Applied Condition Monitoring

Raj Subbiah
Jeremy Eli Littleton

Rotor and Structural Dynamics of Turbomachinery

A Practical Guide for Engineers and Scientists

Springer

Applied Condition Monitoring

Volume 11

The book series Applied Condition Monitoring publishes the latest research and developments in the field of condition monitoring, with a special focus on industrial applications. It covers both theoretical and experimental approaches, as well as a range of monitoring conditioning techniques and new trends and challenges in the field. Topics of interest include, but are not limited to: vibration measurement and analysis; infrared thermography; oil analysis and tribology; acoustic emissions and ultrasonics; and motor current analysis. Books published in the series deal with root cause analysis, failure and degradation scenarios, proactive and predictive techniques, and many other aspects related to condition monitoring. Applications concern different industrial sectors: automotive engineering, power engineering, civil engineering, geoengineering, bioengineering, etc. The series publishes monographs, edited books, and selected conference proceedings, as well as textbooks for advanced students.

More information about this series at http://www.springer.com/series/13418

Raj Subbiah · Jeremy Eli Littleton

Rotor and Structural Dynamics of Turbomachinery

A Practical Guide for Engineers and Scientists

Springer

Raj Subbiah
Oviedo, FL
USA

Jeremy Eli Littleton
Saint Cloud, FL
USA

ISSN 2363-698X ISSN 2363-6998 (electronic)
Applied Condition Monitoring
ISBN 978-3-319-73295-4 ISBN 978-3-319-73296-1 (eBook)
https://doi.org/10.1007/978-3-319-73296-1

Library of Congress Control Number: 2017963016

Printed on acid-free paper

This Springer imprint is published by Springer Nature
The registered company is Springer International Publishing AG
The registered company address is: Gewerbestrasse 11, 6330 Cham, Switzerland

Preface I

In the late 70s, at the beginning of my career, I have developed interest in learning the aspects of vibration in general. I had very limited knowledge on how vibration would impact structures and the associated damages, etc., until I pursued graduate studies in Indian Institute of Technology (IIT) in Delhi where I took a preliminary course on vibration. Following this, I took advanced courses on vibration and rotor dynamics. These courses dealt with highly mathematical approach and were challenging in the beginning to relate them to real life. They were difficult to comprehend but were interesting and arose my curiosity to work on those areas. Rotor dynamics course taught by Prof. J. S. Rao introduced me to the subject; however, until I worked on a project on vibration and rotor dynamics issues on a compressor rotor, I really was not able to grasp the core of the subject.

This formed a sound basis for my rotor and structural dynamics career path. After I completed my graduate studies at IIT, I have accepted a fellowship offered to pursue my doctoral studies on rotor dynamics at Concordia University in Montreal, Canada. Excellent laboratory facilities boosted my learning further. I grasped more on the subject thanks to my supervisor, Prof. R. B. Bhat, whose great inspiration helped my learning tremendously.

After my doctoral studies, I started to work for Stress Technology Inc., a mechanical consulting company, in Rochester, New York, founded by Prof. Neville Rieger on rotor dynamics-related industrial problem; this time, for a major turbine manufacturer in Switzerland. In this position, I have developed rotor dynamic software for linear and nonlinear rotor dynamics in addition to handling other turbomachinery vibration issues.

During the late 80s, I moved to Orlando to work for Westinghouse Electric Corporation where I started working on various aspects of rotor and bearing designs as applied to fossil and nuclear power plants. New R&D projects initiated during that time helped to expand my horizon on fatigue, fracture mechanics, creep, etc. While I was working in Westinghouse, I also taught courses on vibration and rotor dynamics at the University of Central Florida (UCF) as an adjunct faculty for a few years. Siemens took over Westinghouse in the late 90s. I had challenging assignments to work on multifarious problems including structural and concrete foundation issues due to normal and earthquake type of loadings. These studies also helped to understand the influence of impact and random loadings on various components associated with the turbomachines.

During this period, I had the opportunity to conduct tailored 3- or 5-day vibration courses in turbomachines to students in academics, engineers, and managers at various industries and universities globally. The motivation to write this book came from the feedback provided by my students during the course of these lectures. Their feedback and suggestion enabled me to venture writing a book that would simplify the concepts and explain them in simplistic terms with minimal mathematical equations. I am sure that this book will cater to every engineer's needs to apply their learning to resolving their turbomachinery problems.

I have been an active member of national (USA) and international (ISO) vibration committees for about 25 years. The opportunities to work on a few projects enhanced my exposure to meeting with global experts and learn and apply their experiences in resolving complex vibration issues.

Oviedo, USA Raj Subbiah
June 2017

Preface II

My career started with working in my father's residential and commercial construction company in the late 80s. Working in this industry spurred my interest into how various forces interacted on structures. In the early 90s, I decided to pursue my bachelors in mechanical engineering from the University of Pittsburgh. During my time there, I concentrated my studies in mechanical design, finite element modeling, and vibration. Upon graduation, I joined Buck's Fabricating where I worked in the design of various types of shipping containers and hydraulic motion applications. This work with hydraulic motion built a sound understanding how forces of motion acted on their support structures. It also inspired my interest in vibration.

In the late 90s, I joined Siemens Westinghouse Power Generation in Orlando, Florida, as a field service engineer. Working in the Field Technology Services group, I was exposed to specialized work including hydraulic controls, impact testing, vibration analysis, and field balancing among other work. My manager, Fred Mynatt, and assistant manager, Fred Laber, both mentored me in field balancing. In a short time, I became proficient in field balancing and moved into complex vibration analysis on turbine-generators. By the mid-2000s, I was considered the field expert in vibration analysis for Siemens.

In 2010, my career shifted from working in the field to moving into an office role to support Siemens as the Subject Matter Expert (SME) in field balancing and vibration analysis. Since then, I have received my M.S. in Industrial and System Engineering from the University of Florida. In this role as the SME, I was involved in supporting all field balancing and vibration analysis operations in the North, South, and Central America. During each year, I conduct classes in field balancing, vibration analysis, and advanced vibration analysis for field engineers. I also have presented at a number global conferences on various vibration issues throughout the years. During the design stage on new rotors, I collaborate with the team on field actual vibration responses of rotors versus theoretical calculations. I am also involved with the field testing of these new rotors. This has given me significant insight into how the rotors react under various conditions.

Raj and I found that the best way to train practical users was to keep the concepts to what is needed to excel and not get wrapped up in theoretical concepts. This book was written with that goal in mind. Based on the feedback from the years of training field engineers, the sections in this book have been tuned to benefit the reader with practical knowledge and know-how.

Saint Cloud, USA Jeremy Eli Littleton
June 2017

Acknowledgements I

Majority of the sections in this book were taken from my lecture notes and technical papers published in ASME, IFToMM, and IMechE journals and proceedings. Chapter 5 on balancing was co-authored by Jeremy Littleton who is a “Subject Matter Expert” in the area of rotor balancing in Siemens, Orlando. I take this opportunity to thank my colleagues. I am indebted to many who read my manuscript and made suggestions for improvement. Most notable mention is my ISO colleague Mike McGuire, Chair of the ISO vibration SC2 committees, who read the first two chapters and provided valuable comments within short time despite his busy schedule. Primarily, his input helped me shaping up the core content of the book.

My sincere thanks are due to my colleagues Avinash Balbahadur, Joseph Hurley, and Justin England, Siemens Generator Engineering, Orlando, for their excellent suggestions and quick review of the text. Review and/or help rendered by Richard Goodfellow, Ashley Ammon, Todd Bentley, Manish Kumar, Vivek Choudhry, Dharmen Tailor, Gabor Tanacs, Jim Dorow, Ryan Boone, John Mellers, Larry Fowls, Lewis Gray, Stuart Weddle, George Altland, John Thomas, Roger Heinig, Joe Berelsman, and Mike Steedle all from Siemens is gratefully appreciated. Helpful review by Dr. Uli Ehehalt, Florian Hiss, and Uemit Mermertas from Siemens, Germany, came handy. Diane Schell’s help in formatting illustrations is highly appreciated.

I want to thank Mark Cottrell, Steam Turbine Service Engineering Manager, and Attorney Daniel Ryan of Siemens for their timely review and suggestions. Daniel Ryan’s helpful gesture at every step of the way made easier to come up with the copyright format as needed by the publisher.

Bearing illustrations provided by Waukesha Bearings Corporation, Kingsbury, Inc. and copyright permissions by publishers John Wiley and New Age International, New Delhi, are kindly acknowledged.

Thanks are due to Dr. Leontina Cecco Di and the publisher Springer, Germany, for their concerted effort providing timely guidance, review, and suggestions to improve the book.

Last but not least, I am indebted to my beautiful wife Kala lifelong for her patience, support, and understanding throughout the arduous process of writing the book that lasted for almost 18 months. Thanks are due to my beautiful daughters Suki and Nithya and my brother-in-law Prof. C.V. Ramakrishnan and Dr. Krishnamurthy for supporting me as well.

June 2017 Raj Subbiah

Acknowledgements II

I like to give special thanks to Fred Mynatt and Fred Laber for all the mentoring that they had given me over the years. Their support has been instrumental to my advancement to become the technical expert that I am.

My mother, Constance, instilled in me from an early age to set and achieve goals. Without her continuous support, I would not be where I am today, thank you.

Last but certainly not least, I want to acknowledge and thank my wife Claudia. She has been my rock since I met her. Throughout this process of writing this book and my career, she has taken on the extra burden to fill the gap, while I pursued my career. She has dedicated her time and efforts to raise our son Jonathan and daughter Katarina. Thanks to both Jonathan and Katarina for their support and understanding of the time missed being with them during this process.

June 2017 Jeremy Eli Littleton

Contents

Chapter 1
Basics of Rotor and Structural Vibration

1.1 Introduction

The inspiration for writing this book came from the feedback provided by global audiences during my lectures on the vibration theory of rotating machinery. Many felt the need for a simplified approach to better understand the theory of rotor and structural dynamics. The intent of this book, is therefore, to introduce an easy-to-grasp concepts on rotor and structural vibration issues. Although steam turbines were used as examples throughout the book, the methods discussed are equally applicable to all rotating machines. The content has been divided into eight chapters which discuss various dynamical aspects that cause vibrations in rotating machines. More practical examples are compiled at the end that provide in-depth knowledge of symptoms to problems faced by turbo-machinery engineers. The information can be found useful for scientists to pursue further research on this topic.

1.2 General

This chapter lays the foundation by introducing the basic rotor and structural dynamic terminologies, concepts and differences between them. They will form a sound basis for the readers to grasp the concepts of the subject when larger and more complex rotor systems are studied in later chapters. A simple rotor dynamic model, widely known as the "Jeffcott Rotor" is utilized to discuss the influences of fluid-film (Fluid-film or Oil-film terminologies mean the same. Both terminologies are used in this book) bearing dynamic properties and structural support stiffness on rotor frequencies. Studies include backward and forward rotor whirl occurrences and their role in shaping the elliptical orbits.

R. Subbiah and J. E. Littleton, *Rotor and Structural Dynamics of Turbomachinery*,
Applied Condition Monitoring 11, https://doi.org/10.1007/978-3-319-73296-1_1

Chapter 2 discusses the details of rotor modeling methods as applied to lateral (bending) and torsional (twist) vibration analyses. Rotor models for lateral analysis include gyroscopic effects, rotor asymmetry, mass unbalance, fluid-film bearing dynamic characteristics and steam/gas-induced force unbalances. For torsional vibration studies, grid induced torques, developed by negative sequence currents and short-circuiting, are studied for their impact on rotor fatigue life. Further, various test methods used to measure rotor frequencies are discussed. The test results are used to validate shaft train models and detune frequencies of the hardware, if necessary.

Chapter 3 focuses exclusively on variations of bearing pedestal stiffness in service. These pedestals are fabricated steel structures. Pedestal stiffness is one of the dominant parameter that influences rotor dynamics. Stiffness reduction in pedestals were observed in certain category of LP turbine designs that were applied in half-speed or 30 Hz machines. Test data supports that excessive pedestal oscillations could eventually lead to deterioration of the pedestal stiffness in those designs. Several tests involving the use of electrical shakers consistently proved that they are suitable for imparting sufficient energy to excite rotor and structure frequency spectrums for the pedestal structures discussed. Shaker tests on more than 100 bearing support pedestals produced consistent frequency spectrums that enabled identification of rotor frequencies and pedestal stiffness values. Various structural modifications applied to stiffen the degraded pedestal structures are also discussed.

Chapter 4 is dedicated to oil film bearing configurations and their influence in rotor dynamics. Various journal bearing types and their geometries are extensively covered. Pros and cons of several bearing types are discussed in controlling and maintaining their dynamical behavior. Additionally, special bearing types that are applied to solve complex turbo-machinery problems are covered. Thrust bearings that control axial loads (developed by steam or gas medium in the axial direction) and maintain rotor axial travel are discussed as well. At the end of the chapter, a list of common symptoms observed in both the journal (or radial) and the thrust (axial) bearings are covered including their root causes and possible solutions.

Chapter 5 deals with rotor balancing. Detailed rotor balancing fundamentals such as influence co-efficient and modal balancing methods are discussed to provide insight into the subject. Rotor balancing is typically performed at the factory and follow up rebalancing on site may be required to help control and reduce vibrations below ISO specified levels. Rotor balance strategies are discussed using polar plots and the relative phase angle references. Keeping a log of balance weight angular positions of a machine is always helpful for subsequent or future balance moves. Several examples are discussed on balancing of various rotor configurations applied in turbo-machinery.

Rotor alignment processes, applied in turbo-machinery, are discussed in Chap. 6. Basically, coupling alignment is central to keep the rotor vibration within acceptable limits. The two major parameters, viz., "Concentricity and Parallelism" in a coupling pair (coupling radial displacements and axial gaps) are of paramount importance for good alignment. The tools used to measure these parameters are discussed with illustrations. In addition, two different shaft alignment philosophies are discussed. These philosophies include (a) assembling the shafts with zero bending moments at the couplings or (b) assembling them with zero bending moments at the bearings. The choice of choosing one or the other is by “tradition of design” rather than the best practice.

Chapter 7 discusses the diagnostic methods generally practiced in the turbine industry. Various diagnostic tools utilized to measure rotor and structure vibration levels are described in the text. Measured data is used to diagnose symptoms of common problems confronted in turbo-machinery. Potential solutions are discussed as well. Turbine operating issues and their impact on rotor vibration has been added to this section.

Chapter 8 lists commonly experienced vibration issues in turbo-machinery. Eleven case studies are presented. An example of a rotor crack is among them and discussions include observed symptoms and potential solutions.

1.3 Fundamentals of Rotor Dynamics in Turbo-Machinery

Rotating shafts, in general, are known as “rotors” play a central role in all turbo-machines. Examples range from small machines such as automobile axles, motors, pumps, chemical processing equipment, sugar and paper mills to large machines applied in power generation such as steam, gas and wind turbines and electrical generators.

This introductory chapter discusses the basic principles and terminologies applied in rotor dynamics using the well-known “Jeffcott Rotor” as an example. This will lay the foundation for understanding the problems associated with rotating machinery. Steam turbines are used as real-world examples during discussions of various design analyses methods. The main emphasis is on rotor dynamics and discussion of its role in the overall turbo-machinery design process. The problems and the associated solutions discussed in this book are applicable to most rotating machines. The two-major vibratory modes due to rotor bending and torsion are introduced to demonstrate their distinct characteristics and behaviors. Suitable modeling tools, that can be applied to understand the dynamic response of turbine-generator (T-G) systems, are discussed when these systems are subjected to various forcing functions.

Lateral rotor dynamic fundamentals are mainly discussed in this introductory chapter, deferring advanced discussions on both torsional and lateral vibration to Chap. 2.

1.4 Why Rotor Dynamics Plays a Vital Role in Rotating Machinery Design?

Let us briefly go over the various aspects of turbine design to understand how rotor dynamics plays an important role in rotating machinery. The first example shown in Fig. 1.1 is an opposed and symmetric flow Low Pressure (LP) steam turbine applied in a large turbine-generator (T-G) system.

Steam enters through the mid-section of the rotor and expands equally in opposite axial directions shown by the red arrows. When steam travels through the rows of stationary and rotating blades, it expands and produces mechanical work. Similar working principles can be observed in High Pressure (HP) and Intermediate Pressure (IP) turbines which are often coupled to the LP turbines. The mechanical energy produced in the turbine section is then converted to electrical energy by the generator that is coupled to the steam turbine.

As the steam expands through a steam turbine, its specific volume increases. Longer blade rows in progression are designed along the steam path to accommodate the increase in the volumetric steam flow. Hence, the longest blades in a steam turbine are located at the last few rows of the LP rotor. The longer LP-end blades, by virtue of their flexibility, could participate in either lateral and/or torsional rotor vibration.

Mass variations in the LP blade rows can cause mass unbalances in the rotor leading to increased lateral vibration. Variations in rotational inertia and/or the natural frequencies of the longer and more flexible blades could affect torsional vibration. Depending on the configuration of the rotor, one to three last row LP blade stages can participate in torsional vibration near the operating speed. The HP

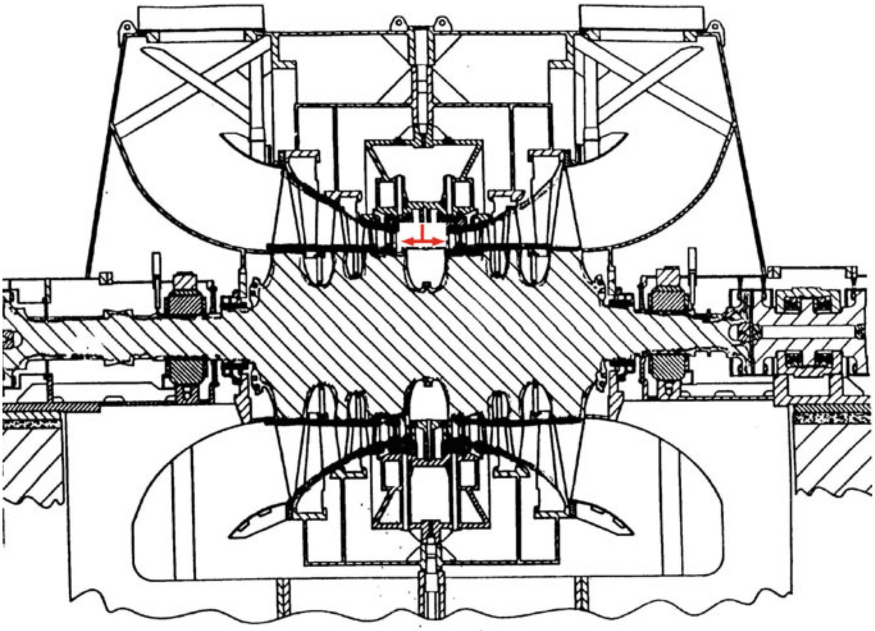

Fig. 1.1 Opposed flow LP steam turbine (courtesy of Siemens)

and IP blades, being shorter and rigid, rarely participate in torsional vibration at or near the operating speed.

A second example is a gas turbine rotor, which is shown in Fig. 1.2. Air is compressed along the compressor blade stages to a certain maximum pressure. The compressed air is then mixed with fuel in the combustion chamber where the air-fuel mixture ignites thus attaining higher pressure and temperature. The resulting high-pressure gas stream expands in the turbine blade stages producing mechanical energy.

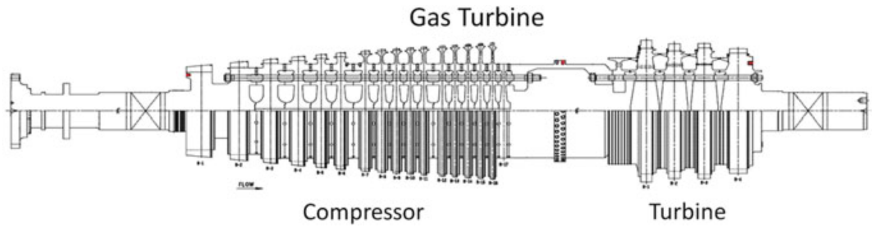

Fig. 1.2 Example of a gas turbine (courtesy of Siemens)

In both steam and gas turbines, blades are designed in accordance with thermal and aero-dynamical design requirements. In addition, peripheral structures such as casings, fluid-film bearings, bearing support structures and concrete foundation are designed to meet structural and rotor dynamic requirements.

A third example is a wind turbine. It consists of a set of rotating blades at the front end of the shaft and is connected to a generator on the same shaft as illustrated in Fig. 1.3. Wind velocity drives the turbine blades, which rotate at variable speeds. This converts the wind power into mechanical work, which is then converted into electrical power in the generator.

Fig. 1.3 Cross section of a wind turbine

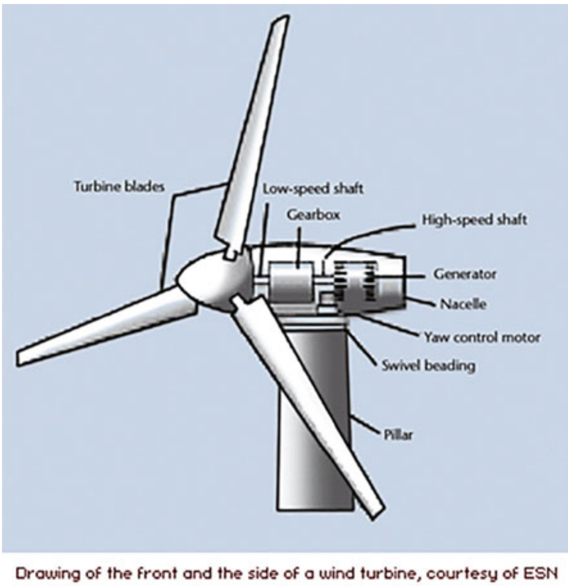

A fourth example is a generator. The generator consists of a stator and a rotor as illustrated in Fig. 1.4. The stator of the generator houses several electrical coils (known as armature coils). They circumferentially, surround the generator rotor. The generator rotor is a large rotating electromagnet, which creates a rotating magnetic field. As the magnetic field rotates (driven by the turbine), the conductors in the stator coils cut the lines of electromagnetic flux thereby generating electrical energy by the process of electromagnetic induction.

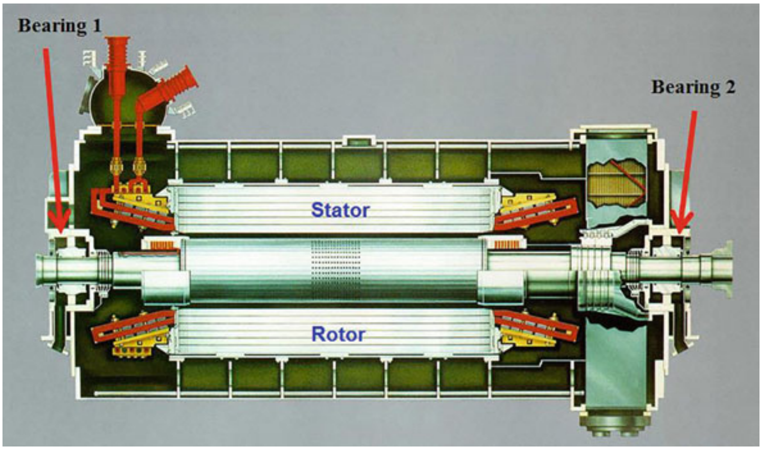

Fig. 1.4 Example of a generator

Although the four examples discussed above are related to turbo-generators, the general design principles discussed here and in the subsequent chapters (in one way or other) are applicable to almost all rotating machines. A brief overview of the various dynamical analyses performed in a steam/gas turbine design is listed below:

- ***Thermo-dynamic analysis*** is used to define the envelope/boundary of the blade path for the target performance and efficiency. This is the first analysis performed in a turbine design that determines the boundaries of the turbine enclosure, which accommodates the stationary and the rotating blades. The blade path design is used to determine the optimal length of blades and the associated rotor profile from turbine inlet to exhaust. The turbine cylinder or casing to enclose all turbine parts is designed next.

- ***Aero-dynamic analysis*** focuses on the stream-lined flow path by minimizing secondary flow interruptions from the thermo-dynamic design. This analysis is used to minimize flow loss and maximize the thermal performance and efficiency.
- ***Structural dynamic analyses*** are performed for casings, bearing support pedestals and foundation structures to make sure that calculated stress levels met the design strength and fatigue life targets for turbine-generators.
- ***Rotor dynamic analyses*** are done to identify and avoid rotor system resonant frequencies near the operating speed of the machine. Additionally, sub-harmonic frequency analyses are performed to eliminate or minimize rotor instability caused by oil film and/or steam/gas.

Discrepancies in either thermo-dynamic or aerodynamic designs result in reduced performance or efficiency of the machine, but the turbine still will be operable. Whereas, if the structural design is inadvertently deficient, the machine may experience lingering vibration issues. For example, structural components such as bearing supports may be resonant with rotors and may degrade overtime as a result with deteriorating stiffness. This can lead to high vibration. While the machine may still be operable with balance moves in the near term, the machine may continue to experience intermittent high vibration until the structural deficiencies are corrected.

However, in the event of a severe oil whip or significant steam induced whirl, the rotor system can become in-operable. This often requires a major redesign effort to resolve before the unit can be put into operation successfully. Thus, it becomes obvious that rotor dynamics plays a crucial role in the rotating machinery design. This chapter describes the salient aspects of rotor dynamics. The behavior of oil film bearings and their interaction with rotors will be discussed in detail in Chap. 4.

1.5 Rotor Failure Modes

Before delving into the details of rotor dynamics, it is important to understand the major failure modes of a rotor system are: (a) Torsional Vibration and (b) Lateral Vibration.

1.5.1 Torsional Vibration (Due to Rotor Twist). See Fig. 1.5

- Shaft end A (in Fig. 1.5) is fixed and a twisting moment is applied at the free end B. This causes the shaft to twist (or subject to angular displacement) with its node located at the fixed end of the shaft. The shape of the shaft condition is known as mode-shape. A mode-shape is always associated with a natural frequency of the shaft.
- When the shaft vibrates under the influence of an external torque, angular displacement increases resulting in torsional vibration of the shaft. When the

Fig. 1.5 Shaft twist

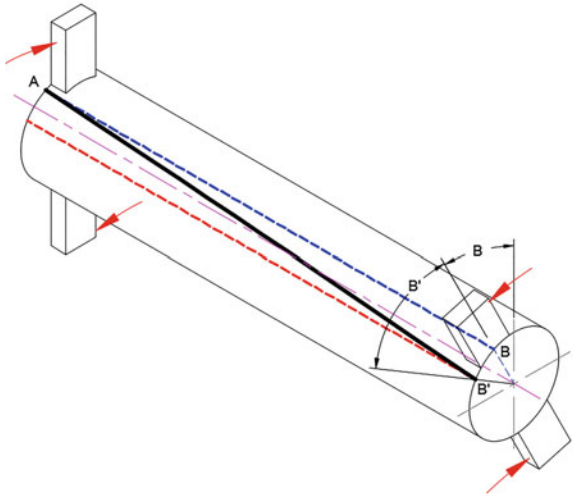

frequency of the external torque matches with a natural frequency of the shaft, vibration reaches its peak value. The rotor is said to be in resonant with the frequency of the applied torque. At this point, the mode-shape is fully developed (such as pure twist mode) and the shaft will experience increased torsional vibration.
- Excessive grid electrical disturbances could lead to torsional resonance of the shaft train.

Torsional dynamics involves the determination of rotor system torsional natural frequencies and their associated twist modes. The accurate determination of these frequencies is critical for safe operation of a rotating machinery. As illustrated in Fig. 1.5, excessive torsional vibration can cause fatigue damage of the shaft, if it is operated for longer periods of time in that condition. Other components coupled to the train such as turbine blades will be impacted as well. Therefore, torsional frequency evaluation becomes an essential part of the rotor design process.

For large rotor systems (such as multi-component steam turbines), several torsional frequencies and their associated modes are possible. When one or more of the rotor train frequencies come close to the operating frequency, the shaft system will experience resonant condition. This can be harmful to the turbo-generator system. More detailed discussions are deferred to Chap. 2.

1.5.2 *Lateral Vibration (Due to of Rotor Bending). See Fig. 1.6*

- Similarly, mass unbalance forces excite rotor bending (or lateral) natural frequencies and their respective bending modes as illustrated in Fig. 1.6.
- When the natural frequency of the excitation force matches with any one of the rotor natural frequencies, rotor vibration becomes excessive.
- Mass imbalances could cause large rotor vibration when the excitation frequency is resonant with its natural frequency.

Rotor bending and lateral vibration are synonymous to angular twist and torsional vibration.

In comparison to rotor twist that occurs about the shaft axis, rotor bending occurs in two orthogonal planes of the rotor. Consequently, a rotor supported in dissimilar supports (such as fluid-film bearings plus pedestals) have distinct lateral frequencies in the vertical and the horizontal planes (or directions). The lateral frequencies are different from those due to torsion unless the bending and twist motions are mechanically coupled. The predominant driving force for lateral vibration is “mass unbalance” present in the rotor system.

Lateral vibration is caused by several factors. Most prominent ones are: (a) mass unbalance, (b) fluid-film forces, (c) steam induced unbalance loads or (d) degraded pedestals. Excessive vibration generated by these forces could damage the rotor system in various degrees. These effects will be discussed in Chaps. 3 and 4.

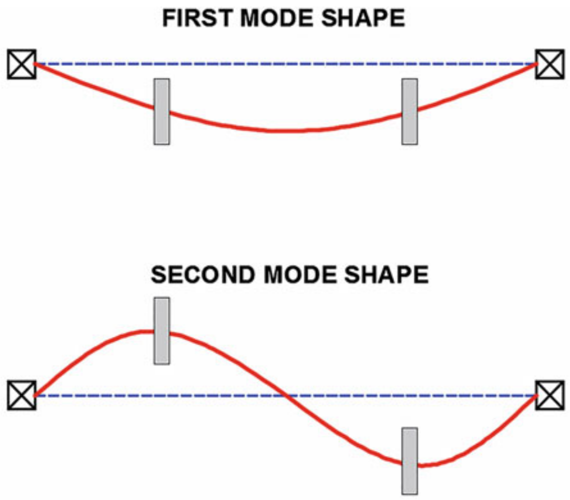

Fig. 1.6 Shaft bending

It is important to understand that ***fluid film and pedestal degradation effects impact rotor lateral behavior only, but do not impact torsional behavior***. By default, the term "rotor dynamics" typically refers to lateral dynamics.

For a better appreciation of the terminologies used in rotor dynamics, an attempt was made to compare them to the well-known terminologies used in structural dynamics as shown below in Table 1.1.

1.6 Rotor Dynamics Versus Stationary Structural Dynamics

Table 1.1 provides a list of terminologies used in rotor and structure. They are further discussed in the sub-sections that follow.

Table 1.1 Comparative terminologies used in a stationary structure and a rotor

#	Stationary structure	Rotor	Remarks
1	Vibration (Fig. 1.7a)	Whirl (Fig. 1.7b)	Terminologies
2	Natural frequency, in cycles/s or Hz	Critical Speed in RPM $N_{cr} = \frac{60}{2\pi}\sqrt{\frac{K_{eq}}{m}}$	Rotor natural frequency is converted to speed
3	Mode shapes are called 1st, 2nd, 3rd… etc.	Mode shapes are named based on the characteristics of the rotor whirl such as "Cylindrical Whirl" (represents 1st rotor bending) and "Conical Whirl" (represents 2nd rotor bending) (Fig. 1.7c)	
4	Structural response $y = \frac{F}{(-m.\omega^2 + k)}$	Rotor response is a combination of forward and backward whirl components $Y(t) = e^{-jwt} + e^{+jwt}$ (Fig. 1.7d)	
5	Structure can be excited by single and/or multiple external sources	Rotor is predominantly excited by the residual mass unbalances present in the rotor system	Unbalance response always occurs at synchronous speed only (the whirl speed and the spin speed of the rotor are the same)
6	In general, for a stable structure, no de-stabilizing forces are generated within the system	Rotor *is susceptible to de-stabilizing forces* that are internal to the system. Examples: oil whip and steam whirl	

1.6.1 Structural Vibration Versus Rotor Whirl

A structure undergoes oscillatory motion with respect to a reference point whenever it is disturbed from this reference position by an external force (see Fig. 1.7a). The cycles of oscillations are known as “vibration”. In the case of a rotor suspended in a fluid-film bearing, the rotor whirls within the bearing clearance space whenever it is disturbed. The locus of the center of the rotor is measured as “rotor whirl” as shown in Fig. 1.7b. The rotor whirls about its statically bent shape and does not oscillate as one piece like a structure. Rotor vibration is a term loosely used to refer to rotor whirl amplitude.

1.6.2 Structural Natural Frequencies Versus Rotor Critical Speeds

A stationary structure has several vibratory modes and their associated “natural frequencies”. Whereas, when a natural frequency of a rotor (converted to RPM) coincides with a rotational speed, the rotor response reaches its peak value. The rotor speed corresponding to that peak response is known as “critical speed”.

1.6.3 Structural Mode Shapes Versus Rotor Whirl Motions

Frequencies of stationary structures are identified with their mode shape patterns such as 1st, 2nd, 3rd,… etc. In rotor dynamics, rotor modes are identified based upon their whirl pattern. The first rotor mode is described as either “translatory whirl or cylindrical whirl” which is associated with the rotor 1st critical speed and the rotor second mode is referred to as “conical whirl” [2]. In cylindrical whirl mode, the rotor whirls in the shape of a cylinder exhibiting circular whirl motions at the two ends. Conical whirl is like two cones revolving in opposite directions with their common apex at the center of the rotor. A comparison of these rotor whirl modes is shown in Fig. 1.7c.

1.6.4 Structural Responses Versus Rotor Whirl Responses

Whenever a natural frequency of a structure is subjected to an excitation force, it responds with an increase of vibration. Similarly, when a rotor is subjected to residual mass unbalance forces, the rotor whirls. The resulting whirl is a combination of a forward and a backward whirling components. In a forward whirl motion, the rotor spins and whirls in the same direction (usually counterclockwise)

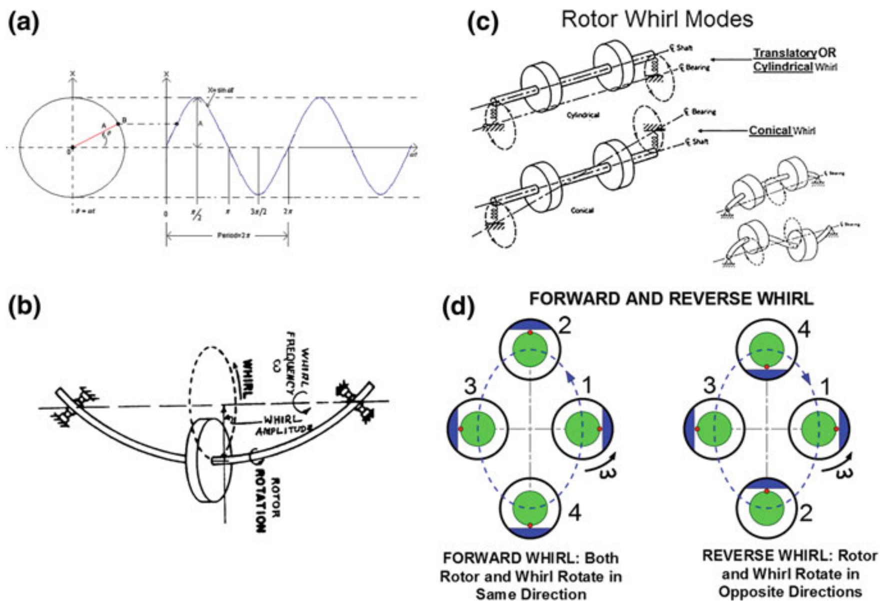

Fig. 1.7 **a** Vibration of a structure. **b** Rotor whirl. **c** first and second rotor whirl modes. **d** rotor whirls in forward and backward directions [1]

whereas in the backward whirl motion, the rotor spins and whirls in opposite direction to each other. See Fig. 1.7d. As a result, the whirl (or rotor vibration) due to mass unbalance excitation is dominated either by a forward or by a backward whirl depending on the dynamic characteristics of the fluid-film.

1.6.5 Structural Excitation Versus Rotor Excitation Forces

Any type of forced excitation (such as single frequency or harmonic or random types) can cause back and forth oscillations in a stationary structure, usually known as vibration. The most common source of excitation in a rotor is "mass unbalance". The shaft eccentricity, which is caused by the mass center being non-coincident with the geometric center, is instrumental in amplifying the mass unbalance force. The eccentricity value depends on the delta between the geometric and the mass centers of the rotor. Eccentricity in shafts is due to one or more of the following:

- Non-uniform circular forging
- Eccentric machining centers
- Eccentricity created by assembly of dissimilar blade weights, shaft runouts, misalignment etc.

Rotor unbalance excitation always occurs when the spin and whirl speeds of the rotor are identical causing “synchronous whirl”. Non-synchronous shaft whirls are the ones where the spin and the whirl speeds are not the same. For example, sub-synchronous rotor whirl occurs at ½ x (or half times) or less than the spin speed of rotor; whirl due to rotor asymmetry occurs at 2x or two times the spin speed.

1.6.6 Stability of Structures Versus Rotor Stability

For stationary structures, the unstable vibration conditions are rare. However, for a rotor suspended in fluid-film bearing, a condition known as “oil whip” can occur at a sub-synchronous frequency of the rotor. Prior to oil whip, both the spin and the whirl speeds of the rotor go together. During oil-whip, the whirl speed separates from the spin speed of the rotor and is locked at the sub-synchronous natural frequency of the rotor. From this point on, the whirl amplitude continues to grow unabated while the rotor spins towards the rated speed. This rotor dynamic condition is also called, “sub-synchronous frequency whirl”. Steam/gas unbalance forces can cause steam or gas whirl. The steam or gas whip has similar characteristics as oil whip, although the source of excitation is different. Both oil and steam whirl occur below the operating frequency, they are called, “sub-synchronous whirl”.

A few examples of simple rotor-modeling methods are discussed below. They are intended to provide better insight into the rotor dynamic characteristics already discussed. The equations of motion of a rotor are derived from energy principles as referenced in [2] and in numerous textbooks and technical publications. Hence, the details are not duplicated here.

1.7 Examples

Four example cases, with increasing complexity, are discussed primarily utilizing a Jeffcott rotor model in the following sub-sections.

1.7.1 Example-1

In Example-1, a very simple rotor model is discussed. Rotor dynamists [2–6] utilized the classical Jeffcott rotor model to explain rotor dynamical characteristics. A Jeffcott rotor carries a single disc that is centrally mounted on a massless shaft and is rigidly supported at the two ends as shown in Fig. 1.8. **Although the vertical and horizontal rotor motions described here are in y and z axes respectively, these rotor motion descriptions may have changed to x and y in later chapters**

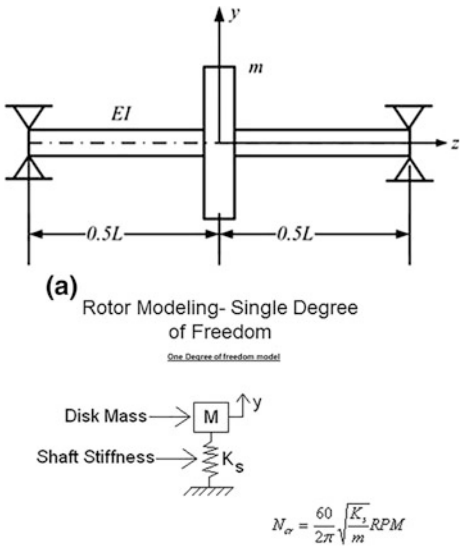

Fig. 1.8 Jeffcott rotor. **a** representation of Jeffcott rotor with lumped mass/stiffness model

due to usage of results obtained from different analytical tools. However, the results obtained from either of the co-ordinate systems are identical. This rotor system can be idealized by a simple lumped mass/stiffness model shown in Fig. 1.8a.

The Jeffcott rotor shown in Fig. 1.8 can be modelled with a disk mass "m" and a shaft stiffness "K_s as illustrated in Fig. 1.8a". The resulting equation of rotor motion "y" can be written as

$$m\ddot{y} + K_s y = 0 \tag{1.1}$$

Assuming sinusoidal motion for y $= A \sin \omega t$
Equation (1.1) becomes

$$-A\,\omega^2 \sin \omega t + K_s A \sin \omega t = 0 \tag{1.2}$$

$$\omega = \sqrt{(K_s/m)} \tag{1.3}$$

ω is cycles/sec or Hz and can be converted into critical speed in RPM as

$$\mathrm{N_{cr}} = \frac{60}{2\pi}\sqrt{\left(\frac{Ks}{m}\right)} \tag{1.3a}$$

Rotor frequency in (1.3) is converted to critical speed $\mathrm{N_{cr}}$ in (1.3a). This is the fundamental bending frequency of the Jeffcott rotor when a lumped mass assumption is made. It should be borne in mind that this approach can only be used to obtain approximate information of a rotor frequency. Estimates of higher frequencies become grossly inaccurate when this simple lumped mass approach is applied. Therefore, a more elaborate rotor model with several degrees of freedom should be considered when there is a need for this.

1.7.2 Example-2

In this example, the Jeffcott rotor shown in example-1 (on rigid supports) is now placed on flexible pedestal supports with equal spring stiffness at the two ends as illustrated in Fig. 1.9. In this configuration, the disk mass “m” is the same as before; however, the system stiffness now becomes a combination of shaft stiffness K_s and the support stiffness K_p. The system stiffness is obtained by combining the two springs in series that results in “the effective stiffness K_{eq} of the system.

Using this simple spring-in series approach, the equivalent stiffness becomes

$$\frac{1}{\mathrm{Keq}} = \frac{1}{K_s} + \frac{1}{2K_p} \tag{1.4}$$

$$\mathrm{Keq} = \frac{K_s \quad 2.K_p}{2.K_p + \quad K_s} \tag{1.4a}$$

K_{eq} in example-2 is lower than K_s used in example-1. How? Let us apply numerical values in Eq. (1.4a) to demonstrate that K_{eq} is lower than K_s. Let K_s be 5 units and K_p be 7 units, K_{eq} is calculated to be 3.68 units, which is lower than K_s of 5. With the same rotor mass and lower system stiffness K_{eq}, the new critical speed of the rotor in example-2 is calculated to be N_{cr1} which is lower than N_{cr}.

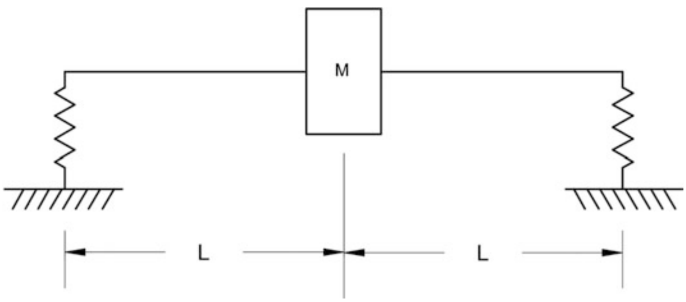

Fig. 1.9 A Jeffcott rotor on two springs

In the above example, if we use a pedestal stiffness K_p at 4 instead of 7 and the same shaft stiffness $K_s = 5$ units, the new equivalent system stiffness K_{eq} now becomes 3.08. This is also lower than 3.68 from the previous step. The rotor critical speed Ncr_2, in this case, would be lower than Ncr_1.

The above numerical examples demonstrate that the rotor critical speed is sensitive and varies when pedestal stiffnesses vary, even though the shaft stiffness remains constant. Fluid-film stiffness is another system variable that should be considered in addition to pedestal stiffness. This will be discussed later.

So far, we have discussed single plane motions with one degree of freedom (y-displacement) models for simplicity. In real life, a rotor simultaneously whirls around two orthogonal planes (YX and ZX) as shown in Fig. 1.10. It has a minimum of two degrees of freedom. This is discussed in example-3 below.

1.7.3 Example-3

In example-2, we applied a 1-DOF Model and obtained the fundamental bending frequency of the rotor. Let us place the planar Jeffcott rotor model on two spring supports (shown in Fig. 1.9) into two planes that are orthogonal to each other as shown in Fig. 1.10. The mass of the rotor remains "m". The rotor model now becomes a 2-degree of freedom system.

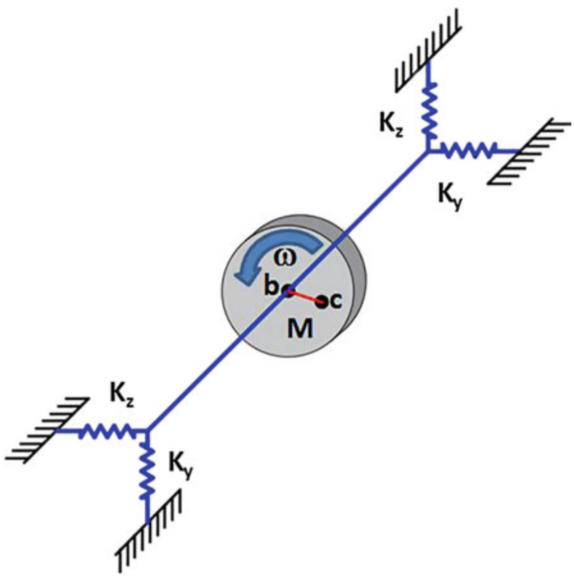

Fig. 1.10 Jeffcott rotor on two equal spring supports on two orthogonal planes

When the springs have equal stiffnesses along Y and Z, the rotor motion is equal at the two orthogonal planes when excited. In this case, the rotor executes a circular whirl motion.

When the spring stiffnesses in the orthogonal planes are dissimilar, the resulting rotor motions become dissimilar as well. Consequently, the rotor whirl no longer remains circular; the rotor executes a non-circular or elliptical whirl orbit.

Let us use this simple Jeffcott rotor model with dissimilar support stiffnesses to further investigate this rotor dynamical behavior. The simple two-plane approach represents a realistic rotor dynamic model and can be applied for complex rotor systems with several masses. For simplicity, damping is not considered for now.

1.7.4 Example-4

Let us use the Jeffcott rotor shown in Fig. 1.5 and apply a mass unbalance eccentricity **"a"** at the central disc as shown in Fig. 1.11. This is viewed in the fixed coordinate system **XYZ** (where X is the origin, Y vertical and Z horizontal). Geometric center has shifted from X to G. As a result, mass center M has an eccentricity "a" from the geometric center G.

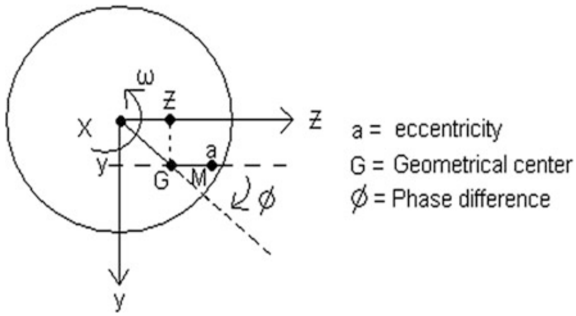

Fig. 1.11 Rotor unbalance parameters

The purpose of this exercise is to perform unbalance response of a rotor suspended in an-isotropic bearings. If $\mathbf{K_s}$ is the stiffness of the rotor shaft and neglecting damping in the system, the equations of motion of the rotor can be written in the two orthogonal planes Y and Z as follows:

$$\left.\begin{aligned} m\frac{d^2}{dt^2}(z + a\sin\omega t) + K_s \bullet z = 0 \\ m\frac{d^2}{dt^2}(y + a\cos\omega t) + K_s \bullet y = 0 \end{aligned}\right\} \tag{1.5}$$

Where m = $\frac{w}{g}$

Equations (1.5) can be expanded as:

$$\begin{aligned} m\ddot{z} + K_s \cdot z &= ma\omega^2 sin\,\omega t \\ m\ddot{y} + K_s \cdot y &= ma\omega^2 cos\,\omega t \end{aligned} \tag{1.6}$$

Equation (1.6) can be solved by assuming the rotor is executing harmonic motion. For a symmetric support stiffness condition, the rotor motion is identical along the two orthogonal planes XZ and XY and the rotor executes a circular whirl. In practice, a rotor applied in turbo-machinery is supported on fluid-film bearings, which add anisotropic fluid-film conditions to the rotor system.

1.8 Fluid-Film Stiffness

The non-isotropy of the support stiffness coefficients (both fluid-film and pedestal) is responsible for different rotor whirl motions along the two orthogonal planes resulting in an elliptical whirl motion. The non-isotropy of the oil-film bearing stiffnesses are also responsible for forward and backward whirl formations in a rotor. Fluid-film damping is not considered here for simplicity.

The equivalent stiffness of the rotor and the fluid-film stiffness become

$$\left.\begin{aligned} \frac{1}{K_y} &= \frac{1}{K_s} + \frac{1}{K_{by}} \\ \frac{1}{K_z} &= \frac{1}{K_s} + \frac{1}{K_{bz}} \end{aligned}\right\} \tag{1.7}$$

1.9 Forward and Backward Rotor Whirl Vectors

Now introducing the bearing properties (represented by linear springs in Z and Y axes) in the two planes, the equations of motion [7] can be written as follows:

Applying Eqs. (1.7) in Eq. (1.6) and converting trigonometric functions to exponential form results,

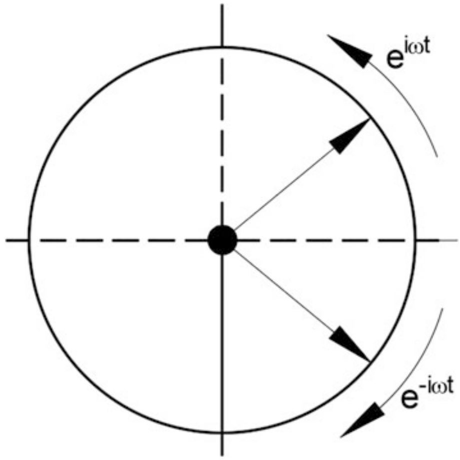

Fig. 1.12 Forward and backward rotating vectors

$$\begin{aligned} m\ddot{z} + K_s \cdot z &= \frac{ma\omega^2}{2i}\left(e^{i\omega t} + e^{-i\omega t}\right) \\ m\ddot{y} + K_y \cdot y &= \frac{ma\omega^2}{2}\left(e^{i\omega t} + e^{-i\omega t}\right) \end{aligned} \tag{1.8}$$

Where $i = \sqrt{-1}$
Assume

$$\begin{aligned} \mathrm{z}(t) &= z_F e^{i\omega t} + z_b e^{-i\omega t} \\ y(t) &= y_F e^{i\omega t} + y_b e^{-i\omega t} \end{aligned} \tag{1.9}$$

Substituting Eq. 1.9 in Eq. 1.8 results (Fig. 1.12)

$$\begin{aligned} \mathrm{Z_F} &= \frac{2ma\omega^2}{K_z - m\omega^2} \\ \mathrm{Y_F} &= \frac{2ma\omega^2}{K_y - m\omega^2} \end{aligned} \tag{1.10}$$

The maximum rotor amplitude is a combination of forward and backward whirls as shown below:

$$\mathrm{R(t) = Y(t) + iZ(t)} = \frac{1}{2}\left(\frac{ma\omega^2}{K_y - m\omega^2} + \frac{ma\omega^2}{K_z - m\omega^2}\right)e^{i\omega t} + i\frac{1}{2}\left(\frac{ma\omega^2}{K_y - m\omega^2} - \frac{ma\omega^2}{K_z - m\omega^2}\right)e^{-i\omega t} \tag{1.11}$$

$= r_F(forward) + r_B(backward)$ Which corresponds to elliptical whirl.

1.9.1 Split Critical Speeds of a Rotor

Case 1: If $K_z = K_y$, then the second term in Eq. (1.11) vanishes resulting in a forward whirl only and the whirl becomes circular.

Case 2: If $K_y > K_z$

$$\omega_{by} = \sqrt{\frac{K_y}{m}}, \omega_{bz} = \sqrt{\frac{K_z}{m}} \omega_{ny} > \omega_{nz} \tag{1.12}$$

The plot of rotor response Versus rotor speed in RPM provides the so called, "Critical Speed Map" of a rotor system shown in Fig. 1.13. In this case, ω_{ny} is greater than ω_{nz}.

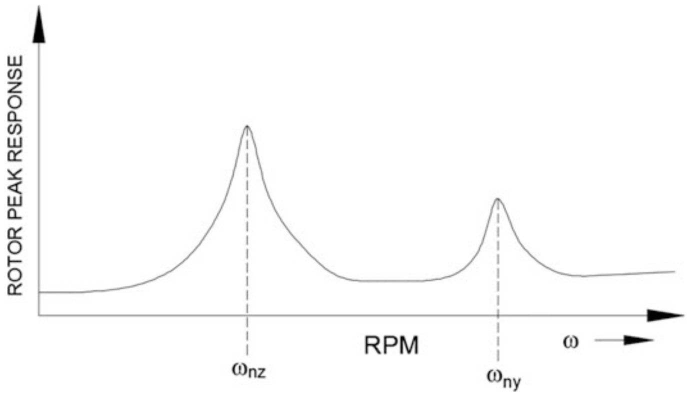

Fig. 1.13 Critical speed map

Three scenarios exist here. They are:

(a) When rotational speed ω is situated below ω_{nz} which represents rotor horizontal critical speed

$$\begin{aligned} \text{Mag } r_F &= \frac{ma\omega^2}{2}\left[\frac{1}{m\left(\omega_{ny}^2 - \omega^2\right)} + \frac{1}{m\left(\omega_{nz}^2 - \omega^2\right)}\right] \\ \text{Mag } r_B &= \frac{ma\omega^2}{2}\left[\frac{1}{m\left(\omega_{ny}^2 - \omega^2\right)} - \frac{1}{m\left(\omega_{nz}^2 - \omega^2\right)}\right] \end{aligned} \tag{1.13}$$

When Mag r_F is $>$ Mag r_B, the rotor executes a "Forward whirl" as illustrated in Fig. 1.14.

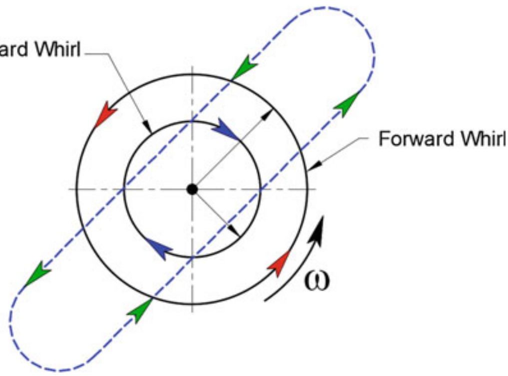

Fig. 1.14 Forward whirl

1.9.2 Construction of Whirl Plots

Draw circles of forward and backward whirl amplitudes. Draw the S-max line combining forward and backward whirl amplitudes. Draw the S-min line orthogonal to this line, subtracting forward from the backward whirl amplitudes. Connect the two end points of the lines in the form of parabola. Adjust the orientation of parabola with the known phase angle between major and minor axes.

(b) When rotational speed ω is situated between ω_{nz} (Horizontal) and ω_{ny} (Vertical)

Mag r_B is larger than Mag r_F, the rotor motion is dominated by backward whirl; hence the rotor executes a "Backward whirl" as shown in Fig. 1.15.

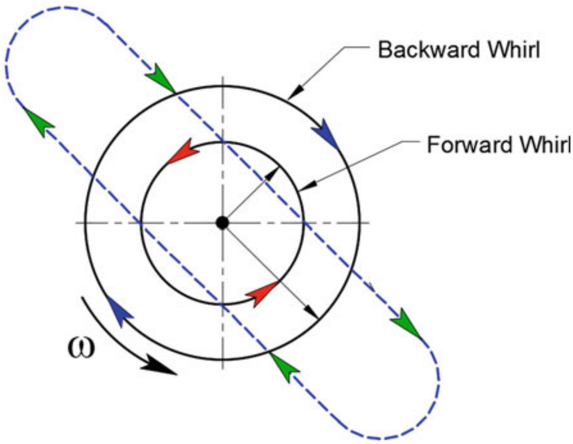

Fig. 1.15 Backward whirl

(c) When rotor speed $\omega > \omega_{ny}$ (Vertical Critical speed), then

Mag $r_F >$ Mag r_B, the rotor executes a "Forward whirl"

As illustrated in the critical speed map in Fig. 1.13, the rotor whirl stays forward until it reaches the peak response corresponding to the first horizontal rotor bending critical frequency ω_{nz} *due to horizontal plane* $Z - X$. As the rotor speed increases further, the rotor motion changes to backward whirl until the response reaches the next peak amplitude corresponding to the first vertical rotor bending critical frequency ω_{ny}. Thereafter, the whirl continues to be in the forward motion.

Typically, two critical speeds with similar first bending mode shapes in the horizontal and in the vertical planes are called, "Split Critical Speeds" of the rotor.

It is clear from the discussions above that the rotor whirl direction is backward in between the two peak responses of the first rotor bending (or U-mode) modes as shown in Fig. 1.13. This is the unique behavior of rotors supported on oil film bearings.

The above change of a forward to a backward whirl motion was also observed in laboratory tests conducted and reported by Subbiah [4].

Split critical speeds are not observed on a rotor supported on rolling element bearings which are isotropic (equal support stiffness at all speeds).

The simple rotor system models discussed in this chapter provide the basic understanding of rotor dynamic characteristics. These basics will help when multi-degree of freedom systems are applied in large and multiple rotor trains.

1.10 Closure

In this chapter, we have covered the following:

- Various design analyses applied in turbo-machinery and the importance and uniqueness of rotor and structural dynamic analyses.
- Dynamic behaviors of stationary structures were compared with those of rotors to provide a better understanding and appreciation of rotor dynamic characteristics.
- Simple equations of motion of a Jeffcott rotor (with added levels of complexity) were discussed.
- Two main rotor failure modes viz., rotor twist (torsion) and rotor bending (lateral) were introduced deferring the details to Chap. 2.

References

1. Tse F, Morse I, Hinkle R (1978) Mechanical vibrations. Prentice Hall, New Jersey
2. Vance JM (1988) Rotordynamics of turbomachinery. Wiley, New York
3. Nordmann R (1984) Identification of modal parameters of an elastic rotor with oil film bearings. Trans ASME, 83-DET-11
4. Subbiah R (1983) Experimental verification of simultaneous forward and backward whirling at different points of a Jeffcott rotor supported on identical journal bearings. J Sound Vib:379–388
5. Lund JW (1965) Rotor bearings dynamics design technology, part V: computer program manual for rotor response and stability. Mechanical Technology Inc., Latham, NY, AFAPL-Tr-65-45
6. Rao JS (1983) Rotor dynamics. Wiley, New York
7. Subbiah R (1985) Dynamic behavior of rotor systems with a compehensive model for the hydrodynamic bearing supports using modal analysis and testing. PhD thesis, Concordia University, Montreal, Canada

Chapter 2
Mathematical Model

2.1 Introduction

In Chap. 1, we have discussed simple mathematical models to idealize the rotor and support systems using Jeffcott rotor. Simple rotor and structural dynamic systems, terminologies and characteristics learnt in Chap. 1 will lay a solid foundation when we extend the studies to larger systems. Methods to articulate mass and stiffness elements to formulate accurate rotor system models will be the focus of this chapter. Advanced rotor modeling methods such as Finite Element (FE), traditional Transfer Matrix (TM) and the combined methods will be discussed in detail. In addition, numerical solutions that are applied in lateral and torsional vibration analyses will be presented.

2.2 General

The following were accomplished in Chap. 1:

- Importance of rotor dynamics in rotating machinery design using steam turbine as an example.
- The dynamic behaviors of stationary structure vs. rotor structure, their similarities and differences for a better appreciation of rotor dynamic characteristics.
- Basic rotor dynamic terminologies, primarily using Jeffcott rotor model including stiffnesses of fluid-film and support pedestals.
- Two main rotor failure modes viz., rotor twist (torsion) and bending (lateral) including one and two degrees of freedom models.

In this chapter, the lateral and the torsional rotor modeling methods will be discussed in detail.

R. Subbiah and J. E. Littleton, *Rotor and Structural Dynamics of Turbomachinery*,
Applied Condition Monitoring 11, https://doi.org/10.1007/978-3-319-73296-1_2

2.3 Lateral (Bending) Rotor Dynamic Model

A lateral rotor dynamic system comprises of

- Rotor
- Fluid-film Bearings
- Steel Pedestals supporting the bearings
- Concrete Foundation or Base Supports

See Fig. 2.1. Let us go over each sub-component as follows:

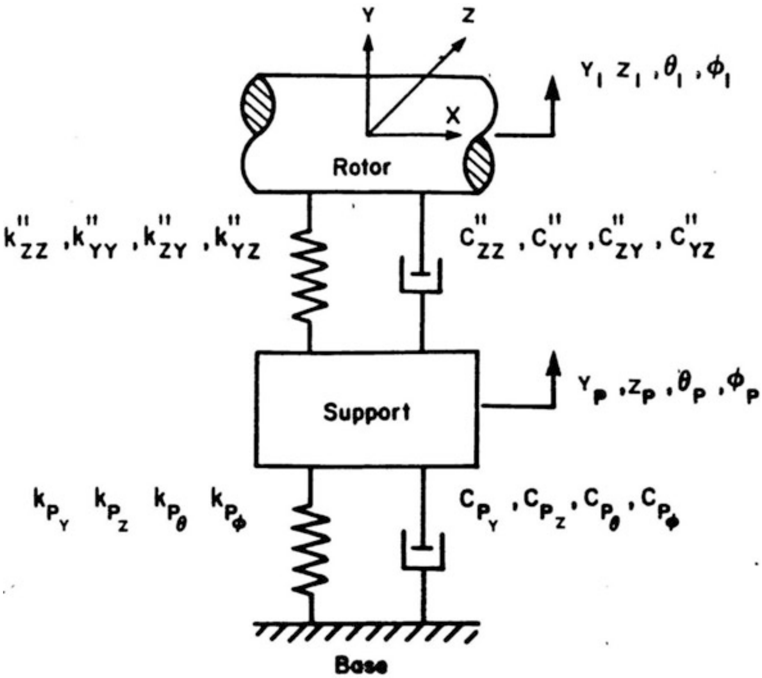

Fig. 2.1 Rotor-Bearing-Pedestal-Foundation Model

2.3.1 *The Rotor Modeling*

Discretize rotor continuum (typically, 2:1 ratio for length to diameter) using beam elements with two nodes per element. Each node represents two displacements (due to bending forces in Y and Z axes) and two rotations θ and ϕ (due to bending moments about Y and Z axes). The fluid-film bearing and the pedestal elements are connected in series to the rotor at the appropriate node point. The fluid-film bearing element consists of stiffness and damping coefficients (the superscripts “tt” for fluid-film coefficients shown in Fig. 2.1 indicate translational motions only; effects due to rotational motions are not significant) whereas the pedestal characteristics are represented by their translational stiffness only. The effects due to rotations in θ and ϕ directions for pedestals are irrelevant. Although more sophisticated Finite element rotor models increasingly become standard, the less time-consuming beam models are more than adequate for modeling and analysis of rotor systems. **It should be remembered that axial degree of freedom X in a lateral rotor dynamic model is always constrained.**

2.3.2 The Fluid-Film Bearing Modeling

A fluid-film bearing element is added at an appropriate node point on a rotor. Typically, a bearing element **c**onsists of eight dynamic linear coefficients, i.e., four of them are due to film stiffness and the other four due to film damping [1–3]. Further, each of the four coefficients represent two collinear and two cross-coupled planar forces in the Y and Z axes. It should be noted that linear bearing coefficients are relatively accurate for small amplitude rotor motions under steady-state operation. When amplitudes exceed the bearing clearance values, rotor motions become non-linear; consequently, linear models no longer are useful to predict rotor whirl amplitudes accurately.

2.3.3 Bearing Support Pedestal Modeling

Traditionally, pedestals are structures made of steel and are part of a complex casing structure in turbines. Pedestal elements are basically pipes or struts welded between the bearing cones, yokes and the cylinder horizontal joints in a steam turbine. They are modeled as single degree of freedom springs, one each in the two orthogonal planes together with the associated pedestal mass where appropriate. Unlike fluid-film bearings, cross coupled stiffness effects in pedestal structures are insignificant and are not considered in rotor dynamic analyses.

2.3.4 Concrete Foundation Modeling

Concrete foundation is typically stiffer by at least ten or more times than the bearing support steel pedestals. Hence, they are considered very rigid. As a result, concrete foundation has very little influence on rotor dynamics under normal operating conditions. So, concrete foundation influences are not discussed any further.

2.3.5 Steel Foundation Structures

It is commonly applied in Europe and elsewhere; they are rarely applied in turbines installed in the USA. Since steel foundations use structural steel, they provide additional flexibility to the overall rotor support systems.

2.4 Solution Methods

Continuum shaft modeling of rotor systems, in general, are carried out using two well-known numerical approaches in rotor dynamics. They are:

(a) Transfer Matrix (TM) Method
(b) Finite Element (FE) Method

The intent here is to familiarize the readers with various sub-systems that go into the rotor system modeling, but not to overwhelm with intense mathematical equations. These modeling discussions made here will come handy for users when they consider applying commercial or in-house software to model rotor systems. Advanced modeling methods are discussed later in the chapter.

2.4.1 Transfer Matrix (TM) Approach

Figure 2.2 shows discretized rotor shaft using TM model.

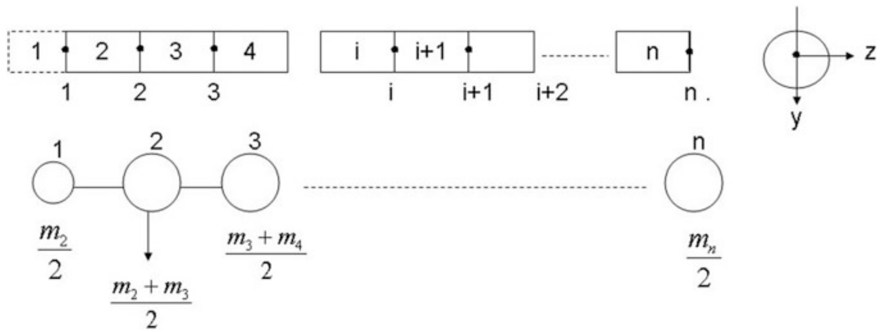

Fig. 2.2 Transfer Matrix modeling of shafts

The rotor is divided into small number of discrete beam elements with each element having two nodes. The mass of each element is equally lumped at the two nodes. Planar rotor displacements (Y and Z axes), rotations (ϕ, θ), associated forces (F) and moments (M) are defined at the nodes. Equations of motions for the mass and the stiffness properties are developed for the discrete beam elements consistent with the nodal displacements and forces. They are illustrated in Fig. 2.3 for the O-X-Y plane (Vertical). Similar representations apply for O-X-Z plane (Horizontal). References by Lund [1] and Rao [2] provide details of TM formulations and are not repeated here.

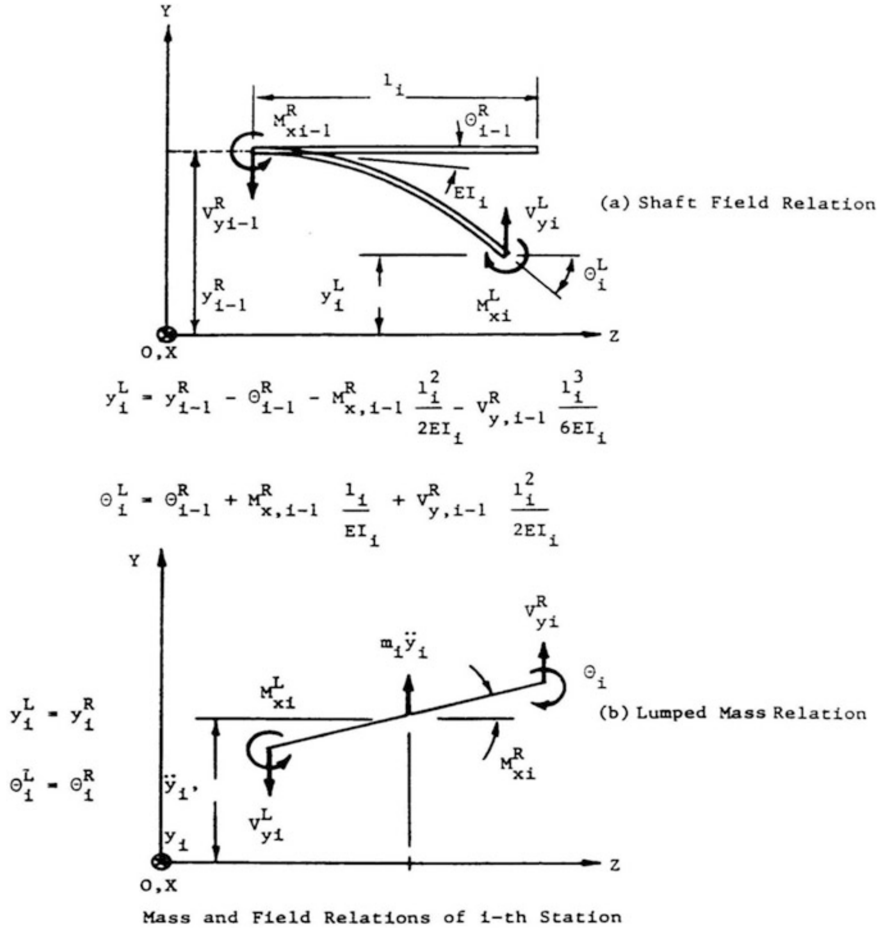

Fig. 2.3 Beam stiffness and mass properties

Nodal vector represents displacements (y, z), rotations (ϕ, θ) shear forces (V_Y and V_Z) and bending moments (M_x) respectively. The articulation of elemental mass and stiffness of beams are shown below in Fig. 2.4. A beam element is connected to two nodes.

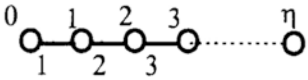

Fig. 2.4 Node and element representation

The numbers in the superscript represent nodes and the numbers in the sub-script represent elements. Starting with station 1 of the shaft, the state vector S connecting stations 1 and 0 through a field matrix is written as

$$\{S\}_1^L = [F]_1\{S\}_0 \tag{2.1}$$

In Eq. (2.1), the state vector S includes displacement (y), rotation (θ), moment (M) and force (V) at any node. Element 1 has nodes 0 and 1. So, state vector at the left of node 1 is connected to state vector at 0 through a "Field Matrix" that represents stiffness properties of beam.

Then, in Eq. (2.2), the state vector to the right of node 1 connects the lumped mass properties called, "Mass Matrix" to the state vector at the left of node 1. The equation connects right and left state vectors of node 1 through a mass matrix.

$$\{S\}_1^R = [P]_1\{S\}_1^L \tag{2.2}$$

When Eq. 2.1 is substituted in Eq. 2.2, the resultant left and right vectors of element 1 become

$$\{S\}_1^R = [P]_1[F]_1\{S\}_0 \tag{2.3}$$

Similarly, for n_{th} number elemental system, the Eq. (2.3) becomes

$$\{S\}_{n+1} = [F]_{n+1}[P]_n[F]_n[P]_{n-1}\cdots[F]_1\{S\}_0 \tag{2.4}$$

With the known boundary conditions at node 0, state vector $\{S\}_1^R$ properties can be solved and so on for the rest of elements.

Elements like the bearing, concentrated mass or rigid disks and the unbalance force can all be attached at the appropriate rotor nodal points as shown in Fig. 2.5.

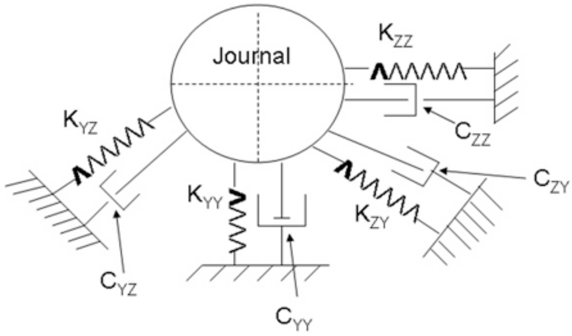

Fig. 2.5 Fluid-film bearing properties, rigid disk and mass unbalance force

2.4.2 Two Dimensional Finite Element Formulation

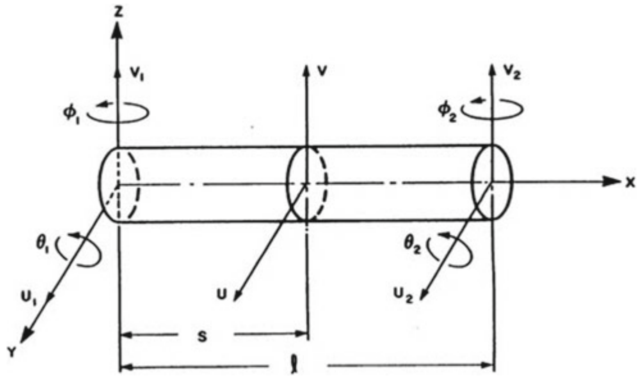

Fig. 2.6 Finite beam element discretization of a shaft

Rotor continuum is modeled using finite elements as shown in Fig. 2.6. Rotor is modelled as several finite elements. Each shaft element has two nodes. Each node has four degrees of freedom (dof), viz, *two translations y and z in Y and Z planes and two rotations about Z and Y axes such as* ϕ *and* θ *respectively*. Elemental mass properties are distributed across the element unlike the transfer matrix formulation where masses are lumped at the nodes. Stiffness properties are distributed among the elemental matrices. Elemental mass and stiffness matrices are assembled consistent with nodal degree-of-freedom (dof) parameters. An example of element stiffness matrix assembly is shown in Fig. 2.7. Significant amount of research has been done in this area. Therefore, readers who are interested in details are directed to references listed under the bibliography at the end of this chapter. One of the notable references is the paper by Nelson and McVaugh [3] that details methodical approach for FE modeling of the rotor-fluid-film and pedestal systems. Subbiah [4] and Ratan [5] simplified the rotor modeling process combining the benefits of TM and FE. Subbiah and Rieger [6] presented transient analysis of rotor systems.

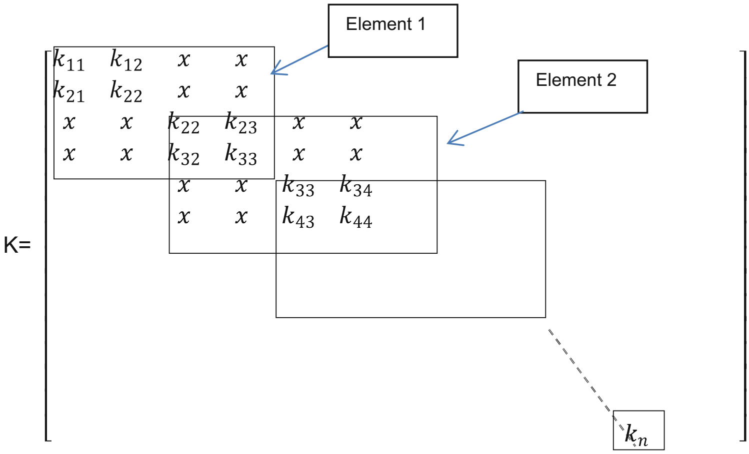

Fig. 2.7 Assembly of elemental stiffness matrices

2.4.3 Gyroscopic Effect in Rotor Systems

It is important to understand the influence of "**Gyroscopic Moment**" on rotor frequencies. Gyroscopic moment is generated when a spinning disc on a flexible shaft precesses in the orthogonal planes as illustrated in Fig. 2.8.

Impact of gyroscopic moment on a rotor system are:

- The axially spinning disc in a rotor also precesses in the two orthogonal (lateral-vertical and horizontal) planes perpendicular to the spin axis, thus causing gyroscopic couples or moments in the two planes. The resulting gyroscopic moment of the disc could stiffen the shaft and could increase shaft natural frequency.
  - For a rotor with central disc similar to a Jeffcott rotor, the gyroscopic moment of the disc has no impact on the first rotor frequency since the disc is located at an anti-node point (U-shaped mode).
  - The gyroscopic couple tends to stiffen the rotor shaft and increases the rotor 2nd natural frequency (S-shaped mode) associated with the conical mode, since the disc or discs are located at the node point.
  - The 2nd rotor frequency could be underestimated by not modeling the gyroscopic effect (specifically for a rotor with a central disc) in a rotor dynamic model.
- **It should be noted that turbine rotors have very little impact due to gyroscopic couples since they do not typically have a massive central disc in the mid-plane or angular displacement is not large without massive disc at the center**.

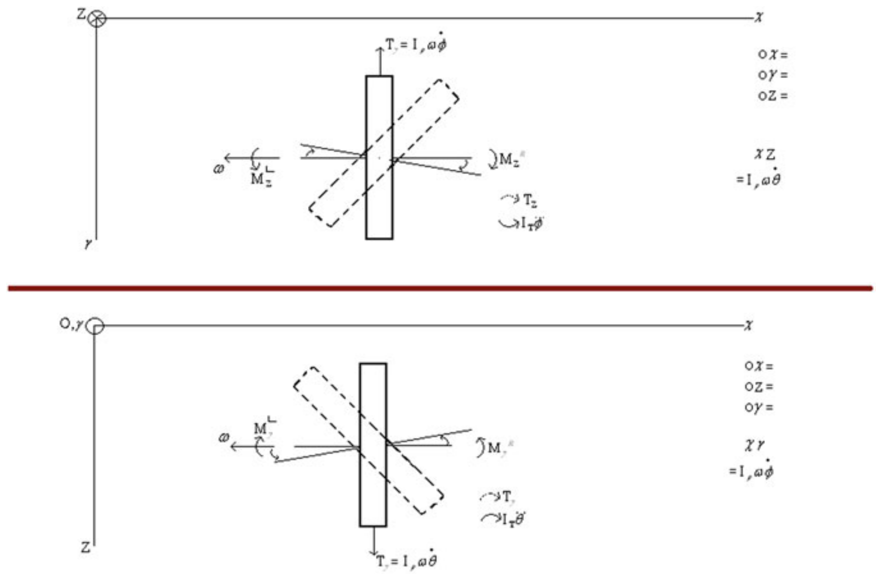

Fig. 2.8 Gyroscopic moments of rotor disc in two orthogonal planes

- When an axially spinning disc is located at the end of an overhang rotor, resulting gyroscopic effect increases the rotor stiffness and hence the rotor frequency. In this case, gyroscopic modeling of disc is essential.
- The classical work by Den Hartog [7] provides in-depth insight into this topic.
- Gyroscopic moments generate velocities in the spin and translational planes as well. The inertias I_p (polar moment of inertia) and I_T (transitional moment of inertia) with their respective angular responses ϕ and θ generate gyroscopic moments in the rotor system. The resulting gyroscopic effects in XY and XZ planes as presented by Rao [2] are shown in Fig. 2.8. They should be included in the equations of motion in the rotordynamic model to understand the influence of gyroscopic effects.

2.4.4 Asymmetric Stiffness Effects in Rotor Systems

The stiffness diameter evaluation of a non-circular or a non-symmetrical rotor body sections such as a generator rotor is challenging. Generator rotor body cross-sections (Example of two pole generator is shown) are asymmetric due to slots machined in selective segments around the circumference of the rotor body to accommodate copper conductors.

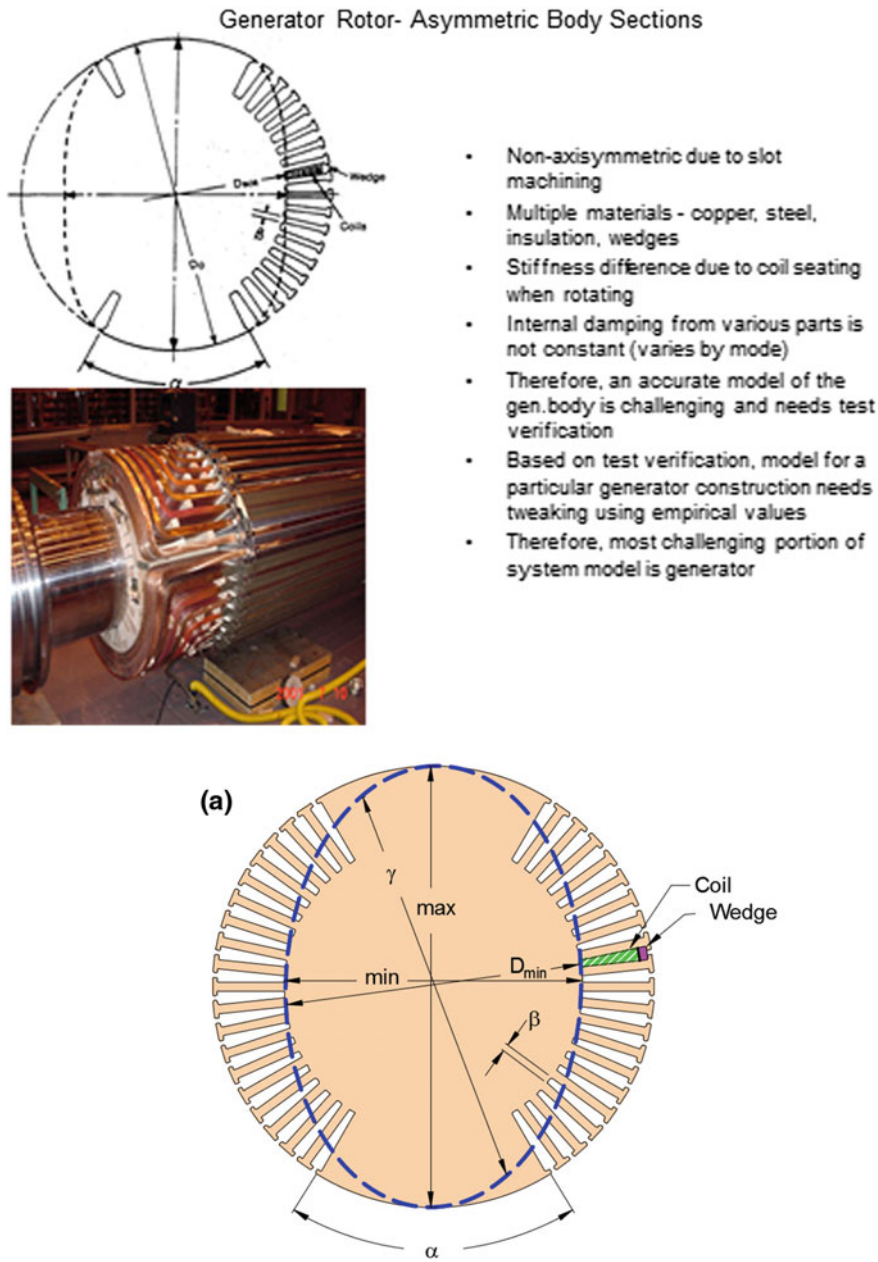

Fig. 2.9 Generator body stiffness configuration (courtesy of Siemens)

Consequently, the rotor body sections become non-circular as shown in Fig. 2.9 and the rotor body exhibits two dissimilar stiffnesses (in the orthogonal axes as shown in Fig. 2.9a) in one rotation of the rotor. As a result, the vibration spectrum could exhibit slightly higher amplitudes of 2× components, the degree of which, depends on how well the slots are compensated by driving wedges to make the rotor cross-sections closer to a circular shape. In most cases, a small magnitude of 2× vibration component can still be observed in the generator rotor spectrum plots. Therefore, accurate modeling of dissimilar rotor body of a generator requires test verification and model validation.

2.5 Advanced Rotor Modeling Methods

In Chap. 1, simple lateral modeling approach was introduced using Jeffcott rotor for a better understanding of the basics of rotor dynamics. In this chapter, we will discuss advanced techniques such as 3-D FEM (3-dimensional finite element model) applied in developing rotor models for lateral analyses. Let us use steam turbine as an example as we did before.

2.5.1 Lateral Rotor Model

Until the recent past, it has been the practice to build 2-D axi-symmetric FE rotor beam element models for the following reasons:

(a) Rotor is a symmetrical structure on two orthogonal planes.
(b) Blade masses can be lumped.
(c) Economical and quicker way of solving rotor dynamic problems.

The rotor continuum is discretized into numerous finite elements and nodes. The rotor model is constrained in the axial direction and bending moments and shear forces are applied at the two ends. The model is solved for elemental strain energies (SE). Strain energy results are used to compute stiffness diameters using the formula shown below.

$$D_e = \sqrt[4]{\frac{32M^2L}{\pi EU}}$$

where M- Bending moment, L- Section Length, E- Young's Modulus and U-strain energy

Using the stiffness and the mass diameters and the length of the section, lateral dynamic model input can be generated using any general-purpose rotor dynamic software. This model is being applied in rotor dynamic analyses by properly including fluid-film dynamic and pedestal characteristics.

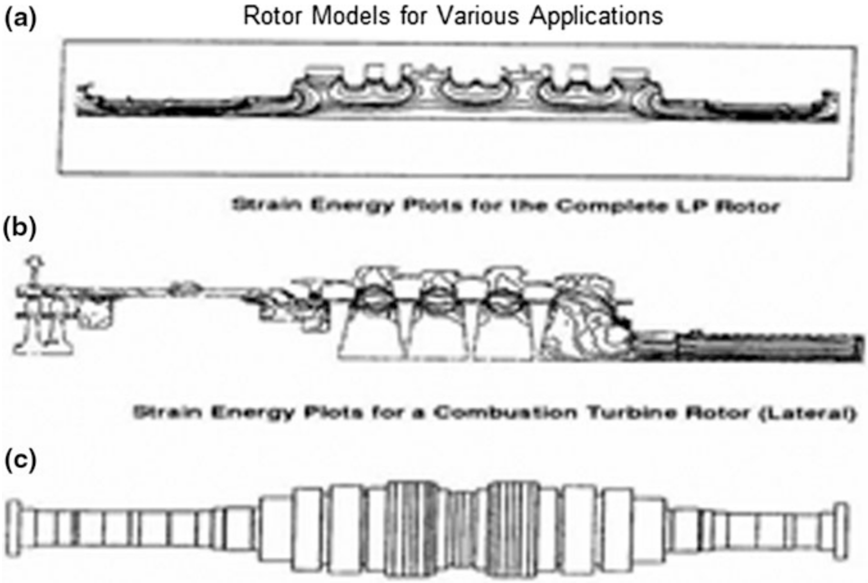

Fig. 2.10 **a** Strain energy plots of an LP Rotor. **b** Strain energy plots of a gas turbine rotor. **c** Lateral rotor model of the LP rotor shown in Fig. 2.10a, b and c

Figures 2.10a, b show the strain energy plots for an LP rotor and a gas turbine rotor respectively as illustrated in Figs. 1.1 and 1.2 in Chap. 1.

Effective lateral stiffness diameters of the rotor can be computed for the discretized sections of a planar (or 2-D) axi-symmetric FE model as illustrated in Fig. 2.11 for an opposed flow LP rotor.

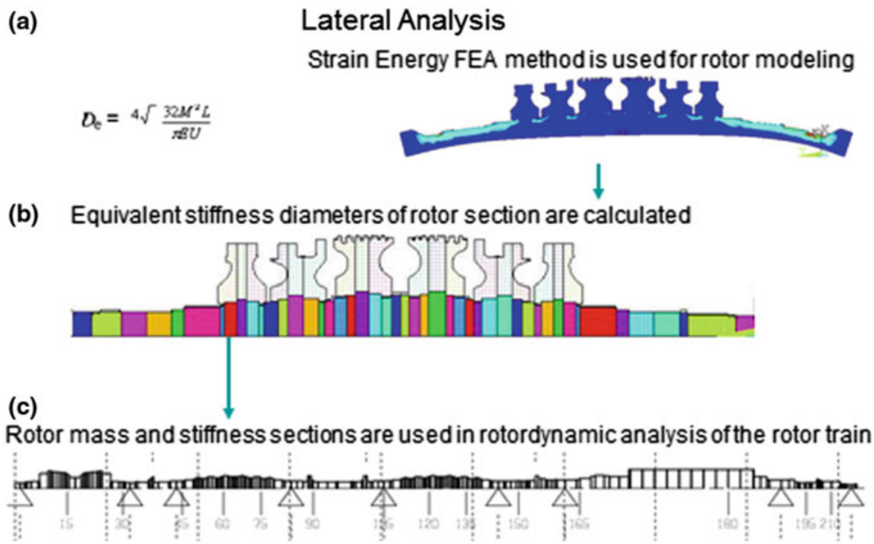

Fig. 2.11 Lateral modeling of rotor using strain energy method (courtesy of Siemens)

Commercially available software can be used to create a FE model of the rotor. Boundary conditions for the FE rotor model are to release the Y and Z degrees of freedom (and the associated rotational degrees of freedom) and constrain the axial degree of freedom in the X-axis.

- Simulate bending moments at the two ends of the rotor as shown in Fig. 2.11a.
- Resulting elemental strain energy plots (in planar view) are shown in Fig. 2.11b using 2-D FE analysis. They provide strain energy distribution which can be used to calculate stiffness diameters using $D_e = \sqrt[4]{\frac{32M^2L}{\pi EU}}$
- The data from the previous step can be used to generate rotor models utilizing any commercially available or in-house rotor dynamic software. Two-dimensional lateral rotor models for an entire train that consists of a HP rotor, two LP rotors, a generator and an exciter are shown in Fig. 2.11c. including bearing supports by upward arrows.

Until the recent past, computer storage had limitations to build and solve 3-D rotor models. With the advent of advanced technologies in computer architecture, optimal storage capability and the increased computer power enabled solving 3-D problems significantly quicker than before. 3-D Finite Element lateral model of a rotor train is shown in Fig. 2.12. The casing is only shown on one turbine for simplicity.

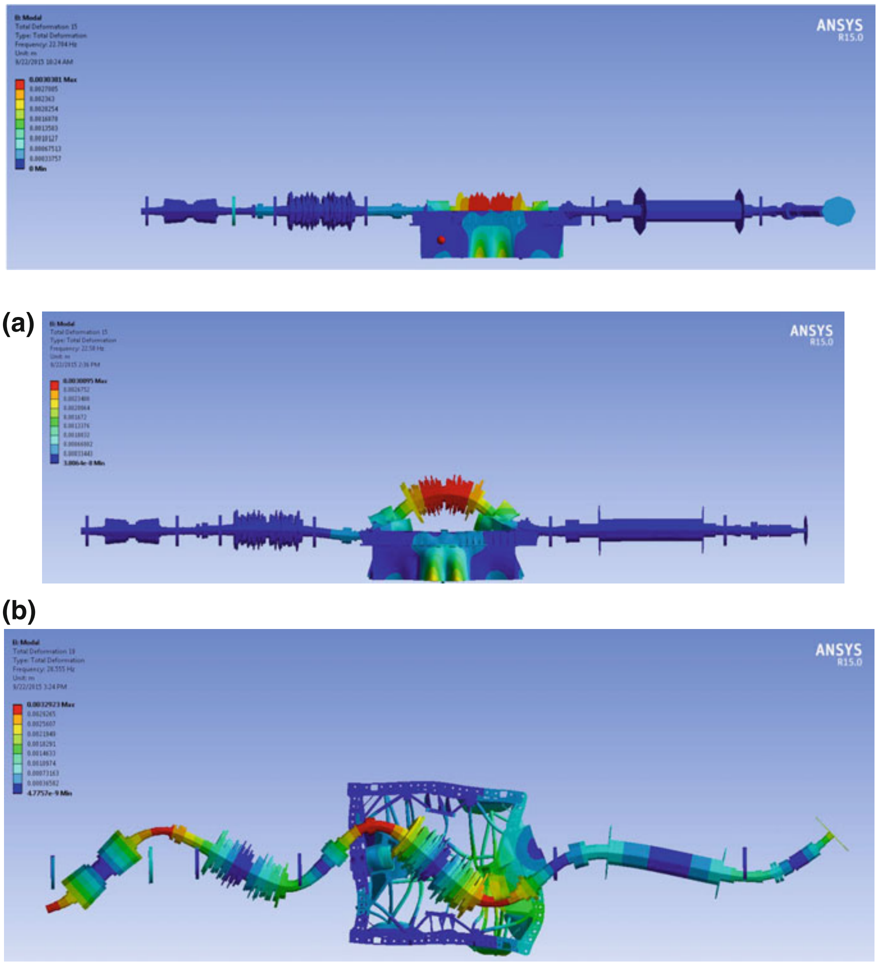

Fig. 2.12 3-D Lateral model of a rotor train. **a** Lateral U- Mode shape of LP2 rotor in the train. **b** Lateral S- Mode shape of LP rotors in the Train (courtesy of Siemens)

3-D rotor model can be built using any commercially available software products. The example shown in Fig. 2.12 is built with 3-D brick elements. Auto meshing of rotor shapes significantly reduces the model building effort. Features enable automatic model checking of node connectivity and makes the modeling effort foolproof. Importing CAD models of rotor geometries into FE software accelerates model-building efforts smoother and easier.

Two-rotor modes viz., the U-mode (shown in Fig. 2.12a) that represents first bending mode of the rotor and the S-mode that represents 2nd bending (shown in Fig. 2.12b) or conical mode.

The following analyses are required to evaluate to determine the acceptability of design for operation. They are:

2.5.2 *Mode-Frequency Analysis or Modal Analysis on Rigid Supports*

Mode-frequency analysis is performed without fluid-film properties and bearing support pedestals. The rotor model used is known as "rigid support" condition. The calculated rotor frequencies in this case are always higher than those calculated including oil film and pedestal properties. The oil film and pedestal supports soften

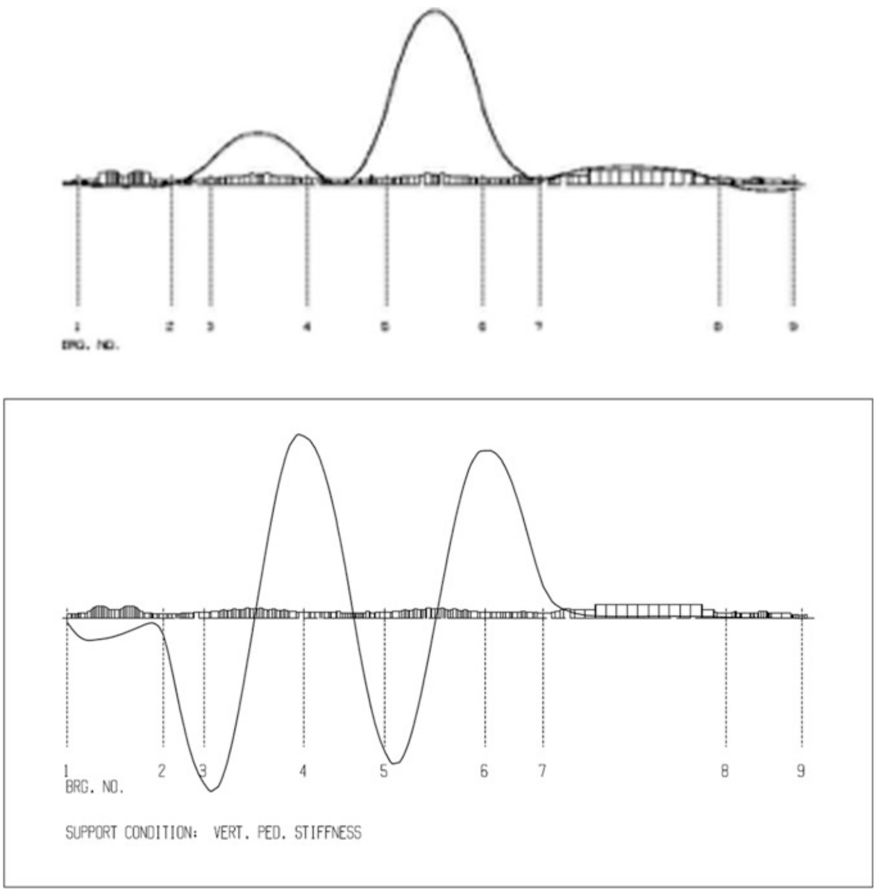

Fig. 2.13 LP Rotor 1st and 2nd modes of a rotor train (courtesy of Siemens)

the overall system stiffness by reducing rotor frequencies lower than those by rigid supports. This rigid rotor analysis provides preliminary information of the rotor frequencies prior to an in-depth rotor dynamic analysis. Figure 2.13 provides the first (U-mode) and second (S-mode) bending modes of an LP rotor discussed before. This analysis is also known as “Eigen Frequency” analysis.

2.5.3 Unbalance Response Calculations

Rotor unbalance response calculations are performed including the speed-dependent fluid-film effects, the pedestal stiffness and the mass unbalance forces at the rotor balance planes. Resulting responses and phase angles for a rotor system are plotted as shown in Fig. 2.14. Both vertical (solid line) and horizontal (dotted line) rotor motions are plotted (at the bottom) along with phase angles (at the top).

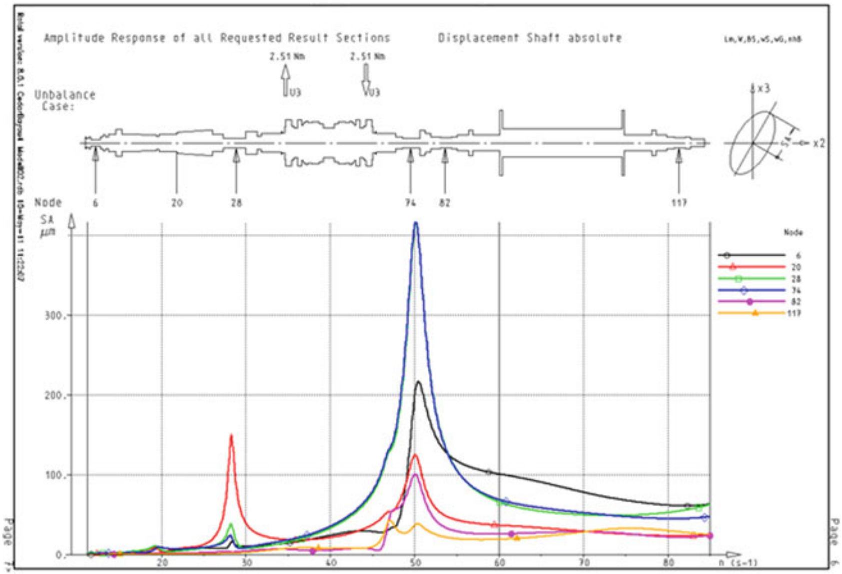

Fig. 2.14 Unbalance response with phase (courtesy of Siemens)

In general, unbalance response analysis provides more accurate rotor critical speeds since speed-dependent fluid-film model is included. However, the vibration amplitudes calculated by simulated unbalance forces in the rotor model may not reflect the real mass unbalance magnitudes and the relative phase angle positions at the various balance planes of the rotor system; hence the unbalance response amplitudes may not be representative of the in-service rotor configuration. In addition, it should be noted that when the rotor responses reach resonance speeds, they become non-linear and it is not possible to predict non-linear responses accurately with the linear fluid-film models applied.

In general, the industry guideline is not to have lateral frequencies (or critical speeds) within ±10% of the operating speed. If frequencies are calculated within the frequency exclusion range, it is customary to calculate Q-factor (see Fig. 2.15) and assess the design acceptability condition. Lower Q-factors indicate better-damped modes. Higher than the acceptable Q-factors indicate the unit needs additional balancing in the factory and on-site as well.

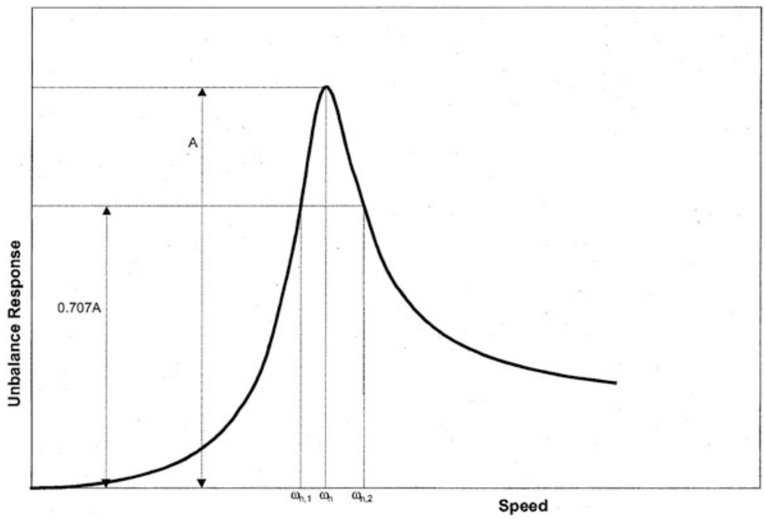

Fig. 2.15 Q-Factor measurement

2.5.4 Q-Factor Evaluation

Amplification factor is an indirect measure of the damping present at a peak response of the rotor.

Amplification factor is calculated using "Half Power Point Bandwidth" method where the side band frequencies are evaluated at 0.707 of the peak response amplitudes. The theory is based on electrical signal measurements in RMS (Root Mean Square). Peak amplitude value is obtained by multiplying the RMS amplitude by 1.414. Q-factor is the ratio between the peak response frequency and the delta of side band frequencies (on either side of the peak frequency).

For the nth mode, the dimensionless Q-factor can be calculated from the following equation: (see Fig. 2.15)

$$Q_n = \frac{\omega_n}{\omega_{n,2} - \omega_{n,1}}$$

where

ωn = nth critical speed measured at the peak response
$\omega_{n,\ 1}, \omega_{n,\ 2}$ = Rotor speeds at the half-power point level (responses at 0.707 A) about the nth critical speed

2.5.4.1 An Important Note About Q-Factor Evaluations

Q- factor is an index of damping and measures the sharpness of response at the peak amplitude corresponding to a rotor critical speed. The calculations are based on linear rotor dynamic models. As was discussed before, the following conditions could cause non-linear behavior.

(a) When rotor amplitudes are large enough to exceed the bearing clearances, the linear hydrodynamic film coefficients used in response calculations are no longer valid.
(b) The mass unbalance estimates applied in the model may not reflect the true unbalances in the rotor and the associated phase angle positions for the following reasons: (a) Variable eccentricities produced by rotor machining, blade assembly and blade mass variations within a row of blades. (b) Inaccurate fluid-film forces applied in the model.

The above factors could lead to errors in the estimated Q-factors and hence, they may not reflect the reality. Under those circumstances, the best approach would be to review the operating data of a similar or a representative rotor system to evaluate and justify the design.

2.5.5 Rotor Stability Calculations

Detailed rotor dynamic stability discussions due to oil film bearings are deferred to Chap. 4. Stability analysis essentially provides the damping present in the system due to “oil whirl/oil whip and steam induced whirl”. Complex modal analysis is used to compute the sub-synchronous critical speeds and the damping present at the associated modes.

The complex modal analysis calculates Eigen values of the rotor as shown below:

$$\pm\alpha \pm j\omega$$

where

The real part "α" provides the damping characteristics of the rotor mode. A positive α indicates responses grow monotonically and the rotor is unstable. A negative α indicates responses diminish and the rotor is stable. "ω" is the associated rotor frequency. It should be noted that the two conjugate frequency modes are computed, i.e., one with a positive sign $+j\omega$ and the other with a negative sign $-j\omega$; for the same frequency ω.

Figure 2.16 shows the whirl plot obtained for one of the sub-synchronous mode of the rotor system.

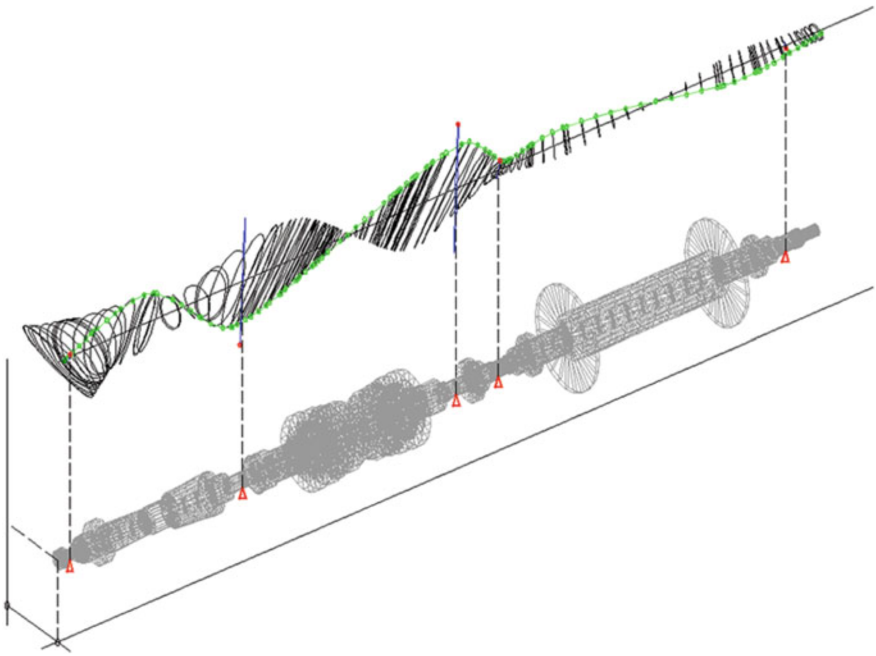

Fig. 2.16 Rotor Whirl Plots for an LP mode (courtesy of Siemens)

When the rotor system is calculated to be unstable due to oil whip, the solution is to use a more stable bearing type to meet rotor stability. Stable bearings such as tilting pads eliminate oil whip.

Like oil whip, steam whirl also causes unstable rotor. Excessive steam pressure across the rotating seal segments at the steam inlet could lead to steam induced vibration or steam whirl. More detailed discussions are deferred to Chap. 4.

2.6 Various Rotor Constructions

A rotor develops mechanical energy by the expansion of fluid medium in the turbine. Series of rotating blade rows, that produce mechanical work, are designed either impulse or reaction type. Modern machines use impulse blade designs for HP turbine and reaction types for IP and LP turbines.

Most HP and IP rotors are of mono-bloc construction or made from a single forging. However, LP rotor types can be:

(a) Mono-Bloc
(b) Shrunk-on disc
(c) Welded

2.6.1 *Mono-Bloc Rotor*

Mono-bloc rotor is shown as illustrated in Fig. 2.17. They are made of one-piece forging with or without bore. Ultra-sound inspection is used to detect and correct core impurities, gas shrinkage and non-metallic inclusions that could otherwise reduce fatigue life of a rotor. One-piece forgings need longer time to manufacture.

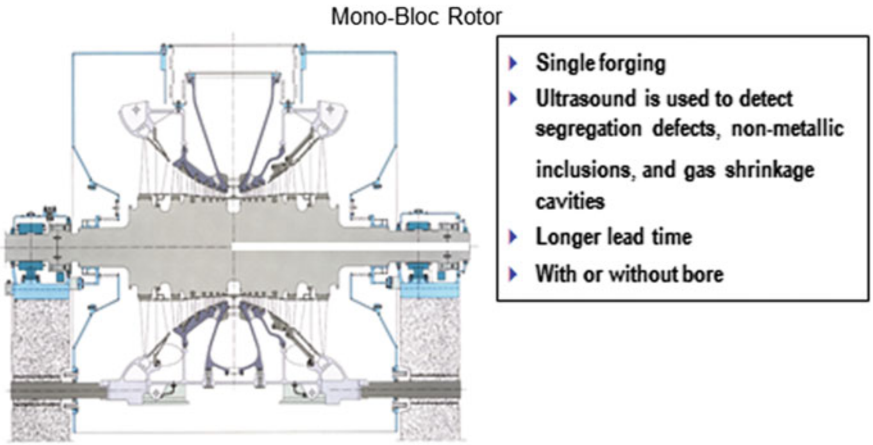

Fig. 2.17 Mono-Bloc rotor

2.6.2 Shrunk-on Disc Rotor

Shrunk-on rotor is illustrated in Fig. 2.18. Individual discs are shrunk-on to a shaft. Discs are finish-machined before they are shrunk onto the rotor. Individual disc forgings take less time to manufacture than a mono-bloc rotor forging. In addition, manufacturing time reduces significantly, if multiple vendors supply discs.

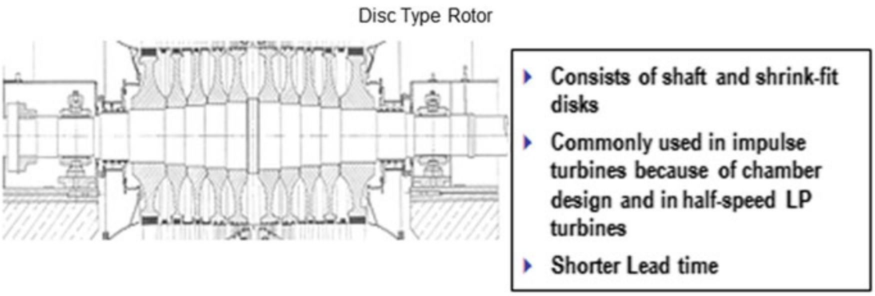

Fig. 2.18 Shrunk-on Disc rotor

2.6.3 Welded Rotor

Welded rotor construction (drum type rotor) is shown in Fig. 2.19. Separate discs are axially aligned and are welded together. The advantage of this type of rotor construction is that the end stage blades can be designed not to couple with the associated disc or shaft frequencies unlike the other two rotor constructions. Consequently, this type of construction offers more flexibility to design the blade alone frequencies not to interfere with the shaft system frequencies and their harmonics. However, the major effort is welding of the discs. When welding process is automated, welded disc-rotor can be produced with shorter lead-time since procuring individual discs are less time-consuming.

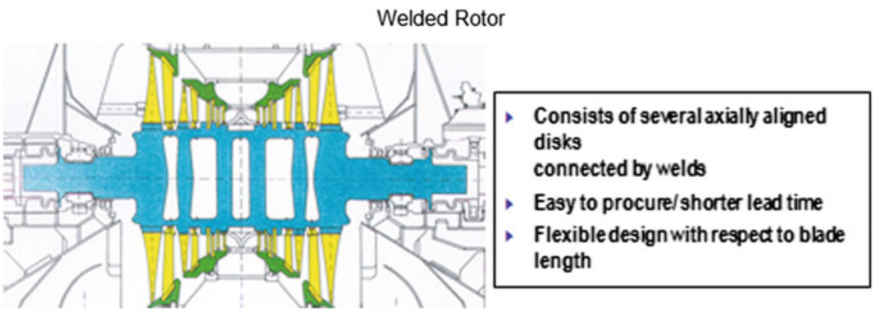

Fig. 2.19 Welded Rotor (courtesy of Siemens)

2.7 Rotor Mechanics

In addition to rotor dynamics calculations, rotor mechanics calculations are also important. Rotor mechanics calculations, among other requirements, mainly focus on the strength and fatigue life requirements of the rotor. These calculations are briefly listed below:

- Stress Analyses are done by including the maximum operating steam/gas pressures, temperatures, centrifugal forces of blades and thrust loading of the working fluid.
- Shaft alignment is required for better control of bearing loading and reduction of high cycle fatigue (HCF) at small fillets and grooves where bending stresses typically concentrate.
- Fracture Mechanics calculations are performed to assess the acceptability of rotor with the contaminants and impurities in rotor forging process including rotor surface damages/defects etc.
- Stress corrosion resistance is important for rotors operating in wet steam environment
- Duty-cycle analyses are done for transient load cycles that lead to low cycle fatigue (LCF) assessment. They account for meeting rotor design life for various operating cycles such as cold, warm, hot starts, load changing cycles and others.

2-D FE rotor models are sufficient to perform accurate rotor stresses due to the axi-symmetric contour of the rotor. Boundary conditions and the various operating loads under stead-state operating conditions are shown in Figs. 2.20 and 2.21.

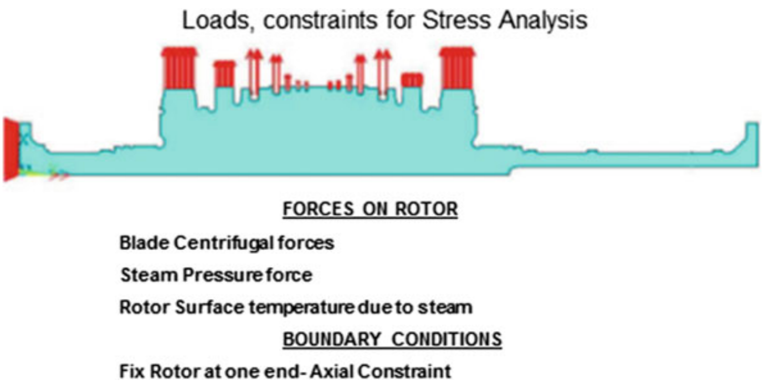

Fig. 2.20 Rotor modeling with forces and constraints (courtesy of Siemens)

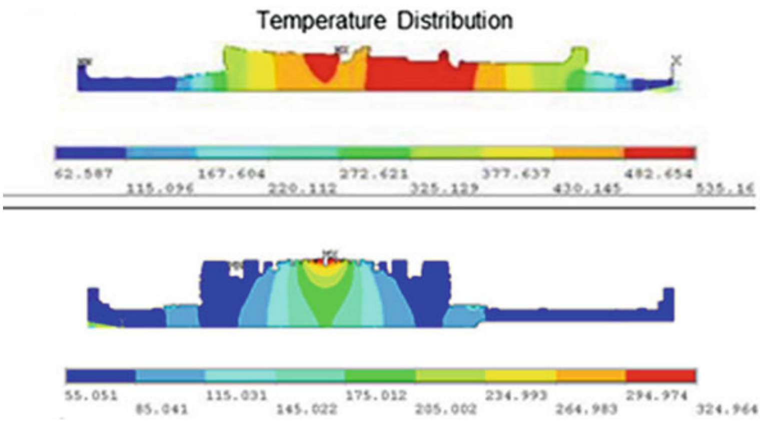

Fig. 2.21 Rotor temperature distribution (Top) and stress distribution (Bottom) due to combined mechanical and thermal loads (courtesy of Siemens)

Computed stresses are compared to design limits for acceptance. If calculated stresses exceed design limits, re-design of the rotor discs may be required. Acceptable steady-state stresses confirm that the rotor can be operated for the specified design life. However, rotor stresses due to transient operating conditions may exceed rotor material elastic limits and consume the design life as a result. Therefore, transient analyses including operating load cycles are required to assess their impact on the rotor design life. Damage fraction of each operating event can be assessed and cumulatively added to estimate the remaining rotor life.

2.8 Torsional (Twist) Rotor Dynamics

As discussed before, the other potential failure mode of a rotor is “torsion”. It is important to analyze torsional frequencies of a rotor system to evaluate their impact with the operating frequencies and the resulting torsional vibrational behavior in the operating cycle. In general, torsional modeling of rotors has been discussed in numerous books and technical publications [9–15]. Interested readers are directed to read those references for basic understanding of the mathematics involved. The objective here is not to overwhem the readers with the mathematics of torsion; instead, to touch upon salient aspects of torsion that could influence the turbo-machines in an adverse manner, recognize them and mitigate them for continuous and reliable operation.

2.8.1 Lumped Mass Model

In earlier times (in the 1960s), major rotor component masses were lumped and connected by springs that represent shaft stiffness. A representative lumped mass model of a steam turbine-generator train is shown in Fig. 2.22.

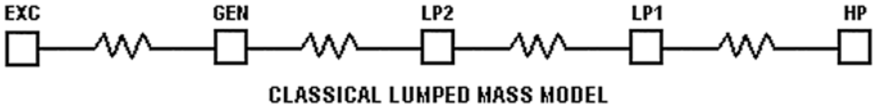

Fig. 2.22 Lumped mass model of a rotor system. *Notes* HP- High Pressure; LP1, LP2- Low Pressure; Gen- Generator and Exc- Exciter

This simple model can be used to analyze torsional rotor system frequencies. They provide fundamental shaft frequencies accurately and comparable to those obtained by advanced continuum models. However, long and flexible blade systems are crucial in torsional rotor system analysis and cannot be modeled by simple lumped mass modeling approach. Consequently, an advanced continuum model of the turbine-generator (T-G) system is required that includes large LP blades as shown in Fig. 2.23.

Fig. 2.23 Continuum model of a Turbine-Generator shaft system (courtesy of Siemens)

A turbine-generator shaft system comprises of several rotor components that interact dynamically. Alteration of inertia or stiffness of any rotor component in the system will affect the torsional natural frequencies and mode shapes and must be accounted for in the design phase.

Shaft elements that are typically sensitive for torsional vibration are low pressure (LP), generator and exciter rotors for a steam turbine train. It is important to know that the last few rows of LP blades (which are longer and flexible) could interact with the turbine-generator shaft system and bring the system torsional frequencies closer to operating speed. Under those circumstances, one or more natural frequencies of the shaft system could become resonant with the electrical frequencies of the potential grid faults, causing eventual component damages.

It is important to note that such blade and rotor disc frequency coupling is typical for torsion. Such frequency coupling does not affect the lateral vibration behavior of a rotor system.

2.8.2 Blade and Rotor Disc Frequency Coupling

Let us begin discussing the blade-disc interactions and how they influence torsional frequencies in general. An example of bladed-disc system is shown in Fig. 2.24.

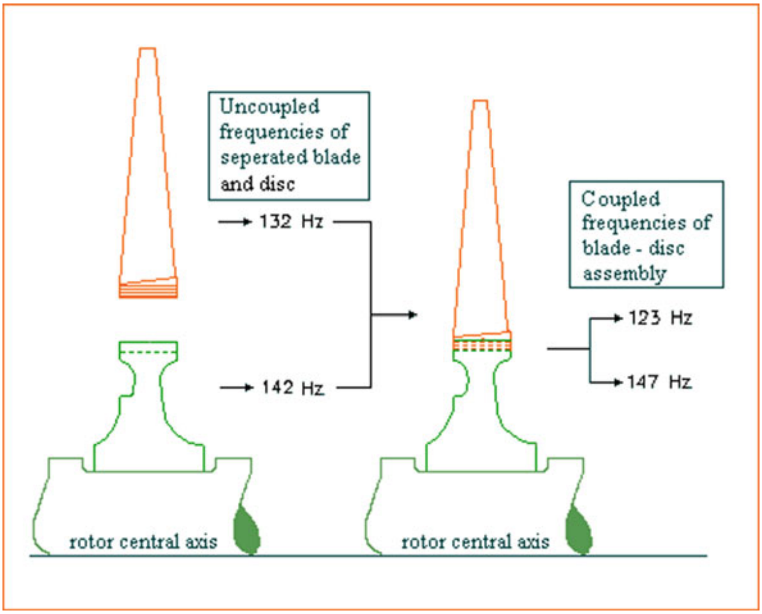

Fig. 2.24 Blade and rotor disc frequency coupling for Torsion (courtesy of Siemens)

For the example shown in Fig. 2.24, the assembled bladed-disc frequencies split into 123 and 147 Hz. Before assembly, the individual disc and blade frequencies were at 142 and 132 Hz respectively. The blade alone frequency before-assembly at 132 dropped to 123 Hz and the disc alone frequency at 142 moved up to 147 Hz after-assembly. It should be noted that the lower blade frequency at 123 Hz is closer to twice line frequency for 60 Hz machines and can be excitable by grid faults. This will be discussed in detail in the forthcoming sections. Figure 2.25 shows how blade frequencies could vary with rotor speed.

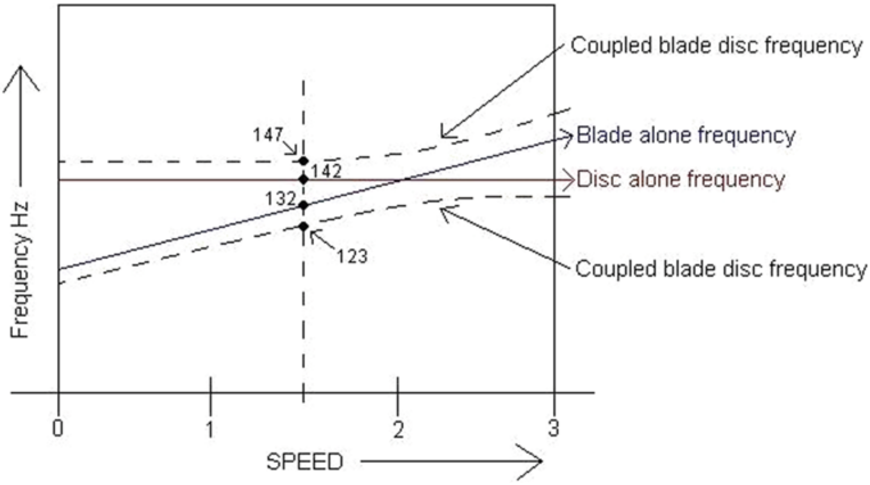

Fig. 2.25 Coupled blade and disc frequencies

2.8.3 Three-D Finite Element Model of a Bladed-Disc

An example of a last row blade and the associated rotor disc is modeled in a 3-D FE as shown in Fig. 2.26. A row of blades is fixed to the disc rim. For a shrunk-on

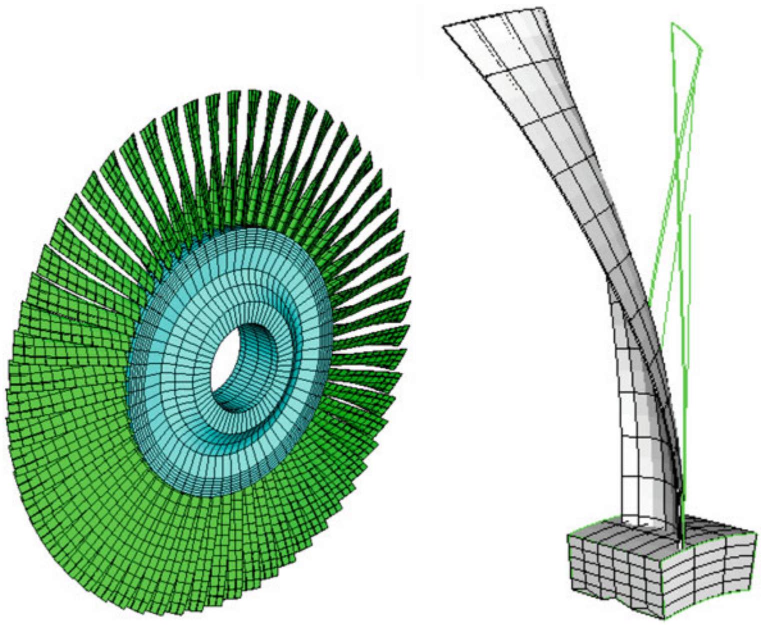

Fig. 2.26 Zero-nodal diameter modes of bladed-disc/umbrella modes (courtesy of Siemens)

rotor disc configuration, nodes in the lower end of the disc are coupled to the underlying shaft. In operation, this row of blades moves in unison like an "umbrella" in the fundamental mode of vibration; hence the name umbrella or zero nodal diameter mode. Blades are modeled with 3-D brick elements using general-purpose software. All degrees of freedom of the entire blade row are fixed, except the torsional or tangential degrees of freedom in the model.

Blades can have zero, first, second and higher order nodal diameter modes as shown in Table 2.1. Blade-umbrella mode (see Fig. 2.27) or zero nodal diameter mode is the fundamental mode in which the node at the center of the blade-row moves in and out like opening and closing of an umbrella. Essentially, the blade

Table 2.1 Example zero nodal diameter frequencies with varying rotor speeds

Order	Example of zero nodal diameter frequencies of a bladed disc	
	600 rpm	**1800 rpm**
1	70	80
2	140	150
3	200	220
4	270	280

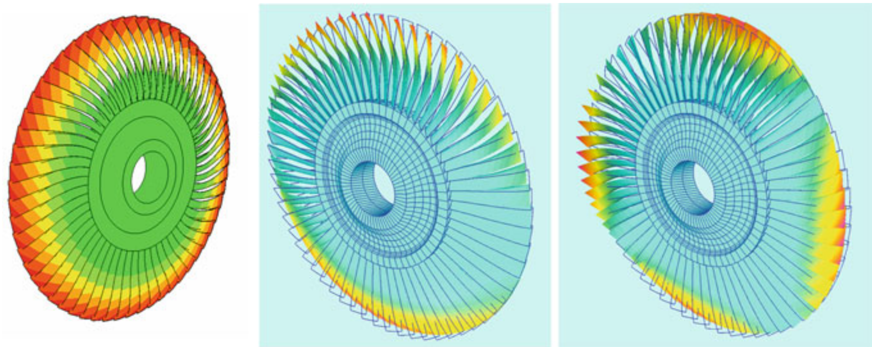

Fig. 2.27 Blade umbrella modes (courtesy of Siemens)

row and the disc moves unison in the zero-nodal diameter mode. Since the mode is mainly static, it can be compared to a rigid body mode of a rotor. In both cases, rigid-body modes exhibit very little dynamical motions.

Nodal diameter modes move about the diameter. Assume the blade row as a circular vibrating membrane. This circular membrane creates various combinations of diametric and concentric node points. Nodes or nodal points remain at rest while the other parts of the membrane are in a state of motion.

So, one-nodal diameter mode splits equally about the diameter and the two segments move opposite to each other. Similarly, two-nodal diameter modes split about two diametric planes with four nodal segments that move opposite to each other as shown in Fig. 2.27.

Example nodal diameter frequencies are listed in Table 2.1 and can be noticed that they vary with different operating frequencies. These frequency variations are applied in generating a Campbell diagram to show how they interact with the various operating speeds of the rotor and how they position themselves with respect to various blade harmonic frequencies. Campbell diagram consolidates all the nodal diameter data versus rotor frequencies and is used by a blade designer to tune blade frequencies as needed.

2.8.4 Effects of Blade-Disc Coupling on Lateral Dynamics

- Blade-disc dynamical coupling affects torsional behavior only
- They have no effect on bending or lateral vibration parameters unless there is a strong coupling between torsion and bending at any frequency.
- When one of the coupled frequencies approaches near line (50 or 60 Hz) and Twice-line (100 or 120 Hz) grid frequencies, modes become resonant and get energized. Under these circumstances, high distress in blades can lead to fatigue failure during continuous operation. One blade row of the rotor disc is shown modeled by FE in Fig. 2.28.

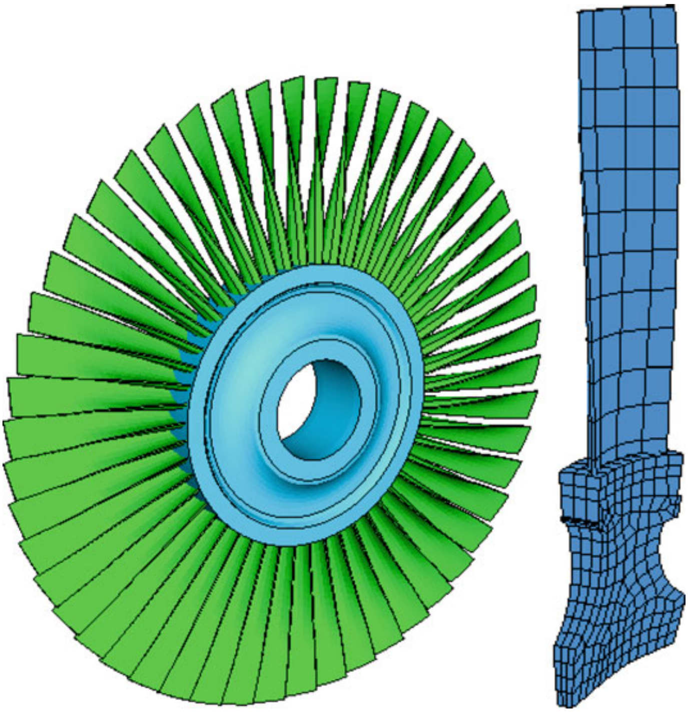

Fig. 2.28 A segment of bladed-disc FE model (courtesy of Siemens)

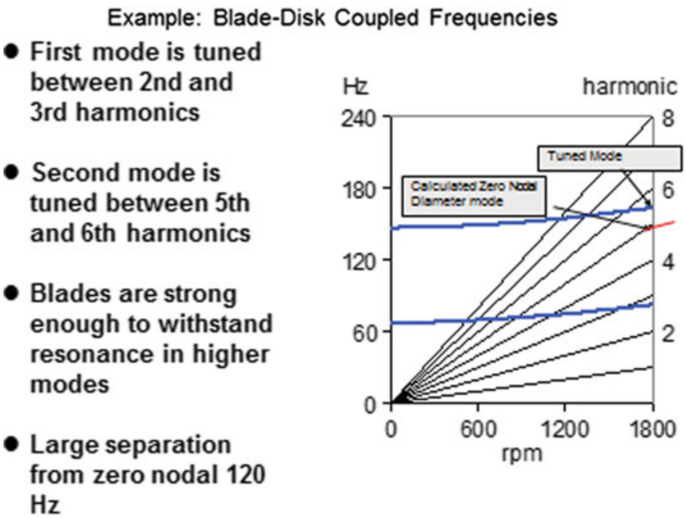

Fig. 2.29 An example Campbell diagram for a bladed-disc system

Figure 2.29 shows an example of a Campbell diagram that is being developed and used to map out blade frequency interactions with rotor speeds. A row of blades excites multiple blade harmonics depending on the number of blades in a row. It is important to design blade systems to keep the frequencies of concern away from the harmonics of excitation; typically, away from the lower harmonics, which are the most energetic. The blades can be tuned between harmonics at any operating frequency by modifying the blade airfoil profile and/or steeple and platform areas.

2.8.5 Rotor Torsional Model

In rotor shaft modeling, it is important to evaluate shaft stiffness and inertia accurately. The shaft inertia is straightforward to compute using the physical shaft dimensions of the section, whereas the shaft stiffness is not straightforward to evaluate when a shaft section abruptly transitions into a large diameter disc resulting in a drastic step change in diameters. This applies equally to lateral stiffness modeling as well.

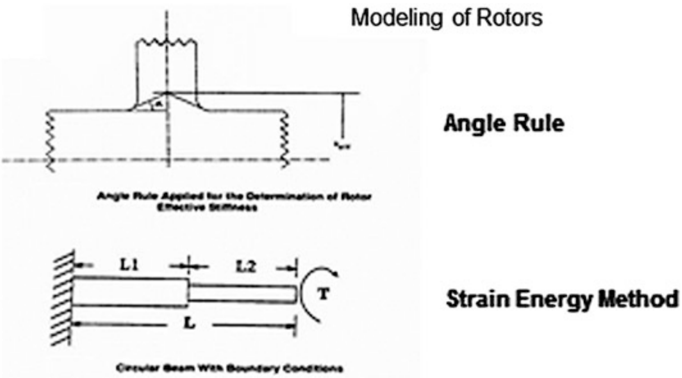

Fig. 2.30 Angle rules to define stiffness diameters

For a uniform diameter shaft, inertia and stiffness can be evaluated using the same physical diameter. However, in steam, gas and generator configurations, it can be noticed that the rotor body diameters are not uniform. Empirical angle rules (based on limited experience) were used in earlier times for the determination of rotor stiffness diameters. One example of using angle rule for a rotor configuration is shown in Fig. 2.30. The drawback of this angle rule is that one rule does not fit different rotor configurations. Therefore, a consistent method of evaluating the rotor stiffness diameters for variable geometrical configurations became necessary. One

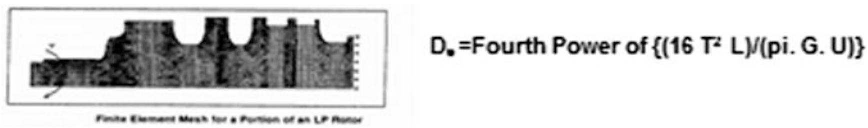

Fig. 2.31 Strain Energy Method to calculate stiffness diameters (courtesy of Siemens)

such method is using strain energy principle to evaluate stiffness diameters. They proved to provide rotor stiffness diameters accurately and consistently regardless of rotor-disc geometries. An example of a rotor disc modeled by FE is shown in Fig. 2.31. A fixed torque was applied at one end and the resulting strain energy plots were obtained. The rotor stiffness diameters were obtained at different rotor segments using the 4th power diameter relationship using strain energy illustrated in Fig. 2.31.

For torsion, release axial degrees of freedom (X-axis) and constrain Y and Z degrees of freedom. Apply torque at one end of the rotor by holding or fixing the other end. Sum up elemental strain energy for a chosen rotor segment and the stiffness diameters for that segment can be evaluated using the 4th power equation. Detail sequence of rotor modeling for torsion is shown in Fig. 2.32.

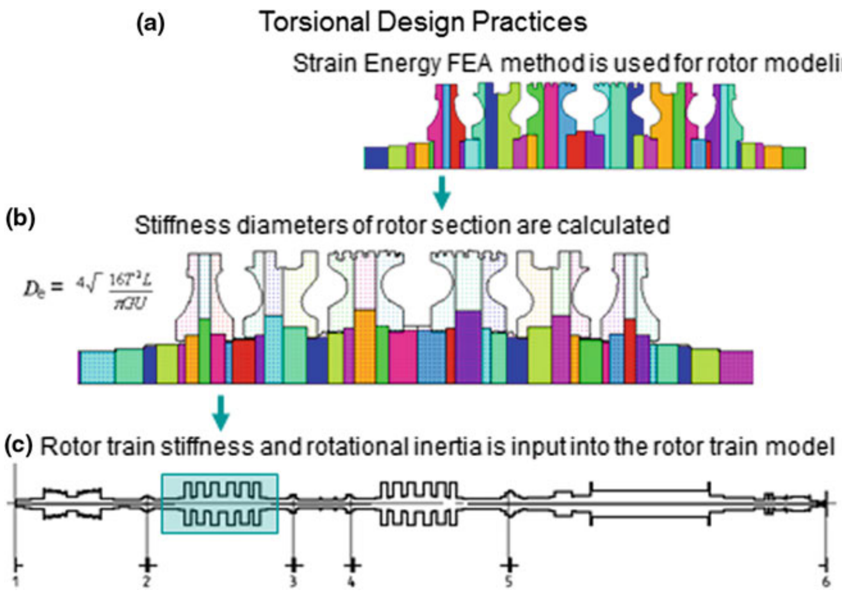

Fig. 2.32 Torsional stiffness diameters of an LP rotor (courtesy of Siemens)

Please note that the lateral and torsional effective stiffness diameters are different and cannot be used interchangeably.

The derivation of torsional stiffness diameter evaluation using elemental strain energies (U) is provided below.

$$\mathrm{U} = \frac{T\phi}{2} \text{ where } \phi = \frac{\mathrm{TL}}{\mathrm{GJ}}$$
$$\mathrm{U} = \frac{\mathrm{T}^2 L}{2GJ}$$

where

U = strain energy
T = applied torque
L = shaft or section length
G = shear modulus
J = polar moment of inertia

Torsional Stiffness Diameter

$$D_{\mathrm{e}} = \sqrt[4]{\frac{16\mathrm{T}^2 L}{\pi G U}}$$

Shaft inner diameter is assumed as zero in the above equation. The stiffness diameter derivation can be applied for circular rotor geometries only.

2.8.6 Three-D Torsional Modeling of Rotors

3-D FE mesh can be developed for the rotor torsional system. To reduce modeling complexity, the circular rotor sections are modeled as 2-D circular beam sections and the blades are modeled in 3-D since they are not axi-symmetric. The LP rotor and the LP blade models are merged. The HP and generator rotors are combined with the LP rotor to make the rotor train model shown in Fig. 2.33. Boundary condition applied is to free axial degrees of freedom and constrain lateral degrees of freedom in Y and Z-axes.

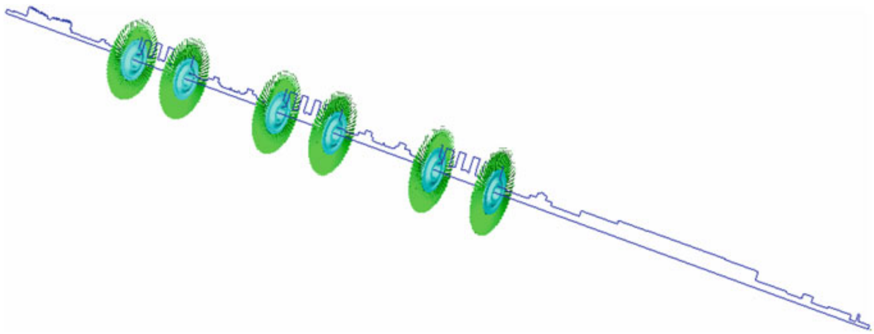

Fig. 2.33 3-D model with blade-disc coupling (courtesy of Siemens)

2.8.7 *Modal Analysis*

When rotor system modeling is complete (Fig. 2.33), torsional frequencies and mode shapes are calculated using modal analyses features in the FE modeling tool. Some of the torsional sub-synchronous frequencies (below line frequency, say 50 or 60 Hz) and the associated mode shapes are shown in Fig. 2.34. Super-synchronous (above line frequency) frequencies of the rotor system are shown in Fig. 2.35.

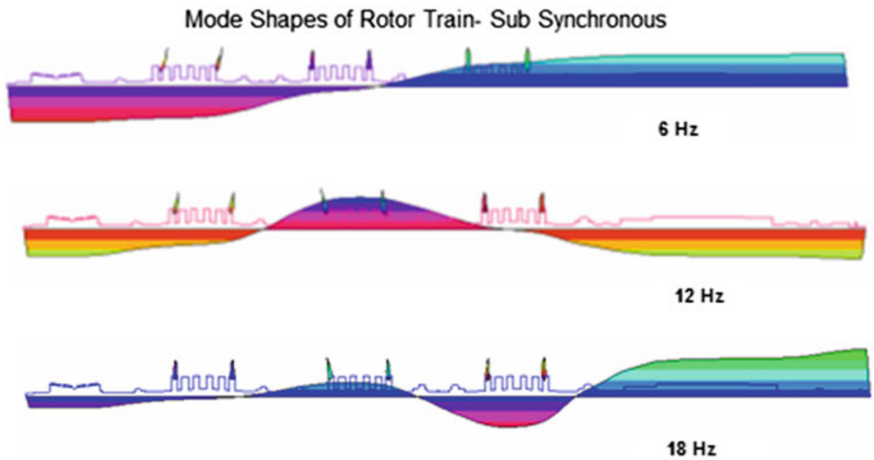

Fig. 2.34 Rotor train frequencies for sub-synchronous modes (courtesy of Siemens)

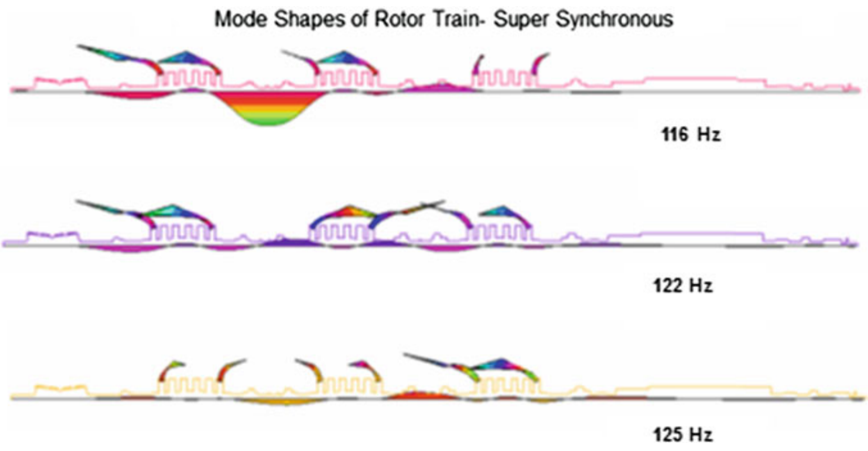

Fig. 2.35 Super-synchronous modes (courtesy of Siemens)

Whenever a system mode has no torsional activity, then the mode shape plot shows a flat horizontal line as shown in Fig. 2.36 below. In such cases, external excitation through the generator cannot transmit torque to other parts of rotor train and hence, the shaft system is not excitable. In general, exclusive last row blade umbrella and exclusive connector shaft (sometimes called as Jack Shaft) modes have less energy and are hard to excite by an externally induced torque.

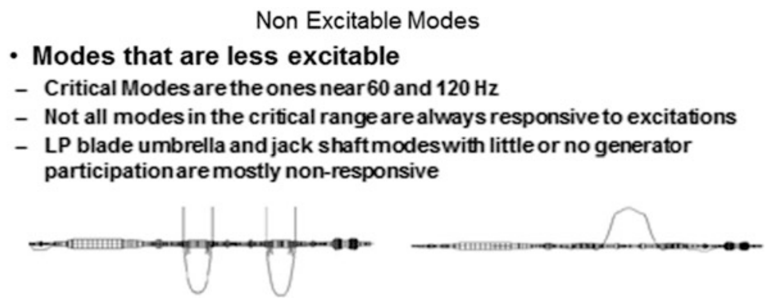

Fig. 2.36 Non-excitable modes

In a steam turbine shaft train, the most excitable elements are LP, Generator and the Exciter rotors. As shown below in Fig. 2.37, HP rotor typically does not have an energetic mode near the line and/or twice the line grid excitation frequencies because the rotor is relatively rigid and does not have longer blades like LP rotor does. Consequently, HP rotor is not a candidate of torsional concern. However, flexible coupling sections between HP and IP rotors in some designs may pose a concern for torsion. Therefore, total train torsional analysis will be required to determine rotor frequencies.

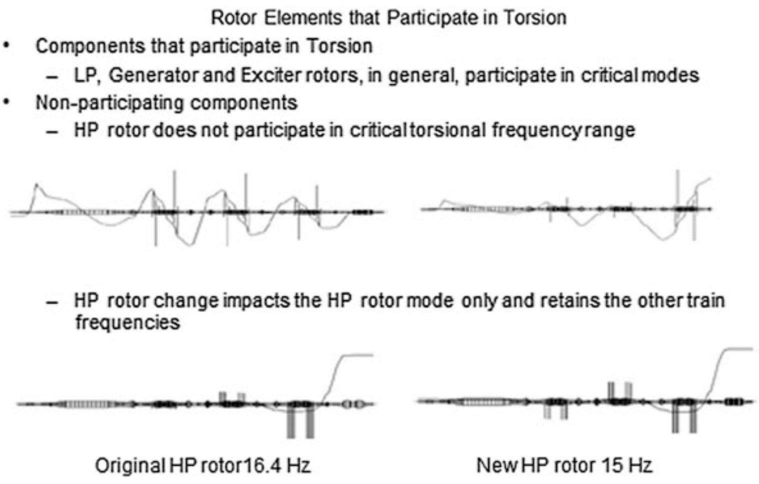

Fig. 2.37 LP, Gen and Exciter rotor modes are excitable and HP rotor modes are non-excitable

In the example shown in Fig. 2.37, the replacement new (heavier) HP rotor frequency drops (because larger inertia with same stiffness reduces frequency i.e. k/m effect) compared to the original HP rotor. However, both original and new HP rotor modes are not excitable by line or twice line frequencies at 16.4 and 15 Hz.

The next step is to assess the frequency results in relation to line and twice line frequencies. Depending on the position of the calculated frequencies to operating frequency, additional analyses may be required to validate the shaft train frequency results for acceptable and continuous operation of the machine. ISO 22266-1 standard [16] provides frequency avoidance zones as shown in Table 2.2 as guidance for design.

Table 2.2 Torsional frequency exclusion zones

Grid frequency (Hz)	Single line, Avoidance zone (Hz)	Double line avoidance zone (Hz)
50	47.0–53.0	94.0–106.0
60	56.4–63.6	112.8–127.2

The frequency avoidance zone includes margin to account for calculation uncertainty and necessary separation to limit responsiveness. It should be noted that only the torsional natural frequencies that can be excited by the energy from the generator air gap torque are subject to the frequency avoidance zone criteria. Several non-excitable modes may exist within the frequency avoidance zones. For those modes, more detailed stress response calculations are needed to discount them from torsional concerns.

Before we go into the details of additional analyses in a rotor train, it is important to identify the probable external torsional excitation sources that affect the turbine-generator-exciter system. Primarily, the external excitation torques can induce variations of current in the generator stator windings resulting in variations in the resisting torque to the generator rotor through the flux linkages.

The excitation sources can be broadly classified into two types. They are:

1. Steady State and
2. Transient

2.8.8 Steady-State Excitations

Steady state excitation analysis is required if the system has responsive modes in the Primary Frequency Exclusion Zone (PFEZ) shown in Table 2 per ISO 22266-1 requirements. The excitation torque requirements are defined by IEEE Standard C50.13-2005, "IEEE Standard for Cylindrical- Rotor 50 and 60 Hz Synchronous

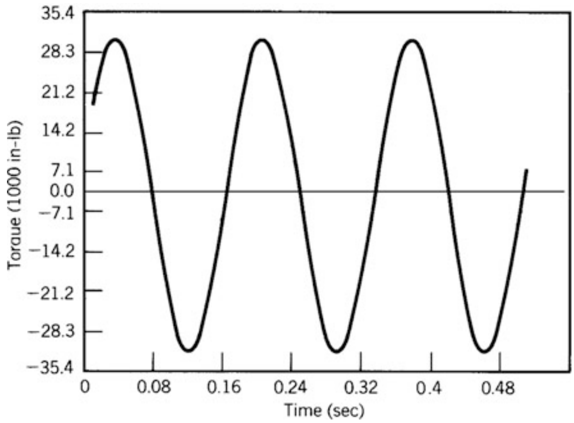

Fig. 2.38 Steady-state stress behavior

Generators Rated 10 MVA and above", Table 2: Short-time negative-sequence current capability" [17]. This states that the rotor system "shall be capable of withstanding a continuous current unbalance corresponding to a negative-phase sequence current providing the rated KVA are not exceeded and the maximum current does not exceed 105 percent of rated in any phase.

Steady-state excitation (as shown in Fig. 2.38) produces torque variations at twice the electrical line frequency, which is commonly known as "line unbalance". The magnitude of the torque is determined by the amount of the unbalance currents in the three phases of the system at any instant.

- Disturbances that occur at the generator rotor transmit torque to the entire shaft train
  - *Steady state- Oscillatory*

    Line Unbalance (Negative Sequence Current) currents cause air-gap torque at the generator rotor
    Excites the shaft train at 2× grid frequency (120 Hz in US and 100 Hz in Europe, Australia or most of Asia)

If a mode falls within the frequency exclusion zone, then the steady state stresses due to a phase unbalance must be calculated, evaluating all critical areas such as blade and low diameter shaft locations. As a conservative measure, the calculated frequencies in the PFEZ should be assumed to be resonant with the grid frequency for stress calculations. The resulting stresses are compared to allowable values and, if the stresses in the train are within acceptable limits, no further analyses are necessary. The negative sequence current that cause steady-state torque could last anywhere from a fraction of a second to a few seconds, the strength of which could be anywhere from 1% to sometimes as high as 100%.

2.8.9 Positive and Negative Sequence Currents

Line unbalances are caused by positive and negative sequence currents. They are explained below.

Positive sequence: Two magnets (rotor and stator) showed in Fig. 2.39 rotating in the same direction and at the same frequency. When the three-stator phase currents are balanced, the direction of rotating flux in the stator is in the same

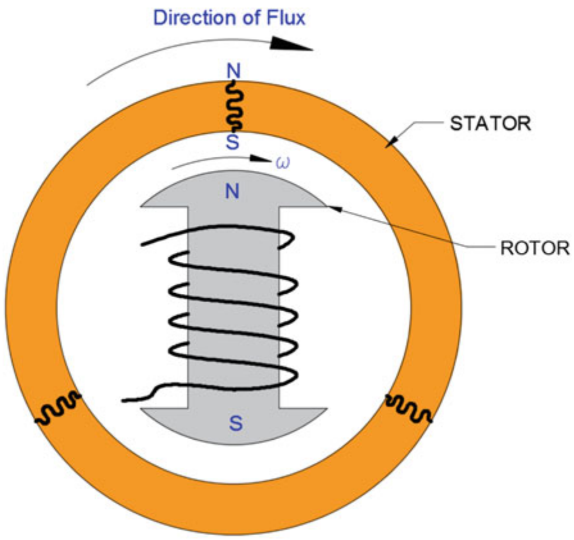

Fig. 2.39 Positive sequence currents

direction as the rotor rotation. When there are no unbalances in the stator phase currents, the resulting magnetic interaction between the rotor and stator causes a steady torque with no torsional oscillations.

Negative sequence: Two magnets rotating in the opposite direction. This occurs when the stator phase currents are not balanced. See Fig. 2.40.

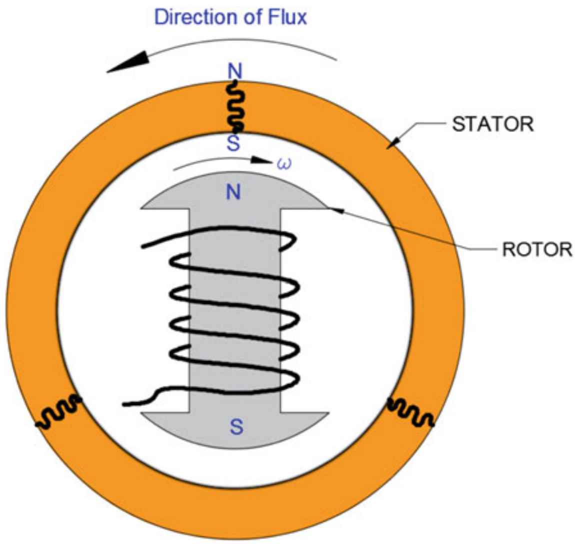

Fig. 2.40 Negative sequence current

For the negative sequence current situation, two torque pulsations during each rotation, are experienced and therefore, the frequency of torque oscillations due to negative sequence current occurs at twice (2x) the electrical frequency. When the three-stator phase currents are unbalanced, the resulting negative sequence current generates electrical torque oscillations.

For cases where frequencies are calculated within the avoidance zone and/or steady state stress criteria are not met, it is required to "tune" the train frequency away from single and/or double line frequency. Frequency tuning can be done in two ways:

(a) Increase or reduce stiffness where twisting rate is high
(b) Increase or decrease inertia where amplitude is high
(c) Both tuning options need to be verified by on-site torsion tests to confirm that the tuned frequencies are outside the zone of concern.

Frequency tuning options include installation of inertia rings at the coupling locations to move frequencies lower. Removing inertia at a shaft location can alter stiffness. Calculations are needed, prior to making decisions on frequency tuning. It is important to review the torsional mode shapes of concern closely and identify locations where inertia or stiffness tuning can be effective. Torsional tuner is also used to reduce amplitudes.

2.8.10 Transient Excitations

Unbalanced transient grid events (short circuits (SC), etc.) result in transient torques at single and double line frequency (e.g. 60 and 120 Hz on 60 Hz systems and 50 and 100 Hz on 50 Hz systems). Primary requirement is avoidance of rotor train frequency resonance with single and double line excitation frequencies. Although the transient torque dies down eventually and reduces the energy input to the rotor train, the oscillating torque amplitudes, to begin with, could be much higher than that due to steady state event. Repeated high amplitude SC events could accumulate damage in shafts and are detrimental to the life of the rotor train. It has also been observed that the off-resonant response decreases more slowly during a transient short circuit event. Therefore, the frequency avoidance range must be greater to be effective.

Many types of transient excitations are possible. A severe transient excitation that shall be considered for steam turbine-generator shaft system design is a "**Line-to-line short circuit** (SC)" at the generator terminals. This transient produces primarily a step change in torque level at both line and twice line frequencies simultaneously and decays in time. An example of SC event is shown in Fig. 2.41. In general, SC event at the generator terminals is rare.

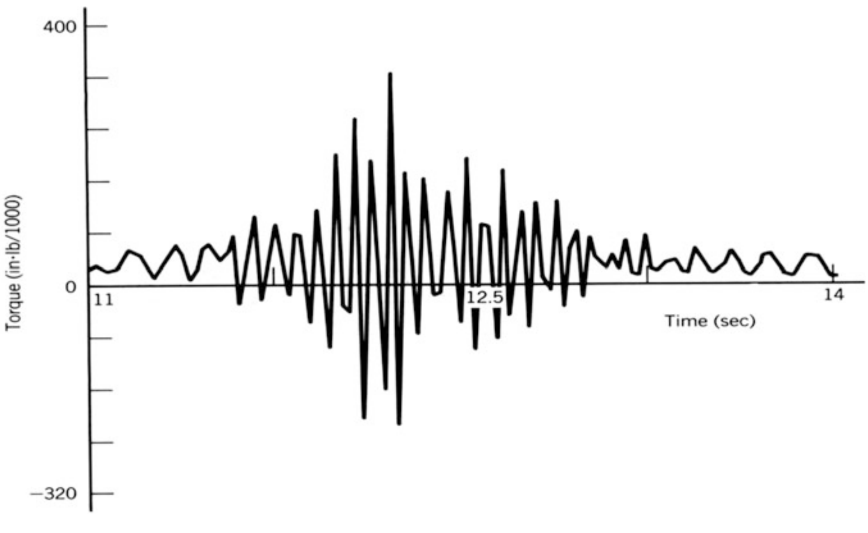

Fig. 2.41 Short circuits (Two and Three phase)- Excites 50 or 60 Hz and 100 or 120 Hz modes simultaneously

An example short-circuit incident occurred in a power plant is captured as shown in Fig. 2.42. Normalized amplitudes over 2s of short-circuit incident is recorded as shown. The amplitudes tend to reach steady state eventually after the SC event was initiated. Signals are synthesized for frequency responses as shown in Fig. 2.43. Two frequencies 1x (60 Hz-Line frequency) and 2x (120 Hz-twice line frequency) have dominant amplitudes. Resulting blade stress amplitudes are shown in Fig. 2.44. Blade stress amplitudes for at the two ends of a symmetric flow machine

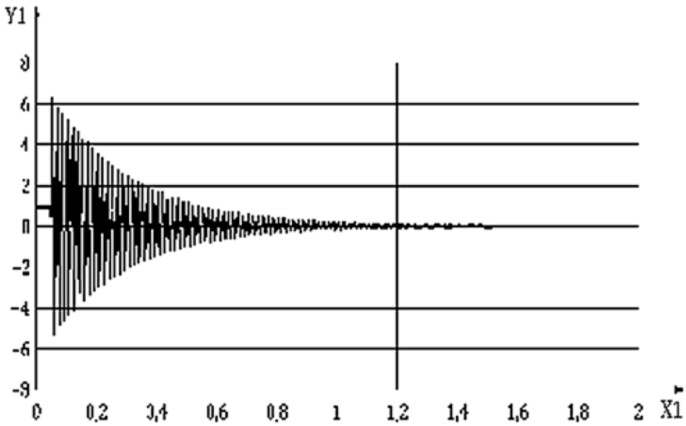

Fig. 2.42 Shot circuit fault—Amplitude versus Time

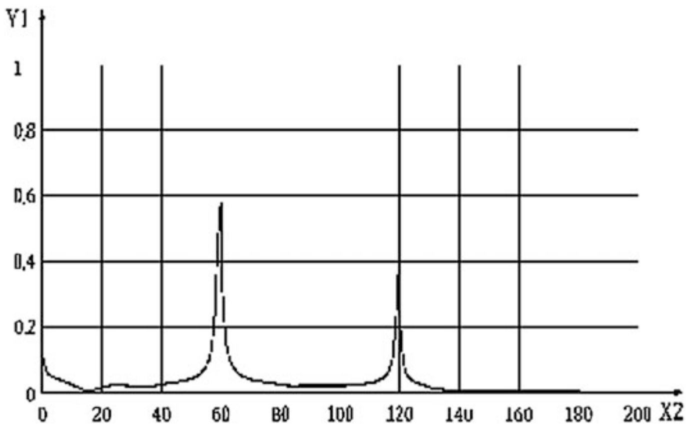

Fig. 2.43 Short circuit fault—Frequency response spectrum

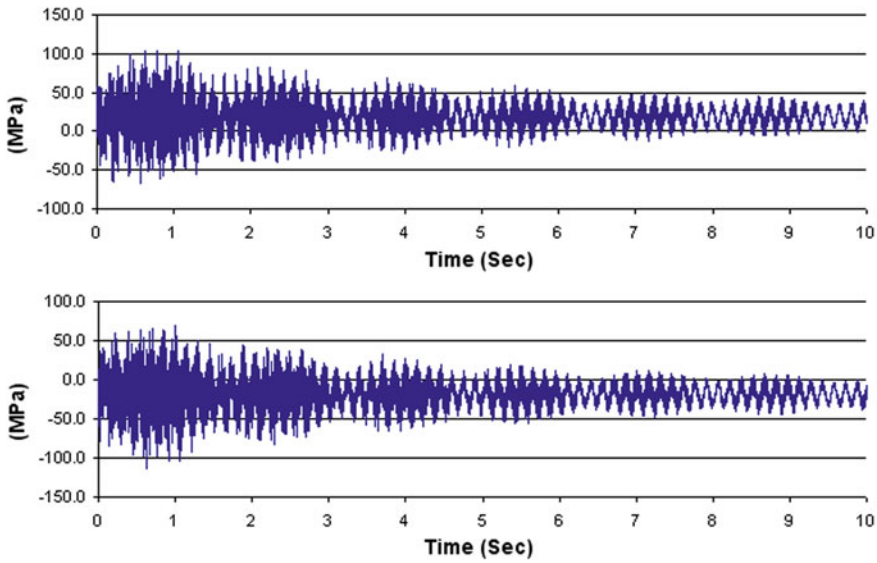

Fig. 2.44 Blade stress response plots due to short circuit fault—MPa versus Time

are shown. As can be seen, stress amplitudes dampen out within a short duration. For example, it can be noticed that stresses reduced by about 50% within a second after the SC event.

While designing a rotor system, it is important to know that torsional modes near single and double line frequencies should have low vibratory stress. Considerable torque is developed in the shafts due to the step change in air gap torque, which occurs during a SC transient. This step change will excite the lowest modes of the system more prominently. Therefore, it is important to identify and include a frequency range with the lowest frequency when performing the transient response calculation. The shaft line should be designed for strength to avoid damage due to SC events.

For turbine shafts, coupling bolts, shrunk-on couplings, coupling keys and LP blades, it is important to evaluate shear stresses due to a SC event and compare them to allowable stresses for the specific material and ambient conditions.

The total stress is the sum of the transient and steady state stresses (centrifugal force stress, untwist stress and steam bending stress for blades). In general, the total allowable shear stress should be limited to an acceptable percentage or at maximum to material yield.

2.8.11 Loss of Life Calculations

If the nominal shear stress exceeds the acceptance limit, a loss of life calculation must be performed. Loss of life calculations are done by adding damages due to various electrical fault events that occurred/or can occur over the life of the unit and provide the remaining fatigue life margin for the rotor system.

An example is illustrated in Fig. 2.45 that shows the calculated linear elastic stress-strain of a component (either a rotor or a blade) that is made from steel. The actual material elasto-plastic stress-strain behavior for steel components is also shown. Neuber postulated that the area of strain energy (1/2 Sε) under the elastic material line can be related to linear stress and strain in the form of parabolas. When the parabola crosses the elasto-plastic material curve, the true stress and strain are

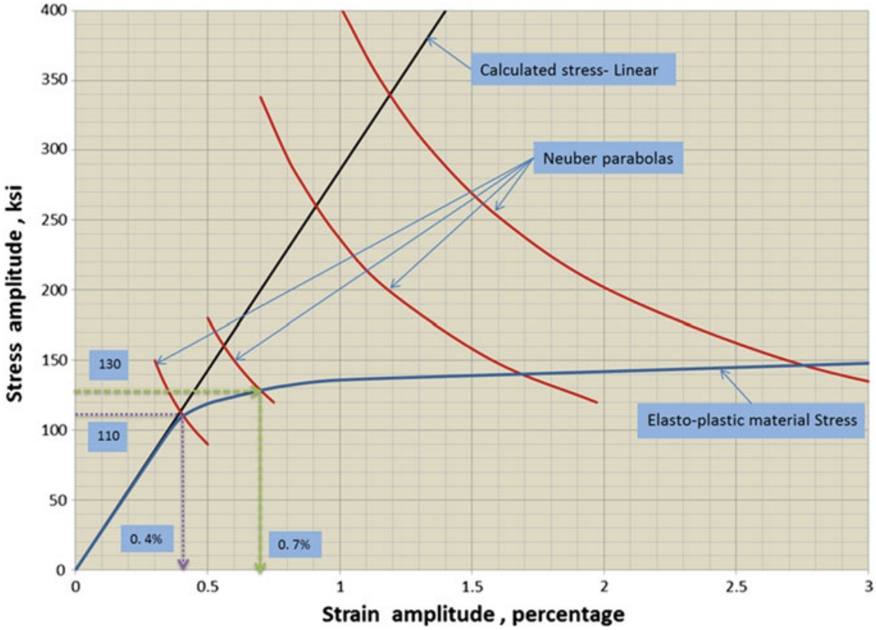

Fig. 2.45 Neuber's diagram for damage assessment

estimated. Wherever the parabola crosses the material stress line, the corresponding component stress and strain provide "True Stress/True Strain". Few examples (parabolas) are generated for various component distress conditions as shown in Fig. 2.45. Wherever a parabola for true stress cuts the elasto-plastic material line, the corresponding strain amplitude is used to estimate the component life using Fig. 2.46.

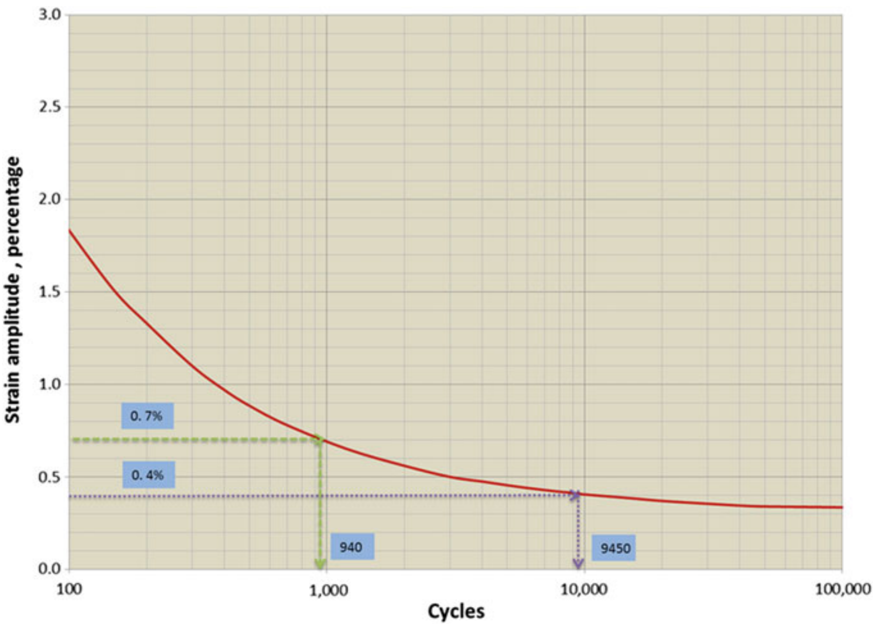

Fig. 2.46 Example life versus Strain amplitude curves

Life estimation of a component can be assessed using curves 2.42 and 2.43. Example shows when the estimated % strain is 0.7%, the component life is estimated at 940 cycles, whereas when the % strain expended is only 0.4%, the life of the same component lasts longer at 9400 cycles, a ten-fold increase. Strain (or stress) thus arrived can be used to assess the remaining life of a part or component using Fig. 2.46.

2.8.12 *Out-of Phase Synchronization (OPS)*

Another transient excitation that occurs in electrical power plants is out-of-phase synchronization. Always some amount phase-mismatch between the generator and the grid system voltages exists when the breaker is closed. This causes out-of-phase synchronization. In general, small phase-mismatch in the order of less than 30 degree is tolerable; however, larger phase mismatch could cause excessive torque, that could be equivalent to or sometimes exceeds the amount of line-to-line short circuit. OPS Excites line frequencies only (50 or 60 Hz modes)

2.8.12.1 Sudden Impulse or Repetitive Industrial Loads Near Power Plants—Excites Sub-synchronous Modes

Line Switching and Resonance Due to Series Capacitor Compensated Transmission- Excites Sub-synchronous Modes

2.8.13 Sub-synchronous Excitations

Potentially damaging transient is known as "sub-synchronous" excitation. They are assessed as part of SSR (Sub-Synchronous Resonance) net-work studies. Power plant management routinely conducts sub-synchronous resonance (SSR) studies time-to-time because the actual sub-synchronous frequencies may vary with the frequencies programmed in the network configuration developed and used. It is impossible to tune the frequencies of the rotating hardware with the varying network frequencies. Therefore, utilities (owners of power plant) design their own network system that synchronizes with the frequencies of hardware for protection. For this purpose, unit owners request the turbine generator (T-G) torsional design data from designers to match them with their network system design. Typically, shaft system data below the line frequency are calculated using simplified torsional

Fig. 2.47 Lumped mass model of the T-G shaft system

spring-mass model shown in Fig. 2.47.

In summary, the goals of torsional system design/analyses are

(a) Frequency avoidance near line and twice line frequencies per ISO guidance.
(b) Design rotor shafts for strength due to (a) steady-state line unbalance and (b) line-to-line short circuit torques.
(c) Tune rotor system frequencies sufficiently away from line and twice line frequencies when needed.
(d) Torsional testing helps to verify the predicted torsional frequencies and validate models.

2.8.14 Impact on Shaft Torque Due to Grid Events

During normal steady-state operation, the mechanical power or torque produced by the turbine is being converted to electro-magnetic torque in the generator air-gap, which in turn is converted to electrical power and transmitted to the grid. The generator air-gap torque is defined as the electromagnetic reaction between the current in the rotating field winding and the current in the stationary armature winding, and the air-gap torque is constant during steady-state operation.

However, grid disturbances such as transmission line short circuits, line switching events and/or other disturbances develop transients on generator-armature currents and impact generator air-gap current as a result. Consequently, the air-gap torque in the generator also varies. Let us discuss how these transient events will impact the mechanical torque conditions of the rotor train.

Steady-state torque and power conditions are being disturbed during any of the transient grid events. Short circuits and other disturbances in the grid induce transient currents in the generator (stationary) armature winding that interacts with the (rotating) field winding thus producing transient generator air-gap torque, which is responsible for torsional oscillations in the turbine-generator shaft system. These transient- torques, typically, produce instantaneous step changes in both the generator air-gap power and the air-gap torque at one and two times of the electrical frequency.

Grid short circuits and related disturbances that occur at the generator terminals produce air-gap torque transients that are greater in magnitude, as the induced generator armature currents are larger.

Similarly, in the case of exclusive generator terminal short circuit condition, the induced generator armature currents become very large in magnitude and transmit large mechanical torques in the rotor train.

(a) The *torque due to transient disturbances* could induce stresses in the shaft as high as the material yield and could lead to fatigue damage.
(b) Transient oscillatory frequencies may get closer to one or more of the shaft system frequencies resulting in resonance condition.
(c) *Disturbing resonant torques* (if the shaft frequency is close to the excitation frequency) could produce high stresses and increase fatigue damages in shafts
(d) The step-change in *steady-state torque* in shaft system could potentially distress blades, retaining rings, exciter shaft and low diameter journals by high cycle fatigue (*HCF*)
(e) The *transient torque* is capable of damaging blades, coupling bolts and shafts by low cycle fatigue (*LCF*)
(f) Both mechanisms can reduce fatigue life of the shaft system anywhere from few hours to few years.

2.9 Testing for Torsional Frequencies and Modes

Torsional shaft testing can be done for individual rotors at the factory. This test is performed in two ways.

2.9.1 Stationary Frequency Testing

Stationary testing has limited value (may be useful in verifying natural frequencies of blades or retaining rings) and only validates the tested rotor in uncoupled condition. When rotors are coupled, rotor system becomes flexible and creates a new system. As such, the single component test verification may not be relevant. This type of testing is obsolete.

Torsional frequencies can be verified for the rotor in stationary condition applying mechanical torque by impact hammer at one point and measuring the resulting responses at all other points. The response points in the rotor can be used to draw the rotor wire-frame model as illustrated in Fig. 2.48. Responses generated

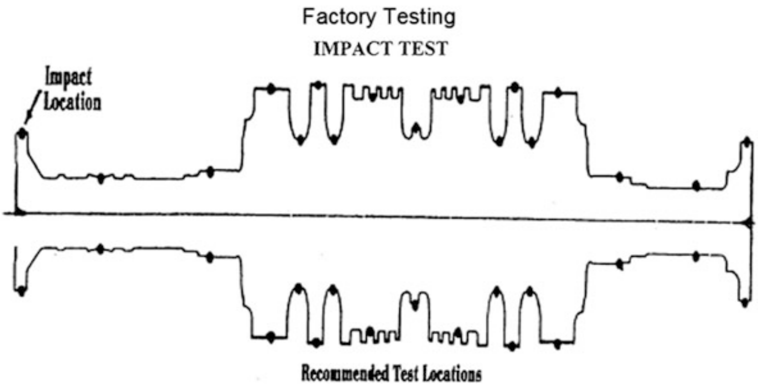

Fig. 2.48 Stationary rotor (Un-bladed) Test at the Factory

by the applied torque by the hammer are measured. The measurements are applied at the appropriate nodal points in the model simulating modes and frequencies using modal analysis software. This will help to verify the theoretical model of individual rotors in uncoupled condition and could help calibrating the rotor model in the shaft train. Usually, LP and Generator rotors may be tested in the factory. Rotor modes can be verified; however, the most important blade-disc coupled frequencies that vary with rotating speeds cannot be verified with the stationary test.

Figure 2.48 shows an example LP rotor configuration tested in the factory with impact hammer. Measured first LP rotor twist mode and corresponding frequency is shown in Fig. 2.49.

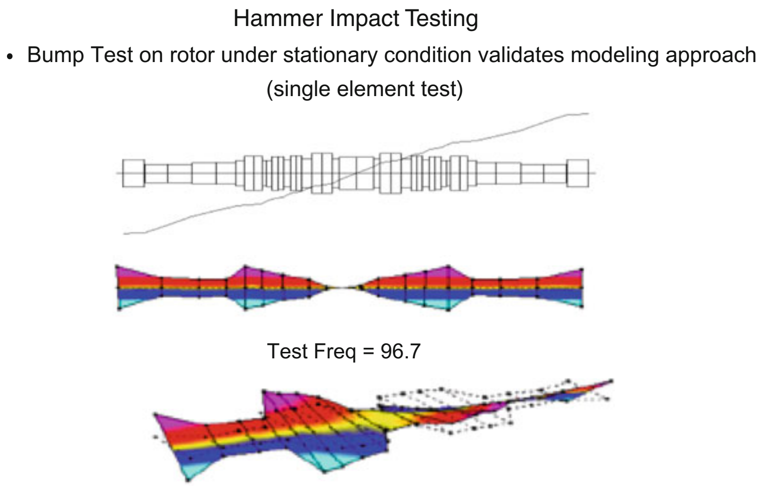

Fig. 2.49 Rotor mode tested with impact hammer at the factory

2.9.2 Rotating Tests

Dynamic testing or rotating component testing can improve modeling. These are factory testing, that are done to verify rotor-to-blade coupled frequencies at the operating speed. However, when the individual rotors are connected in a train, the system frequencies can generate additional modes/frequencies that were not measured in the factory testing. Such rotating test results of the rotor in the train can be used to calibrate the overall rotor shaft model.

On-site testing is most useful to identify and confirm the actual system torsional frequencies at the operating speed. They help to understand the modal behavior of individual frequencies and enable detuning of them to be sufficiently away from line and twice line frequencies as needed. On-site torsion testing is more appropriate for the in-service or modernized rotor systems.

Filed torsion tests can be carried out using sensitive measuring devices such as strain gages at the most effective shaft locations, based on the calculated mode shapes. Additionally, torsional motions can be measured at a turning gear location or on a tooth wheel (that measures the elapsed time between teeth) mounted on the shaft using magnetic probes. The test can be performed during speed ramp. Measured frequencies can be compared with calculations.

2.10 Closure

The following topics were discussed in this chapter

- Advanced 3-D lateral and torsional rotor dynamic modeling
- Rotor frequency and response evaluations
- Mass unbalance excitations and Q factor evaluations
- Various forcing functions due to grid excitations for shaft torsional vibration
- Rotor stress and fatigue evaluations
- Factory and on-site torsional testing for validation of shaft models

References

1. Lund JW (1965) Rotor bearings dynamics design technology, Part V: computer program manual for rotor response and stability. Mechanical Technology Inc., Latham, NY, AFAPL-Tr-65-45
2. Rao JS (1983) Rotor dynamics. Wiley
3. Nelson HD, McVaugh JN (1976) The dynamics of rotor-bearing systems using finite elements. J Eng Ind Trans ASME 98(2)
4. Subbiah R, Kumar AS, Sankar TS (1988) Transient dynamic analysis of rotors using the combined methodologies of finite elements and transfer matrix. J Appl Mech Trans ASME 448–452
5. Ratan S, Rodriguez J (1989) Transient dynamic analysis of rotors using successive merging and condensation (SMAC) techniques. J Vib Acoust 482–488
6. Subbiah R, Rieger NF (1988) On the transient analysis of rotor-bearing systems. ASME J Vib Acoust Stress Realiab Des 110/515:515–520
7. Den Hartog JP (1956) Mechanical vibration. McGraw Hill, New York, p 301
8. Dimarogonas AD, Haddad S (1992) Vibration for engineers. Prentice Hall
9. Thomson W (1988) Theory of vibration with applications. Prentice Hall
10. Subbiah R, Moreci J (1995) Turbine rotor torsional dynamics: analysis, verification and standardization. Power-Gen Asia Conference, Singapore
11. La Rosa JA, Kung GC, Rosard DD (1980) Analysis of turbine blade vibrations induced by electrical-mechanical interactions. In: ASME joint power generation conference
12. Ramey DG, Kung GC (1978) Important parameters in considering transient torques on turbine-generator shaft systems. In: IEEE/ASME/ASCE state-of-the-art symposium turbine-generator shaft torsionals, pp 25–31
13. Walker DN (2003) Torsional vibration of turbomachinery. McGraw-Hill
14. Huster J, Eckert L, Prohle F (1999) Calculation and measurement of torsionals in large steam turbosets. Machine, Plant & Systems Monitor, March/April 1999, pp 22–27
15. Torsional Vibration Standrad, ISO 22266-1, 2009
16. ANSI C50.13-1989, Rotating electrical machinery—Cylindrical-rotor synchronous generators (Note: this standard has been withdrawn)
17. Detuner for tuning torsional mode of a rotating body, US Patent 8013481 B2

Chapter 3
Rotor-to-Structure Interaction

3.1 Introduction

We discussed that the rotor and the bearing support structure (called pedestals) can be modeled as two linear springs in series using the classical Jeffcott rotor in previous two chapters. The core points discussed were listed as follows:

- Equivalent stiffness of the shaft and the pedestal is used to compute rotor critical frequencies and the corresponding mode shapes.
- The rotor stiffness mainly influences the first bending frequencies (U-mode), whereas the pedestal stiffness has prominent influence in shaping the rotor second mode (S-mode) frequencies.
- The above concepts are tested in real turbines and are proven to be so with more than 100 tests.
- Therefore, this section is very important for both Engineers and Scientists who may pursue further research into this complex support system subject.
- Number of operating and structural parameters were collected and analyzed whether they can contribute to the degradation of bearing support pedestals in service.
- This new topic is a result of research done on steel pedestal supports over a decade and are exclusively presented in this book.

3.2 General

The focus of this chapter is to expand on the findings of the pedestal structure stiffness deterioration in real machines during service and its impact on the rotor critical frequencies. In worst cases, the pedestal stiffness degradation could shift original rotor frequencies toward the operating frequencies and may lead to

R. Subbiah and J. E. Littleton, *Rotor and Structural Dynamics of Turbomachinery*,
Applied Condition Monitoring 11, https://doi.org/10.1007/978-3-319-73296-1_3

catastrophic damages. In preparation for the deep dive approach on the subject, it is important to understand the various rotor mode shapes, viz. U-mode, S-mode, and W-mode as illustrated for an opposed flow LP rotor in Fig. 3.1.

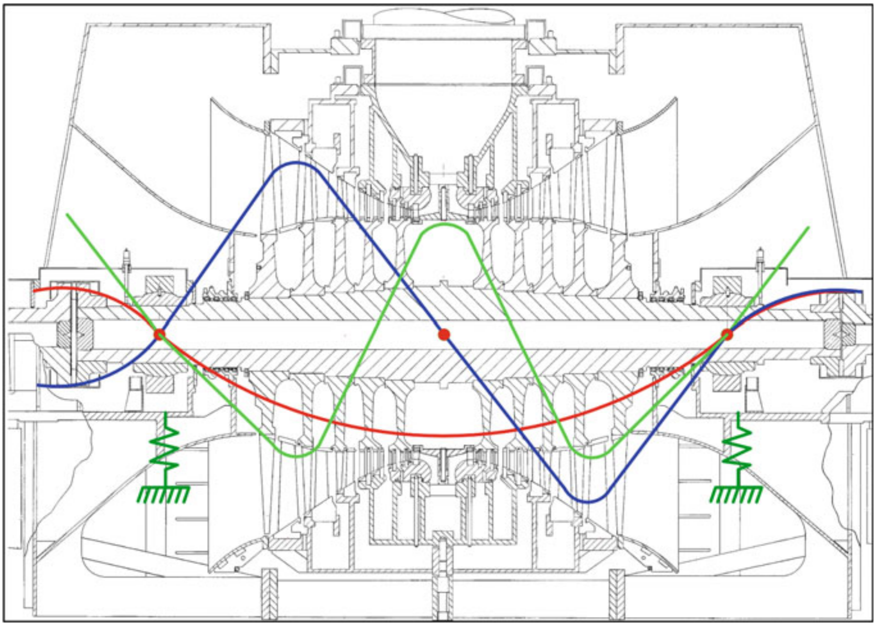

Fig. 3.1 Major modes of rotor [red—first mode (“U”), blue—second mode (“S”), green—third mode (“W”)]

3.3 Influence of Bearing Support Pedestal Stiffness on Rotor Critical Frequencies

Let us discuss some real-life examples which indicated the bearing pedestal structure degradation lead to the reduction of rotor S-mode critical speeds exclusively. The steel pedestal designs applied in certain category of steam turbines (mainly in designs applied in half-speed machines, 30 Hz) fall under two major categories: (a) rigid pedestals and (b) flexible pedestals. They are discussed in detail in the following sections.

3.3.1 Rigid Bearing Support Pedestals

Rigid bearing support condition is defined when turbine bearing supports are directly mounted on the concrete pillars through a few solid blocks of steel.

Figures 3.2, 3.3, and 3.4 are examples of rigid bearing supports that are applied in high-pressure (HP), intermediate-pressure (IP), and low-pressure (LP) steam turbines, respectively. Similar bearing pedestal structures are shown for gas turbines in Fig. 3.5. Rigid support pedestal designs are also common for small turbine components as well.

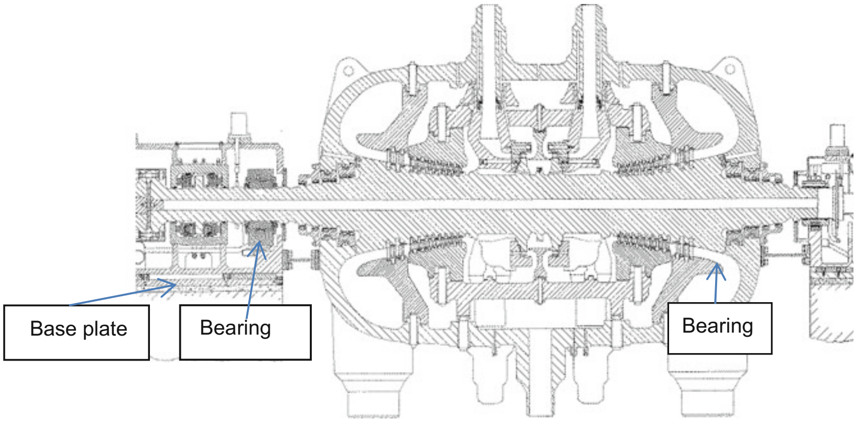

Fig. 3.2 High-pressure turbine (courtesy of Siemens)

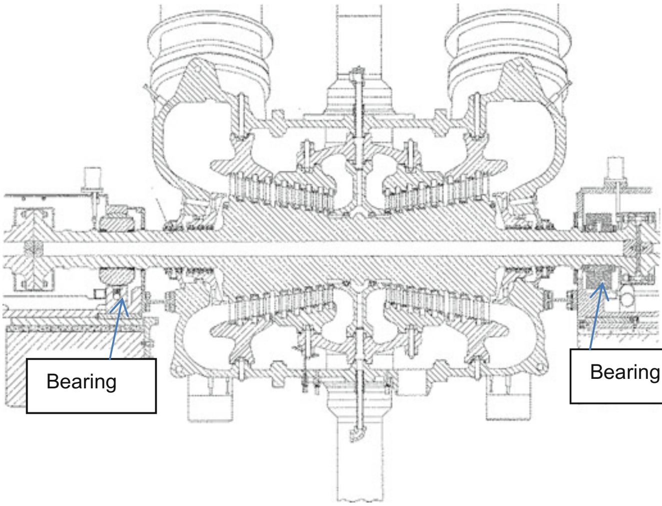

Fig. 3.3 Intermediate pressure turbine (courtesy of Siemens)

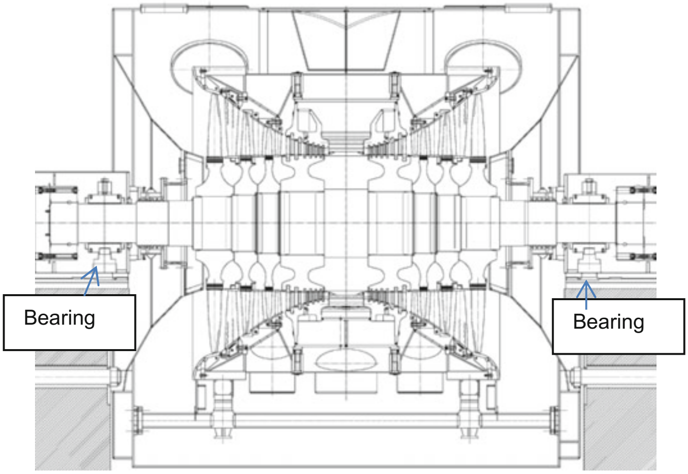

Fig. 3.4 Low pressure turbine (courtesy of Siemens)

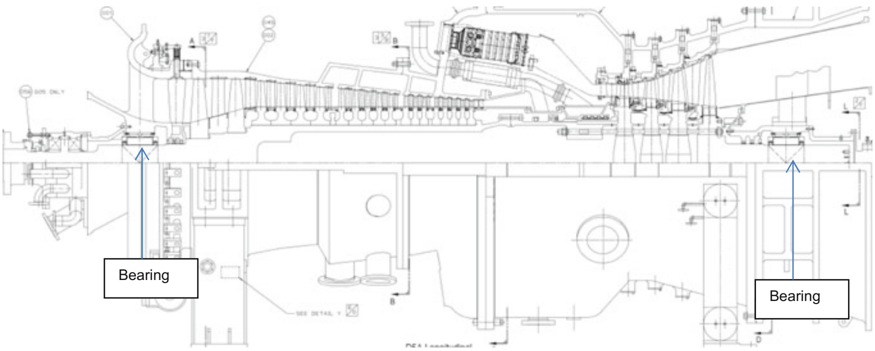

Fig. 3.5 Gas turbine (courtesy of Siemens)

3.3.2 Flexible Bearing Support Pedestals

In comparison with rigid bearing supports discussed in Sect. 3.1, a flexible bearing support pedestal system comprises of sets of steel struts and pipes which connect the bearing cones and the base plate of the casing. Such flexible connecting

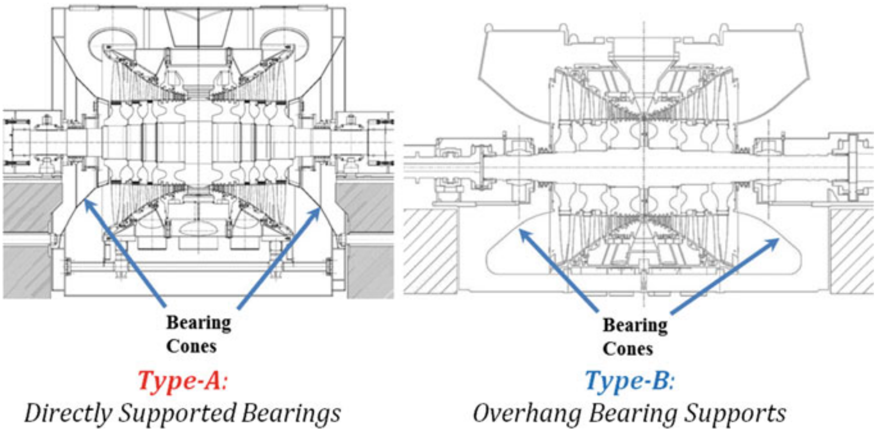

Fig. 3.6 Two different LP bearing pedestal support systems (courtesy of Siemens) (use the uploaded pictures)

members make the pedestals less rigid. A side-by-side comparison of a representative rigid (Type-A) and flexible pedestals (Type-B) in Fig. 3.6 allows for better appreciation of the structural differences.

Type-A Pedestal System: Bearing cones are directly mounted on concrete foundation or pillars via solid blocks of steel with no flexible connecting members between the bearing cones and the base plate. Hence, they are considered rigid. There are no reported pedestal stiffness degradations observed for Type-A pedestals.

In contrast,

***Type-B Pedestal System**: It* has flexible struts or pipes welded between the bearing cones and the casing base plates. In addition, the bearing cones overhang from the concrete pillar, which add more flexibility to pedestals, mainly in the vertical direction.

Owing to their flexibility, Type-B pedestals are susceptible to gradual decline in stiffness over long operating cycles. Consequently, reduced pedestal stiffness was found to drop the S-rotor frequencies lower than they were originally designed for. It should be noted that these vintage steel pedestals were built anywhere between 30 and 50 years ago with limited structural inspections during their service life. Details of the flexible pedestal system are shown in Fig. 3.7.

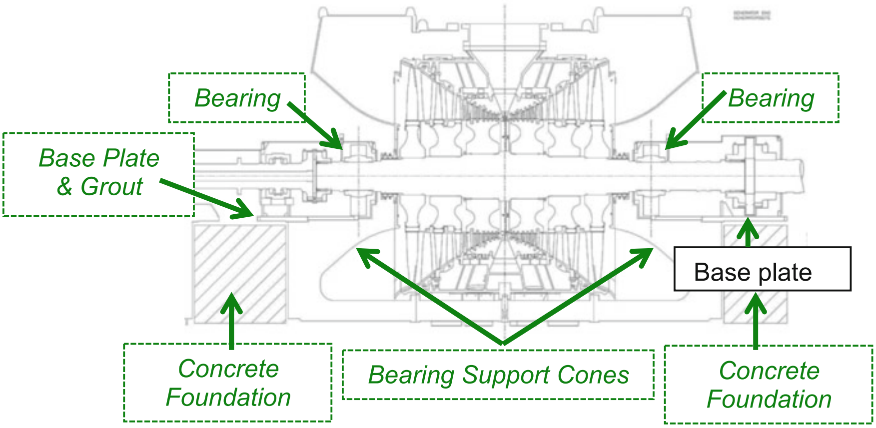

Fig. 3.7 Details of flexible bearing supports an LP turbine (courtesy of Siemens)

This chapter discusses the Type-B pedestal degradation effects or similar flexible pedestal designs only unless stated otherwise. The operating speed of the Type-B LP turbine is 1800/1500 RPM (30/25 Hz). Another example of flexible support system is also shown in Fig. 3.8 for a Generator design.

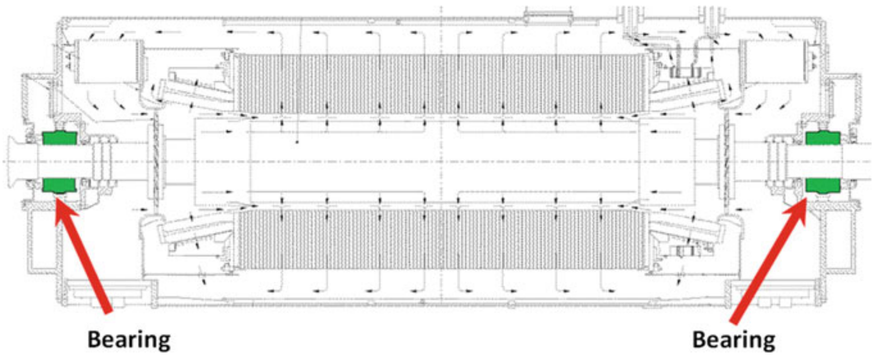

Fig. 3.8 Generator rotor support systems

3.3.3 Background on Flexible Bearing Support Pedestal Degradation

A high vibration event reported on a unit with flexible bearing pedestals similar to the one shown in Fig. 3.7 motivated the bearing pedestal degradation studies [1, 2]. During the event, the LP rotor second critical speed gradually dropped toward the operating speed. Detailed analytical studies correlated well with the pedestal dynamic stiffness drop that was associated with the second critical speed of the rotor. A summary of the events is listed as follows:

- Second rotor frequencies (also known as conical or S-mode) dropped from the originally designed values for the degraded (Stiffness reduced) bearing support pedestals. For the nominal pedestal design conditions, the rotor frequencies were well above the over speed limit of 110% of the operating speed (OS).
- The dynamic stiffness corresponding to the S-rotor frequency for the degraded bearing pedestals was lower than that of the original design.
- Shaft absolute vibration was measured higher than ISO 20816 C/D limits; but it was not clear from the absolute vibration data whether the vibration was dominated by the structure or by the rotor. Assuming the rotor was reactive to imbalance forces, the unit was balanced to reduce dynamic forces on the bearing support pedestals.
- Within few months after the balance move, the S-rotor mode frequencies further shifted lower until they became resonant with the operating speed. This event caused significant structural damages to the machine.
- Figure 3.9 sums up the progression of support structure degradation as the S-rotor critical speed dropped toward the operating speed.

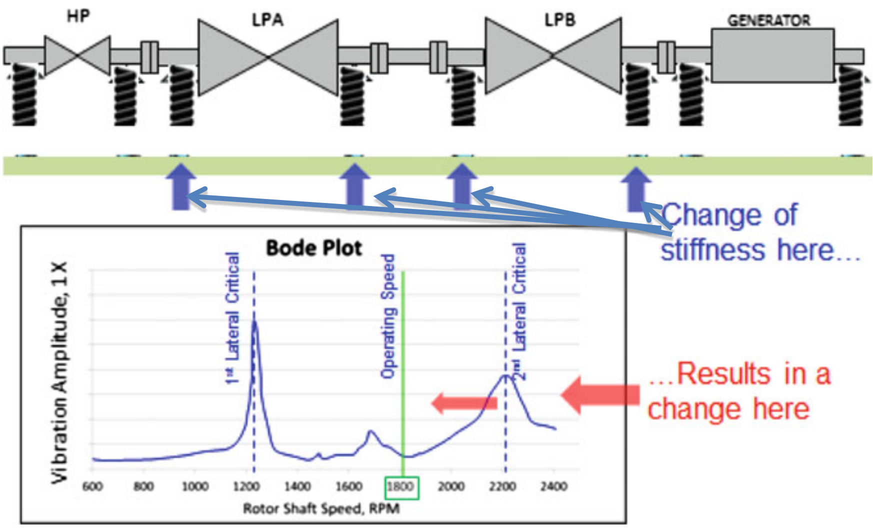

Fig. 3.9 S-mode frequency shift due to pedestal stiffness reduction

3.3.4 Pedestal Degradation Experience in Power Plants

The author has been associated with more than 100 shaker tests on Type-B support structures and a few generator-bearing pedestals [1, 2] as well. About 20% of steam turbine pedestals tested were "degraded" meaning their second rotor critical speeds dropped below they were originally designed for (at 110% of operating speed). For the pedestals tested, the visual, magnetic particle inspection (MT), and dye-penetrant (PT) inspections did not provide any indications of physical damage that otherwise should have matched with the definition of "pedestal degradation." More intrusive ultrasonic (UT) inspection technique could have helped to identify microscopic damage. But it was not applied due to prohibitive inspection cost and long outage schedule. Since no structural damages were evident through limited inspections, material experts speculated that micro-cracks at the strut weld joints could have caused gradual decline of the pedestal stiffness (or degradation) and the associated second rotor critical speed.

Shaker test results proved whenever the S-rotor frequency dropped from the original design, the associated pedestal stiffness also reduced. In some cases, pedestals were stiffened to increase the rotor second critical speeds well above the operating speed. Post-stiffening shaker tests confirmed the second rotor critical speeds and the pedestal dynamic stiffness moved up; in many cases, closer to their original design condition or better.

Although the examples cited above are directly related to steam turbine products applied in nuclear applications, structural degradation/damages can occur to any flexible support systems of similar construction including cross-compound fossil machines where some of the LP turbine bearing support pedestals are flexible. According to the author's knowledge, more than 1200 [3] such flexible pedestal configurations are operating globally.

It is important for the readers to understand the physics behind the two primary rotor modes of the turbine structures and their role in the pedestal degradation process. For simplicity, only rotor and pedestals are considered in the discussions ignoring oil film effects for the time-being.

3.4 First Rotor Mode or U-Rotor Mode

A pictorial representation of rotor and pedestal behavior for the U-rotor mode is shown in Fig. 3.10. In the U-rotor mode, rotor shaft bends in "U" shape with two-end pedestal support springs compressed. The phase angles of the bent rotor at the two pedestal ends are the same in the U-rotor mode shape. In this configuration, the rotor shaft is flexible compared to bearing support pedestals, which behave as *hard springs* [4, 5]. As a result, the equivalent stiffness that determines the U-rotor frequency is heavily influenced by the rotor stiffness. Hence, pedestal degradation does not impact the U-rotor frequency.

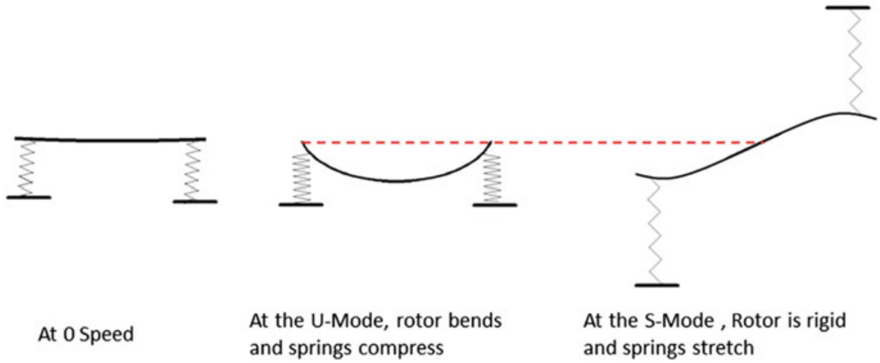

Fig. 3.10 Dominant rotor behavior

However, rotor cracking is an observable symptom for significant rotor stiffness reduction. See Rotor crack example discussions in Chap 8.

3.5 Second Rotor Mode or S-Rotor Mode

In the S-rotor mode configuration, the rotor shaft is rigid (contrary to U-mode) and the bearing support pedestals behave as *soft springs* [4, 5]. The phase angles of the rotor at the two pedestal ends are 180° out-of-phase to each other. They are in line with the S-rotor mode shape shown in Fig. 3.11. Because the pedestal stiffness (spring) is softer than that of the rotor, pedestal stiffness plays a key role in shaping

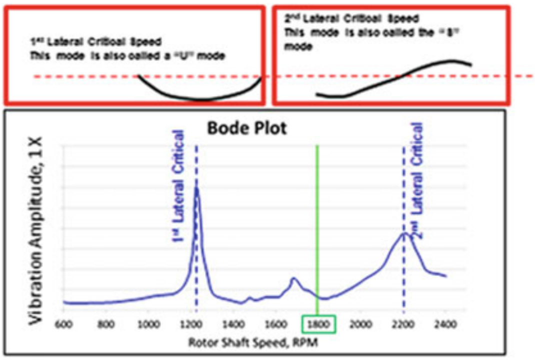

Fig. 3.11 Dominant pedestal structure behavior

the S-rotor mode and the associated frequency. Hence, the S-rotor frequency reduction provides symptoms of pedestal (stiffness) degradation. Soft pedestals in the S-rotor mode could soften further, if they are exposed to operating forces over a long period of service.

U- and S-rotor modes for a turbine are shown in Fig. 3.11.

3.6 Rotor and Bearing Support Pedestal Modeling

For better appreciation of the pedestal stiffness impact on rotor frequencies, a simple mathematical model of the rotor and the pedestal is considered as illustrated in Fig. 3.12. Oil film modeling is not included for simplicity. The concrete foundation is very rigid for the rotor systems discussed. Similar mathematical models are also discussed in numerous rotor dynamic books and technical papers [6, 7].

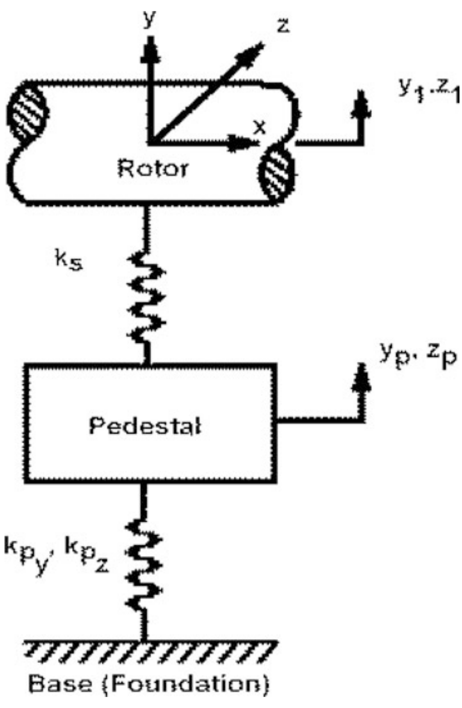

Fig. 3.12 Rotor and the bearing support pedestal

The equation of motion of the rotor-pedestal system in Fig. 3.12 can be written as follows:

$$[M]\{\ddot{x}\} + [K]\{x\} = me\omega^2 \tag{3.1}$$

M and K represent 4 × 4 matrices representing mass and stiffness properties of the system.

ks and kp are rotor shaft and support pedestal stiffness, respectively.

Vector {x} represents 4 × 1 rotor and pedestal displacements in two orthogonal planes.

And meω2 represents rotational mass imbalance force applied on the rotor.

Solution to Eq. 3.1 provides U- and S-rotor critical frequencies, responses, and mode shape information. Any general-purpose rotor dynamic computer code would be able to compute rotor frequencies and other parameters.

3.7 Testing Methods

The U- and S-rotor frequencies and mode shapes of any turbine structure can be obtained through testing. Tests can be performed using:

(a) Impact Hammers or
(b) Electrical or Pneumatic Shakers.

In both cases, rotor and pedestal frequencies can be excited.

Both hammer and shaker tests were performed on one of the LP turbine (Type-B), and the results are discussed below:

LP rotor and bearing pedestal frequency responses obtained by **hammer impact tests** (also known as, “bump test”) are shown in Fig. 3.13a. Although hammer tests produced reasonable results for simple structures, the frequency spectrums obtained for the large LP turbine structures were very noisy with no well-defined peaks compared to the spectrums obtained by the electrical shaker shown in Fig. 3.13b. The following reasons can be attributed to the weak signals obtained in impact testing.

1 Impact hammer excites random frequencies and is typically distributed among all frequencies in the test range. Moreover, the LP bearing support pedestal structure is a complex one with several welded subassemblies. These subassemblies act like speed breakers diffusing the already low impact energy produced by the hammer. As a result, only a fraction of the energy is used for exciting the modes of interest. Therefore, the hammer signals are weaker and nosier.
2 On the contrary, rotating imbalance force generated by shaker motor is speed dependent and provides a more focused single frequency excitation. When a shaker rotational speed matches with the rotor or the pedestal natural frequency, response reaches a peak as seen in the Bode plots. The red and blue lines seen in the shaker spectrum plots in Fig. 2.13b represent ascending and descending speed ramps of the shaker motor, respectively.

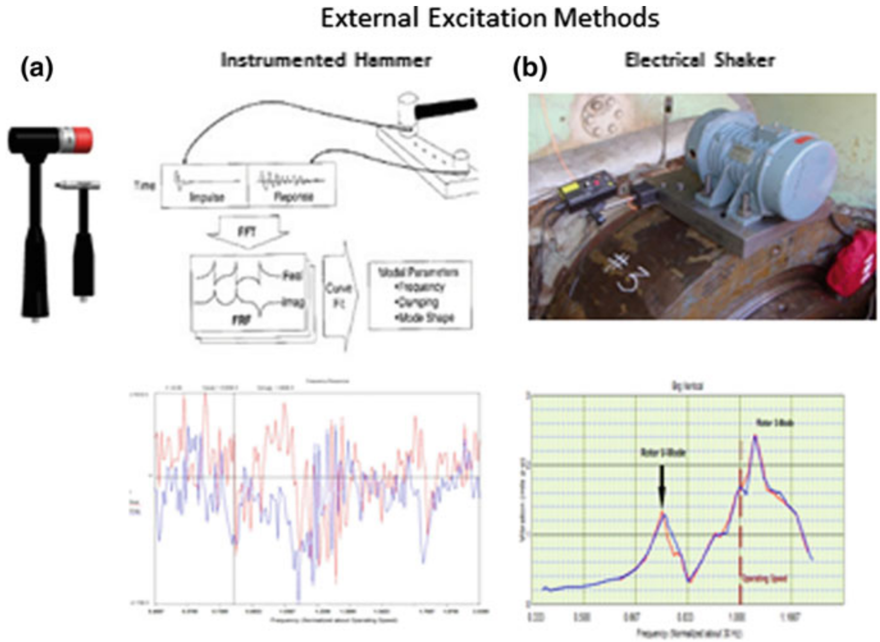

Fig. 3.13 **a** Hammer impact test. **b** Electrical Shaker test

In a nutshell, electrical shakers consistently provided prominent and low noise response spectrums compared to those produced by impact hammer for the rotor and bearing pedestal structures tested. References [8, 9] discuss shaker and impact hammer testing for a simple steam turbine support structure. In their investigations, the bearing support stiffness for the split critical speeds pertaining to the rotor U-modes was measured. Although details of the shaker used is not clear, the signals produced by the shaker seem to be surprisingly weaker. Most probably, the mass unbalances applied may be very low.

3.7.1 Electrical Shaker

The electrical shaker applied to test the Type-B LP turbine structures are discussed here.

- The shaker consists of an electrical motor housed in a casing (See Fig. 3.14).
- The motor has two adjustable masses at both ends that enable varying the mass eccentricity positions. Consequently, applied forces can be adjusted.
- The shaker is mounted on the bearing casing and secured through bolts.

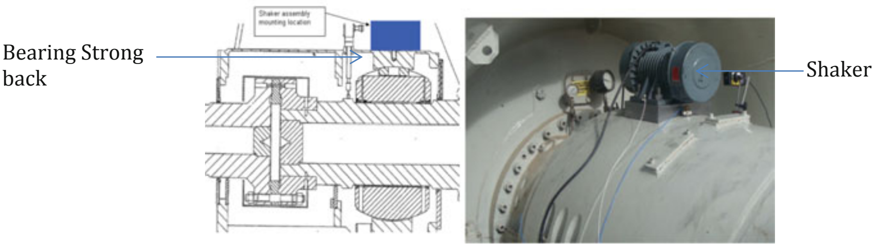

Fig. 3.14 Electrical shaker mounted on an LP bearing strong back (courtesy of Siemens)

3.7.2 *Shaker Test Process*

A preferred shaker test configuration is to have all rotors in the train coupled with their bearing oil lifts deactivated. The test should be performed with rotors at standstill (0 RPM), and the turbine should be assembled to the operating configuration. Installed electrical shaker on one of the LP turbine bearings is shown in Fig. 3.14. During the test, the shaker excitation frequency could be varied from 0 to 40 Hz (for machines that operate at 25/30 Hz) through a variable frequency drive (VFD). An example shaker test configuration of an LP turbine similar to Type-B is shown in Fig. 3.15.

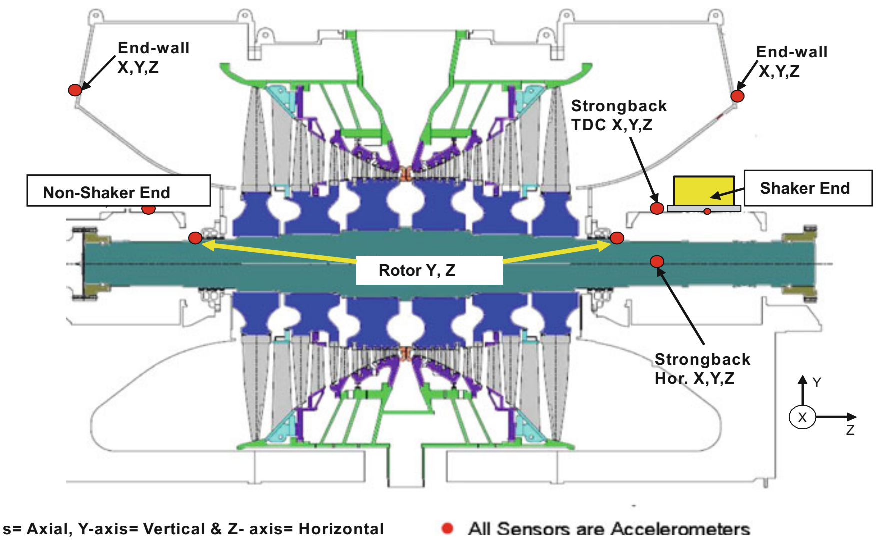

Fig. 3.15 Instrumentation details for shaker test (courtesy of Siemens)

Accelerometers were placed at the rotor, and the bearing pedestal supports to measure responses to applied forces. Force and response signals at the shaker end (SE) and at the non-shaker end (NSE) of the rotor were fed through a signal analyzer which would display the frequency spectrums on the screen. When a rotational frequency matches with one of the natural frequencies of the rotor or the pedestal, peak response can be observed. Corresponding phase angles for the rotor can be measured at the SE and the NSE to identify and confirm the U- and the S-rotor modes. At each bearing, the frequency sweep should be repeated to confirm the repeatability of the measured data.

3.7.3 Shaker Test Spectrum Plots

Figure 3.16 shows the rotor response amplitudes and phase angles (in the ordinate or vertical axis) versus the shaker speed (in the abscissa or horizontal axis) for the LP rotor configuration shown in Fig. 3.15. Similar results were also reported in Refs. [1, 2].

For the example shown, the U- and the S (vertical)-mode frequencies of the LP rotor were measured, respectively, at 68.2 and 122.5% of the operating frequency. Since the S-rotor frequency was measured well above the typical design target limit of 110% of operating frequency, the bearing pedestals were considered nominal (not degraded).

3.7.4 Shaker Test Pedestal Stiffness Plots

Typical shaker unbalance force versus shaker speed spectra are shown in Fig. 3.17.

Stiffness values (k) of the LP bearing pedestals were obtained from the shaker imbalance forces (mef2) and the corresponding vibration response (x) as shown below:

For Imperial Units

$$\mathrm{k} = \left(\frac{8\pi^2}{386,000}\right)\cdot\left(\frac{(me)f^2}{x}\right) \tag{3.2a}$$

For SI Units

$$\mathrm{k} = \left(\frac{8\pi^2}{9,806,000}\right)\cdot\left(\frac{(me)f^2}{x}\right) \tag{3.2b}$$

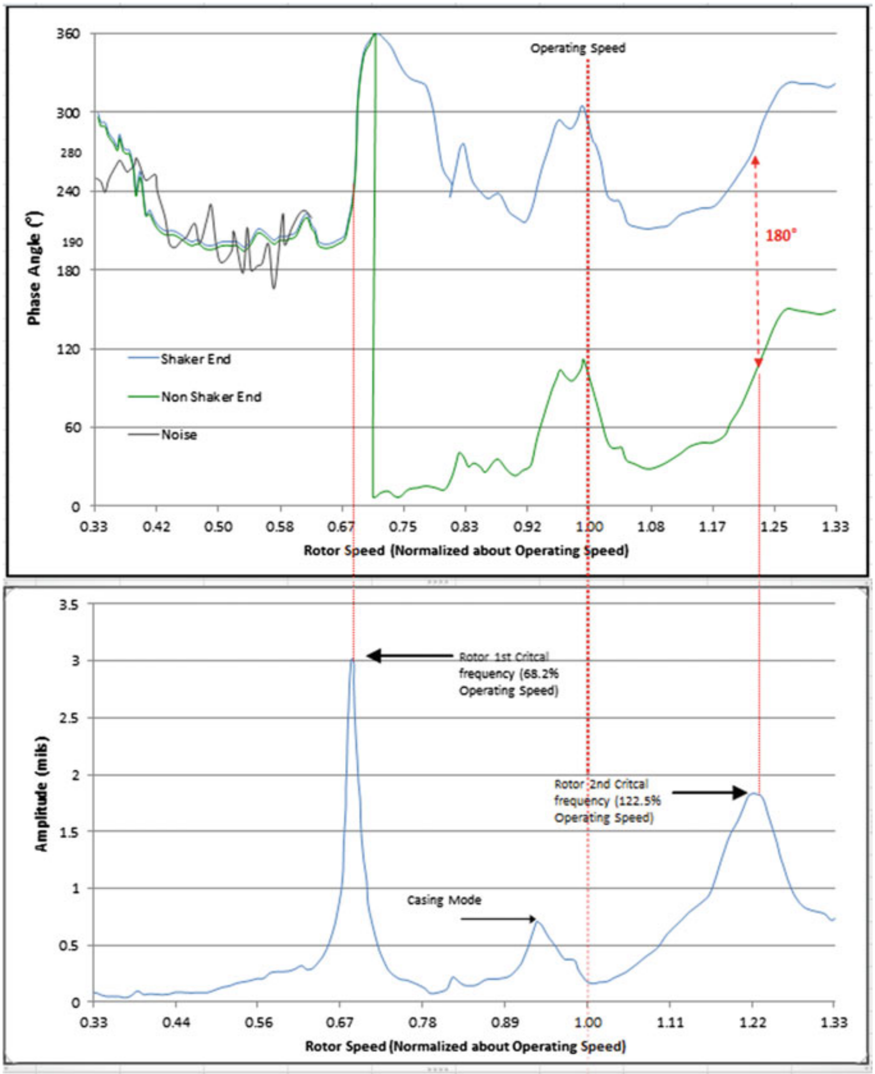

Fig. 3.16 An example of rotor critical frequencies of LP turbine measured by electrical shaker

where

k = stiffness in million lbf/in or N/mm
me = unbalance, in-lb or mm-kg
f = rotational frequency, Hz
x = measured response, mils p-p or Microns p-p

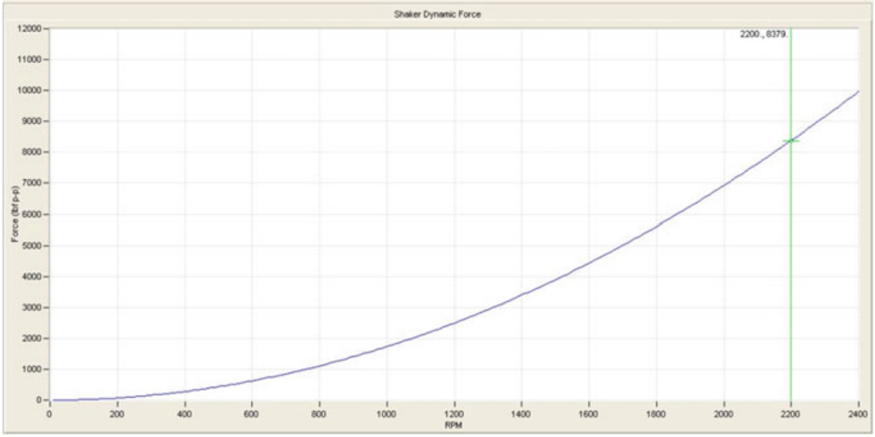

Fig. 3.17 An example of shaker force versus shaker speed

Using Eqs. 3.2a or 3.2b, pedestal stiffness can be calculated at any shaker speed as shown in Fig. 3.18. Electronic noise of the test instrumentation dominates the stiffness measured in the lower speed range (0–600 RPM) since the shaker imbalance forces are too small to overcome the noise. When the shaker speed picks up above 600 RPM and when it reaches between 700–1000 RPM, pedestal static stiffness usually stabilizes. The errors in pedestal stiffness estimation could be due to (i) noise in measured signals, (ii) noise emanating from weak structural members and joints, and (iii) conversion errors from acceleration to response. Any of the above could impact the accuracy of the estimated pedestal stiffness values.

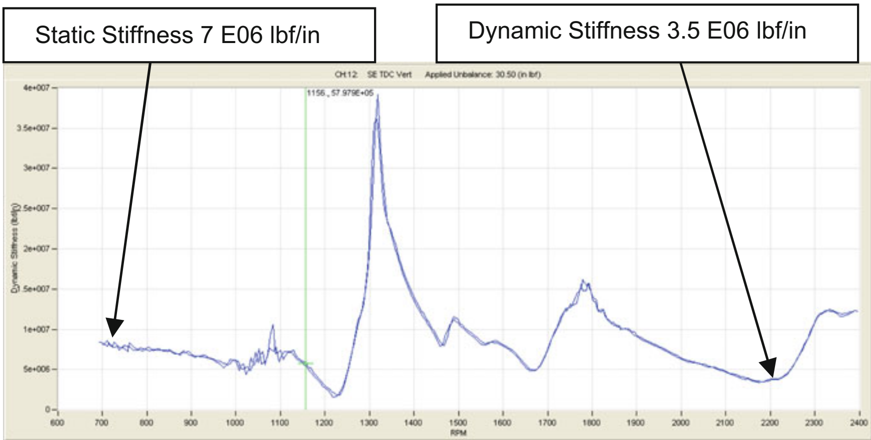

Fig. 3.18 Example of measured LP bearing vertical pedestal stiffness plots

Stabilized stiffness in the 700–1000 RPM range is referred as, "***static stiffness***" (due to hard pedestal springs) of the pedestal and is used to compute the U-rotor frequency. Stiffness corresponding to the S-rotor frequency is referred to as "***dynamic stiffness***" (due to soft pedestal springs). Pedestal stiffness in the vertical direction has always been less noisy compared to those measured in the horizontal direction. This is because the rotor rests at the bottom dead center of the bearing cone in the vertical plane while the rotor has no contact with the bearing cone in the horizontal direction. As a result, air gap between the rotor and the bearing clearance produces noisier spectrums in the horizontal or lateral plane.

Measured pedestal stiffness values by shaker tests can be applied in rotor dynamic models to compute the first and second rotor critical frequencies. For Type-B turbine designs or similar structures, only S-rotor vertical frequency drops toward the operating frequency when pedestals degrade. However, minor change in U-rotor frequency can be observed. The best design practice is to have the S-rotor vertical frequency well above the 110% of operating frequency.

Depending on the size of the turbine structure, the measured *static stiffness* of Type-B pedestals could vary anywhere between 7 E06 and 14 E06 Lbf/in in the vertical direction. Corresponding *dynamic stiffness* values of pedestals are usually about half of static stiffness. A list of measured pedestal stiffness values for nominal, degraded, and stiffened design conditions are provided in Table 3.1. It can be clearly inferred from the table that only dynamic stiffnesses provide symptoms of pedestal degradation.

Table 3.1 Measured static and dynamic pedestal stiffness of the LP turbine in vertical direction, $\times\ 10^{-6}$ Lbf/in

Bearing supports	Nominal		Degraded		Stiffened	
	Static	Dynamic	Static	Dynamic	Static	Dynamic
Figure 6	7.0	3.5	7.0	1.2	7.0	4.0

As seen in Table 3.1, for degraded pedestal condition, dynamic stiffness had reduced significantly. The dynamic pedestal stiffness measured after the pedestals were stiffened provided slightly higher dynamic stiffness values than their original design. A series of struts were applied to stiffen the LP bearing pedestal supports are shown in Fig. 3.19. Various strut positions can use to stiffen the pedestals. They are (a) direct vertical, (b) A-frame type with two struts about 45° on both sides of the bottom dead center of the bearing cones, (c) combination of direct vertical and A-frame struts.

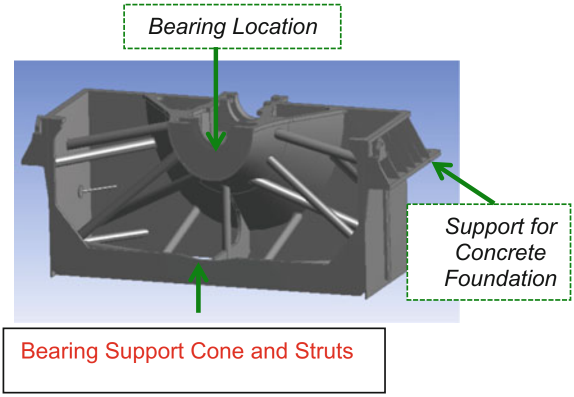

Fig. 3.19 Stiffening of bearing pedestals by vertical and/or A-frame type struts (courtesy of Siemens)

Hiss et al. [10] performed elaborate testing for similar steel supported flexible bearing pedestals to understand the influence of the coupled motions in other degrees of freedom over the direct stiffness measured in the vertical and the horizontal planes. Measured harmonic response functions (HRF) representing the stiffness matrix of the pedestal system were obtained. HRF is a populated matrix that consists of both diagonal terms that represent direct stiffness and the non-diagonal terms representing the cross-coupled stiffness due to other degrees of freedoms. The measured HRF stiffness matrix indicated that the off-diagonal stiffness values were anywhere from 3 to 5 times smaller than those of the diagonal values measured. This study corroborates with the traditionally established single degree of freedom pedestal stiffness (similar to those obtained in shaker tests) values that were typically applied in rotor dynamical calculations.

References [11,12] have reported and documented studies related to support structural characteristics.

Shaker Tests in a nutshell:

- Static stiffness of bearing support pedestals was always higher than the dynamic stiffness.
- Dynamic stiffness is measured approximately 50% of the static stiffness for nominal pedestal designs.
- Static stiffness variations between the nominal and the degraded pedestals were minimal.
- Measured dynamic stiffness for the degraded pedestals varied anywhere between 25 and 75% of the nominal value for the LP (Type-B) turbines tested. One example is shown in Table 3.1.
- Based on 100 tests, the reduction of dynamic stiffness is consistent with the drop in S-rotor frequencies for the degraded pedestals.

3.8 Calculation of Lateral Frequencies Using Shaker Data

- ***General***
  - The shaker test configuration (including rotor and pedestals only) with the operating configuration can be simulated in a rotor dynamic model for rotor frequency calculations.
- ***Calculation Data***
  - The calculation data should represent the complete shaft system and stiffness of bearing pedestals. This data set is capable of simulating shaker test configuration to match the rotor and pedestal frequencies measured. For the operating configuration, speed-dependent fluid-film dynamic coefficients must also be included in addition to the data used to simulate shaker test configuration.
- ***Calculation Results***
  - Rotor dynamic calculations provide rotor natural frequencies and the corresponding mode shapes (U- and S-modes); see Fig. 3.20. Commercial rotor dynamic codes, in general, may not have the modeling capability of the complex pedestal supports that enable calculating pedestal stiffness. So, finite element models should be developed as described in Sect. 3.6.1

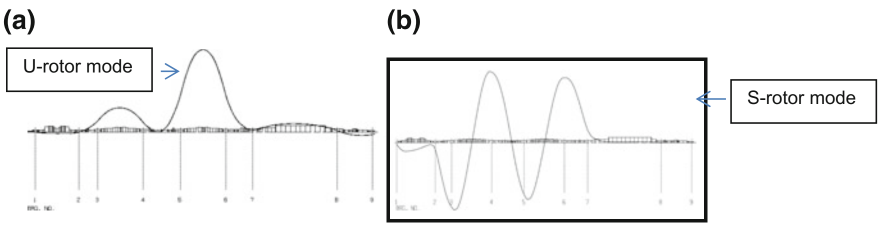

Fig. 3.20 Typical rotor U- and S-mode shapes

3.8.1 Mode Shapes of LP Rotor Systems Connected with an Extension Shaft

Some turbine configurations have the LP rotors connected with extension shafts or sometimes called, "jack shafts" (JS) between them as shown in Fig. 3.21. The JS typically splits the LP rotor conical modes into two. The first JS mode (in-phase) is described as a partially developed LP rotor conical or second mode as shown in Fig. 3.22. The second JS mode (out-of-phase) generates the fully developed second LP rotor mode as shown in Fig. 3.23.

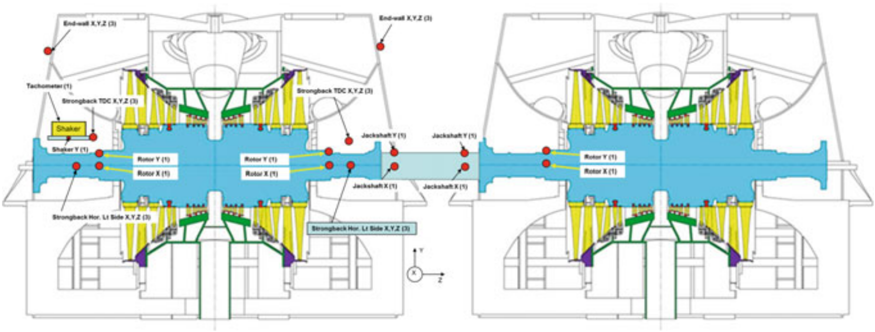

Fig. 3.21 Two LP rotors are connected by a JS

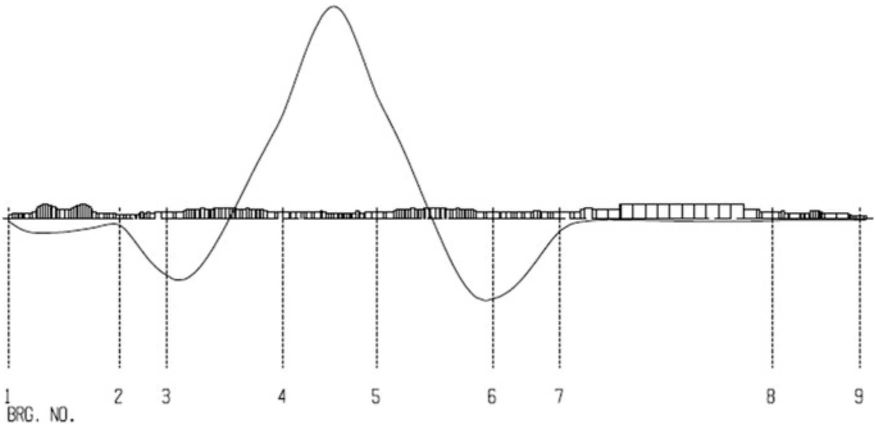

Fig. 3.22 JS (in-phase) with partially developed LP rotor second critical speed

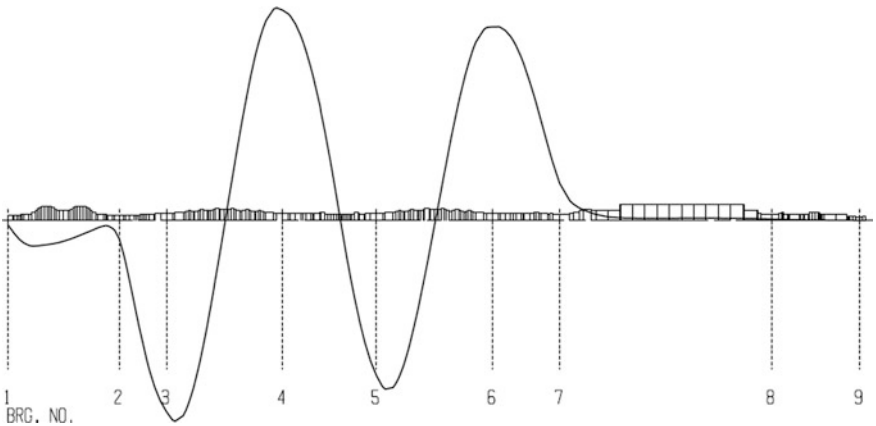

Fig. 3.23 JS (out-of-phase) dominant fully developed LP rotor second critical speed

3.8.2 Finite Element Model and Results

- Finite element models can be developed including rotor, casing, and pedestal for the LP turbine as shown in Fig. 3.24. Mode shape results show that the bearing cones on either end of the turbine are moving 180° opposite to each other confirming rotor conical mode predominantly in the vertical direction. Some call this mode as "reverse vertical." Analysis of the mode shape indicates that stiffeners are required in the vertical direction to stiffen the pedestals. Detailed finite element calculations help choosing suitable locations where the stiffeners can be applied.

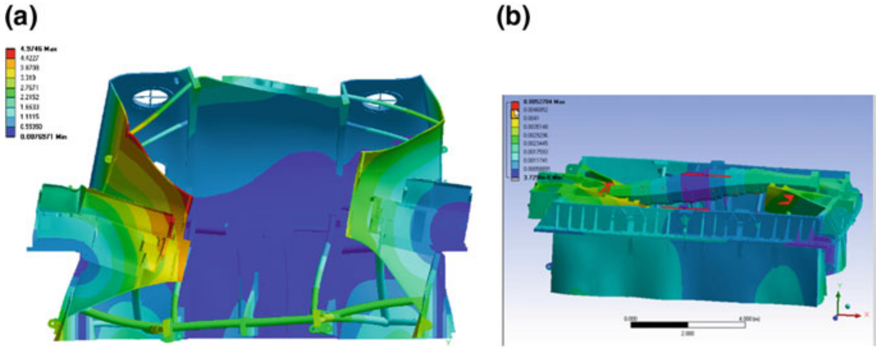

Fig. 3.24 Finite element simulation of S—rotor mode shape (courtesy of Siemens)

- Calculation Report
  - In general, the report should contain relevant data of the unit, configuration of the shaft system (including total weight, bearing information, direct pedestal stiffness values), and the calculation results.

3.9 Evaluation of Pedestal Degradation Condition

3.9.1 Primary Evaluation

If the S-rotor frequency were tested above 110% of the operating frequency, then the pedestal condition is considered as "nominal" and pedestals are deemed healthy.

If the S-rotor frequency were tested below 110% of the operating speed, then the LP pedestal condition is considered as "degraded." This means that the health condition of LP pedestals has deteriorated since installation.

3.9.2 Secondary Evaluation

Static stiffness of pedestals hardly changes due to pedestal degradation, whereas dynamic stiffness drops due to degradation. Typically, pedestal dynamic stiffness is approximately 50% of static stiffness for “nominal” designs. Significant reduction of dynamic stiffness of pedestal would also indicate the S-mode rotor frequency dropped from the nominal design.

3.9.3 Stiffening of Flexible Pedestals

If the tested pedestals were found degraded, stiffen the pedestals. Stiffening can be done either with a single strut in the vertical direction or A-frame type struts or a three-strut as shown in Fig. 3.19. The optimal and stable stiffening condition is a three-strut stiffening design. Bode plots or the static deflection shape (SDS) plots obtained during shaker test or the Operation Deflection Shape (ODS) obtained at the rated RPM of the unit would provide the direction in which stiffening be most effective. Supplier or the supplier’s authorized contractor is in a better position to determine the suitable stiffening configuration.

3.10 Recommended Guide Lines (GL) to Assess Safe Operational Condition of Flexible Bearing Pedestals

3.10.1 Primary Assessment

(a) For a category of LP steam turbine designs with flexible bearing supports (Type-B), pedestal degradation can be assessed by measuring the S-rotor frequencies and comparing them to the original design. When S-rotor frequency is tested below 110% of OS, the pedestals are considered degraded.
(b) Historical mechanical over speed test data (if over speed limit of 110% of the OS can be achieved) may sometimes help identifying the S-rotor frequencies. Oftentimes, historical bode plot data sets may not be consistent with one another due to the variations of rotor balance quality and rotor positions between maintenance outages. So, shaker tests should be considered for confirmation of frequencies in evaluating pedestal degradation. If S-rotor frequencies are not identified below 110% of OS through shaker tests, the pedestals are considered “nominal.” No degradation might have occurred.
(c) If S-rotor frequencies were tested between 105% and 110% of OS, tracking of the S-rotor frequencies at all subsequent scheduled maintenance outages is recommended to make sure that S-rotor frequencies do not drop below 105% of OS through shaker testing. In addition, continuous seismic vibration monitoring

is recommended per ISO 20816-2 [13]. Increase in seismic vibration levels could accelerate the pedestal degradation process.

(d) If S-rotor frequencies reach 105% of OS, it is recommended to move the S-rotor frequencies up and above 110% of OS by stiffening the pedestals. It is not possible to determine the pace of degradation and the associated risk from this point on. Under those circumstances, it is also recommended to limit the seismic vibration levels below 20816 C/D levels until the pedestals are stiffened that moves the S-rotor frequency above 110% of OS.

(e) If S-rotor frequencies are tested between 100 and 105% of OS, the pedestals are considered to have degraded to the extent that they pose high risk of operating the machine any further. At that point, mechanical inspections are recommended as a first measure to investigate damages and repair them as necessary. If inspections were to prove inconclusive or did not indicate any clues leading to damages, it is recommended to stiffen the pedestals immediately.

If stiffening option is postponed at this stage, it is recommended to continuously monitor bearing structure seismic vibration levels and limit them below 20816-2 C/D levels by balancing the rotor; in addition, continuous phase angle monitoring is required to understand the pace of degradation. Typically, 3–4° phase angle change in a 24 h span is considered that the pedestal degradation is worsening.

3.10.2 Secondary Assessment

Compare the measured dynamic stiffness (corresponding to the S-rotor frequency) with the nominal design value; see Fig. 3.18. This assessment mostly complements the primary frequency data when the data is relatively noise-free. It is recommended to compare dynamic stiffness as designed versus degraded condition to understand variations over the period of the service of the unit.

3.10.3 Inspections

Generally, inspections of the affected pedestal parts and assembles are recommended. With the complex structures discussed here, there may be challenges to get into intricate areas and capture defects or physical damages. When inspections proved inconclusive, it is recommended to stiffen the pedestal structures. There are methods to stiffen pedestal structures based on tests and analysis. One example of commonly applied stiffening methods is shown in Fig. 3.19. Post-stiffening shaker test is required to confirm how far the S-mode rotor frequency has increased after the pedestals were stiffened.

3.10.4 Other Influences

Listed below are some of the known turbine issues that could increase pedestal seismic vibration levels. Pedestal degradation could occur if seismic vibration levels continuously stay at or increase well and beyond the ISO 20816 C/D limits.

3.10.5 Seasonal Changes in Condenser Pressure

Seasonal changes in condenser backpressure can influence the seismic vibration changes particularly in flexible bearing pedestals. Between fall and spring months (October through March in USA), condenser water temperature gets cooler; as a result, condenser pressure drops with cooler water circulation. In that condition, the pedestal seismic vibration increases. Whereas the opposite trend (lower seismic vibration levels) has been observed during the summer months (April through September in USA) when the condenser pressure reaches higher with increased circulating water temperature. Consequently, the seismic vibration levels drop during the summer months. Figure 3.25 provides the seasonal trends of a representative flexible bearing pedestal (Type-B) vibration in a steam turbine plant.

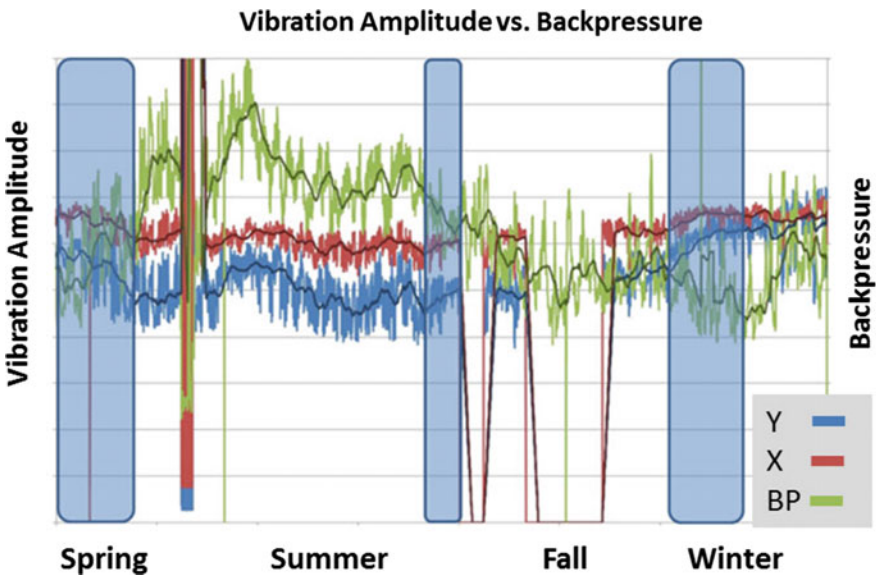

Fig. 3.25 Typical seasonal changes of pedestal vibration

3.10.6 Influences Due to Electrical Grid Events

A grid event in the power plant could increase the pedestal seismic vibration levels as well. Depending on the intensity of grid event, a step change in pedestal and rotor vibrations may be observed after the grid event. No pedestal degradation was observed or reported entirely by grid events.

3.10.7 Influences Due to Grout Degradation

Grout is a powdery substance (aggregate of cement, water, and other chemicals) filled tight in the space between the base plate and the concrete surface of the foundation for positive turbine casing contact. In some cases, epoxy is pumped to fill the space as well. Over long periods of service, the grout wears away opening clearances between the base plate and the concrete surface. As a result, pedestal seismic vibration levels may increase leaving with “loose grout” condition. Based on a limited number of inspections, it is considered that grout damage is unlikely to be a contributor to pedestal stiffness decline.

3.11 Closure

Pedestal degradation of a category of flexible bearing steel supports (Type-B) in medium and large nuclear steam turbine applications (60 Hz/1800 RPM machines) was discussed. Based on several bearing support pedestal tests, reduction of second rotor critical speeds (S-mode or conical mode) from original design provided symptoms of pedestal degradation. These findings were also confirmed with the measured reduction of dynamic stiffness in the degraded pedestals. Shaker tests can help identifying rotor critical frequency drop on any rotor systems. Guidelines were developed to identify various levels of pedestal degradations and associated actions for steam turbines in Sect. 3.7.

Two different pedestal stiffness values (static and dynamic) are required to calculate the rotor first and the second mode frequencies. In general, dynamic stiffness is about half the static stiffness for the steam turbine structures reported. However, tests are required to validate the ratio of static and dynamic stiffness findings for other pedestal support structures or other configurations.

References

1. Subbiah R (2015) Evaluation of pedestal stiffness variations in steel supported structures for steam turbines In: Proceedings of 9th IFToMM international conference on rotor dynamics held in Milan, Italy, September 2014. Springer International Publishing, Switzerland, pp 2149–2164
2. Subbiah R (2012) On the determination of bearing support pedestal conditions using shaker testing. In: Presented in the IMechE conference, London, UK, Sept 2012. pp 99–111
3. Nuclear News (1993) September 1993, pp 43–61
4. Malcolm Leader (1984) Introduction of rotor dynamics of pumps without fluid forces. In: Proceedings of the 1st international pump symposium, Texas A&M. pp 133–146
5. Vance J (1988) Rotor dynamics of turbo machinery. Wiley
6. Subbiah R, Bhat RB, Sankar TS (1985) Response of rotors subjected to random support excitations. J Vib Acoust Stress Reliab Des
7. Rouch KE, McMains TH, Stephenson RW, (1989) Modeling of rotor-foundation systems using frequency-response functions in a finite element approach. ASME J 157 pp
8. Nicholas JC, Barrett LE (1985) The effect of bearing support flexibility on critical speed prediction. In: Presented at the 40th annual meetings, 6–9 May 1985, Paper No. 85-AM-2E-1
9. Nicholas, John (1999) Utilizing dynamic support stiffness for improved rotor dynamic calculations. In: Proceedings of the 17th [i]nternational modal analysis conference, vol 3727. pp. 256–262
10. Florian H, Gerta Z (2014) Updating of rotor models by means of measured frequency response data. In: Presented in ASME technical conference turbo expo, Dusseldorf, 14–20 June
11. Kirk RG, Gunter EJ (1972) The effect of support flexibility and damping on the synchronous response of a single mass flexible rotor. ASME J Eng Ind 94(1)
12. Lund JW (1965) The stability of an elastic rotor in journal bearings with flexible, damped supports. ASME J Appl Mech 87(Series E):911–920
13. ISO 20816 Mechanical vibration—measurement and evaluation of machine vibration—part 2: land based gas turbines, steam turbines and generators in excess of 40 MW, with fluid-film bearings and rated speeds of 1500 r/min, 1800 r/min, 3000 r/min and 3600 r/min”

Chapter 4
Fluid-Film, Steam and/or Gas Seal Influences on Rotor Dynamics

4.1 Introduction

Thus far, the complex fluid-film bearing modelling and analyses were deferred to make technical discussions simpler. Before we get into the core subject of bearing dynamics, it is important to be aware of the fact that a variety of fluid-film bearing configurations were utilized in turbo-machinery applications for various reasons. For example, cylindrical bearings were chosen for better load bearing capability. However, they were prone to oil whirl in certain operating conditions leading to rotor instability. Consequently, tilting pad bearings became popular. Multiple-pad configurations (such as 2, 3, 4, 5 and 6 pads) were, therefore, developed to cater to specific needs. Thus, tilting-pad bearings increasingly found their place in modern turbo—machinery.

Other bearing types such as elliptical, groove and damper bearings were also considered for cost and other specific operating reasons. Since fluid-film bearing dynamics influences and addresses most turbo-machinery vibration issues, it is worthwhile to get into some details of fluid-film bearing modeling and calculations for familiarity. To this end, Reynolds linear mathematical equations are utilized to derive oil film dynamic coefficients. Special bearing types are introduced to provide other options to solving machinery problems. A list of common bearing issues, symptoms observed and potential solutions, is provided at the end.

4.2 General

In Chap. 3, pedestal stiffness influences on rotor frequencies were exclusively discussed. This chapter is devoted to oil-film bearing dynamics. An example LP rotor, mounted on various support configurations, is used to demonstrate support influences on rotor frequencies as listed in Table 4.1.

R. Subbiah and J. E. Littleton, *Rotor and Structural Dynamics of Turbomachinery*,
Applied Condition Monitoring 11, https://doi.org/10.1007/978-3-319-73296-1_4

The example LP rotor weighs 37,700 kg and is supported on two 380 mm (15 inch) cylindrical fluid-film bearings. The static and dynamic pedestal stiffnesses used are 12 million (2.1 million N/mm) and 6 million (1.05 million N/mm) Lb_f/in respectively.

Level 1—***Rigid condition*** involves Rotor + Rigid support (directly mounted on concrete foundation)
Level 2—***Flexible condition*** involves Rotor + Flexible Steel Pedestal supports
Level 3—***Most flexible condition*** involves Rotor + Flexible Steel Pedestal supports + Oil film bearings

Table 4.1 Rotor frequencies in RPM for different support conditions

Support conditions	First bending	Second bending
Level 1 − Rotor + Rigid support	**2301**	**5310**
Level 2 − Rotor + Pedestals	**1454**	**3101**
Level 3 − Rotor + Pedestals + Oil film bearings	**1300**	**2677**

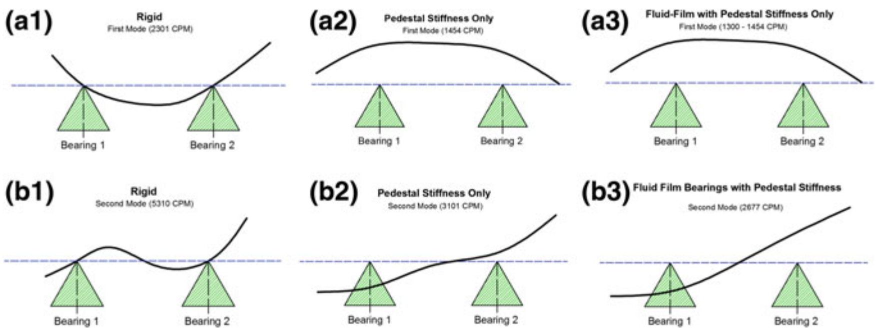

Fig. 4.1 **a** First Mode of rotor on various support conditions (use uploades figures). **b** Second Mode of rotor on various support conditions (use uploades figures)

Figure 4.1a1–a3 illustrate the first rotor bending natural frequency variations for the three levels of support (from left to right) respectively. Figures 4.1b1–b3 similarly illustrate the rotor second bending frequency variations under the same support conditions. The rotor configuration with oil film bearing + pedestal stiffness provides the most flexible condition with the lowest rotor frequency.

In addition to lowering the overall support stiffness, fluid-film bearings provide the single most source of damping for a rotor train and is mainly responsible for reducing peak response amplitudes at critical speeds during start-up, coast down and at rated operating conditions. The fluid-film dynamic characteristics and their influence on rotor frequency and vibration are discussed exclusively in this chapter.

Bearings are primarily chosen for the load they support, the temperature they generate and the vibration they sustain for continuous operation of a rotating machinery. Majority of rotors applied in steam, gas and industrial turbines, generators and exciters, are supported by fluid-film bearings. In addition to load, temperature and vibration considerations, rotor stability is another important phenomenon that needs to be considered when selecting a bearing.

Bearings are broadly classified as follows:

4.3 Bearing Types

- Contact Type
  - Ball Bearings
  - Roller Bearings
- Non-Contact Type (Fluid Film Type)
  - Radial Bearings—Maintain rotor radial position
    - Hydro-static—Operate at constant oil pressure
    - Hydro-dynamic—Operate at variable oil pressure
  - Axial or Thrust Bearings—Maintain rotor axial positions and balance the thrust developed by the operating fluid medium of the turbine

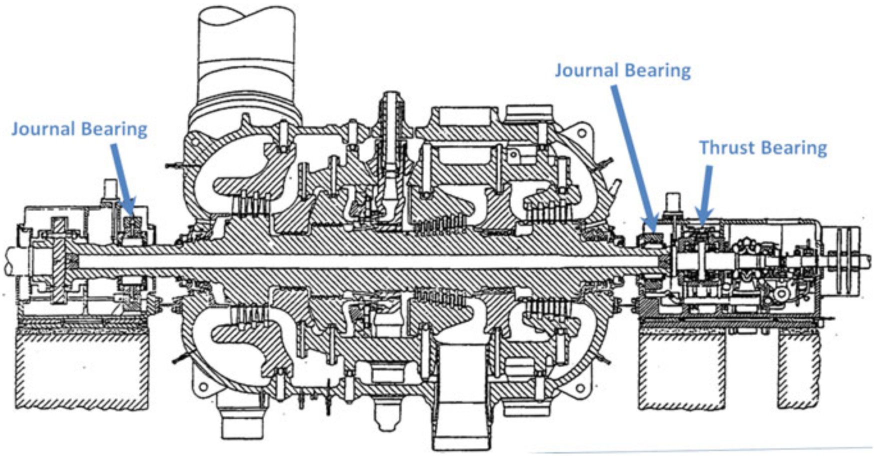

Fig. 4.2 Bearing locations in a turbine

- Levitated Bearings
  - Magnetic Bearings

The bearings applied in turbo-machinery, in general, are to maintain the radial and axial positions of rotors in a very precise manner within their bearing casings. As illustrated in Fig. 4.2, journal bearings support rotors radially whereas axial or thrust bearings support rotors axially. Since non-contact type bearings exhibit a variety of rotor dynamic behaviors than those of contact-type bearings, the focus is centered on the non-contact type or fluid-film bearings only in this chapter.

4.4 Capabilities of Various Bearing Types

The bearing types used in turbo-machines and their unique qualities are discussed here.

4.4.1 Fluid-Film Bearings

- Hydro-dynamic bearings support heavy loads and last longer (low maintenance and long service life)
- Hydrostatic bearings operate at constant pressure and are applied in machine tools and as oil lifts in small, medium and large turbo-machinery
- The journal rises inside the bearing shell in hydrodynamic bearings due to increased fluid pressures at various rotor speeds and loads
  - Hydrodynamic bearings, except for the tilt-pad type, exhibit cross coupled effects (A force applied in the Y-direction has direct response on the Y-direction and also causes coupled response in the Z-direction)
- Squeeze film bearing is a special type of hydrodynamic bearings that provides additional damping due to the "bearing-inside-a-bearing" configuration. This bearing is a special design that operates well for a particular operating condition only where other bearing types fail. However, this type may not be operable outside the specific operating zone for which it was designed.

4.4.2 *Rolling Element Bearings (Ball and Roller)*

- Compact design that provides good dimensional stability because the ball or rollers are always in contact with the rotor they support
- No cross-coupling effects
- Provide early warning sign of any impending failure
- Used as main bearings in all aircraft engines because of reliability considerations

4.4.3 *Magnetic Bearings*

- Journal forces can be controlled
- No cross coupling
- Very low losses
- Low load capability; hence their usage is restricted to small turbines/machines
- Need backup (fluid-film) bearings in case active control fails

Among the fluid-film bearing families, the following types find common usage in turbo-machinery

- Plain Cylindrical or circular
- Partial Arc Type
- Elliptical or Lemon Type
- Multi-Lobe Type
- Pressure dam Type
- Tilting pad Type
- Squeeze Film Damper
- Magnetic Type
- Multi-pad special bearings

4.5 Plain Cylindrical Bearings

An example of plain cylindrical bearing configuration is shown in Fig. 4.3. In this configuration, the clearance between the journal (rotating component) and the bearing (stationary part) is constant around 360°. These types of bearings are used commonly in older units and in some smaller size (diameter) bearing configurations (usually under 3” (75 mm) diameter) such as steady-rest or laboratory bearings where the journal floats within a copper ring or a floating seal.

Plain cylindrical or circular bearings also fall under the category of “fixed arc” type, which is attributed to active loaded arc they support.

Fig. 4.3 Plain cylindrical bearing

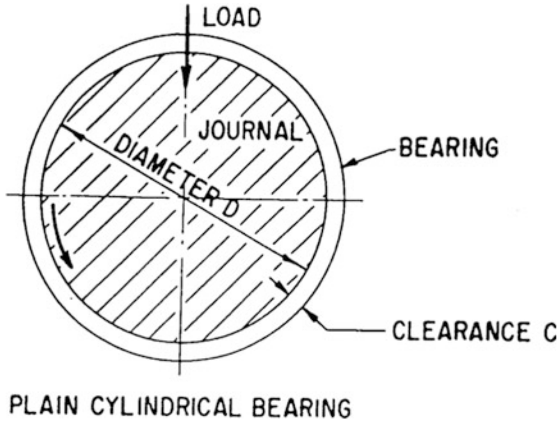

4.5.1 Hydrodynamic Film Formation

The hydrodynamic fluid-film pressures developed inside a bearing vary with the journal speed, viscosity, film temperature, load and oil density. Typical pressure distributions in fluid-film bearings are shown in Fig. 4.4a, b respectively for counterclockwise and clockwise journal rotations. The speed-dependent fluid-film pressure generates distinct dynamic stiffness and damping coefficients at each speed. In general, the pressure distribution for all types of fluid-film bearings are parabolic in shape. The maximum resultant fluid-film pressure is generated at the minimum oil film zone.

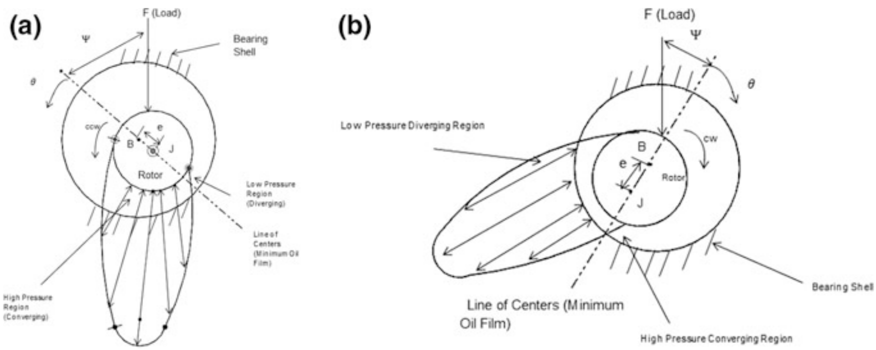

Fig. 4.4 Hydrodynamic pressure distribution in an oil-film bearing

Let us assume that air is filled in the space between the journal and the shell. It is conceivable that the journal tends to move straight down inside the clearance space. Instead of air, if the clearance space is filled with oil, the oil viscosity tends to resist the journal taking a straight path down. Instead, the journal takes an angular path with respect to the vertical load line. The angle between the vertical load line and the line connecting the centers of the journal and the bearing is called, "Attitude Angle" and the straight line that connects the centers of the journal and the bearing is "Attitude Line" as illustrated in Fig. 4.4a, b. This line moves away from the vertical load line at an angle, which depends on the magnitude of the applied load, speed of the journal, oil temperature and the viscosity of the oil film. Depending of the direction of rotation of the journal, the attitude angle ϕ and the minimum oil film thickness move clockwise or counterclockwise. The locus of the journal at an instant (within the clearance space) can be defined by attitude angle ϕ with respect to the vertical load line. The attitude line moves as load increases as illustrated in Fig. 4.5.

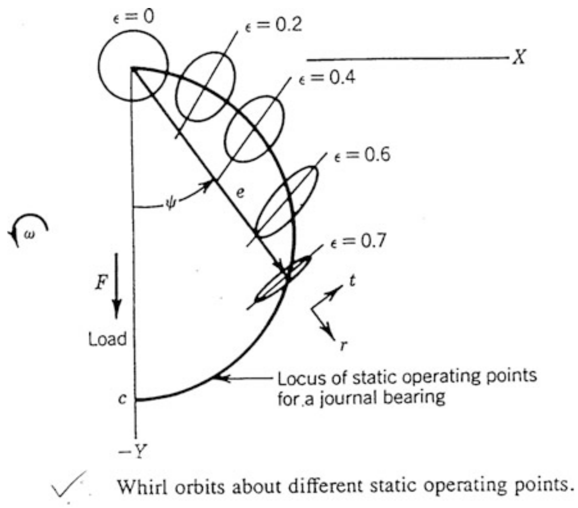

Fig. 4.5 Variation of orbital shape at various loading conditions [4]

4.5.2 Journal Position in Oil Film

As shown in Fig. 4.5, the locus of the journal varies within the bearing clearance circle. For the condition, where the bearing and the journal centerlines coincide (eccentricity $\varepsilon = 0$), the rotor executes a circular whirl. When the load on the journal increases causing the journal to move on the clearance circle, line of centers bear an angle ϕ called, "attitude angle" with the load line. At any loading condition, the position of the journal can be defined by ε and ϕ. As can be seen, when bearing load increases, the orbital shape of the journal also varies. At the extreme condition when $\varepsilon = 1$, the journal touches the bearing shell at the bottom. To avoid this condition, heavily loaded bearings have oil lift systems that supply oil at high pressures lifting the journal up at lower operating speeds. Depending upon the direction of rotation of the journal, the attitude angular positions change as shown in Fig. 4.4a, b.

4.5.3 When Does a Bearing Need an Oil Lift?

Oil film pressure is generated mainly by the rotation of the journal; however, it also depends on oil viscosity and oil temperature as well. Oil is supplied at nominal pressures between 12 and 15 psi (in certain abnormal cases pressures may vary as low as 8 psi and as high as 26 psi) that fills the clearance space between the journal and the bearing shell. At low journal speeds, very thin oil film sustains the rotor load and this condition is called "Boundary Lubrication" as shown in Fig. 4.6. The region of boundary lubrication has more friction compared to the condition of the lifted journal at increased speeds. The dynamic fluid pressure developed in the bearing at low journal rotation barely keeps it sufficiently away from the bottom of the bearing shell. As a result, the oil film temperature is high at this journal condition.

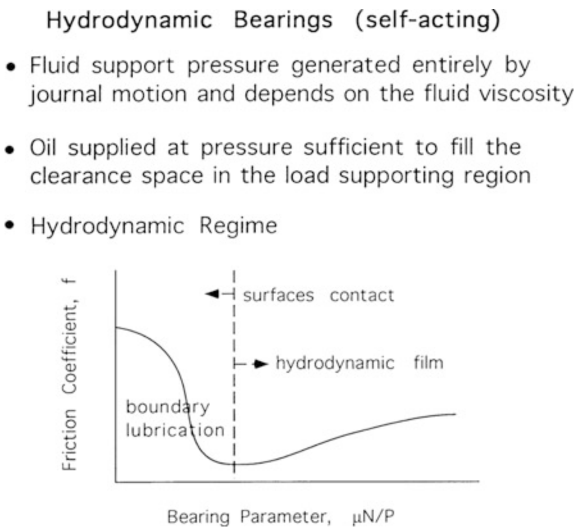

Fig. 4.6 Film formation versus loading condition

A rule of thumb for turbo-machinery bearings is that dynamic film develops at speeds approximately 600 RPM and above to sufficiently lift the journals away from the shell. Between 10 and 600 RPM, the journal mostly stays slightly above the thin boundary film. Again, this speed range, where dynamic film develops, is dependent on the load that the bearings carry. Thus, thin static film at low speeds may not be able to sustain heavy loads; for example, for 1500/1800 RPM turbo-machines, LP journals run the risk of operating at the boundary film frequently. To address this condition, oil lifts are installed to move the journals up, thus protecting the journal surfaces and the bearing babbitt areas as well. Oil lifts are activated starting from zero RPM of the rotor and up until 600 RPM (1000 RPM on certain high-speed turbo-machinery) for the formation of sufficient hydrodynamic wedge to support the rotor load during unit startup. Similarly, while the unit coasts down on speed, lift oil is activated at around 600 RPM.

4.5.4 Partial-Arc Bearings

Partial-arc bearings are a sub-set of plain cylindrical or circular bearings. Arc length of a typical partial-arc type is 160° at the bottom. This active arc is achieved by machining the support shell 10° below on either side of the horizontal line as shown in Fig. 4.7. The upper shell, which represents the remaining 200° arc, is relieved by a slightly eccentric bore with a different arc angle, which distinguishes this type as, “partial arc” bearing.

Fig. 4.7 Partial arc bearing

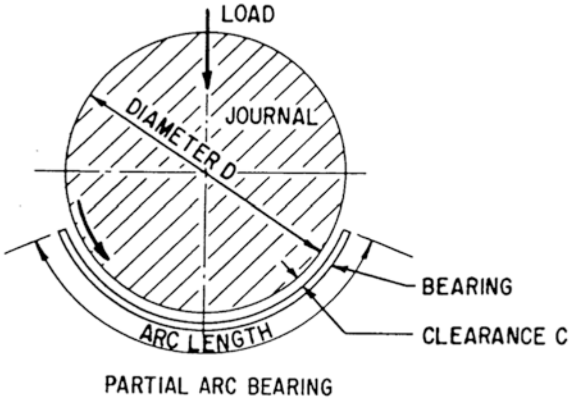

4.5.5 Viscosity Pump Bearings

- A special type of partial arc bearing is known as “Viscosity Pump” (VP) as shown in Fig. 4.8 designed by Westinghouse. The oil inlet, located at the upper half of the shell at 45° from the top dead center, has a specially machined feature that draws the oil by pump action due to pressure variation. This assures continuous oil circulation at all operating conditions. Figure 4.9 illustrates the actual VP bearing upper and lower halves. The lower half has a machined oil lift pocket that looks like a “bow tie” which is typical for Westinghouse bearing designs. Rectangular oil lift pockets are also common in other bearing

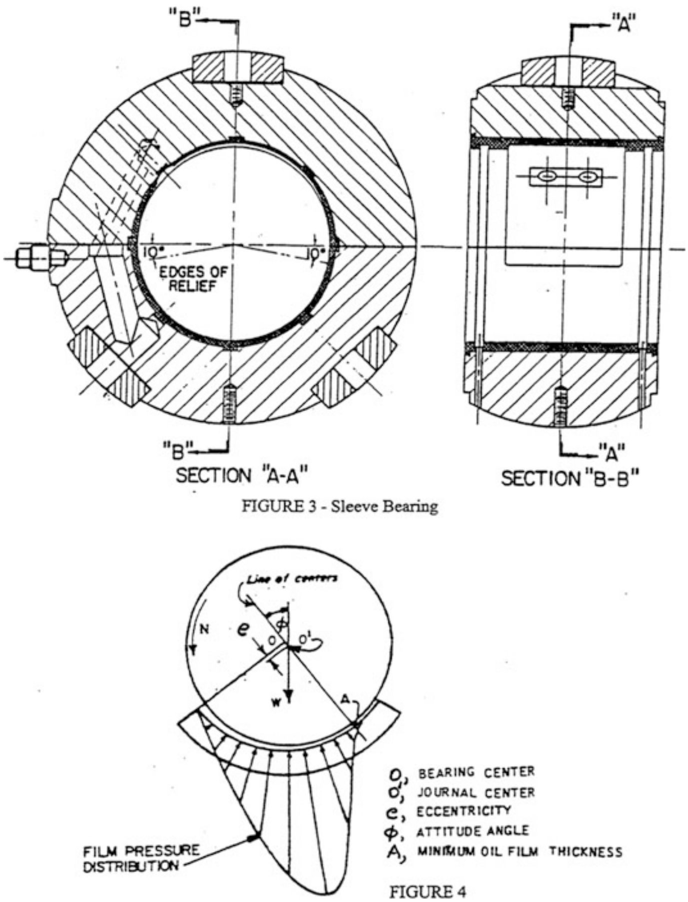

Fig. 4.8 Viscosity pump bearing

configurations manufactured by Siemens and other vendors. Oil discharges through oil drain holes that are located at the bottom of the lower half of the shell. Figure 4.10 illustrates the exploded view of the assembled parts for the viscosity type bearings.

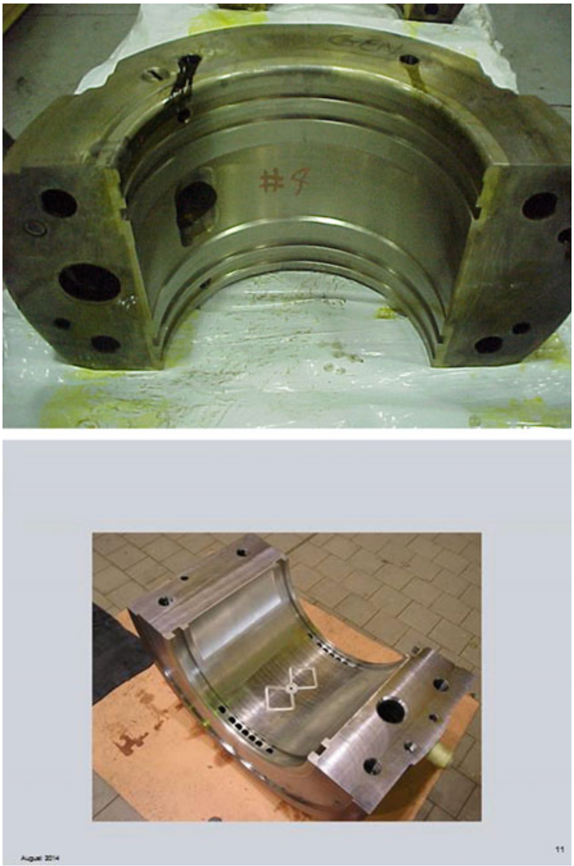

Fig. 4.9 Actual bearing halves (upper and lower) (Courtesy of Siemens)

Spherical surface profile should be maintained between the outer surface of the bearing shell and the inner surface of the stationary pedestal for the best alignment condition of a bearing. A rule of thumb is about 80% surface conformity of the mating surfaces are acceptable. This allows the rotor to be concentric to the pedestal bores. Also, note that the mating pedestal spherical bore has reliefs between the contact areas. These details could be overlooked, but are very important to maintain for good bearing alignment.

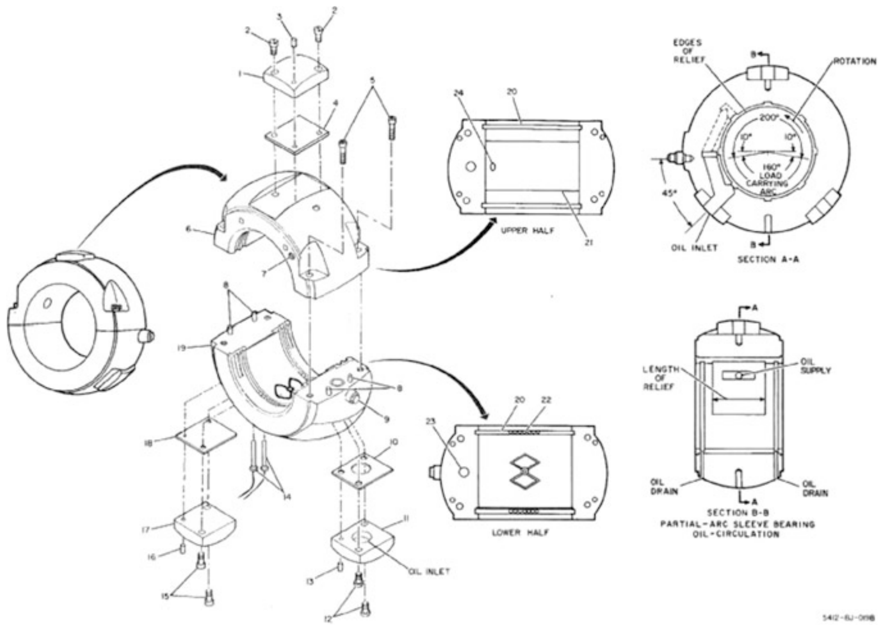

Fig. 4.10 Exploded view of a VP bearing (Courtesy of Siemens)

4.5.6 Common Construction Features on All Hydrodynamic Bearings

- The anti-rotation pin keeps the top and bottom shells in position against rotation.
- The babbitt material that is thin and soft, (Tin base alloy) offers low friction and is applied on the inner surface of the top and bottom bearing shells.
- The part of the rotor that stays inside the bearing shell is known as "journal".
- The effective length l is the axial distance between the drain holes. The effective length to diameter ratio l/D is included for the bearing dynamic coefficient calculations.
- For static bearing load calculation, typically l/D of 0.9 or higher are used.
- Smoothly machined journal (less than 16 microns) and the soft Babbitt material provide less friction and enable the journal to roll effortlessly in the oil film.
- Turbine oil to grades VG 32 or VG 46 are mostly applied.

4.6 Elliptical Bearings

Elliptical type has two dissimilar bearing clearances in the two orthogonal planes. This feature differentiates from plain cylindrical bearing, which has constant clearances all around. Typically, the clearance ratio between the vertical and the horizontal directions in an elliptical bearing is about 1:2. Reduced vertical clearance in elliptical type bearings provides more damping. The two halves of the bearing shells are assembled to circular bearing shape with inserted shim packs on either end of the horizontal joints. When the shim packs are removed, the bearing takes an elliptical shape or lemon-bore having two dissimilar clearances in the vertical and the horizontal directions as shown in Fig. 4.11.

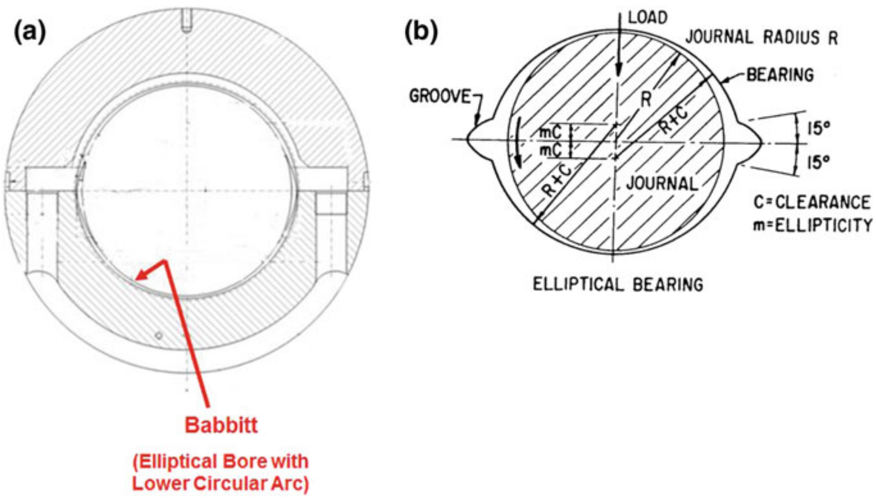

Fig. 4.11 Elliptical bearings. **a**: Siemens bedded-arc type elliptical bearing

A special type in this category is developed by Siemens and is called, "Bedded-arc" (or lower circular arc) type that has a finely machined feature with a shallow arc at the bottom. See Fig. 4.11a. This feature provides additional damping to the bearing. These bearing types can be considered for heavily loaded bearing applications where additional damping is needed to run the rotor smoothly through critical speeds during turbine startup and/or coast down and at the operating speed as well.

4.7 Axial Groove Type Bearings

An example of an axial groove type bearing is shown in Fig. 4.12 with four axial grooves. The groove feature defines the active arc of the bearing. These grooves provide oil flow discontinuity. This feature improves stability of the bearing compared to a plain cylindrical type. However, this type of bearings is limited to low load applications. Hence, they may not be preferable in medium and large turbo machinery applications.

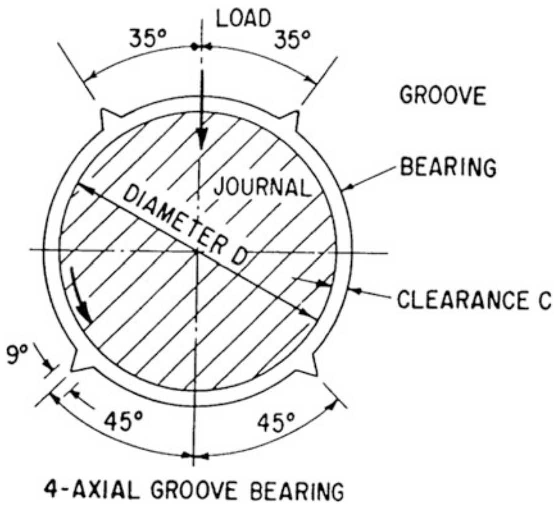

Fig. 4.12 4-axial groove bearing

4.8 Pressure Dam Bearings

The pressure dam bearing configuration is shown in Fig. 4.13. A partial groove is machined in the upper shell. The step at the end of the groove behaves like a dam that builds additional downward force. In operation, the circulating fluid is exposed to a sudden resistance at the dam, which increases local fluid pressure and applies a downward force on the journal as shown by the arrow in Fig. 4.13.

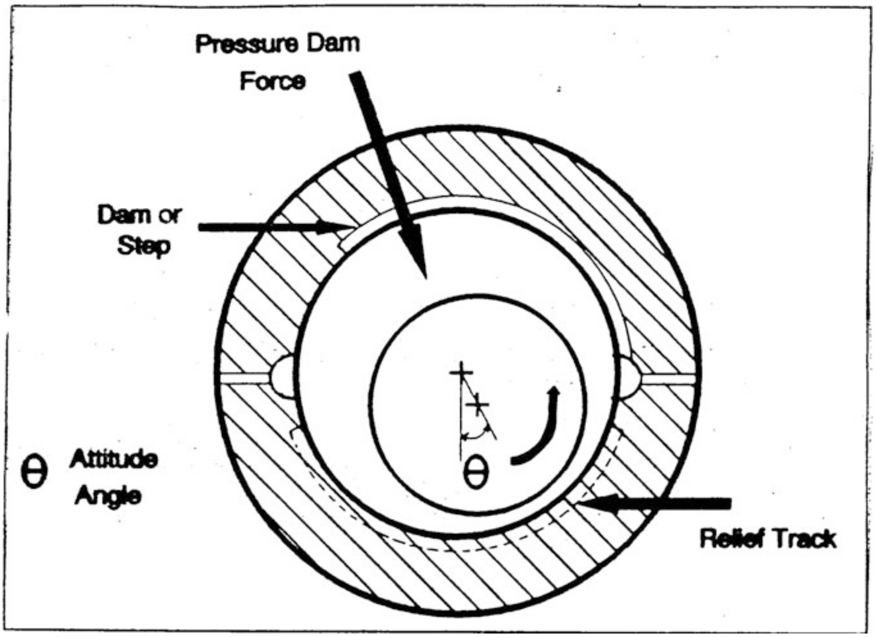

Fig. 4.13 Pressure-dam bearing

The built-in pressure applies a downward force that pre-loads the journal. A relief track machined at the bottom adds damping and can be adjusted to vary L/D ratio. Reduced L/D ratio helps increasing dynamic oil film pressure by improving damping. Both the dam and the relief track features improve rotor stability. The disadvantage of this type of bearing is that contaminants (in the circulating oil) accumulates over time and clogs the dam and the relief tracks making them ineffective.

Lobe, elliptical and pressure-dam type bearings stabilize the rotor condition when they are pre-loaded.

4.9 Tilting-Pad Bearings

The most commonly applied radial bearings in turbo-machinery are "Tilting-pad" types. In general, 4 or 5 pad bearings are common. The pads can be compared to hockey sticks that shove the ball (journal) towards the center of the bearing in all conditions as illustrated in Fig. 4.14. Hence, they are known as, "self-aligning bearings".

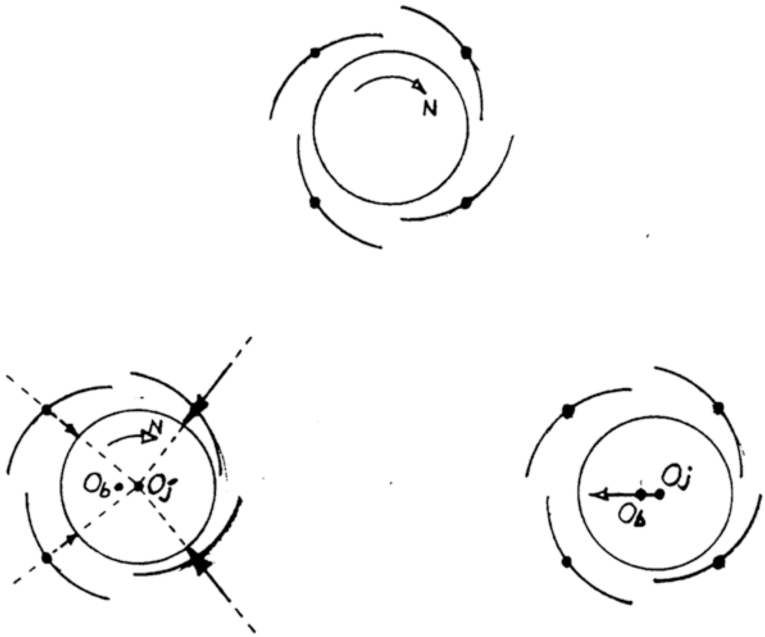

Fig. 4.14 Pads tilt and move the journal to the center

Figure 4.15 shows the cross-section of a 4-pad tilt-pad type bearing. This is the flooded type configuration that has single oil inlet (in most cases) located at the bottom and allows the oil to fill all over the bearing; hence, the name, "Flooded Type". The self-aligning feature of the pads significantly reduces cross-coupled effects, which otherwise are responsible for rotor instability known as oil whirl and/or oil whip. However, in the case of steam/gas whirl, even the self-aligned tilt-pad bearings can be driven into instability by high swirl velocity caused by high pressure differentials exist across the steam or gas seals. The self-aligning feature in pad bearings also reduces damping and the load-bearing capability compared to partial arc types. Tilt-pad types, in general, are not preferable for large and highly loaded bearings. However, more modern and advanced tilt-pad designs with added special features may have overcome the above-mentioned limitations.

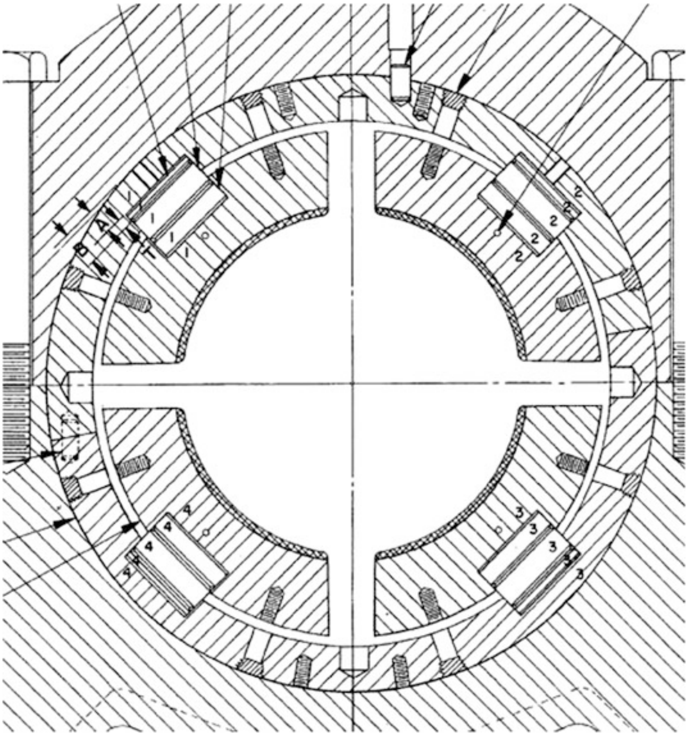

Fig. 4.15 4-pad tilt-pad bearing

4.9.1 Leading Edge Groove (LEG) Bearings

4-pad tilt pad bearing shown in Fig. 4.16 is the leading-edge bearing design (LEG) by Kingsbury. The pads are pivoted at one point on each pad that enables tilting action. Depending on the bearing manufacturers, the overhang pad length from the pivot point may change. The maximum overhang of the arc varies anywhere between 50 and 75%. It was found in older designs that the journal rode on the lightly loaded overhang pad ends located in the upper half, causing pad flutter called, "spragging". Some bearing vendors' [2] design has short arc length at the lightly loaded end to avoid pad flutter. Some others use integral pad-pivot design [3] that increases the natural frequency of the pads, which reduces spragging. Integral pivoted pad bearing configuration is shown in Fig. 4.17.

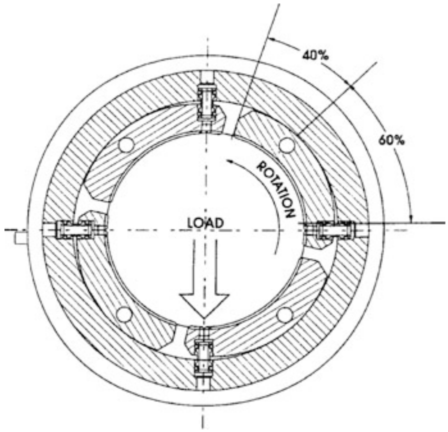

Fig. 4.16 Leading edge groove tilt-pad bearing by Kingsbury

Fig. 4.17 Flexure pivot tilt-pad radial bearing (Photo used by permission of Waukesha bearings)

The leading-edge groove bearing shown in Fig. 4.16 has oil feeds through individual oil inlets located at the leading edge of the pads. Cool oil at the inlet gets hotter when it passes across a pad and mixes with the cool oil that enters through the adjacent pad. This makes the LEG bearing operating cooler than the conventional flooded type pad bearings. Thus, LEG type bearings typically have better performance due to reduced power loss, oil flow and oil circulating temperature.

Experience shows the pad-to-pivot ratio of 3:1 reduces spragging of the trailing edge pads. In some cases, the trailing edge pad edges are taper machined to clear off the riding journal surface to avoid spragging.

Some vendors apply high-pressure spray nozzles at the leading-edge oil inlets. One such configuration is shown in Fig. 4.17.

A cross-sectional view of a bearing and journal is shown in Fig. 4.18 for a glimpse of various parts involved in a bearing assembly.

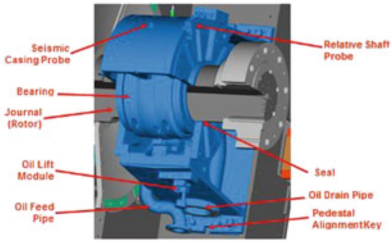

Fig. 4.18 Rotor-bearing assembly and other details (Courtesy of Siemens)

4.9.2 Two-Pad Tilt Pad Bearings

Westinghouse designed two-pad tilt-pad bearing types in the early 70's for better cooling of the bearing and rotor stability. The feature of the top shell looks very similar to a VP bearing whereas the bottom half of the bearing is modified to accommodate two tilt pads as illustrated in Fig. 4.19. This has the advantages of (a) a

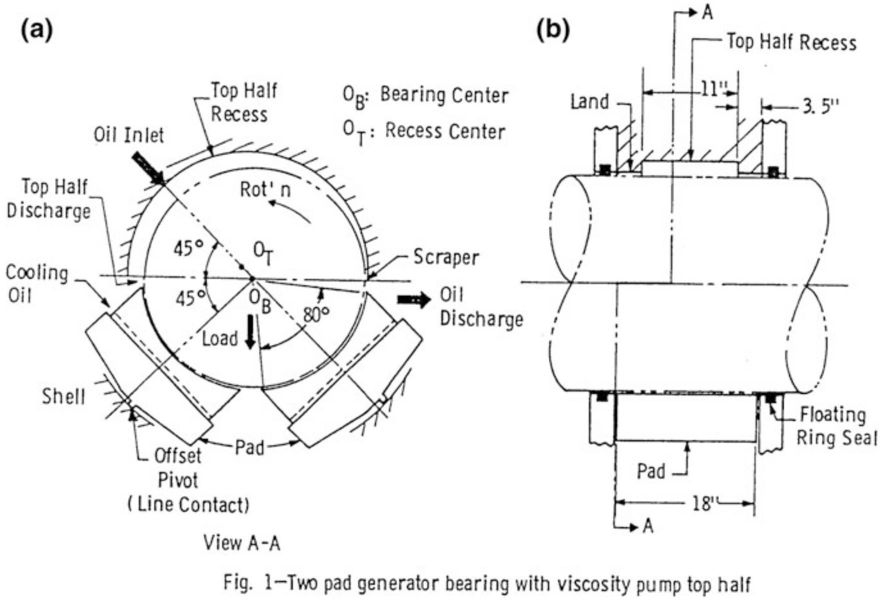

Fig. 4.19 Two-pad tilt-pad bearing by Westinghouse

stable bearing with (b) more space in the upper half for better oil circulation thus making the bearing cooler than other pad bearing types. Generally, bearing pads are made from steel; however, Cu-alloy pads can be employed to improve heat dissipation of oil in highly loaded configurations to reduce bearing metal temperatures.

4.9.3 Three-Pad Tilt Pad Bearings

Three-pad tilting pad is a special design that can carry larger loads. This type has direct lubrication at the pad leading edges through pad support and pad bore holes. Rugged pad design helps easy assembly. This bearing also offers more damping if properly preloaded. It should be noted that all pad lengths are not equal. See Fig. 4.20.

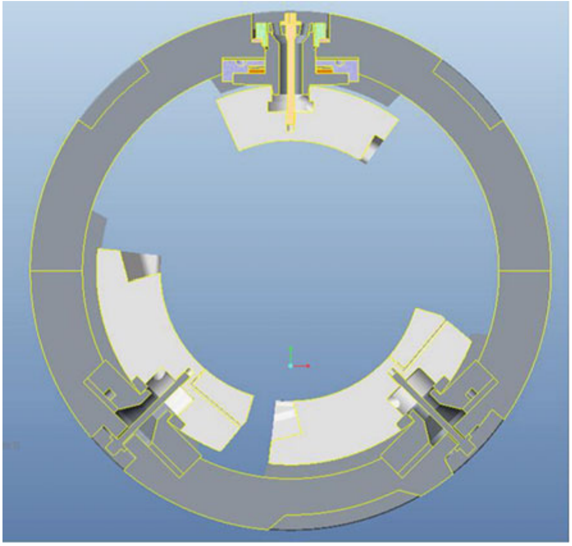

Fig. 4.20 Three-pad tilt pad bearing by Siemens

4.9.4 Five-Pad Tilt-Pad Bearing

Five-pad tilt pad bearings offer better load capability, increased stiffness and damping compared to a 4-pad type. The additional pad provides better maneuverability by pre-loading the journal adequately to achieve rotor stability. The load on pad (Fig. 4.21a) and the load between pads configurations shown in Fig. 4.21b are used to address various operating situations. In general, load between pads is a preferable configuration for more stable rotor operating condition with the top three pads preloaded equally or unequally as needed. As shown in Fig. 4.22, the bottom pad for "load-on-pad" configuration increases damping while the two side pads help centralize the journal by reducing the cross-coupled effects.

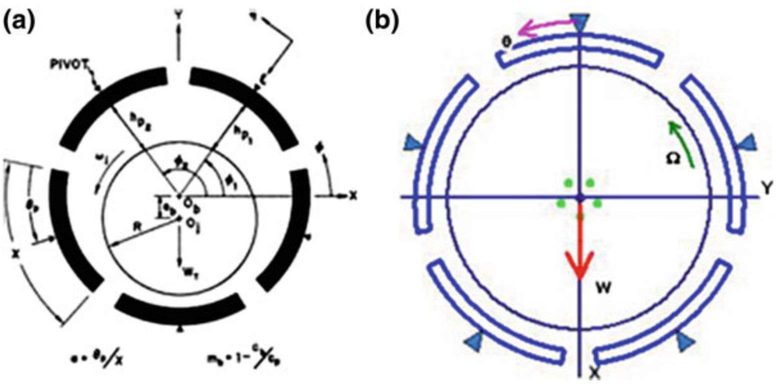

Fig. 4.21 **a** Load on pad; **b** Load between pads

Fig. 4.22 Oil pressure distribution for load-on pad configuration

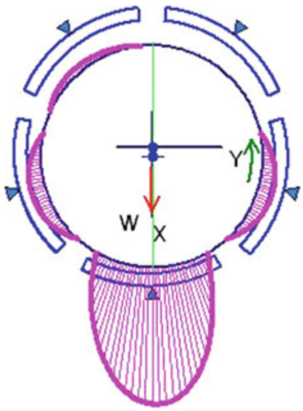

4.9.5 Six-Pad Tilt-Pad Bearings

More number of pads provides better control of the journal inside the bearing. For example, six pads (shown in Fig. 4.23a, b) provide better pad maneuverability to stabilize the journal by moving it towards the center compared to either a 4-pad or a 5-pad type. This feature on six-pad bearing enables the rotor reaching a stable condition under uneven steam/gas loading operation. There are two arrangement of 6-pads that are found to reduce imbalance loads. One arrangement is to load the journal between pads, which potentially increases film stiffness and move rotor frequencies away from unstable region. The other configuration, which is load on pad, adds film damping and reduces sub-synchronous frequency responses. In general, the former type is preferred because it keeps the rotor journal stable under most operating conditions. However, selecting a pad configuration depends on a problem to solve. Some vendors' [4] design has unequal pad lengths and pre-loading suitably applied to impart pre-loading against the steam unbalance forces. Unequal pad bearings were found useful in a steam turbine that experienced medium steam whirl due to partial load operation.

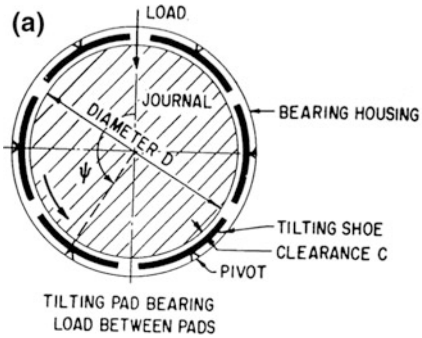

Fig. 4.23 Six-pad tilt-pad bearing (Courtesy of Siemens)

4.10 Special Bearing Types

Special bearing types are the ones applied to address some specific operating needs.

Special needs include controlling mild to medium steam/gas unbalance loads. They can cause bearings to unload either in the vertical or in the horizontal directions. The first course of action is to reduce the unbalance loads by controlling valve positions. If this does not work, the second course of action is to resort to multi-pad bearings such as 6 or higher pads which can control the journal position by bringing it closer to bearing center.

4.10.1 Squeeze-Film Dampers

A squeeze film damper (SFD) by Waukesha Bearings (Fig. 4.24a) is essentially a "bearing-inside-a-bearing". Inner bearing is similar to a cylindrical bearing type which may be susceptible to oil whip. Therefore, this inner bearing is additionally suspended in oil with the outer fixed ring. Oil between the inner bearing's outside shell and the inside surface of the fixed housing generates film pressure as the inner bearing approaches the housing, resulting in added damping to the inner bearing. Basically, the squeeze film action is provided by the outer bearing; hence, the name

SFD. An SFD decreases vibration, which may allow dampening a sensitive critical speed by reducing rotor response to acceptable levels. Unstable inner bearing can be stabilized by the outer bearing with SFD design. The design addresses or focuses only on the specific dynamic condition.

In some special designs [5] shown in Fig. 4.24b, known as integrated SFD (ISFD), stiffness and damping can independently be controlled, which makes the SFD bearings shift critical speeds higher and improve the dynamic stability of the rotor/bearing system.

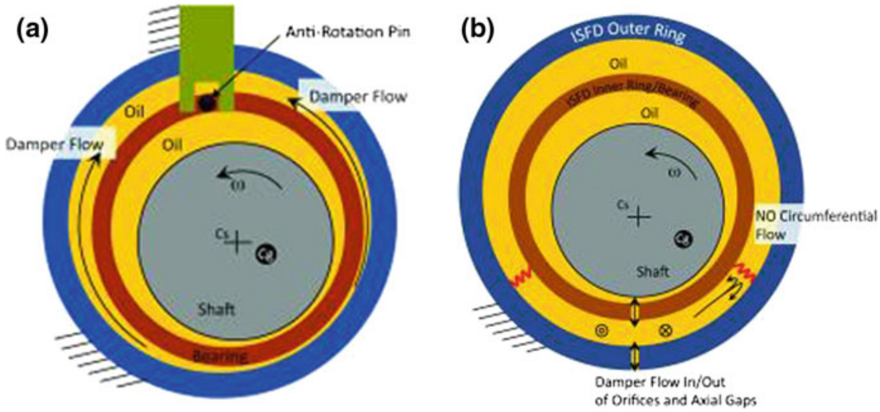

Fig. 4.24 Squeeze-film dampers by Waukesha bearings

4.10.2 Magnetic (Levitated) Bearings

Power amplifiers are used to constantly power the magnetic stator coils in a magnetic bearing as shown in Fig. 4.25. Magnetic bearings are used to support (levitate) rotors using magnetic energy. A ferrous object such as a rotor is known to be attracted to a permanent magnet of an electromagnet such as an electrical coil wound over a ferrous core. The rotor is attracted to an electromagnet located next to it whenever the latter is energized by current. The rotor floats inside the bearing by levitation, due to constant attractive force provided by the electromagnets around the rotor.

Magnetic bearings are applied in small rotating machines such as chemical, sugar processing, paper mills and industrial turbines etc. They are not considered in large turbine applications due to load limitation, added cost for the backup bearings, general maintenance cost and reliability and availability concerns.

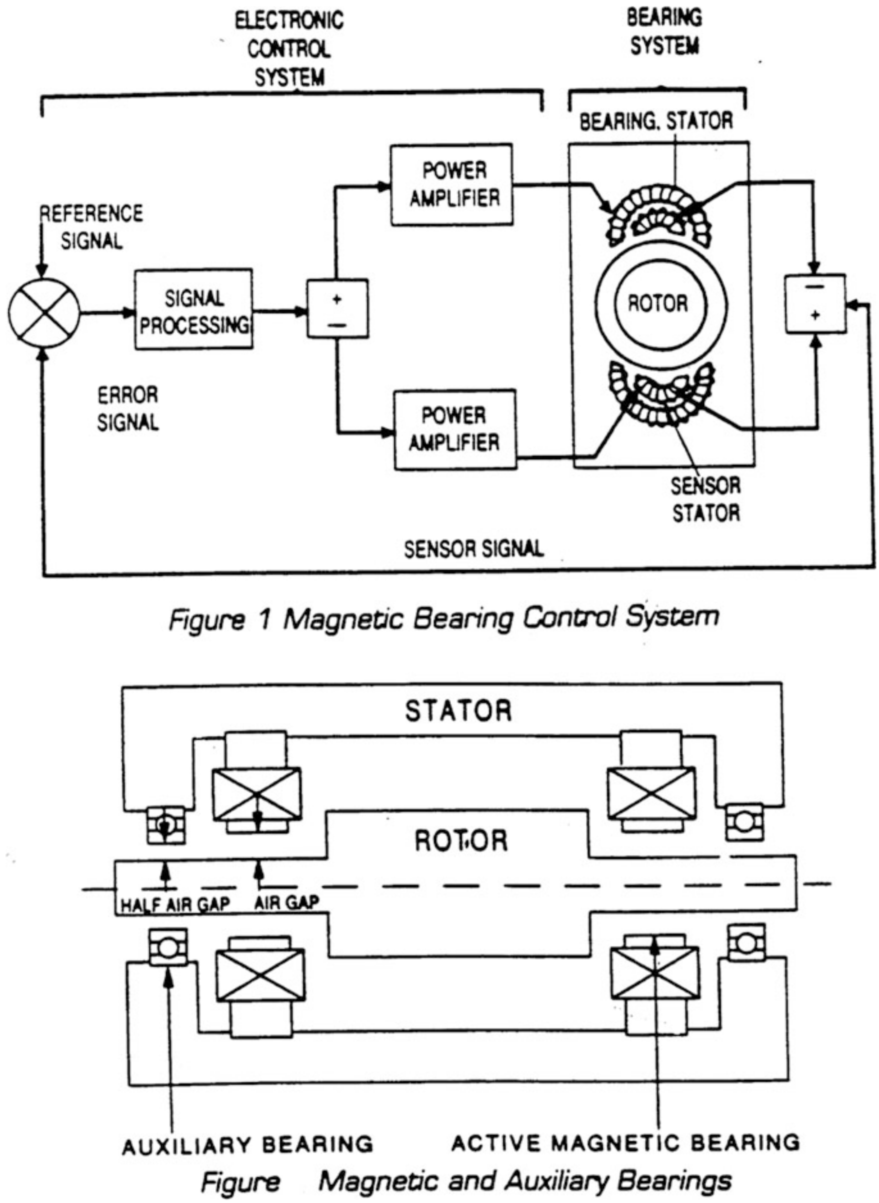

Fig. 4.25 Magnetic bearing

4.11 Comparison of Bearing Types

Different bearing types and their oil film pressure distribution are compared as shown in Fig. 4.26. In all cases, the oil film pressure profiles are always parabolic and obey Reynolds linear assumptions. However, pressure magnitudes of various configurations are different.

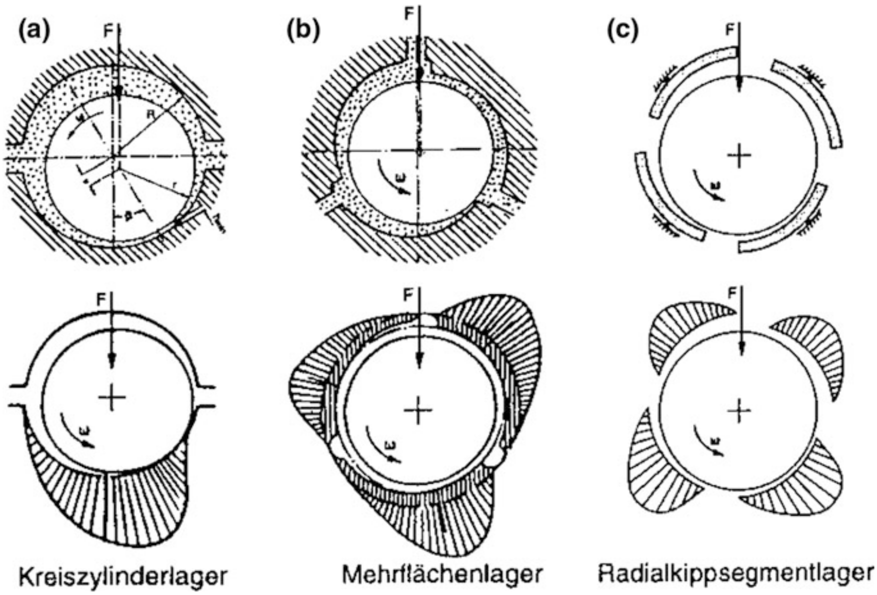

Fig. 4.26 Pressure distribution in **a** cylindrical, **b** 3-lobe and **c** 4-pad bearings

In general, different bearing types can be compared for performance on a scale of 1–10, (10 being excellent and 1 being worse) based on their load bearing capacity, oil film stiffness and damping as shown in Table 4.2 below.

Table 4.2 Relative comparison of bearings

Bearing type	Load capability	Stiffness	Damping	Remarks
Partial-arc or VP type	10	2	8	Susceptible to oil whip
Elliptical	8	4	8	Increases bearing metal temp
Lobe type	5–7	6	3–6	Limited load capability
Pressure dam	8	6	8	Dam may become ineffective in service
4-pad TB	6	6	7	Not capable of controlling steam/gas unbalance loads
5-pad TB	7	9	8	Better control of unbalance steam loads
6-pad TB	8	8	8	Overall better stability control

4.12 Fluid-Film Bearing Theory

Bearing characteristics are very important because they influence the rotor system behavior such as critical speeds, responses and stability in a significant manner. Fluid film bearings offer major source of damping due to the squeeze film effect. Thin film, that separates the journal and bearing shell, supports the journal with multiple springs and dampers. Several authors have extensively covered this subject. Limited references are [1–11] provided and cross-references can be obtained from them. The intention is to introduce very basic mathematical equations for the oil film pressure distribution from where the bearing film coefficients are derived.

The hydrodynamic bearing analysis is carried out to determine the bearing forces of a given bearing geometry. The linear form of generic Reynolds equation is used to obtain fluid-film pressure distribution as shown below in Eq. 4.1 and Fig. 4.27.

$$\frac{1}{R^2}\frac{\partial}{\partial\theta}\left(\frac{h^3}{12\eta}\frac{\partial p}{\partial\theta}\right)+\frac{\partial}{\partial x}\left(\frac{h^3}{12\eta}\frac{\partial p}{\partial x}\right)=\frac{1}{2}\omega\frac{\partial h}{\partial\theta}+\frac{\partial h}{\partial t} \tag{4.1}$$

Sliding velocity term
Provides film stiffness

Squeeze film velocity
Provides film damping

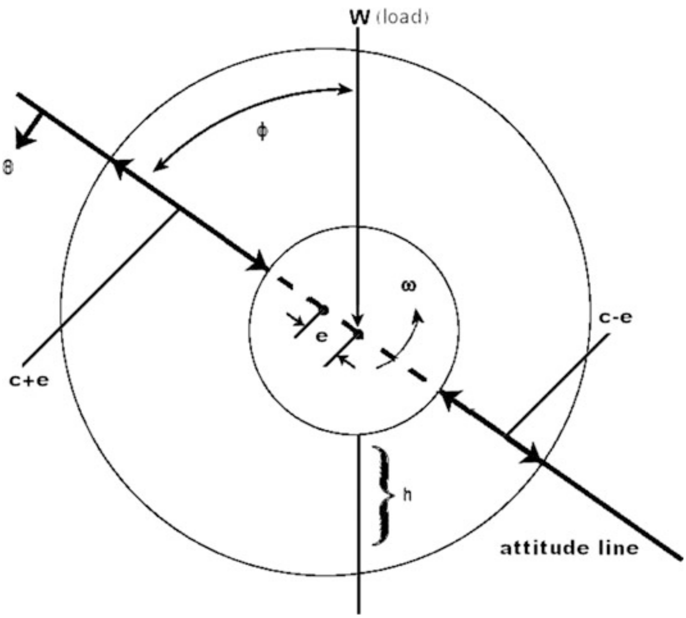

Fig. 4.27 Definition of parameters of a plain cylindrical bearing

Where

p = p (θ, x) is the pressure at a point in the film
h = film thickness
η = viscosity of oil
ω = angular speed of rotation
X = axial coordinate
θ = circumferential coordinate
R = radius of journal
C = radial clearance
e = eccentricity between the centers of journal and bearing

Assumptions of Reynolds pressure equation are:

(a) Film is laminar and incompressible.
(b) Film pressure does not vary across the thickness of the film.
(c) No flow discontinuity between oil and the bearing shell.

It should be borne in mind that the fluid-film dynamic properties are good for small amplitude motions of the journal only. Hence, in linear rotor dynamic evaluations, rotor frequencies (shown in Fig. 4.28) match reasonably well with the measured values whereas log-dec. for stability and rotor amplitudes may not; especially when the rotor amplitudes reach the non-linear fluid-film region.

The shearing action of the rotating journal produces hydrodynamic pressure in the bearing and the resultant force opposes the applied load (see Fig. 4.27). At any given speed, the fluid film reaction force is a function of the position of the journal and the instantaneous journal center velocity.

Fig. 4.28 Oil film Forces verses journal displacement

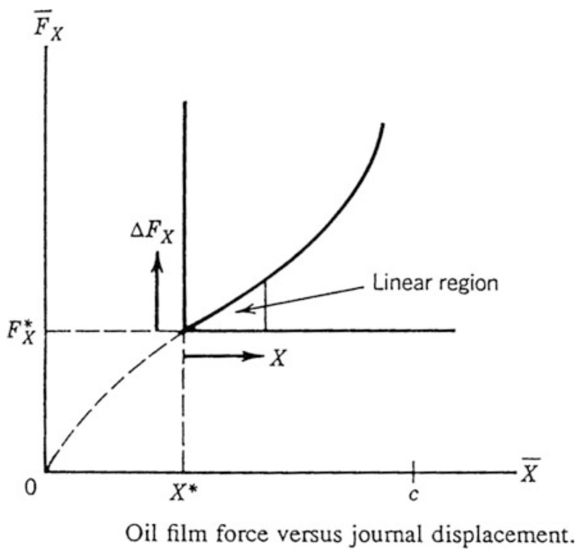

$$F_y = F_y(y, z, \dot{y}, \dot{z}, \omega); F_y = F_z(y, z, \dot{y}, \dot{z}, \omega) \tag{4.2}$$

$h_0 = c + e.cos\theta$ where h_0*is static film thickness* and e is the eccentricity between the journal center motion is described by the amplitudes Δz and Δy, measured from static equilibrium position such that the film thickness at any position becomes,

$$h = h_0 + \Delta\mathrm{y}\ cos\theta + \Delta\mathrm{z}\ \sin\theta \tag{4.3}$$

Assuming the amplitudes are small, a first order expansion of the pressure neglecting higher order terms can be written as:

$$P = P_o + P_y\Delta\mathrm{y} + P_z\Delta\mathrm{z} + P_{\dot{\mathrm{y}}}\Delta\dot{\mathrm{y}} + P_{\dot{\mathrm{z}}}\Delta\dot{\mathrm{z}} \tag{4.4}$$

Where P_o is the film pressure under static equilibrium conditions.

Upon substitution of Eqs. (4.3) and (4.4) into Eq. (4.1) and retaining only the first order terms, five equations are obtained.

$$\frac{1}{R^2}\frac{\partial}{\partial\theta}\left(\frac{h_o^3}{12\eta}\frac{\partial}{\partial\theta}\right) + \frac{\partial}{\partial x}\left(\frac{h_o^3}{12\eta}\frac{\partial}{\partial x}\right)\begin{pmatrix} P_o \\ P_y \\ P_z \\ P_{\dot{\mathrm{y}}} \\ P_{\dot{\mathrm{z}}} \end{pmatrix}$$

$$= \begin{cases} \frac{1}{2}\omega\frac{\partial h_0}{\partial\theta} \\ \frac{1}{2}\omega\left(cos\theta - 3\frac{\sin\theta}{h_0} + \frac{\partial ho}{\partial\theta} - \frac{ho^3}{4\eta}\frac{1}{R^2}\frac{\partial po}{\partial\theta}\frac{\partial}{\partial\theta}\left(\frac{\sin\theta}{h_0}\right)\right) \\ \frac{1}{2}\omega\left(\sin\theta + 3\frac{cos\theta}{h_0}\frac{\partial ho}{\partial\theta}\right) - \frac{ho^3}{4\eta}\frac{1}{R^2}\frac{\partial po}{\partial\theta}\frac{\partial}{\partial\theta}\left(\frac{cos\theta}{h_0}\right) \\ \sin\theta \\ cos\theta \end{cases} \tag{4.5}$$

The boundary conditions are that the pressure is zero at the edges of the bearing.

$$\begin{aligned} &\mathrm{At}\, x = \pm\ell/2 \\ &\left.\begin{aligned} \theta = \theta_{1P} \quad P = P_o = P_y = P_z = P_{\dot{\mathrm{y}}} = P_{\dot{\mathrm{z}}} = 0 \\ \theta = \theta_{2P} \quad P = P_o = P_y = P_z = P_{\dot{\mathrm{y}}} = P_{\dot{\mathrm{z}}} = 0 \end{aligned}\right\} \end{aligned} \tag{4.6}$$

Where ℓ. the effective length of bearing.

The total forces along the y and the z directions can be written as:

$$\left.\begin{matrix} F_y \\ F_z \end{matrix}\right\} = \left\{\begin{matrix} F_{yo} + k_{yy}\Delta y + k_{yz}\Delta z + C_{yy}\Delta y + C_{yz}\Delta z \\ F_{zo} + k_{zz}\Delta z + k_{zy}\Delta y + C_{zz}\Delta z + C_{zy}\Delta y \end{matrix}\right.$$
$$= {}_{\mathrm{P}}\Sigma - 2\int_o^{\ell/2}\int_{\theta_{1P}}^{\theta_{2P}} P\left\{\begin{matrix} cos\theta \\ \sin\theta \end{matrix}\right\} Rd\theta dx \tag{4.7}$$

$$\left\{\begin{matrix} F_{yo} \\ F_{zo} \end{matrix}\right\} = \left\{\begin{matrix} w \\ o \end{matrix}\right\} = \Sigma - 2\int_o^{\ell/2}\int_{\theta_{1P}}^{\theta_{2P}} P_o\left\{\begin{matrix} cos\theta \\ \sin\theta \end{matrix}\right\} Rd\theta dx \tag{4.8}$$

The shearing action of the journal with the fluid-film produces hydrodynamic pressure and the resultant force opposes the applied load. The resistance of the oil film or reaction force can be assessed by journal position ε and ψ and displacement and velocity in the Y and Z planes as described by the mathematics below:

Substituting for p from Eq. (4.4) results in:

$$\left\{\begin{matrix} k_{yy} \\ k_{yz} \end{matrix}\right\} = \underset{\mathrm{P}}{\Sigma} -2\int_o^{\ell/2}\int_{\theta_{1P}}^{\theta_{2P}} P_y\left\{\begin{matrix} cos\theta \\ \sin\theta \end{matrix}\right\} Rd\theta dx \tag{4.9}$$

$$\left\{\begin{matrix} k_{zz} \\ k_{zy} \end{matrix}\right\} = \underset{\mathrm{P}}{\Sigma} -2\int_o^{\ell/2}\int_{\theta_{1P}}^{\theta_{2P}} P_z\left\{\begin{matrix} \sin\theta \\ cos\theta \end{matrix}\right\} Rd\theta dx \tag{4.10}$$

$$\left\{\begin{matrix} C_{yy} \\ C_{yz} \end{matrix}\right\} = \underset{\mathrm{P}}{\Sigma} -2\int_o^{\ell/2}\int_{\theta_{1P}}^{\theta_{2P}} P_y\left\{\begin{matrix} cos\theta \\ \sin\theta \end{matrix}\right\} Rd\theta dx \tag{4.11}$$

$$\left\{\begin{matrix} C_{zz} \\ C_{zyz} \end{matrix}\right\} = \underset{\mathrm{P}}{\Sigma} -2\int_o^{\ell/2}\int_{\theta_{1P}}^{\theta_{2P}} P_z\left\{\begin{matrix} \sin\theta \\ cos\theta \end{matrix}\right\} Rd\theta dx \tag{4.12}$$

The bearing parameters are plotted in dimensionless numbers for usage in computer codes:

$S = \frac{\eta NDL}{w}\left(\frac{R}{C}\right)^2$ Sommerfeld number is a Non-dimensional number

$$\bar{k}_{yy},\bar{k}_{yz},\bar{k}_{zy},\bar{k}_{zz} = \frac{ck_{yy}}{w},\frac{ck_{yz}}{w},\frac{ck_{zy}}{w},\frac{ck_{zz}}{w}$$
$$\bar{C}_{yy},\bar{C}_{yz},\bar{C}_{zy},\bar{C}_{zz} = \frac{c\omega C_{yy}}{w},\frac{c\omega C_{yz}}{w},\frac{c\omega C_{zy}}{w},\frac{c\omega C_{zz}}{w}$$

Where $\bar{k}_{yy},\bar{k}_{yz},\bar{k}_{zy},\bar{k}_{zz}$ and $\bar{C}_{yy},\bar{C}_{yz},\bar{C}_{zy},\bar{C}_{zz}$ are non-dimensional dynamic coefficients.

4.12.1 Oil Film Dynamic Coefficients

The final form of oil film stiffness and damping coefficients are obtained by double integrating Eqs. 4.9 through 4.12 simultaneously along the length of the bearing and around the diameter of the journal. These dynamic coefficients are derived in non-dimensional form plotted against another non-dimensional number known as, "duty parameter" or "Sommerfeld" number in the form of charts. So, suitable dynamic coefficients for different bearing configurations can be calculated with their geometry and oil film parameters.

Example plots of oil film dynamic coefficients versus Sommerfeld number (S) for a pad type bearing are shown in Fig. 4.29 [4]. Similar non-dimensional bearing curves are available for other bearing types.

Fig. 4.29 Representative oil film dynamic coefficients versus Sommerfeld number

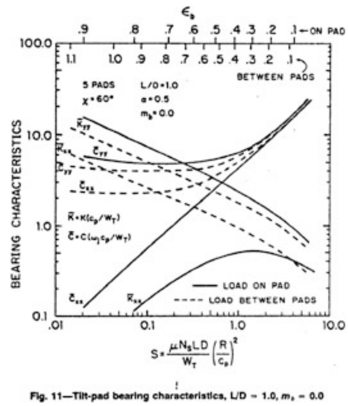

The eight fluid-film bearing dynamic coefficients represented by springs and dampers due to translational degrees of freedom (dof) with superscript "tt" are illustrated in Fig. 4.30. Out of eight, four of them represent oil film stiffness and the other four represent oil film damping. The suffix YY refers to direct coefficients with journal displacement in Y direction due to force in the same direction Y. YZ refers to cross-coupled coefficient of the journal motion in the Y direction due to force applied in the Z direction. Similarly subscripts ZZ and ZY refer to direct and cross-coupled coefficients respectively for the Z-direction. The superscripted "rr" coefficients are due to bending moment as represented by the rotational dof. In general, they are in significant and not considered in turbo-machinery design.

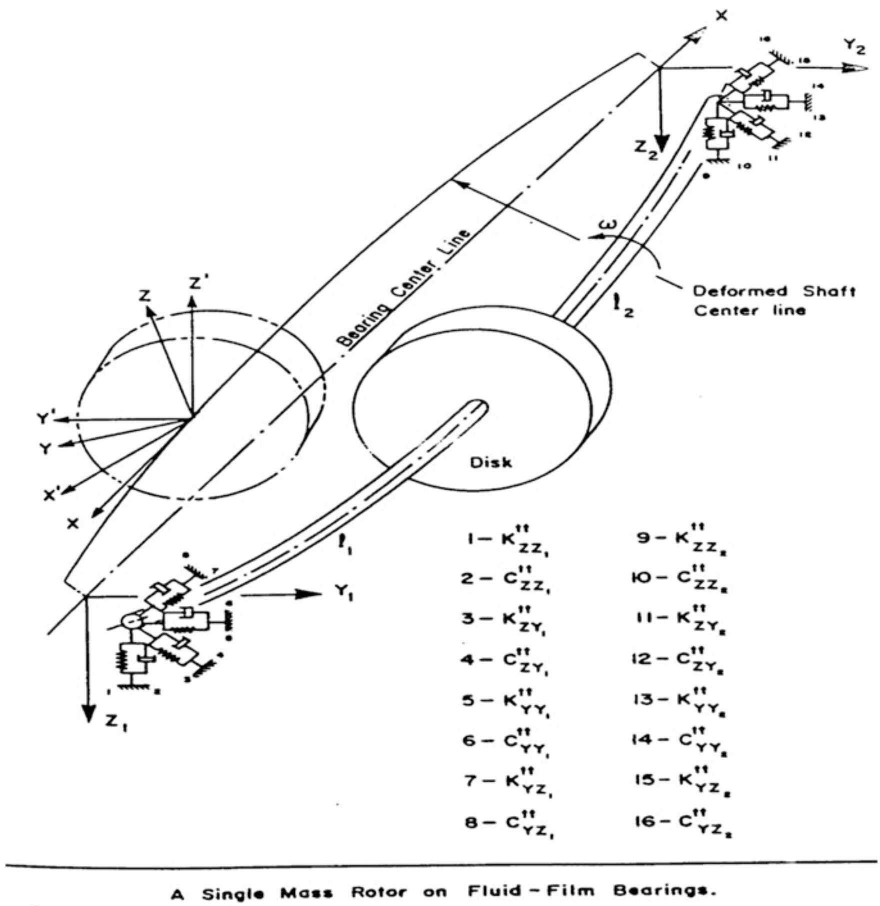

Fig. 4.30 Fluid-film bearing linear dynamic coefficients

4.12.2 Bearing L/D Ratios

The bearings are categorized by their size as "long, finite or short" bearings. A long bearing has L/D > 1. A finite bearing is the one with L/D slightly below 1 and a short bearing, in general, has L/D anywhere between 0.35 to 0.7. Active length of a bearing is measured between the oil drain holes on either side of the center of the bearing as shown in Fig. 4.31. By reducing the distance between the drain holes, a finite bearing can be made into a short bearing with suitable L/D.

Common L/D ratios applied in bearings:

L/D ratio of Long bearing > 1 for example 1.1, 1.2 etc.
L/D ratio for Finite bearing slightly less than1. For example, 0.8, 0.9 etc.
L/D ratio for Short bearing < 1 for example 0.35, 0.4, 0.58, 0.62, 0.7 etc.

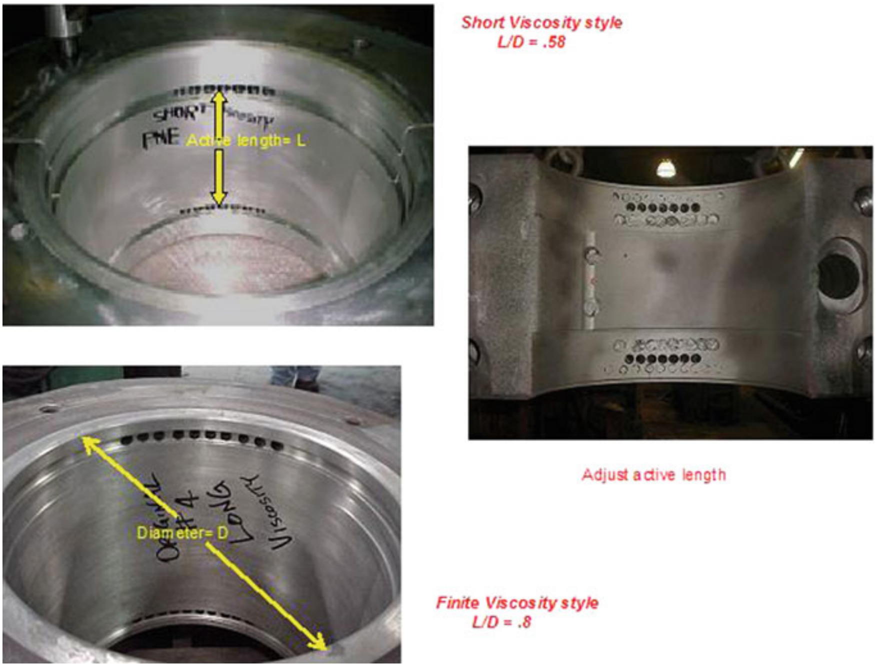

Fig. 4.31 Active Length of bearings (Courtesy of Siemens)

Maximum film pressure increases when bearing active length is shortened. Consequently, the oil pressure distribution changes. An example is illustrated in Fig. 4.32.

In the example illustrated in Fig. 4.32a a finite bearing having L/D of 0.8 is split into (b) Two short bearings with L/D at 0.35 with a central groove.

To eliminate oil whip in cylindrical bearings, a center groove (with a width of 1" (25 mm) and a depth of 0.25" (6.35 mm)) can be machined as illustrated in Fig. 4.32b. The center groove is called, "Oil Whip Groove" that converts a finite bearing of 0.8 L (shown in Fig. 4.32a) into two short bearings of 0.35 L each side of the oil whip groove. The short bearing configuration can be obtained by re-babbitting a finite bearing of 0.8 L with a machined step width of 1" and 0.25"

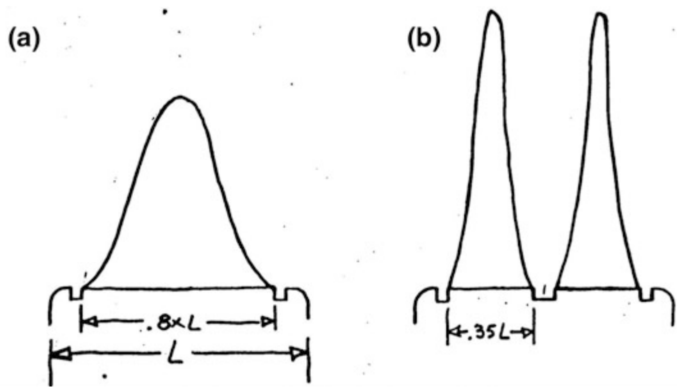

Fig. 4.32 Finite and short bearing configurations

deep at the center leaving the original oil drain groove distances unchanged. The modified oil whip groove changes the bearing pressure distribution as illustrated in Fig. 4.32b. Essentially, the bearing load is supported by two small bearings with large peak pressures of their own. This solution has proven to eliminate oil whip in partial-arc bearings.

4.12.3 Oil Lift Pockets

Heavily loaded bearings typically reduce oil film thickness between the journal and the shell, especially at low turning gear (TG) speeds. Under these circumstances, the journal tends to get closer to the boundary film, frequently wiping bearing babbit surfaces. To eliminate frequent bearing wipes, oil lifts are installed. Lift oil with high static pressure lifts the journal from boundary film, especially at low rotor speeds. One type of bearing oil lift system used by Westinghouse is shown in Fig. 4.33a. Other oil-lift configurations used by other vendors vary and some of them are shown in Fig. 4.33b, c.

Another function of the oil lift is to supress rotor chatter known as “stick-slip” exhibited by bearings at very low speeds. The chatter from long and flexible last row LP blades cause stick-slip phenomenon with audible ringing noise. Repeated stick-slip occurences could damage LP blades if left unaddressed.

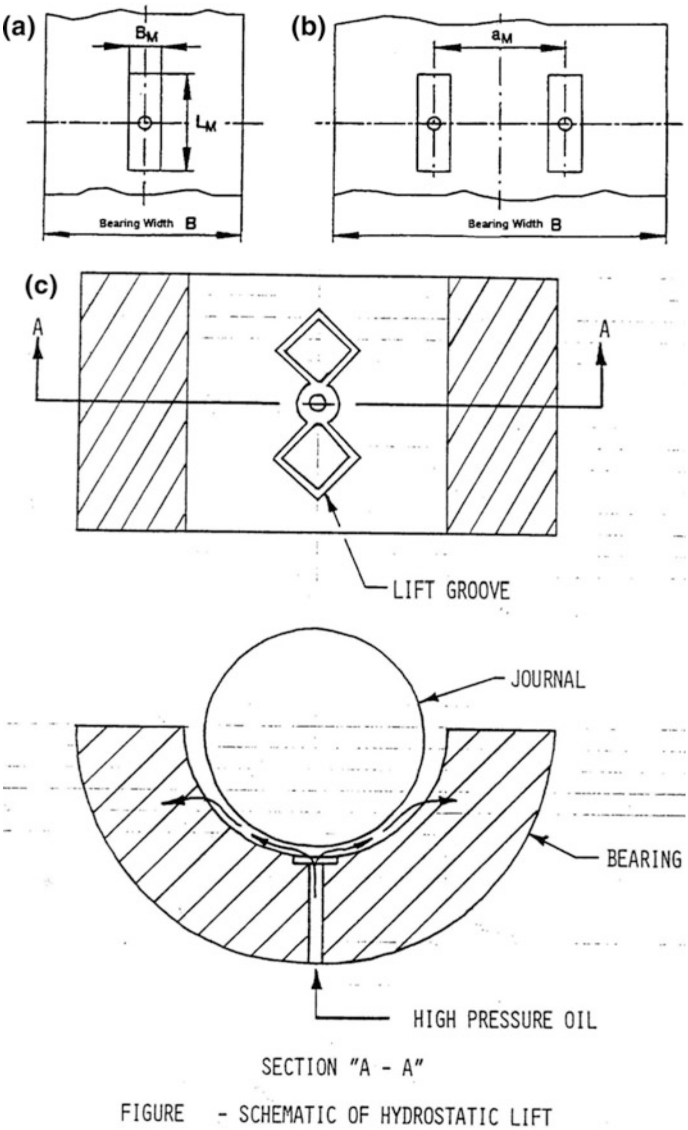

Fig. 4.33 Oil lifts (Courtesy of Siemens)

4.13 Rotor Instability

Rotor stability could be affected by one or more of the following:

(a) Oil whip in circular bearings
(b) Steam whirl due to unbalance steam loads

(c) Parametric Instability due to dissimilar shaft configurations
(d) Hysteretic Instabilty due to friction

Categories (a) and (b) are common in turbo-machinery applications whereas categories (c) and (d) are very rare. So, more detailed discussions will be carried out for the first two categories to understand their impact on rotor vibration behavior.

4.13.1 Oil Whirl/Whip in Bearings

Essentially, oil whirl is the beginning of the rotor instability (also known as self-excitation) and could lead to oil whip which is the ultimate condition at which point severe bearing damage occurs. Both conditions are caused mainly due to bearing unloading by a sub-synchronous whirl component. The main cause for such sub-synchronous vibration is the dominant cross-coupled forces that oppose the effective damping forces provided by the oil film as illustrated in Fig. 4.34.

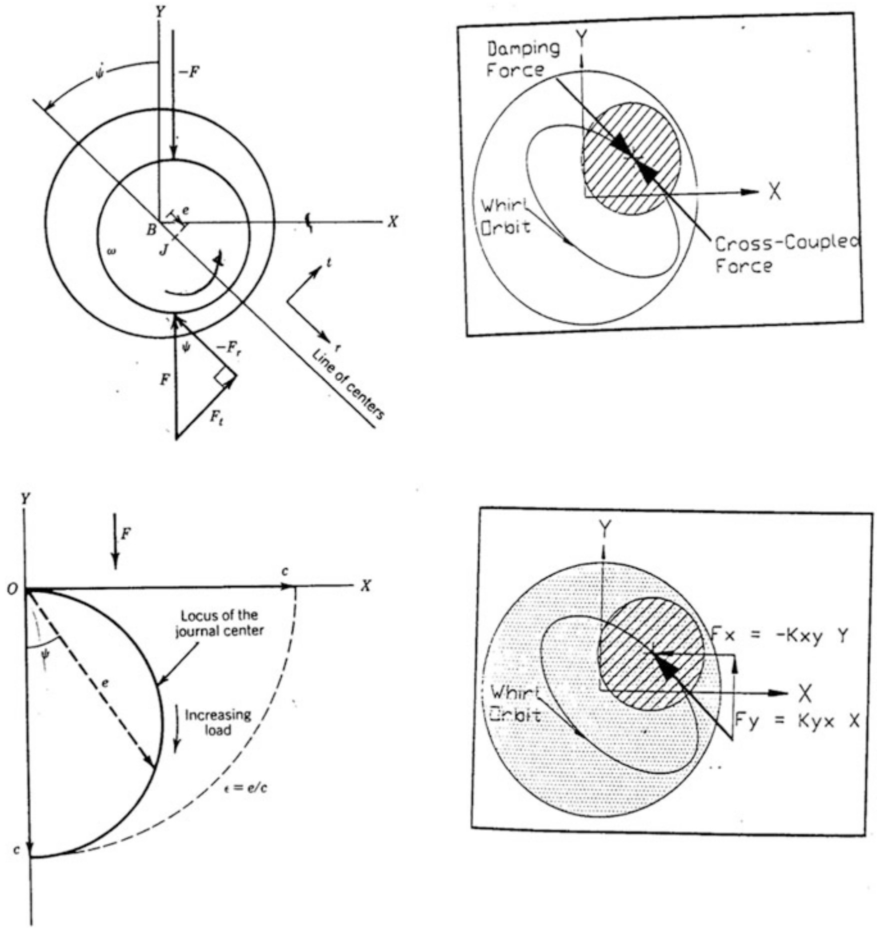

Fig. 4.34 Oil film forces

Oil whirl can be explained in another way [12].

At a certain rotor dynamic condition (mostly for cylindrical and partial-arc bearings), increase in bearing load causes increase of cross-coupled stiffness. When the magnitude of cross-coupled stiffness exceeds the direct stiffness, the shearing action in the oil film increases. The rotor whirl increases as a result and pumps more oil into the converging side of the oil film (Fig. 4.35) while the diverging side is not capable of discharging the oil at the same rate as that of the incoming oil. This uneven flow creates an unstable condition in the bearing. To stabilize the unstable condition, the bearing draws more oil into the converging side which creates more rotor whirl. This cycle continues and the minimum oil film thickness keeps reducing everytime the rotor whirl increases.This is the beginning of the oil whirl.

The unstable condition sterengthens everytime the rotor whirl increases. This action feeds more energy to de-stabilize the rotor. This condition is widely known as "self-excitation" in the bearing. The self-excitation pushes the journal into the thin oil film boundary, eventually breaking the film and causing catestrophic damage to the bearing which is known as "oil whip".

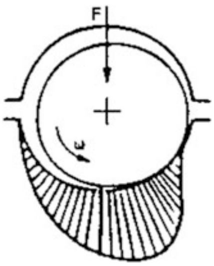

Fig. 4.35 Oil whirl occurrence

4.13.2 Steam Whirl

Steam or gas whirl is another phenomenon of rotor instability by self-excitation like oil whirl. However, the source of excitation, in this case, is unbalance steam/gas forces. This happens during a partial steam entry at the nozzle chamber. When steam is admitted at full-arc, steam forces are balanced whereas at partial-arc mode of operation, the resulting unbalance steam forces cause uneven forces as illustrated in Fig. 4.36. The unbalance steam forces tend to push the rotor towards one end of the casing more than the other side causing unequal clearances around the annular space between the rotor and the casing. This situation is very similar to the behavior of the journal inside the oil film. Rotor whirl in this condition destabilizes the rotor by pushing it into self-excitation. For a rotor supported by two bearings, the steam whirl effect generates uneven bending moments resulting in unloading one bearing and increasing load on the other bearing in the span. The steam whirl symptoms are very similar to oil whirl.

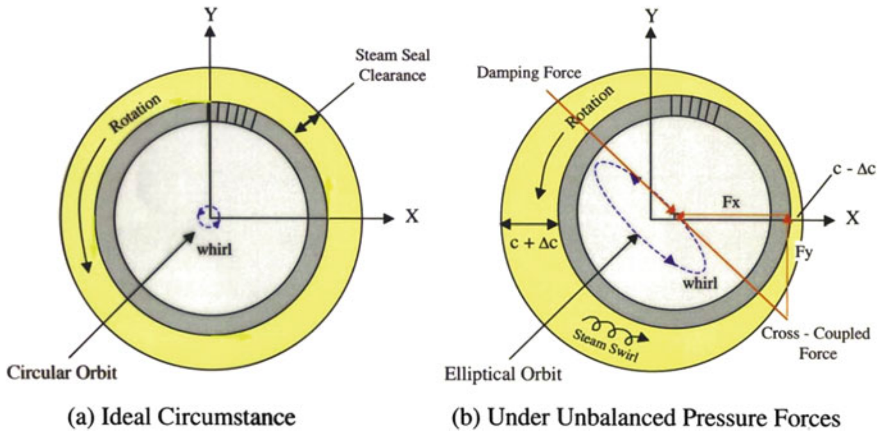

Fig. 4.36 Steam whirl illustration

As illustrated in Fig. 4.36, when a bladed-rotor is moved off-center due to unbalanced steam/gas loads (mainly due to partial steam admission), unequal clearances are created in the annular space. This results in unequal loading on bearings that support the rotor. The lightly loaded side of the bearing is the one unloaded and it is susceptible to self-excitation.

The technical background for steam whirl is briefly discussed here.

Labyrinth seals [13–17] are used in steam/gas turbines to control and minimize leakage flow across seal segments to maintain stage flow and pressures. The difference between the inlet and the exhaust stage pressure ΔP is responsible for initiating higher swirl velocities in the radial direction. The higher the ΔP, the larger would be the swirl velocity. In partial-arc of operation, the increased inlet swirl velocity generates uneven steam forces around the circumference of a bladed-rotor. Thus, the unbalance forces of the working fluid medium impart uneven loads on the bearings. The unloaded end of the bearing associated with the reduction of oil film damping tend to increase rotor vibration. Whereas the loaded end of the bearing

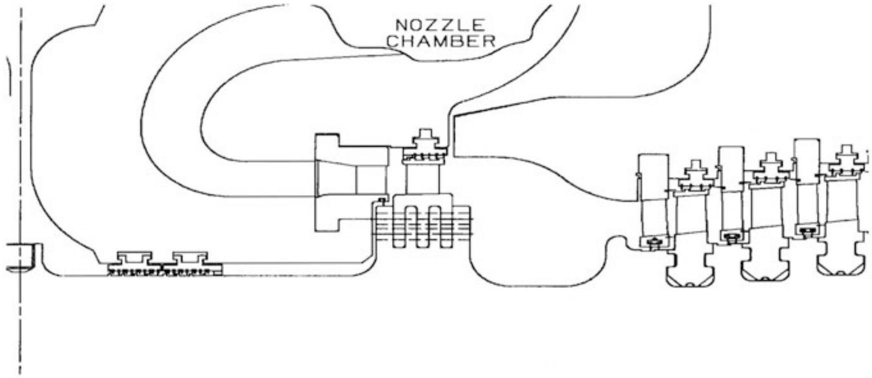

Fig. 4.37 Seal areas shown for a HP rotor control stage (Courtesy of Siemens)

experiences increased bearing metal temperature associated with a reduction of rotor vibration. For the HP turbine shown in Fig. 4.37, typically high steam swirl velocity is experienced at the rotating seals located at the control stage.

Anti-swirl vanes can significantly reduce steam inlet velocity and suppress steam whirl, when installed in front of the seal inlet areas. Potential locations for installation of anti-swirl deflectors and flow dams in a steam turbine are

(a) In front of the control stage rotating row seals
(b) In front of the nozzle chamber and
(c) In front of the rotating row seals in the blade path.

A segment of an anti-swirl vanes and flow dams are shown in Fig. 4.38.

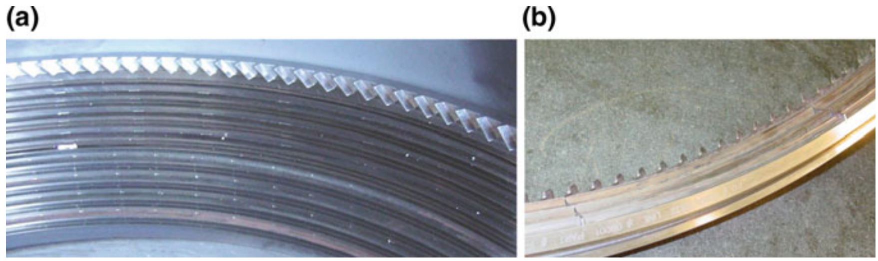

Fig. 4.38 Anti-swirl vanes and flow dams

4.13.2.1 Analysis

In lateral rotor dynamic analysis, it is important to calculate logarithmic decrement (log-dec.) to evaluate rotor stability using complex modal analysis (as discussed in Sect. 2.4.5). Seal dynamic coefficients (like fluid-film coefficients) are applied at the appropriate seal locations in the rotor dynamic model.

Steam whirl computations were made for the rotor system that consists of an HP rotor and an LP rotor as shown in Fig. 4.39. High-pressure seal areas are located between stations 3 and 8 of the HP turbine and the HP bearings are located at stations 2 and 9. The LP Bearings are located at 10 and 11. The LP turbine comparatively has very low-pressure differential and does not participate in steam whirl. Calculations indicated that the HP rotor sub-synchronous mode at 2110 CPM was calculated with a negative damping (logarithmic decrement) of −0.0163 while the rotor was operating at 3600 RPM. The HP rotor whirl pattern is shown as illustrated in Fig. 4.39. Anti-swirl vanes and flow dams were installed to address the steam whirl situation in this case.

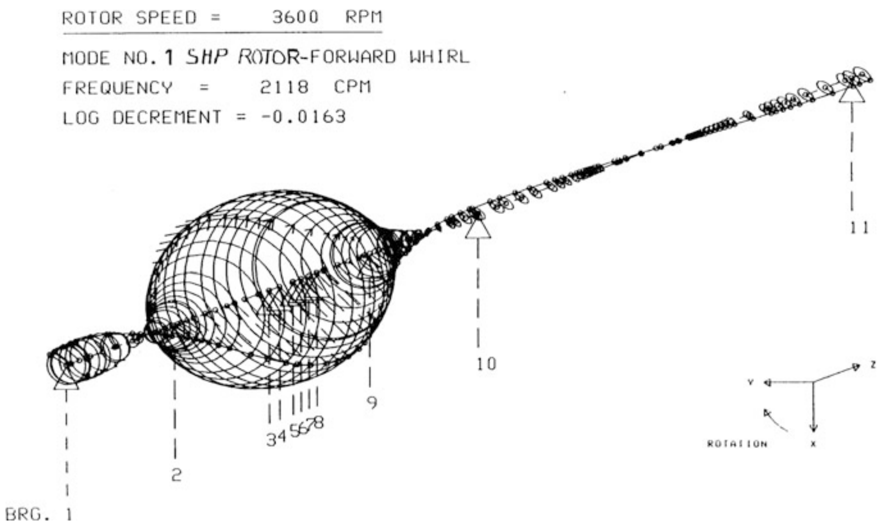

Fig. 4.39 Steam whirl simulation (use this figure)

When steam whirl occurrences were experienced after the turbine was installed, adding anti-swirl vanes and/or flow dams require opening of the turbine cover. This approach is not preferred by customers because of cost and unit down time. Under those circumstances, more self-aligning and preloaded 6-pad bearings can be applied to improve the rotor instability condition.

4.13.3 Discussions of Self-excited Vibration

In general, the rotor spins about its geometric axis and whirls about its static equilibrium position at any speed. For a rotor system that is sensitive to one of the self-excitation mechanisms (oil whirl or steam whirl), the rotor spin speed and the whirl speed go hand-in hand until they reach the sensitive sub-synchronous frequency. Once the rotor reached the rotor frequency (usually first rotor critical speed), the whirl is locked-in at this frequency. The whirl speed and the spin speed separate at this frequency. The amplitude of the rotor frequency keeps increasing while the rotor spins by itself towards the rated speed. The progression of the growth of whirl amplitude is illustrated in Fig. 4.40. Dominant sub-synchronous vibration increase can be observed in the vibration spectrum. In worst cases, the sub-synchronous vibration component could exceed unit trip limits and the rotor is no longer operable until suitable mitigation measures are implemented.

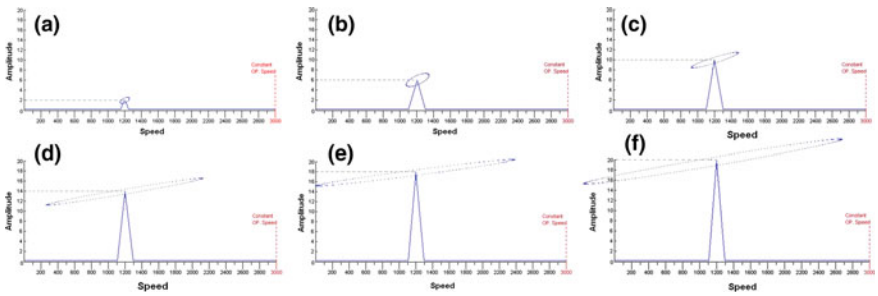

Fig. 4.40 Progression of increased sub-synchronous whirl amplitude leading to steam whirl

4.14 Thrust or Axial Bearings

In a turbine, axial or thrust bearings are designed primarily to maintain axial spacing or axial position between the rotor and the stationary parts.

Thrust bearing as assembled is completely housed inside a cage as shown in Fig. 4.41. Oil enters through two inlet holes at the bottom and flows radially towards the thrust collar and drains circumferentially to the bottom of the case.

Essentially, centrifugal forces pull the oil through the annulus between pads and the thrust collar and flood the entire thrust cage. Some vendors design oil inlets at the leading edges of each individual pads like the LEG radial bearing designs discussed before. Oil seal rings at each end of the case control the leakage flow.

Fig. 4.41 Thrust bearing complete

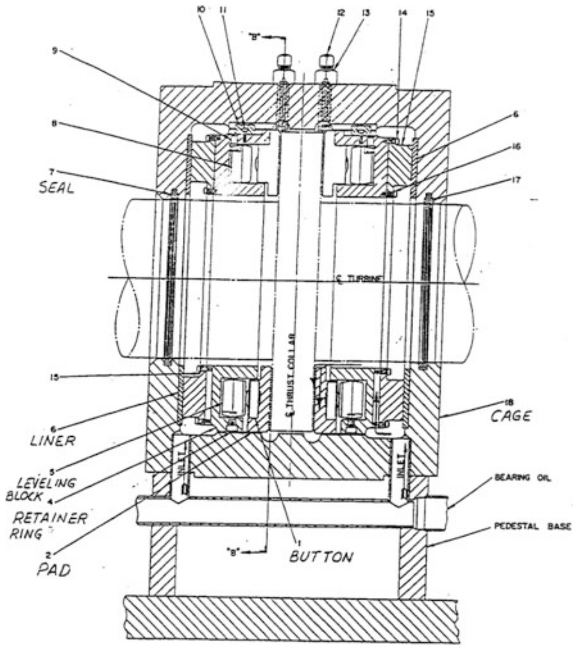

The axial bearings are sized to carry the unbalanced thrust loads generated by the steam or gas medium. Additionally, they are designed to withstand variable thrust loading conditions in operation. Hence, they are also known as, “Thrust Bearings”. In certain applications, the radial and the axial bearings are combined within the same bearing cage.

Fluid-film formation in both thrust and radial bearings is similar. Fixed and pivoted pad thrust bearing illustrations are shown in Fig. 4.42. The thrust force W is the load on the rotating part (thrust collar), N is the speed of rotor and U is the velocity of the oil in circulation, h_1 and h_2 are two end clearances for the oil to leak.

The total flexibility of the bearing system is comprised of a series combination of the flexibilities of the oil film, bearing yoke and cylinder base. If the bearing support is made much stiffer than the oil film and the cylinder base it will not have much affect on the total stiffness. As a guideline, it is desirable to have a support stiffness of about 1×10^8 lb/in.

For designs in which the bearing is very flexible, there is an additional design criterion for support deflection. With the static load applied, the assembly should not deflect such that the bearing radial clearances reduced at any point by more than 20% of its nominal value.

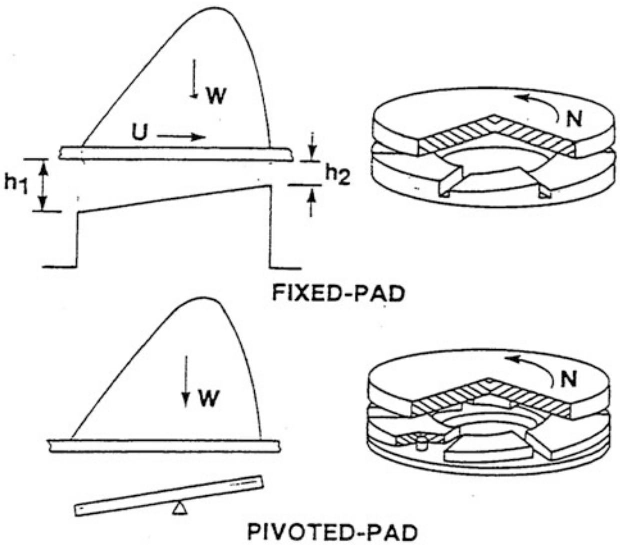

Fig. 4.42 Thrust bearings (Courtesy of Siemens)

4.14.1 How Are Thrust Bearings Built?

A thrust bearing consists of number of stationary babbitted pad segments facing the collar (which is integral part of rotating shaft) on either side of it as shown in Fig. 4.41. Thrust pad load distribution is described in Fig. 4.42. Pads are of equal in size and shape. A thrust bearing typically has a minimum of 6 pads and the maximum depends on the size of the bearing. Each pad is free to tilt about a pivot, which is a hardened spherical surface located behind the pad. Pads are free to incline in both circumferential and axial directions such that it can provide necessary hydro-dynamic lubrication to the bearing. Pads rest on a series of upper leveling blocks that distribute thrust load uniformly around the bearing. The lower

The shoes are supported by a series of levers (or leveling blocks) as shown in Figure 4.43 Because of this lever arrangement, each shoe will carry equal load, within friction limitations, even if the bearing is not perpendicular to the axis of shaft rotation or if the shoes are not of equal thickness. An identical arrangement is located on the opposite face of the collar permitting the bearing to carry load in either direction.

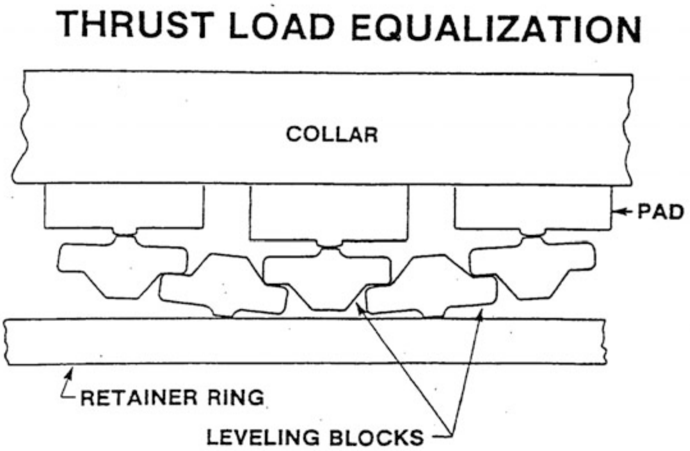

FIGURE 4.43

The design used by Westinghouse in almost all cases is lubricated by flooding the chamber encasing the bearing. This design is shown in Figure 4.44. Due to the fact that pressurized oil flows over the collar O.D. and between shoes, there are parasitic (churning) power losses associated with these areas.

Fig. 4.43 Cross-section of a thrust bearing

leveling blocks support the upper leveling blocks and transmit the total load smotthly to the retainer ring. A cross-section and an exploded view of a thrust bearing is shown in Fig. 4.44. LEG thrust bearing, built by Kingsbury, Inc., has oil feeds built between pads unlike a single feed hole at the bottom of the flooded-bearings in Westinghouse Design.

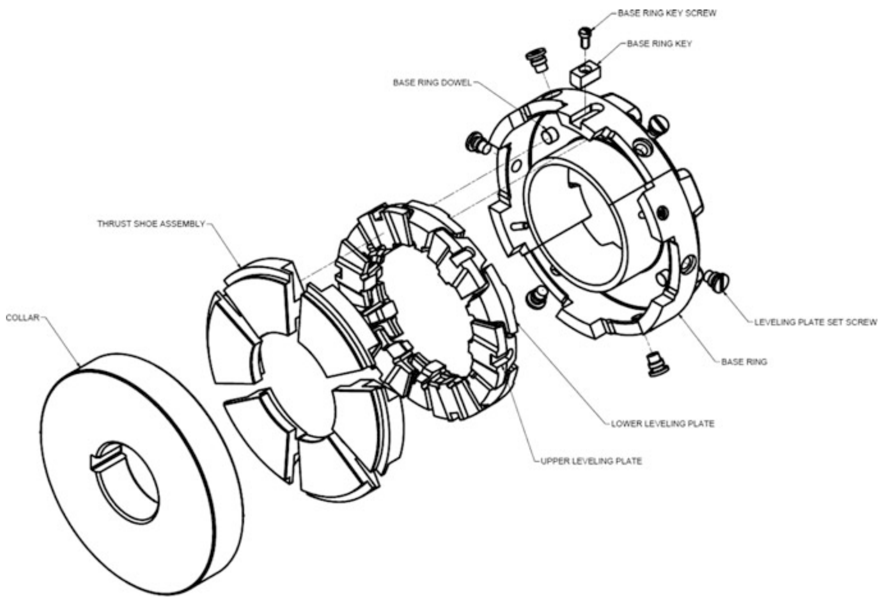

Fig. 4.44 Exploded view of thrust bearing parts

4.15 Symptoms of Issues in Fluid-Film Bearings: Journal (Radial) Bearings

List of symptoms noticed in journal bearings are listed as follows:

- Bearing temperature measured at the minimum oil film location is generally known as, “bearing metal temperature”. This is the most important parameter that provides symptoms of bearing issues along with the rotor vibration associated with it. Continuous monitoring of bearing metal temperatures provides clues on:
  (a) **Shaft misalignment**—a change in shaft alignments from the original design could change the journal positions inside the bearings. This may either shift the journal position away or towards the thermocouples associated with unloading or loading of bearings respectively. When the rotor load increases, the oil film thickness reduces with an increase of oil film pressure and temperature. When the journal moves away from the thermocouple, the bearing is generally unloaded and the metal temperature goes down. Unloaded bearing typically reduces oil film damping and increases rotor vibration. Opposite effect is observed for a loaded bearing.
  (b) **Shaft runouts**—Excessive shaft runout on an overhang shaft, which is supported by a bearing at the fixed end, brings the journal close to the boundary film at low rotor or TG speeds. The bent journal results in higher

bearing metal temperature. If the rotor continues to operate in this condition, the bearing temperature gets amplified every time the rotor passes through a critical speed during start up or coast down. Slow roll vector measurement at low rotor speeds (between 300 and 500 RPM) provides the amount of shaft runout.

(c) **Bearing Load Variations**—(a) Vacuum deflection due to condenser pressure variations in a certain category of steam turbines unloads LP bearings. The vacuum loading effect typically is being observed in fossil-type LP turbines operating at 3000/3600 RPM. (b) On HP turbines, partial arc steam admission loads would unevenly load and/or unload bearings depending on the resultant load directions. (c) In half speed machines (1500/1800 PM), flexible LP bearing support steel pedestals could deteriorate in service causing increased seismic vibration. Under those circumstances, the unloaded journal moves up inside the bearing clearance and increase the minimum oil film thickness; This could reduce damping and bearing metal temperature.

(d) **Oil whirl**—During oil whirl, damping in the oil film reduces (due to dominant cross-coupled stiffness) which increases rotor sub-synchronous vibration component and reduces bearing metal temperature. Unloaded bearings are susceptible to oil whirl and/or whip.

(e) **Steam whirl**—When the steam unbalance forces are dominant (during partial-arc operation), they transfer energy into fluid-film bearings. This could result in unloading one of the bearings that increase rotor vibration and decrease bearing metal temperature. Steam whirl affects HP turbine bearings only.

(f) **Excessive mass unbalance in rotor**—When mass unbalance force levels exceed the nominal residual levels, it could oppose oil film damping. When unbalance forces overcome the damping, the rotor 1× vibration increases. Other associated symptom is the reduced metal temperature due to unloaded bearing.

(g) **Film cavitation** is caused by phase transfer of circulating oil from the liquid phase into vapor phase due to instantaneous and rapid pressure changes in the upper half of the bearing. This phenomenon is very rare and the system corrects the situation during continuous operation. Cavitation could occur at heavier loads with journal reaching boundary film and could cause fatigue damage of Babbit material. One of the effective measures to address this condition is to increase the oil feed pressure to the affected bearing.

(h) **Electrical discharge** in bearings could occur due to faulty grounding or loss of insulation from electrical grounding. This can cause discoloration in a journal surface or a pad surface exposed to grounding. Grounding could cause pitting of journal and bearing surfaces. Mitigation measures include checking the condition of ground brushes and replacing them when they are severely damaged or became ineffective.

(i) **Elevated oil film temperatures** could cause Babbitt or pad material fatigue, creep and pitting of bearing surfaces. Mitigation is to re-babbitt the bearing surfaces.

4.16 Symptoms of Issues in Fluid-Film Bearings: Thrust (Axial) Bearings

Thrust bearing metal temperature (measured at the minimum film thickness), oil inlet and drain temperatures provide symptoms of issues in the machine. Some of the commonly observed symptoms are listed below:

(a) Pad metal temperatures on both active (thrust end) and passive (non-thrust end) sides of a thrust bearing provide symptoms of thrust load conditions of the operating unit. Pad thermocouples installed facing the thrust collar on both sides provide temperatures of the thrust and the non-thrust ends. Measured metal temperature increase indicates one or more of the following: (a) axial thrust is high on the side of the high temperature, (b) Play or excessive wear in the leveling blocks that could disable their function, (c) distorted thrust cage and (d) starved bearing without sufficient oil etc.
(b) Deficiency in oil flow or oil pressure could be the cause of temperature increase in thrust bearing. Check oil inlet/drain temperatures for clues. Turn the nozzle opening by one to two turns to admit more oil. It is also recommended to check oil filters for contaminants and solid particles etc. Frequent oil flush could resolve this issue.

4.17 Closure

This chapter covered the following materials:

- Pedestal stiffness in conjunction with the fluid film stiffness (springs in series) makes the rotor system flexible.
- Pros and cons of contact, non-contact (fluid-film) and magnetic type bearings.
- Hydrostatic bearings use constant oil inlet pressure at all rotor speeds. They are also used as oil lifts to protect bearing and journal surfaces against heavily loaded bearing conditions at lower speeds.
- Non-contact type (journal floats inside the bearing with no metal-to-metal contact) hydrodynamic bearings are used in turbo-machines for better load capability and longer life.

- Among all bearing types, partial-arc bearings provide the most damping and better load carrying capability; however, they are susceptible for oil whirl due to self-excitation caused by cross-coupled stiffness. Hence, they are applied to support heavier LP rotors designed in nuclear powered systems.
- Tilt-pad bearings (such as 3, 4 or 5 pads) eliminate self-excitation due to oil whirl; however, they are not suitable for eliminating self-excitation due to steam whirl.
- Multiple pad bearings provide better stability for mild and/or medium steam whirl conditions with properly aligned pad pre-loading.
- Anti-swirl vanes and flow dams eliminate rotor instability due to steam whirl.
- Special type squeeze film damper bearing could resolve issues due to a specific or unique operating condition where other bearing types were found unsuitable or when additional damping is required. However, studies are required before selection.
- Thrust bearing is applied to control and position rotors in the axial direction due to thrust unbalance loads generated by the working fluid in a turbine.
- General symptoms of faulty bearings and possible causes and potential solutions were discussed for both radial and thrust bearings.

References

1. Lund J (1966) Self-excited, stationary whirl orbits of a journal in a sleeve bearing. PhD thesis, Rensselaer Polytechnic Institute, Troy, NY
2. Lund JW (1965) Stability of an elastic rotor in journal bearings with flexible, damped supports. J Appl Mech 911–920
3. Glienicke J et al (1980) Practical determination and use of bearing dynamic coefficients. Tribol Int 197–207
4. Vance MJ (1987) Rotordynamics of turbomachinery. Wiley
5. Subbiah R, Bhat RB, Sankar TS (1986) Rotational stiffness and damping coefficients of fluid film in a finite cylindrical bearing. ASLE Trans 29(3):414–422
6. Nicholas JC, Gunter EJ, Alaire PE (1977) Stiffness and damping coefficients for the five-pad bearing. In: Presented in ASLE lubrication conference in Kansas City, 3 Oct 1977, pp 50–58
7. Morton PG (1974) The derivation of bearing characteristics by means of transient excitation applied directly to a rotating Shaft. In: IUTAM symposium, dynamics of rotors, Lyngby, pp 350–379
8. Salamone DJ (1984) Journal bearing design types and their applications to turbomachinery. In: Proceedings of thirteenth turbomachinery symposium, pp 180–190
9. Ehrich FF (1999) Handbook of rotordynamics. Krieger Publishing Co. Inc
10. Adams ML (2001) Rotating machinery vibration. Marcel Dekkar Inc., New York
11. Gross WA et al (1980) Fluid film lubrication. Wiley
12. Muszynska A (1986) Whirl and whip—rotor/ bearing stability problems. J Sound Vib 110:443–462

13. Alford JS (1965) Protecting turbo-machinery from self-excited rotor whirl. Trans ASME J Eng Power 333–334
14. Childs D, Kim CH (1986) Analysis and testing for rotor dynamic coefficients and leakage: circumferentially grooved seals.In: Proceedings of second IFToMM international conference on rotor dynamics, Tokyo, pp 609–618
15. Dietzen F, Nordmann R (1987) Finite difference analysis for the rotor dynamic coefficients of turbulent seals in turbo-pumps. In: ASME FED, symposium in thin fluid films, vol 48, pp 31–42
16. Iwatsubo T, Iwasaki Y (2002) Experimental and theoretical study on swirl braked labyrinth seal. In: Proceedings of sixth IFToMM conference on rotor dynamics, Sydney, vol II, pp 564–571, Sept 2002
17. Banckert H, Wachter J (1980) Flow induced spring coefficients of labyrinth seals for application in rotor dynamics, vol 2133. NASA Conference Publication, pp 189–212

Chapter 5
Rotor Balancing: Concept, Modeling and Analysis

5.1 Introduction

In the previous four chapters, we focused on rotor dynamic characteristics, behavior of stationary bearing support steel pedestal structures, rotor and blade mechanical coupling effects influencing blade-disc frequencies and detailed fluid-film modeling and calculations as applied in turbo-machinery. Those characteristics, discussed before, apply for all rotating machines regardless of their size. Another important parameter in rotating machines is "residual unbalance" and the balance-ability condition of rotors. It is important to know what parameters could drive rotors lose their balance-ability condition over the years of operation and become unbalanced. This chapter answers those questions and addresses the art and science of balancing with a few real-life examples.

5.2 General

Rotor balancing was mentioned in the elementary rotor modeling discussions in Chap. 1; but with no details. This chapter is exclusively devoted to rotor balancing methods as applied in the factory and on-site. Rotor should be balanced to ISO 20816-2 levels at the factory before they are shipped out to site for installation. Despite factory balancing, rotors may require additional balancing on-site due to errors caused in rotor train assembly. Essentially, rotor balancing is done to minimize the "excitation forces due to residual mass unbalance" at the critical speeds and at the normal operating speeds of the machine.

In rotor dynamic models, mass unbalance (some use "imbalance" for "unbalance". Both terminologies refer to the same rotor condition) element is simulated to

R. Subbiah and J. E. Littleton, *Rotor and Structural Dynamics of Turbomachinery*, Applied Condition Monitoring 11, https://doi.org/10.1007/978-3-319-73296-1_5

amplify rotor responses to identify critical speeds. The mass unbalances present in a rotor tend to drive the rotor amplitudes higher. So, it is important to learn the various rotor-balancing methods that help reducing the excitation force, which in turn, reduces rotor vibration. Rotor balancing is primarily applied to reduce $1\times$ amplitudes only and it is not the right approach to reduce the sub-synchronous vibration components ($1/2\times$) caused by self-excitation due to oil whirl and/or steam/gas whirl and higher order ($2\times$, $3\times$, … etc.) vibration levels.

5.3 Why do Rotors Need Balancing?

We learnt that the shaft eccentricity increase is primarily responsible for mass unbalance in a rotor. Shaft eccentricity is defined as the deviation between the geometric center and the mass center of a rotor. Shaft runout magnifies eccentricity of a shaft. Bigger the deviation, larger will be the shaft eccentricity. When an eccentric rotor (me) spins, it builds centrifugal force "$me\omega^2$". with rotational speed ω. This is known as "the rotor unbalance force" and is responsible for vibration in rotors.

Errors in rotor machining, assembly and alignment could increase rotor eccentricity either individually or cumulatively. In addition, mass variations in a row of turbine blades add to mass unbalance. In case of generator rotors, the rotor unbalances also arise due to improper compensation of stator coil machining areas. However, they also introduce $2\times$ vibration component as well. Rotor balancing essentially reduces mass unbalance (me) and the rotor vibration as a result.

5.4 Basic Methods of Balancing

Simple way of balancing a shaft is "static balancing" at low speeds. In practice, shaft run outs can be investigated using slow roll vector plots obtained at low speeds. For example, for a two-disc rotor shown in Fig. 5.1a, the mass unbalances at the discs align in the same angular positions (or in-phase) at the top dead center (TDC). When the rotor in this unbalanced condition is placed on knife-edge supports at the two ends, the rotor tends to roll with the unbalances reaching to the bottom dead center (BDC) by gravity. This condition of the rotor is known as, "static unbalance". When equal amounts of balance masses are attached at 180° opposite to the current unbalanced mass positions at the discs, the shaft would be statically balanced; hence, it would stay still at any position without rolling. This is typically done to balance the 1st rotor frequency (U-mode).

Similarly, Fig. 5.1b illustrates a simple example for dynamic unbalance at the rotor discs where the masses are 180 out-of-phase to each other. The rotor can only be balanced using both balance masses and the relative phase angle positions unlike in static balancing where balance masses were directly placed opposite to unbalance positions. This type of balancing is known as "Dynamic Balancing" which is very similar to balancing the rotor 2nd or S-mode discussed in Chap. 3.

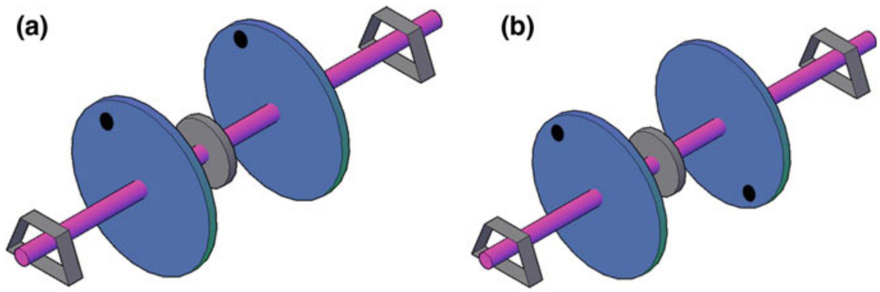

Fig. 5.1 **a** Static unbalance, **b** Dynamic unbalance

5.5 Rotor Classifications

Rotors are, in general, classified as (a) **Rigid Rotor** (b) **Flexible Rotor**.

5.5.1 Rigid Rotor

A rigid rotor is defined as the one that has one frequency prior to the operating or rated speed of a machine. For one frequency and thus one rotor mode to balance, mass unbalances can be corrected in two balance planes. If n is a number of rotor modes, the balance planes required to balance the rotor is n + 1. Essentially, 2 balance planes are sufficient for a rigid rotor balancing. However, by design, a rotor needs to be fully balanced up to 125% of the operating speed. For the LP rotor discussed in Chap. 3, the dynamic mode or the 2nd rotor critical frequency falls within the 125% speed zone. Hence, additional balance plane is added (a total of 3 planes) to balance both static and dynamic rotor frequencies/modes. Over speeding of the rotor ensures blade roots to fully seated conforming to rotor steeple profiles. They are typically high speed balanced at the factory. However, these machines fall under the category of rigid rotors as far as the on-site balancing is concerned. As a result, two end balance planes are used on site to perform additional balancing. Thermal bows are typically developed in high temperature rotors over a long period of service. Excessive thermal bows could trigger increased rotor vibration due to mass unbalance in the static mode. In those cases, mid-balance plane is used on site.

5.5.2 Flexible Rotor

A flexible rotor has more than one frequency to balance before reaching to the operating speed. For example, full speed LP rotors (applied in fossil machines) typically have two critical speeds to balance prior to rated speed. Consequently, they have both static and dynamic balancing conditions to balance and they need more than 2 balance planes to balance the rotor. For these types of flexible rotors, mass unbalances cannot be corrected by low speed balance moves alone. Since the low speed balancing helps balancing one frequency and may not help balancing two frequencies simultaneously. So, those rotors are high speed balanced at the factory and may need additional balancing at the assembly on-site. They must have at least three balance planes for balancing the rotor. Sometimes, additional balance planes are created in some flexible rotors to address special balancing needs.

5.5.3 Methods of Balancing

Basically, two methods are applied to balance a rotor. They are (a) Influence coefficient Method, (b) Modal Balancing Method. Modal balancing was not mostly pursued in practice. Hence, influence coefficient method applied in rotor balancing is discussed here.

Shaft eccentricity is the key parameter in rotor balancing. Therefore, the objective of a balance engineer is to reduce mass-eccentricity and decide whether a static or dynamic balancing is required. The critical points will be covered in this chapter to give a basic to high-level understanding of the techniques needed to perform this task. Techniques and methods described in this chapter are mostly applied in balancing with some exceptions and special needs. However, they have been used successfully for nearly half a century on thousands of Turbine-Generator (T-G) trains.

First, the approach used to balance rotors requires a basic understanding of vectors. The vector adds another dimension known as direction to a force, or a velocity. It must have both a direction and a magnitude. The use of a polar coordinate system will also be needed for plotting. The polar coordinate system used here is with reference to angular positions from 0 to 360° (Fig. 5.2). These angular positions will be used to define the direction of the vectors from the origin of the polar plot. The magnitude of the vibration vectors will be measured in acceleration, velocity and displacement. An in-depth explanation will be covered later in this chapter.

5.6 Practical Field Balancing of Turbine—Generator (T-G) Trains

Before we dive deep into rotor balancing, it is important to understand the many elements associated with it. They are discussed in sub-sections below.

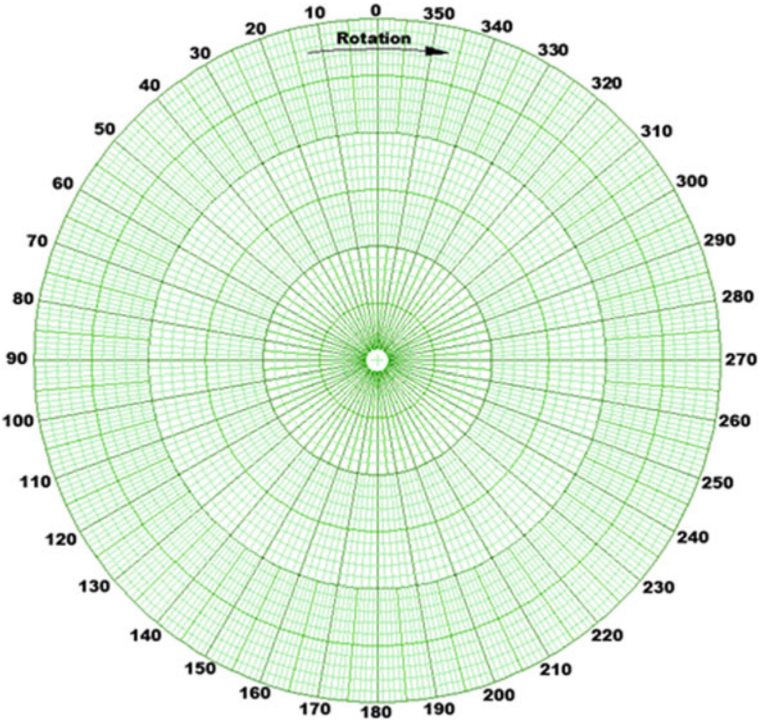

Fig. 5.2 Typical polar plot with angular degree references

5.6.1 Vibration Measurement

Vibration has two main data processing forms: (a) Unfiltered data and (b) Filtered data. Most machine monitoring systems use unfiltered data, which is also known as raw vibration data. The unfiltered vibration is a summation of all the harmonics or frequency components of vibration within a given spectral range. The issue with unfiltered vibration is that since it includes the summation of all the different frequencies, it only gives magnitude of vibration and no phase angle positions. In order to balance a rotor, both magnitude and direction are required. To gather this information, the second form of data is needed; this is known as filtered vibration.

Signal is filtered for a specific frequency of interest, disregarding all other frequencies outside the set bandwidth. Since the most important frequency component in T-G systems is 1× vibration at the rotor operating frequency, by filtering a narrow bandwidth at the running speed frequency, the specific magnitude of the vibration at that frequency can be determined.

Unbalance occurs when an eccentric mass spins about the center of rotation of a rotor. The location of this mass is often referred to as the heavy spot. This causes a once per revolution (1×) oscillation of the rotor resulting in vibration. To determine the angular position of the heavy spot on the rotor, a reference system needs to be setup between the measured vibration and position on the rotor.

The most common industrial technique presently applied is to use a reference signal in conjunction with the vibration signal. In this setup, a notch, keyway, key, reflective tape or mark on the rotor can be used as the reference point. This reference point is then used with a proximity probe, optical tachometer or laser tachometer to generate a once per revolution pulse in the signal. This is known as the reference signal. The timing is measured between the reference signal and the second signal which comes from the vibration probe. The vibration signal is sinusoidal wave that oscillates between maximum (also referred S-max) and minimum (S-min) amplitudes. Measuring backwards in time from the reference signal to the maximum peak of the vibration signal will result in an angular position measured in degrees. This is known as the phase angle and it is considered lagging the reference signal.

Two examples are shown below (Fig. 5.3). The top graph shows a phase that is lagging the reference signal by 90° and the bottom graph shows the phase lagging the reference by 270°. Note that the measured pulse is from the leading edge of the reference signal. This is the actual starting point or considered as 0° on the rotor or shaft. When the notch, mark or piece of tape is narrow on a large diameter rotor, there will be little difference between the angular position and the notch or tape.

On a small diameter rotor with a wide notch, mark or piece of tape, there can be a significant difference in the angular position depending on where the measurement is taken along the reference. For example, if the rotor diameter is 30 inches, then the circumference would be roughly 94.25 inches. To determine the degrees per inch of circumference, divide 360° by the circumference of 94.25 inches. This results in approximately 3.82° per inch. If the notch or mark or piece of tape used has a reference of one inch wide, then the maximum error introduced by picking a random position along the width for zero reference would be 3.82°.

On the contrary, if the same notch or mark or piece of tape were used on a rotor with the diameter of 10 inches, the maximum error introduced would be 11.46°. The rotor or shaft circumference would be approximately 31.42 inches. This would result in the width of the reference notch or mark or piece of tape to be approximately 11.46° per inch. To minimize the introduction of this type of error, it is important to consistently use the leading edge as the reference point for zero degrees.

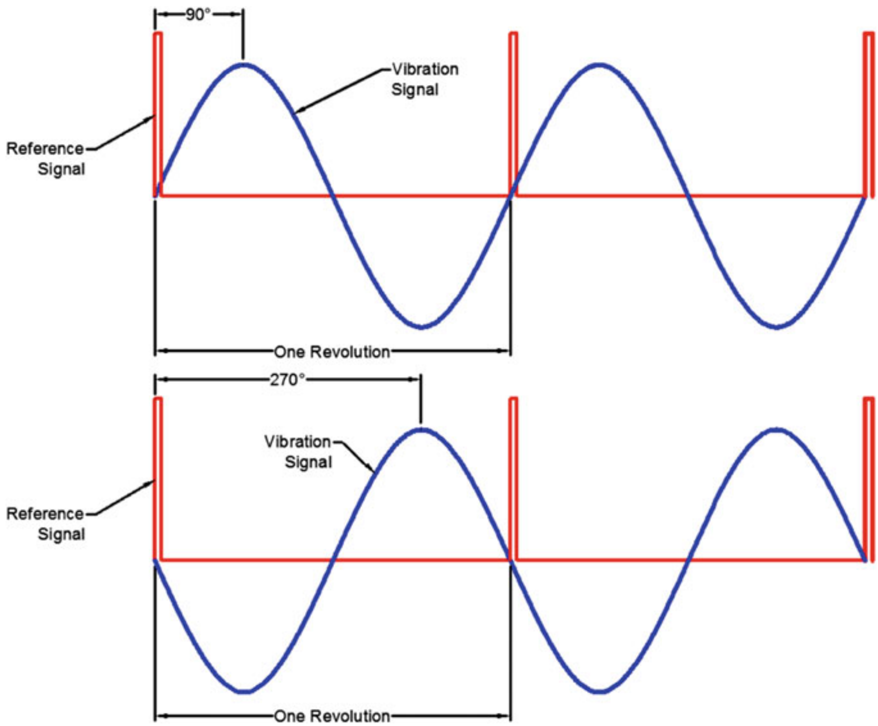

Fig. 5.3 Phase reference top 90° and bottom 270°

Shaft vibration can be measured as acceleration, velocity or displacement. Generally, acceleration is expressed in RMS (root mean square), but it can also be expressed in Peak-to-Peak or 0-Peak. Velocity is commonly expressed in RMS or Peak (0-Peak). Displacement is most commonly expressed in Peak to Peak. The difference between them is determined by knowing how much of the waveform is measured. Peak to Peak uses the entire vertical measurement of the waveform from the minimum peak to the maximum vertical peak. The Peak (0-Peak) measurement uses the vertical measurement from zero to maximum peak of the waveform. The RMS measurement is the square root of the square of the function that defines the continuous waveform. This can be approximated in most cases by multiplying the Peak (0-Peak) value by 0.707. The comparisons of the various measured quantities are shown below (Fig. 5.4). The selection of a measured quantity is determined by reviewing the waveform data. If there is a significant number of erroneous spikes on the signal, then selecting an RMS expression may be order.

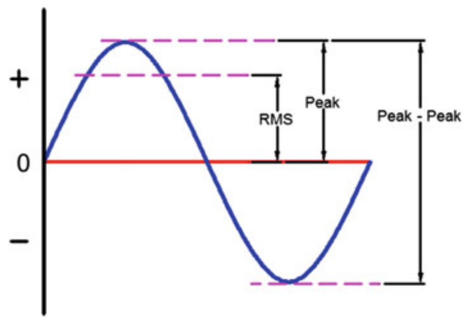

Fig. 5.4 Vibration measurements

It is important to understand how acceleration, velocity and displacement signals rare related to each other. Velocity can be calculated by integrating acceleration. Similarly, displacement can be obtained by integrating velocity signals. Double integration of acceleration signal converts to displacement. The following equations simplify the rigors of integration.

Defined Variables:

A = Acceleration in g's (in/sec^2)
V = Velocity in in/sec
D = Displacement in mils
PI = 3.1415
g = Gravitational constant 386 in/sec^2 (980 mm/sec^2)
f = Frequency in Hertz
$V = (PI) \times (f) \times (D)$
$V = (61.44) \times (A/f)$
$A = (0.511) \times (D) \times (f^2)$
$A = (0.0162) \times (V) \times (f)$
$D = (0.3183) \times (V/f)$
$D = (19.75) \times (A) \times (f^2)$

To convert the phase components between acceleration, velocity and displacement, add 90° each time the amplitude is converted. For example, when acceleration is converted to velocity, add 90° to the phase. Similarly, when converting velocity to displacement add another 90° to the velocity phase. The following Fig. 5.5 shows the waveform relationship between acceleration, velocity and displacement. Acceleration starts with a phase of 90°, then when moving to velocity, there is a 90-degree shift and the same shift is used for displacement calculations.

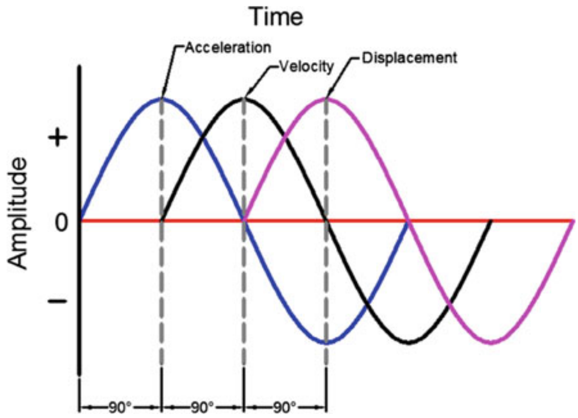

Fig. 5.5 Waveform relationships of acceleration, velocity and displacement

5.6.2 Various Vibration Components

The relationships between the vibration components is the key for a better understanding of balance concepts. There are three components of vibration: absolute, seismic and relative vibration [1, 2]. The absolute vibration (also known as shaft absolute vibration) is the vibration measurement from the rotor to free space. The seismic vibration (also known as casing/bearing vibration) is the vibration measured on the bearing structure to free space and the relative (also known as rotor vibration) vibration is measured between the rotor and the bearing. The relationships between these components can be defined vectorially. When the seismic vibration is added to the relative vibration, the resultant will be the absolute vibration. Also by vectorially subtracting either the seismic or relative vibration from the absolute vibration the resultant will be the missing component. See Fig. 5.6.

- Absolute Vibration Vector − Seismic Vibration Vector = Relative Vibration Vector
- Absolute Vibration Vector − Relative Vibration Vector = Seismic Vibration Vector
- Seismic Vibration Vector + Relative Vibration Vector = Absolute Vibration Vector

These relationships are only valid when the vibration data is taken in the same axial and radial plane along the length of the rotor. Failure to use readings from the same axial and radial plane can skew the vibration data and introduce error into the calculations. A radial variation of less than 10° and axial variation of less than six inches is usually acceptable tolerances for the measurement locations. Calibration should be performed to ensure that the measured readings do not vary greater than the specified axial and radial distances in order to reduce measurement errors.

The other critical variable in the calculations is the unit of vibration and the type of vibration. For example, if absolute vibration is being calculated, then all the vibration readings must be in displacements and they must be of the same representation i.e. peak to peak. This can be accomplished by integrating the seismic readings to displacement. When the formulae are used, add 90° to the phase angle each time the integration is carried out.

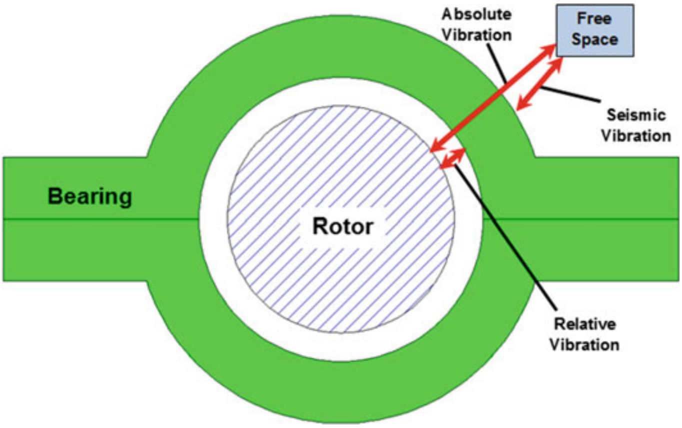

Fig. 5.6 Vibration component relationships

Vibration typically will be shown in terms of the amplitudes and phase angles. The amplitude can be in units of acceleration, velocity, or displacement. The unit for phase angle is in degrees. Below is an example of some sample readings taken to calculate the absolute from the relative and seismic readings.

Given:

Speed = 3600 RPM
Relative = (3.45 mils p-p ∠ 56°)
Seismic = (0.25 in/s 0-P ∠ 296°)
Step 1: Convert the speed to frequency **(3600/60) = 60 Hz**
Step 2: Convert the seismic reading to displacement D = (0.3183) × (V/f) = (0.3183) × (0.25/60) = 0.001326 inches p-p
Step 3: Convert from inches p-p to mils p-p D = (0.001326-inch p-p) (1000 mils/inch) = 1.326 mils p-p
Step 4: Add 90° to the seismic vibration phase due to the single integration was used
Step 5: Vectorially add the relative and the newly calculated seismic vibration.

Absolute Vibration Amplitude = (3.45 mils p-p ∠ 56°) + (1.326 mils p-p ∠ 26°) = **(4.646 mils p-p ∠ 48°)**

The same calculation can be completed by plotting the relative and seismic values on a polar plot as shown below in Fig. 5.7. The red vector is the relative vibration and purple vector is the seismic vibration. By transposing the seismic vector from the origin to the arrowhead of the relative vector (the purple dashed vector), the new blue vector can be obtained from the origin to the head of the purple vector to represent the absolute vibration. Each circle in this polar plot represents 2 mils p-p (Engineers can draw circles of different amplitudes of their choice). From the plot, the vectors show that the absolute vibration is approximately **(4.6 mils p-p ∠ 48°)**.

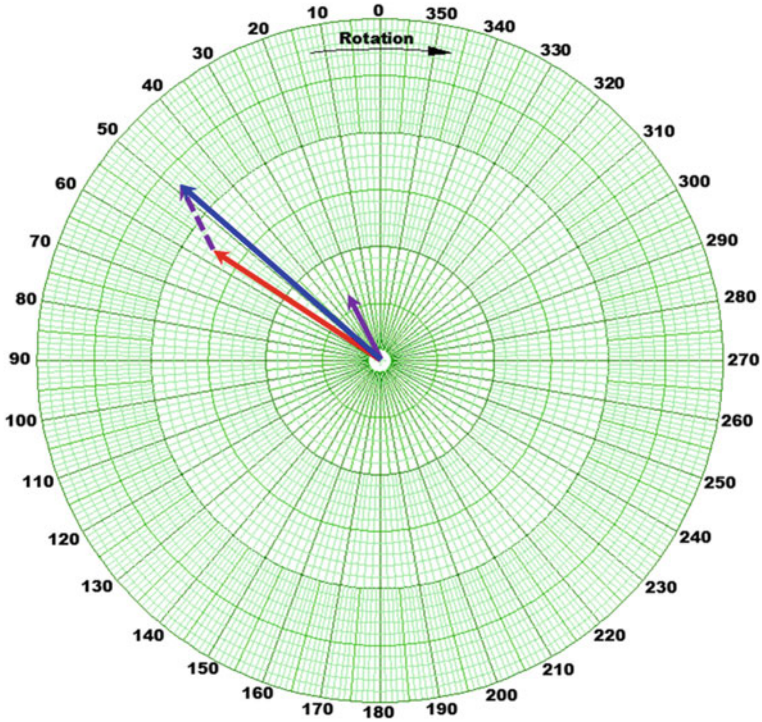

Fig. 5.7 Absolute calculation using polar plot (Scale = 2 mils p-p/major division)

It is important to know these relationships and how they influence each other [3–5]. When one component is known, it is not possible to obtain other vibration components. For example, if the relative component alone is monitored, then the rotor to free space cannot be determined. The rotor may have a very low movement between it and the bearing shown in the plot-display whereas, one may feel the entire floor is vibrating heavily. This is because the rotor is moving in sync with the support system. If seismic readings were also being measured, it would show that there is a significant amount of vibration from the bearing structure to the free space. Similar situations can occur when only the absolute or seismic vibration is monitored. Therefore, it is necessary to monitor at least two of the three components of vibration to fully understand which part is initiating the vibration.

5.6.3 Vibration Data Organization

For the balancing to be effective, it is extremely important to compare datasets before balancing and after balancing that have similar operating conditions. Failure to use similar datasets could skew the calculations and thus making it difficult to predict future balance move strategies.

After the data has been collected, the first step is to organize the data into common categories. The collected data has two main categories and several subcategories. The two main categories are: (a) Transient and (b) Steady State. The transient data includes any data taken while there is a reasonable change in the rotor speed. This would include data during ramp up or coast down of the rotor. Steady State data is when the rotor speed is constant and does not change by more than 50 RPM over a period of at least one hour. When the data does not show a change in speed or measured less than one hour and it is unstable, then such data is considered as transient. Understanding these two main categories will help the analysis of rotor responses to balancing.

The following are the crucial steps when breaking down the transient and steady state data into its subcategories as listed in Table 5.1.

Table 5.1 Data collection for rotor balancing

Transient data	Steady state data
Slow roll	Hold speeds longer than 1 h
Startup	Full speed no load (FSNL) longer than 1 h
Coast down (Shutdown)	Various load conditions longer than 1 h
Critical speeds	
Heat soak speeds	
Full speed no load (FSNL)	

Many units have thermal changes that occur between runs. These sets of data would use the same categories as listed above with a note stating if they were a cold run, or a warm run or a hot run.

5.6.4 Initial Data Required for Evaluation

Under ideal conditions, data needs to be collected for all the operating conditions. For example, if the unit that is being evaluated is a gas turbine which is a peaking unit with cycles on and off the grid based on power demand, then the following data would be important. Prior to site visit for balancing, it is important to collect details such as number of cold, warm and hot start cycles. There may also have large changes in the load demand from minimum load to baseload. With these types of variations in the operation of the unit, it is important to have data from at least one cold startup, online and coast down and one hot restart, online and coast down. This allows accurate evaluation of the transient data when the unit is cold, after the thermal growth has occurred. The online data should contain information of minimum load and base load for several hours. This additional data would allow for a full evaluation as to how the unit reacts under all the various operations. These initial datasets will be referred to as the "**As Found Data**".

5.6.5 Evaluation of Slow Roll Data (Static Imbalance of Shaft Run Out)

Data collected on-site is rarely pristine. Contrarily, the data from a rotor kit in the laboratory or in a closely controlled room will typically produce nice smooth sine wave signals. In those cases, the critical speeds can be easily determined through smooth response peaks and phase shifts. This is rarely the case with data taken from most T-G units on-site. One of the main contributors that skew the data is electrical runout found on the proximity probes. The proximity probes are designed to look at the rotor or shaft surface. Any imperfections of the surface can result in electrical noise on the vibration waveform. Depending on the severity of the imperfections, this can have a significant effect on the total or overall vibration. It can also affect the filtered vibration. Scratches on the rotor surface or pitting or debris are examples that could skew data. A rotor with a single scratch can show up in the waveform. A single scratch can influence the total and 1× vibration readings. Signal alterations due to electrical runout can have impact in the slow roll data, at critical speeds and at rated speed vibration readings. Sometimes, the influence is additive and sometimes it subtracts from the true vibration depending on at what phase angle the vibration occurs.

To address the electrical runout, the slow roll steady state waveform must be subtracted from the waveform data being evaluated. This is difficult to perform; hence, most software packages do not have this function. Since the evaluation will be for balancing, an alternative is to look at the slow roll vector readings for 1× vibration and subtract them from the 1× vector reading of the current data. The following figures show the same data from a startup. Figure 5.8 shows the as-measured data also known as the RAW data. Notice that the 1× amplitude shown by the red line is approximately the same as the Overall (Total) amplitude shown by the black line. The blue dotted line is the phase angle. When determining the slow roll vector reading that will be used to calculate the slow roll compensation, the data should be collected when the phase angles and the amplitudes are steady. For most turbine-generator trains this reading will be between 100–500 RPM. Data below 100 RPM can be noisy and do not provide a true representation of the actual slow roll runout. Data above 500 RPM are influenced by the dynamics of the rotor in fluid-film and hence does not represent the true slow roll runout.

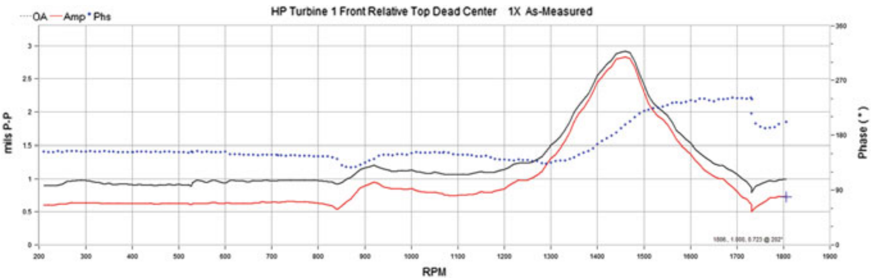

Fig. 5.8 As-measured bode plot during startup

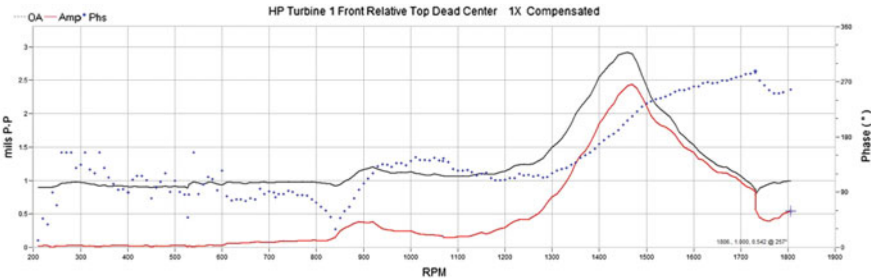

Fig. 5.9 Slow roll compensated bode plot during startup

For the example shown in Figs. 5.8 and 5.9, data gathered at 270 RPM was used as the slow roll reference. The 1× vector was then subtracted vectorially from each reading in the dataset and the results are plotted in Fig. 5.9. From this plot, it can be noticed the difference between the vector compensation versus waveform compensation. If they were the waveform compensation, the Overall (Total) vibration would have approached the highest value similar to the 1× vibration.

Selective software was used in this example, but this can also be done relatively easily using a calculator that can do vector math or by plotting the points on a polar plot. An example is shown in Table 5.2.

Table 5.2 Calculation of data by vector sum

Reading description	Overall value (mils p-p)	1× amplitude value (mils p-p)	Phase angle (deg)
Slow roll reference (270 RPM)	0.96	0.61	155
Steady state (1800 RPM)	1.61	1.40	206

Using the polar plot with a scale of 1 mil p-p circles, the slow roll runout data point is plotted. Instead of drawing the slow roll runout vector from the original data, the vector starts at the slow roll data point and is drawn to the origin. The reason for drawing the vector in reverse is to ensure that when it is transposed, the run out will be subtracted and not accidently added to the vibration reading (purple vector). Next, the steady state data is plotted. The vector is drawn from the origin to the data point (red vector). Transposing the slow roll runout vector such that the tail is placed at the head of the vibration vector (purple dashed vector), the compensated vibration vector (blue vector) is drawn from the origin to the head of the transposed slow roll runout vector. The compensated vibration vector resulted as **1.1 mils p-p ∠ 231°**. When the software was used the compensation, vibration-vector was calculated to be **1.122 mils p-p ∠ 231°**.

In this example, the compensated or "true" vibration was lower than the actual as-measured vibration indicated on the instrumentation. If these amplitudes were higher, action may have been taken to balance the unit unnecessarily. The opposite could have been true as well, when the as-measured readings display a value that was less than the true vibration. An example of this is when the runout vibration is nearly 180° opposite of the vibration. Suppose the as-measured vibration vector was **3.25 mils p-p ∠ 111°** and the slow roll runout vector was **2.05 mils p-p ∠ 345°**, then the slow roll runout vector is subtracted from the As Measured vibration vector to calculate the compensated vibration vector. The resultant would be **4.75 mils p-p ∠ 131°**. This means that the true vibration is higher than the instrumentation indicated. Therefore, it is important to always look at the slow roll runout vector when evaluating the vibration.

A general rule for the slow roll runout of concern is significant enough when the vibration level exceeds 10% of the alarm level. As mentioned earlier, most electrical runout issues are attributed to imperfections on the rotor or shaft surface. Diamond burnishing the surface area that passes under the proximity probes will usually correct the issue. There are cases where the rotor is out of round typically resulting in a large 2× runout, diamond burnishing most likely will not help and more significant machining will be needed to restore a true circular target area for the probes (Fig. 5.10).

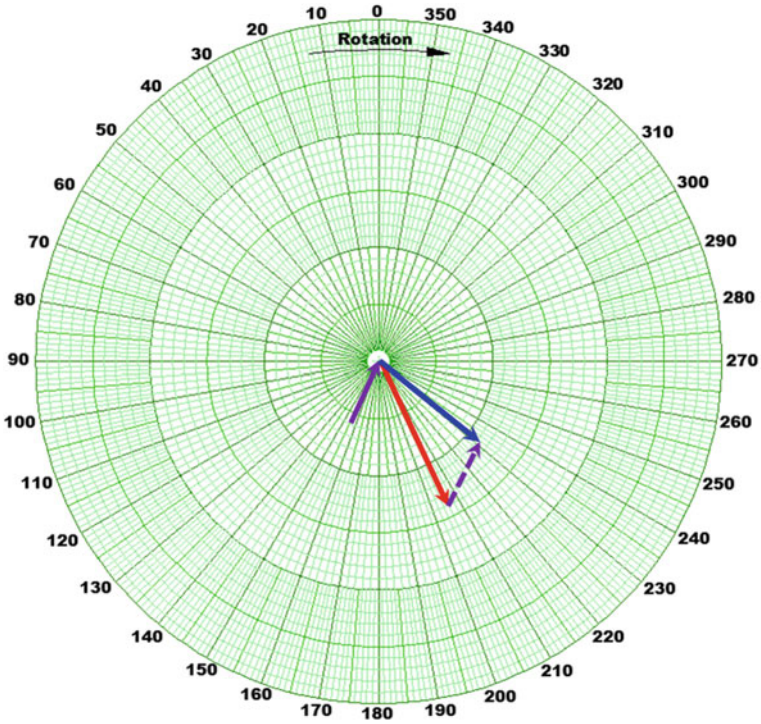

Fig. 5.10 Slow roll compensation using polar plot (Scale = 1 mils p-p/major division)

5.7 Natural Frequency, Mode Shapes and Critical Vibration

The natural frequency of an object is the rate at which an object vibrates once it has been set into motion and not disturbed by an external force. With regards to T-G systems, the natural frequencies that are of most concern are foundation, bearings, housings, rotor and blades. Many times, balancing is used as the least cost solution or temporary solution to an issue. If a unit has known foundation natural frequency that is close to any of the component natural frequencies, the best course of action would be to move that natural frequency through a design change. Sometimes, this could result in a significant cost to redesign. If cost is not the issue, it could be the duration it takes to fix the issue. Under these situations, other alternatives are necessary. Recognizing the fact that forcing function excites the natural frequencies, reducing the forcing function will bring the vibration down and well within the acceptable levels. The dominating forcing functions on a T-G train are the imbalances of the spinning rotors. By balancing the rotor train, they still can operate the machines closer to the natural frequencies of concern.

Determination of natural frequencies of rotors will assist in calculating the best possible balance for the rotors. Most T-G trains operate below their third natural frequency. The steam turbines in half-speed designs operate between their first and second natural frequency. Full speed machines operate between their second and third mode. Generators, boiler feed pump turbines, and gas turbines generally operate between their second and third mode with some operating above their third mode. Exciters and collectors typically operate between their first and second mode, but some operate just below their first mode. Note that there can be some outliers, but the vast majority falling into the natural frequency bands mentioned above.

The First Mode or First Natural Frequency has the mode shape of bow or U-mode. It is often referred to as the bow mode, gravity mode or static mode. If readings were taken at each of the bearing ends, the phase angle would be approximately the same. The highest amplitude occurs at the center of the rotor.

The Second Mode or Second Natural Frequency has the mode shape of S. It is often referred to as the S Mode or dynamic mode. If readings were taken at the critical speed at each of the two end bearings, the phase angle would be approximately 180° from each other with the node point at the center and the vibration amplitude would be minimum.

The Third Mode or Third Natural Frequency has the mode shape of M or W depending on the orientation of mode shape. This mode has a combination of a static and dynamic component. The ends of the rotor are in phase with each other, while the center is approximately 180° out of phase. See Figs. 5.11a, b and c.

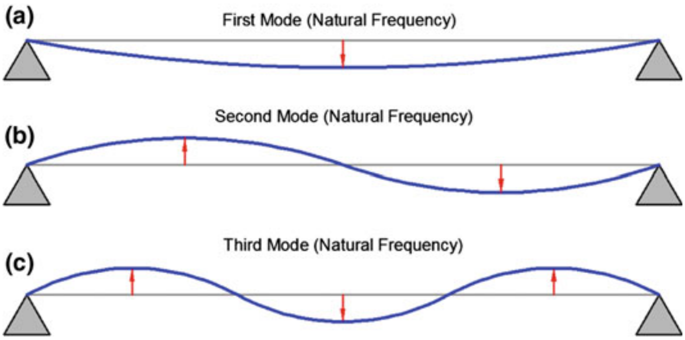

Fig. 5.11 Natural frequency mode shapes

5.8 Actual Heavy Spot Angle Versus Indicated Heavy Spot Angle

The heavy spot is the actual location of the mass imbalance on the rotor. The indicated heavy spot angle is the angle that measured using an analyzer that can filter the 1× vibration. At a very low speed that is below the critical speed, both the actual heavy spot angle and indicated angle will have the same angle (Fig. 5.12a). As the speed increases towards the critical speed the actual angle of the heavy spot will remain the same, but the indicated heavy spot angle will increase. When the critical speed is reached, the indicated heavy spot angle will be 90° greater than the actual heavy spot angle (Fig. 5.12b). After passing the critical speed, the indicated heavy spot angle will continue to increase until it reaches 180° greater than the actual heavy spot angle (Fig. 5.12c). This is commonly known as the low spot angle. It is exactly 180° out of phase with the actual heavy spot. The phase will remain constant until the rotor approaches the next critical speed. At that point, this series of events will repeat for that critical speed. The figures below show an example vibration and phase changes through this process. Corresponding to heavy spot shown by phase angle positions, the high spot is shown by vibration magnitudes.

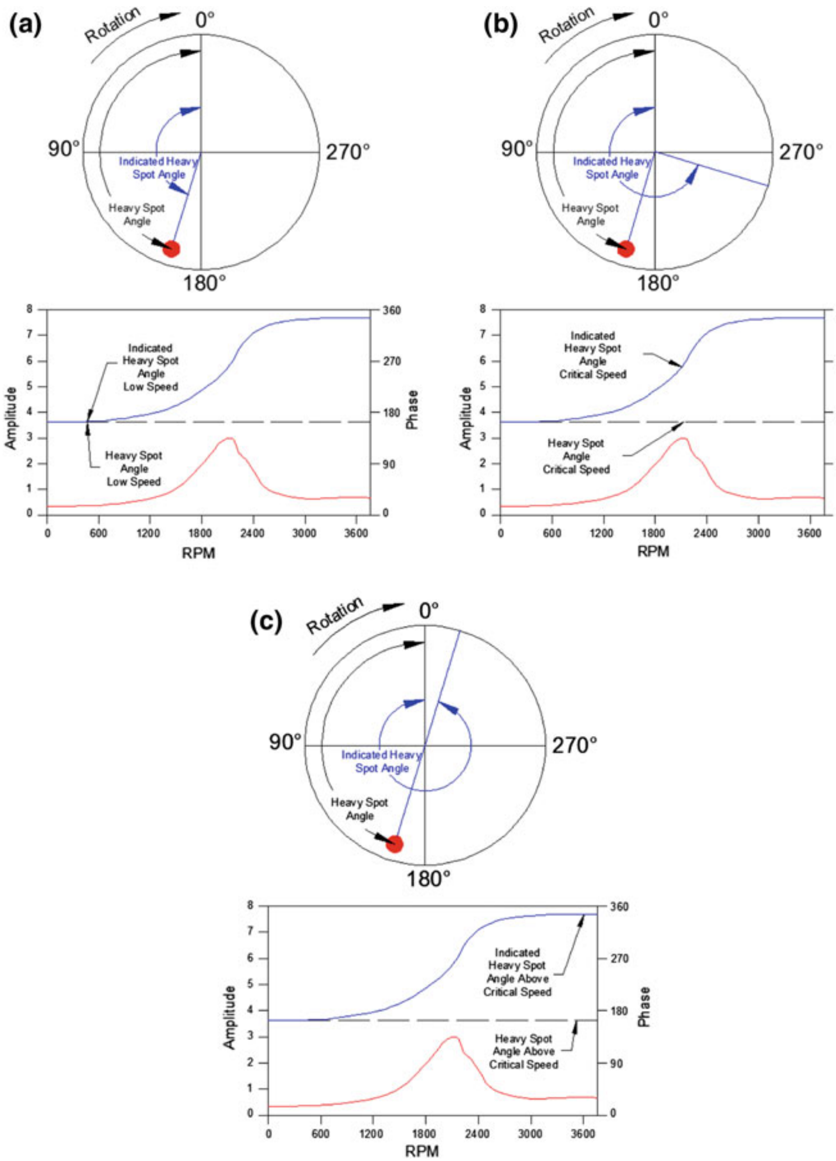

Fig. 5.12 **a** Heavy spot angle position before the rotor critical speed **b** Heavy spot angle position at the rotor critical speed **c** Heavy spot angle position after the rotor critical speed

5.8.1 Calculating Lag Angle to Mode Shape Relationship

Lag angle in reference to weight placement is the angle against rotation that the effect lags or is behind the weight placement angle. To calculate the lag angle, the following equation can be used.

Lag Angle = (Weight Placement Angle) – (Effect Vector Angle)

(Note: If the value results in a negative angle add 360° to make it positive.)

For example, if there is a zero-degree lag, and the weight was installed at 300°, then the effect vector would point directly at 300°. This is shown as the blue vectors and weight on the following Fig. 5.13. Another example is if the lag angle were 50° and the desired effect angle were 80°, and then the weight would have to be installed at 30–50° ahead of the effect angle with respect to rotation. This is shown as the red vectors and weight on the following Fig. 5.13.

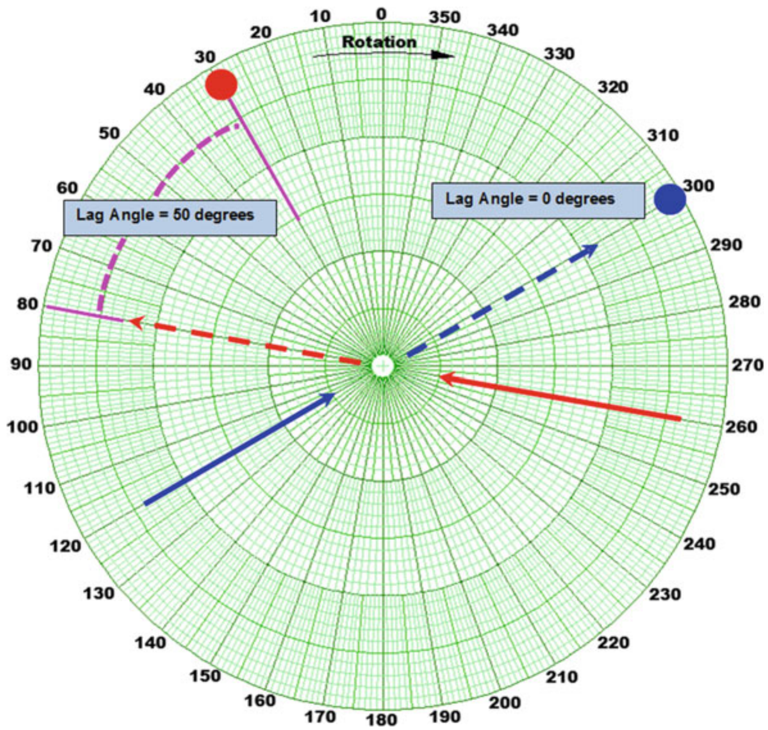

Fig. 5.13 Effect vector to weight placement lag angle

As previously mentioned there are three mode shapes that are of concern in turbine-generators. These mode shapes are excited at various speeds as the unit runs up or down. They are the first mode shape or static (bow shaped) mode, the second mode shape or dynamic (S shaped) mode and the third mode shape or dynamic and static (M or W shaped) mode.

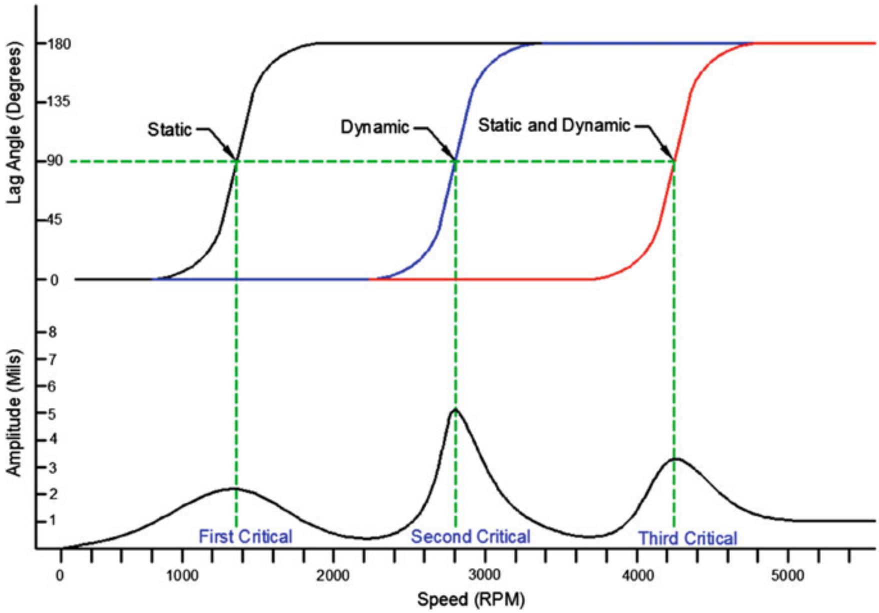

Fig. 5.14 Lag angle to mode shape relationship

To better understand how lag angles, relate to the various mode shapes of the rotor, Fig. 5.14 can be used. As the unit starts at 0 RPM, the lag angle is at 0° as none of the modes have been excited. As the speed increases, in this case past 1000 RPM and approaches the first mode of the rotor (for example) where the lag angle increases shown by the black curve labeled “static”. It should also be noted that the second and third modes are still at 0-degree lag as they have no effect since they have not been excited. As the speed increases to the first critical of the rotor the lag angle reaches 90° and the lag angle remains 0 for the second and third modes. The lag angle increases until it reaches 180° for the static mode. As the speed further increases the second mode or dynamic mode picks up. The dynamic mode follows the same pattern as the first mode and increasing to 180° as the speed increases. Similarly, the third mode follows the same pattern with the third critical having a 90-degree lag and increases to 180° with an increase in the speed.

This phenomenon of lag angle to speed relationship can be a very useful tool when balancing a rotor. By knowing where the rotor is running with an estimated lag angle, it can be made for initial balance moves on the rotor even without knowing the prior effects. With the knowledge of the lag angle to speed relationship and the knowledge of which mode shape is close to speed, an educated estimate can be made as to which plane or planes would be the best for installation of the balance weights. An example of the rotor that was running right at the second critical speed is applied. Two bearings read 180° out of phase to each other and based on this knowledge that it would require a 90-degree lag per end. It is reasonable to place equal amounts of weights at 180° apart and 90° ahead of the desired effect. It is obvious that the center plane will not help as it is a node point and will have no effect.

5.8.2 Identifying Rotor Critical Speeds

With the basic understanding of critical mode shapes, the next step is to determine speeds at which the rotor modes occur. Characteristics that are often observed as a rotor passes through its critical speed are a phase shift and a peak response in the amplitude. In an isolated system with no outside influences, the phase shift will be 180° with the critical speed occurring at the halfway point through the phase shift. In most cases on the T-G trains, the phase shift is typically less than 180°. This is due to a few factors such as bearing oil-film dampening, rotor flexibility, cross effects for other coupled rotors etc. The amplitude peaks can also be influenced by those same factors.

The two most commonly used plots for determining the critical speeds of a rotor are the polar plot and the bode plot. The polar plot when compensated for slow roll runout, the 1× amplitude and phase will start at the origin and make a loop as the speed increases and the rotor passes through its critical speed or speeds. By drawing a line from the origin such that it intersects the loop, the intersection point on the loop indicates the rotor critical speed. This is shown in the Fig. 5.15.

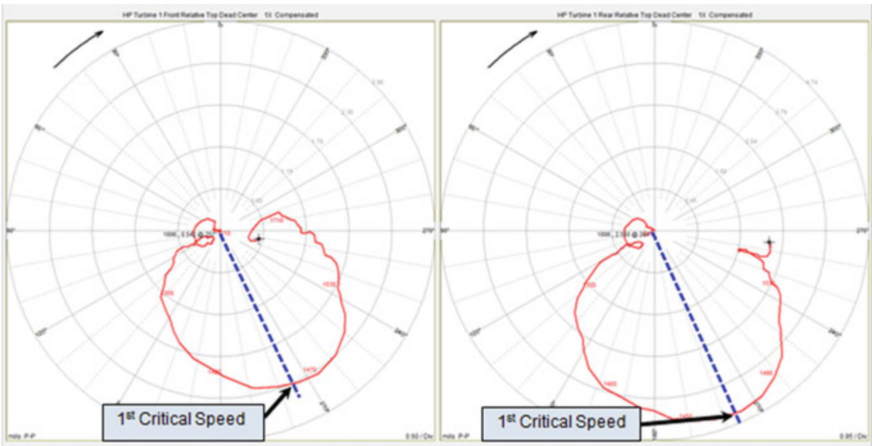

Fig. 5.15 Polar plot identifying the first critical speed

Note on the polar plots that there are small loops near the origin of the plot. Small loops typically represent structure resonances, and/or other effects of rotors within the train or sometimes probe bracketing resonances. The polar plots in this Fig. 5.15 show an example High Pressure turbine (HP) front and rear relative probe orbits. As shown by the intersecting lines on each of the plots, the critical speed is approximately 1460 RPM. The plot provides additional information of this critical speed. When using probes mounted at the same radial angle on each end of the rotor, they can be compared to each other to determine the mode shape of the rotor. If the probes are not radially aligned at the same angle positions, the data can be skewed resulting in invalid determination of the mode shapes of rotors. For this example, both the front and rear probes are mounted at Top Dead Center (TDC) or at 0°. The plot shows that speed of 1460 RPM falls on the first major loop of the polar plot. This indicates that this speed is the First Critical Speed of the rotor. If this speed were identified on the second major loop or third, it would be misinterpreted for the Second Critical Speed or Third Critical Speed respectively. The plots confirm that the phase angle for the front and rear bearings is both approximately 205°. This confirms the rotor mode associated with the first natural frequency. Another important observation that the plot reveals is that the critical speed is roughly 340 RPM from the normal operating speed of 1800 RPM. This means the rotor is operating above the first critical speed and below the second critical speed since the second loop was not noticed.

The second plot that is commonly used to determine the critical speeds of a rotor is the bode plot which uses the speed versus the 1× amplitude and phase. As the rotor goes up in speed and passes through its critical speed, the amplitude will increase to a peak and the phase angle will also shift. As mentioned before, the ideal situation will have a 180° phase shift, but most of the time for the T-G train, the phase shift is observed less than 180°. This is due to soft damping exhibited at the peak responses of the rotor. The peak in amplitude and the mid-point of the phase shift will indicate the critical speed similar to the polar plot. The Fig. 5.16 below shows these typical attributes.

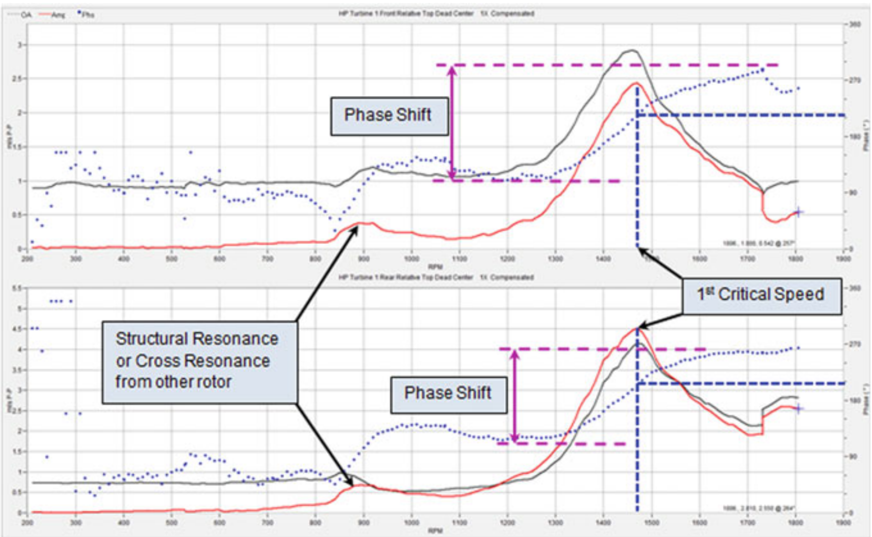

Fig. 5.16 Bode plot identifying the first critical speed

Like the polar plot, the Bode plots help identifying that the rotor is operating between the first and second critical speeds. The first rotor critical speed at approximately 1460 RPM and the phase angles are approximately 205° at the peak amplitudes. There appears to be a non-rotor resonance present prior to 1st rotor critical speed. This resonance could be structural resonance from the support system, from the guarding, probe brackets or even harmonic responses from other equipment operating near the turbine train. Note that the phase shift on the HP front was approximately 170° and the HP rear was approximately 140°.

On units that have orthogonal proximity probes, (accelerometers or velometers can also be used) the orbits can also be used to confirm critical speeds. As the rotor passes through the critical speed, the orbit will go through a transformation. The shape of the orbit will change to a narrower ellipse and in some cases almost a slim straight line at the critical speed. After passing through the critical speed, the orbits usually return to a similar shape of what they were prior to the critical speed. Some influences that can cause this not to behave like this when two rotor critical speeds

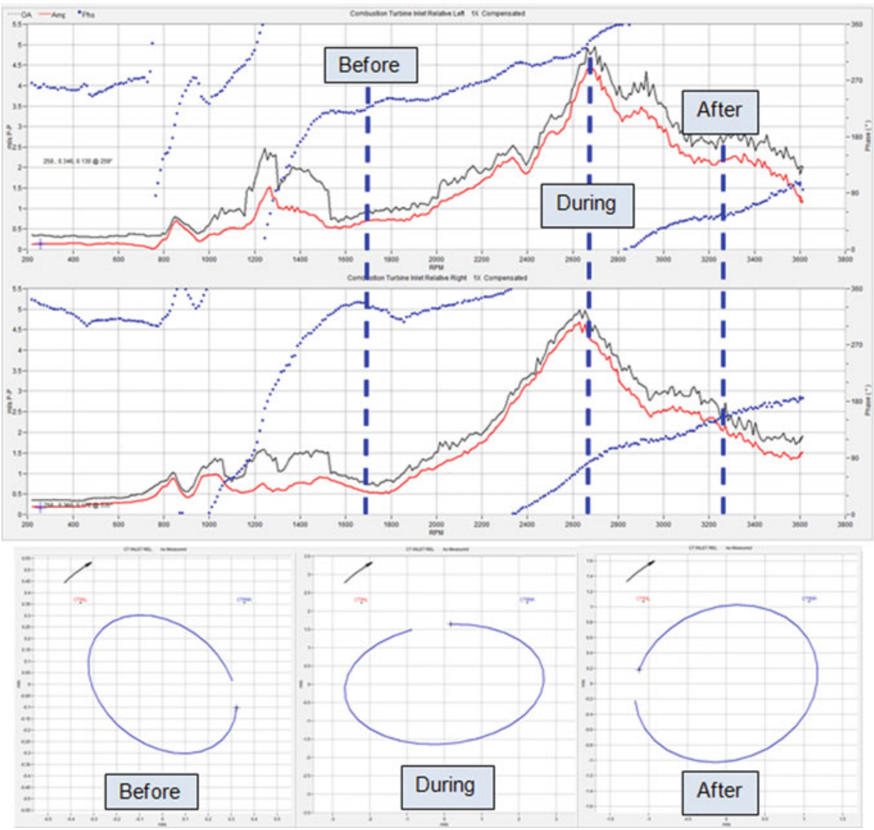

Fig. 5.17 Orbit transformation through second critical speed

are close by to each other or lack of structural dampening, or a rub or fluid film influence etc. An example of the normal behavior is shown in the Fig. 5.17 where the relative probes in the turbine end of the bearing were mounted at 45° right and 45° left of TDC. The blue dash lines correspond to the speeds of the orbits shown below in the bode plots.

Things that are often overlooked are there can be more than one critical speed for a rotor. It should be noted there are differences in the stiffness and dampening of the support system. As a result, it is not uncommon to see split critical speeds when two probes are mounted at different radial angles on each bearing. The following example describes the split critical speeds meaning the mode-shapes are the same. Bode plots show rotor critical speeds one at 1553 RPM and the other at 1621 RPM representing the first mode shape as shown in Fig. 5.18. Most of the time, the speeds are within 200 RPM of each other.

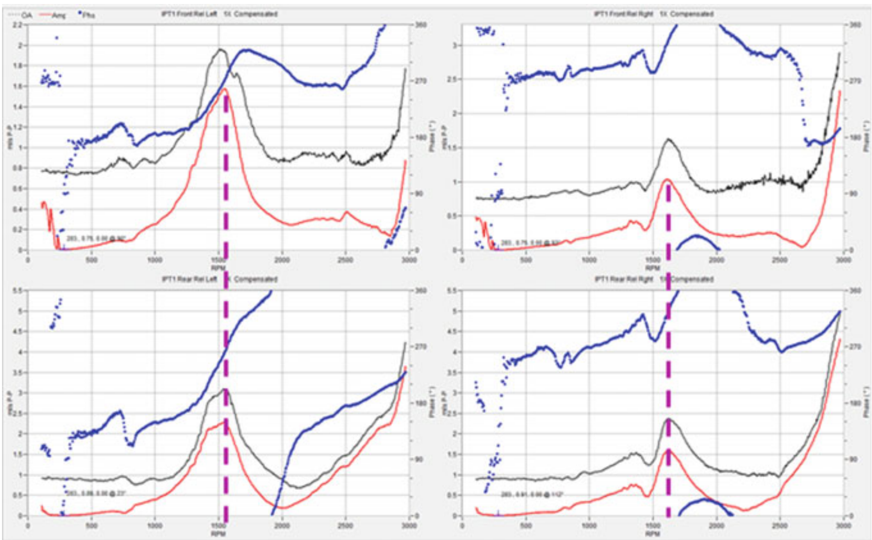

Fig. 5.18 Bode plots showing split critical speeds of the rotor for First Critical Speed

5.8.3 *Determining Static and Dynamic Imbalance Components*

One of the fundamentals to balancing is to determine the type of imbalance that is present. There are two types of imbalance, Static and Dynamic.

Static Imbalance is defined as the $1\times$ vibration at the two ends of the rotor are in phase or have the same angle with each other. For balancing purposes, the two ends of the rotor are considered to have the same phase.

Dynamic Imbalance is defined as the 1× vibration at the two ends of the rotor are 180° out of phase with each other. A combination of Static and Dynamic Imbalance occurs when there is a difference in the vibration amplitude between the two ends of rotor for probes that have same radial measurement angle. In addition, there will be some variation of the phase angles at the two ends that is not the same or not exactly 180° from each other. The following Fig. 5.19 shows both a pure dynamic and pure static set of vibration readings. ***NOTE: The radial angle should be the same for the probes on each end of the rotor that are being used to calculate the static and dynamic components***.

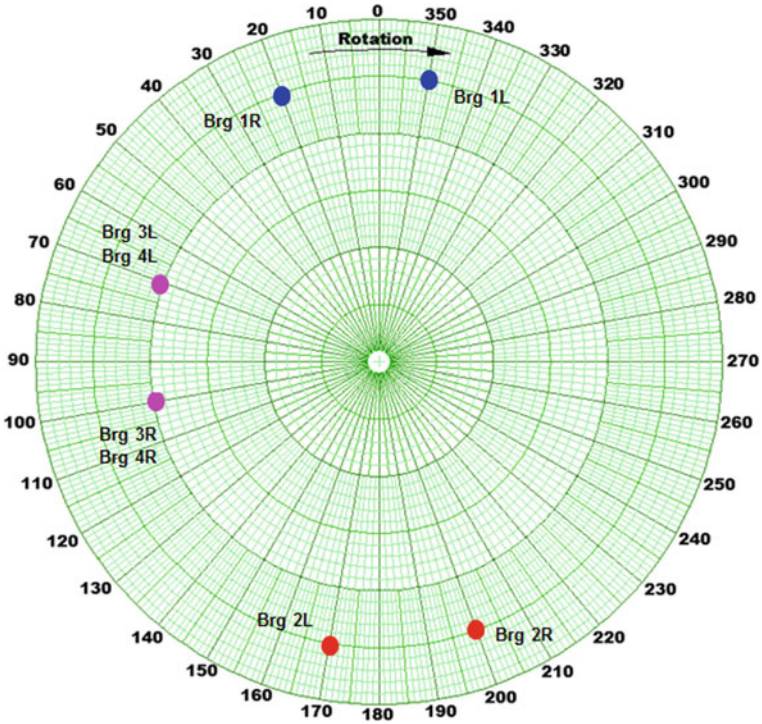

Fig. 5.19 Pure static and dynamic comparison (2 mils p-p/major division)

Bearing 1 and Bearing 2 display pure dynamic motion between the left versus left and the right versus right. The phase is 180° out from end to end and the amplitude is the same. Bearing 3 and Bearing 4 are displaying a pure static between the left versus left and the right versus right. The readings overlay right on top of each other so there is no difference in amplitude or phase from end to end. When the imbalance is pure static or pure dynamic, then the components are equal to the vibration values of the probe readings. For this example, shown, the dynamic components are equal to 5 mils p-p and the static components 4 mils p-p.

In cases where there is a combination of static and dynamic imbalances present, then the dynamic and static components will vary from the measured vibration at the probes. Figure 5.20 describes how to calculate the components when there is a combination. The imbalance static and dynamic components are determined by drawing a line from the same radial probe at end of the rotor (dashed pink line). Next, when this line intersects the orbital curve, draw a line (purple dashed line) from the origin to this intersection point. The dynamic component is the distance from the intersection point to the vibration point in equal and opposite directions. The red vectors on the plot represent this. The static component is the distance from the origin to the intersection point and represented by the blue vector on the plot. To determine the angle of the dynamic vectors, they will be transposed to the origin (represented by the gray dashed line) in the plot. The static vector is read directly from the plot. This results in the following imbalance components.

Static Imbalance Bearing 1 Left/Bearing 2 Left = **(2.0 mils p-p ∠ 43°)**
Dynamic Imbalance Bearing 1 Left = **(4.3 mils p-p ∠ 328°)**
Dynamic Imbalance Bearing 2 Left = **(4.3 mils p-p ∠ 148°)**

This same procedure would be repeated for the right-side probes. Doing so produced the following values for the right side.

Static Imbalance Bearing 1 Right/Bearing 2 Right = **(1.6 mils p-p ∠ 71°)**
Dynamic Imbalance Bearing 1 Right = **(4.3 mils p-p ∠ 3°)**
Dynamic Imbalance Bearing 2 Right = **(4.3 mils p-p ∠ 183°)**

To determine the average Static and Dynamic Imbalance of the rotor, the right and left results are vectorially added together and then divided by two. Performing this task resulted in the following values.

Static Imbalance = **(1.84 mils p-p ∠ 56°)**
Dynamic Imbalance Bearing 1 = **(4.1 mils p-p ∠ 346°)**
Dynamic Imbalance Bearing 2 = **(4.1 mils p-p ∠ 166°)**

To double check this calculation, the answer should fall between the two sets of data.

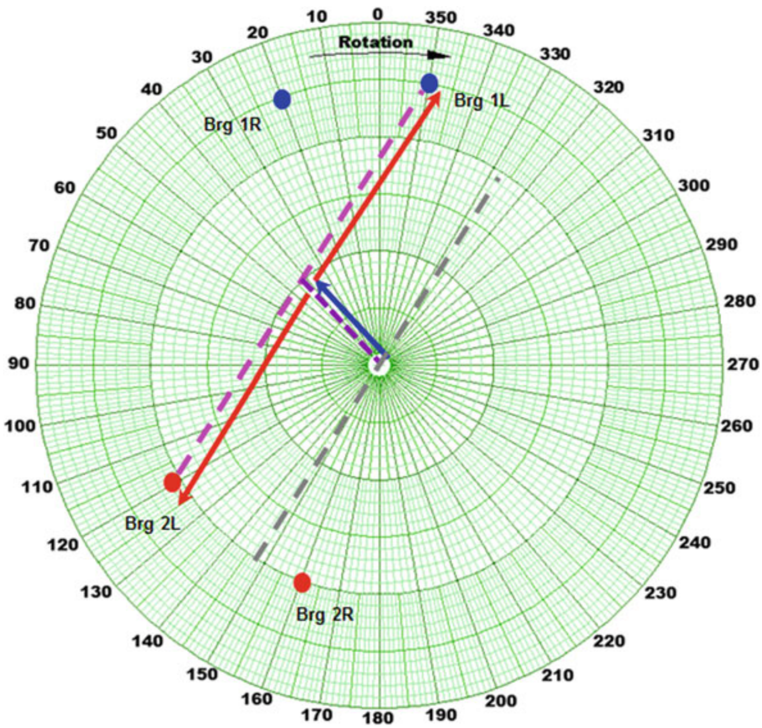

Fig. 5.20 Static and dynamic combination with components (2 mils p-p/major division)

5.9 Balancing Analysis

The basic steps discussed so far help understanding the relationships between the vibration components, organizing vibration data, compensating for the slow roll runout, the understanding of natural frequencies of rotors and how to identify them. This section will now cover the step-by-step analysis to perform balancing analysis.

After the initial As Found data has been collected, the data may need compensation for slow roll runout. To provide the best explanation of the balancing analysis, an example is provided as follows:

Example: Turbine coupled to a generator with a collector

Given:

Normal Operating Speed = 3600 RPM
Turbine Rotor Weight = 71,875 lbs. (32,602 kg)
Exhaust Balance Plane Radius = 18.60 inches (0.47244 m)

After evaluating the bode plots, it was determined that the critical speeds for the turbine were as follows:

First Critical Speed (Horizontal Direction) = 1035 RPM

First Critical Speed (Vertical Direction) = 1254 RPM
Second Critical Speed (Horizontal Direction) = 2630 RPM
Second Critical Speed (Vertical Direction) = 2664 RPM

When the critical speeds are identified, it is important that the speeds after the balance move should be as close to the pre-balance speeds. This is because as the rotor goes through the critical, the phase is shifting. On a well damped rotor, the phase will shift at a slow rate of change, but on a lightly damped rotor, the change can be rapid. In case of exciters, it not uncommon to notice a 20–30-degree change near the critical speed over a 10–15 RPM range. This can have significant effect on the balancing, when the effect vectors are long. Ideally, the variation in the speed between the pre-balance move and post balance move should not exceed ±5 RPM.

The data was evaluated as shown in Table 5.3 and was used as the slow roll reference data. The data was used to perform the slow roll runout compensation in this example. See Fig. 5.21.

Table 5.3 Data for example Table 5.1

			As found slow roll 233 RPM		
No.	TAG	Units	Total	1xAMP as-measured	1xPHS as-measured
1	Exhaust left	mils p-p	0.799	0.519	126
2	Exhaust right	mils p-p	0.771	0.511	216
3	Inlet left	mils p-p	0.338	0.128	263
4	Inlet right	mils p-p	0.350	0.182	341
5	Gen front left	mils p-p	0.382	0.160	291
6	Gen front right	mils p-p	0.444	0.223	147
7	Gen rear left	mils p-p	0.671	0.285	341
8	Gen rear right	mils p-p	0.431	0.108	126

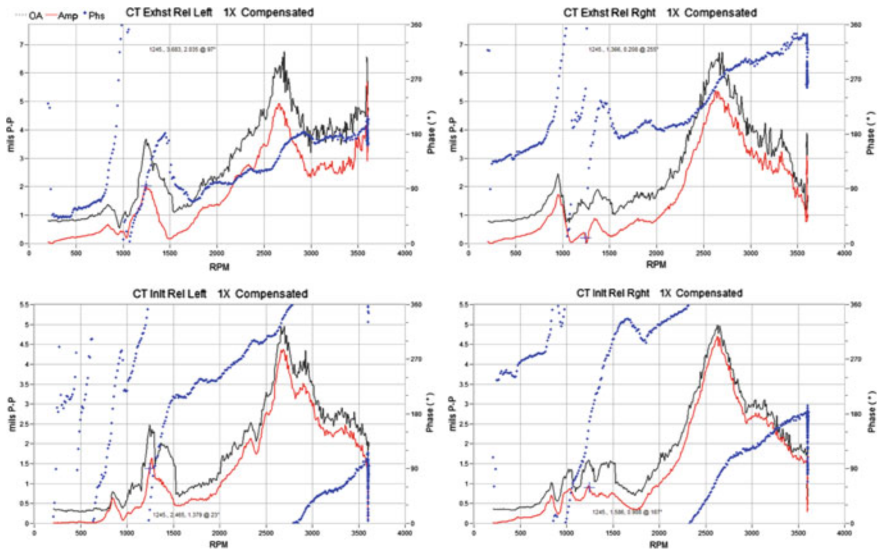

Fig. 5.21 Bode plots as found turbine vibration

The following data shown in a series of Tables (5.4, 5.5 and 5.6) below was compensated for slow roll runout and this data was used as the As Found data set. This data set contains the first and second critical speeds of the turbine along with the steady state online baseload for 8 h.

Table 5.4 Data supporting Table 5.3

			As found 1035 RPM startup			As found 1245 RPM startup		
No.	TAG	Units	Total	1xAMP comp	1xPHS comp	Total	1xAMP comp	1xPHS comp
1	Exhaust left	mils p-p	0.989	0.178	20	3.683	2.035	97
2	Exhaust right	mils p-p	0.764	0.657	354	1.366	0.208	255
3	Inlet left	mils p-p	0.726	0.239	240	2.465	1.379	23
4	Inlet right	mils p-p	1.286	0.863	38	1.586	0.908	167
5	Gen front left	mils p-p	0.797	0.516	231	0.588	0.298	312
6	Gen front right	mils p-p	1.028	0.891	70	1.095	0.687	139
7	Gen rear left	mils p-p	1.000	0.427	309	1.786	1.598	86
8	Gen rear right	mils p-p	0.589	0.255	96	0.812	0.668	240

Table 5.5 Data supporting Table 5.4

			As found 2630 RPM startup			As found 2664 RPM startup		
No.	TAG	Units	Total	1xAMP comp	1xPHS comp	Total	1xAMP comp	1xPHS comp
1	Exhaust left	mils p-p	6.107	4.797	135	6.259	4.930	145
2	Exhaust right	mils p-p	6.457	5.376	258	6.710	5.283	269
3	Inlet left	mils p-p	4.510	3.995	317	4.927	4.364	330
4	Inlet right	mils p-p	4.984	4.700	75	4.837	4.463	84
5	Gen front left	mils p-p	0.989	0.744	236	0.966	0.742	242
6	Gen front right	mils p-p	1.757	1.505	87	1.866	1.548	93
7	Gen rear left	mils p-p	2.391	2.133	276	2.328	2.031	284
8	Gen rear right	mils p-p	1.049	0.931	56	1.035	0.876	63

Table 5.6 Data supporting Table 5.5

			As found online 8 h		
No.	TAG	Units	Total	1xAMP comp	1xPHS comp
1	Exhaust left	mils p-p	5.728	4.834	167
2	Exhaust right	mils p-p	3.096	2.359	266
3	Inlet left	mils p-p	1.493	0.821	85
4	Inlet right	mils p-p	0.773	0.576	159
5	Gen front left	mils p-p	0.710	0.546	19
6	Gen front right	mils p-p	1.284	0.859	160
7	Gen rear left	mils p-p	2.088	1.651	292
8	Gen rear right	mils p-p	1.317	1.145	5

Now that the data has been collected, compensated and organized, evaluation process begins. Review of the data indicated that there was an elevated second critical speed vibration where the levels exceeded 6 mils p-p. See Fig. 5.22. The online data also indicated there was elevated vibration exceeding 5 mils p-p. Ideally for this unit, the recommended levels would be below 5 mils p-p through the transient ranges and below 3 mils p-p at steady state.

From reviewing the bode plots, it appears the turbine is operating above its second critical and below the third critical. When a unit has not been run to the next critical speed above the operating speed, a rough estimate can be calculated. To calculate this, take each of the known critical speeds and divide each of them by the mode shape number they represent. Then sum all these calculated speeds and divide by the total number of critical speeds calculated to get the average critical speed. Next add 100 RPM times the mode number of the unknown critical speed to the average critical speed. This critical speed value can then be added to the highest critical speed available to give a rough estimate of where the next critical speed will occur.

For this example, the first critical speeds are 1035 RPM and 1254 RPM and the second critical speeds are 2630 RPM and 2664 RPM. By calculating as described, the following are arrived [(1035/1) + (1254/1) + (2630/2) + (2664/2)]/4 = 1232 RPM. Since the third mode is the unknown critical speed 300 RPM would be added to the 1232 RPM. Adding this speed to the highest known critical speed the estimated next critical speed is determined (1532 + 2664) = 4196 RPM.

Referring to the Lag Angle to Mode Shape Relationship plot of Fig. 5.13, the lag angle would be expected to be between 0 and 90° since the unit has not passed through the critical speed of third mode. The next step is to plot both the second critical and steady state data. Since the first critical data was relatively low, it is optional if it is plotted or not.

When a rotor has two independent bearings supporting only that rotor and not any other rotor, it can be treated as an isolated system. In these instances, plotting the rotor's bearing vibration and one additional bearing in each direction is typically sufficient to see the effects of the balancing. If balancing is utilizing couplings, then the four bearings surrounding the coupling, two in each direction, should be have their vibration plotted.

The data from the second critical at 2630 RPM in Fig. 5.22 shows the expected 180° out of phase between the Exhaust and Inlet for both the left versus left and the right versus right. This means that at this speed a dynamic imbalance is anticipated. From the Lag Angle to Mode Shape Relationship in Fig. 5.13, we know that the critical is expected to have a 90-degree lag for the plane where the weights would be installed. This means to reduce unbalance, the weight would need to be installed at the following:

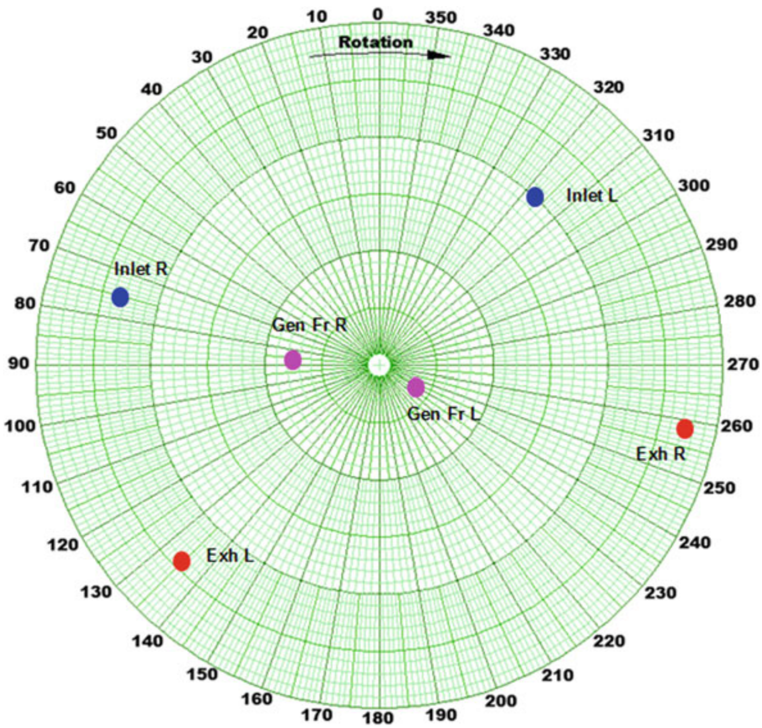

Fig. 5.22 As found second critical 2630 RPM (2 mils p-p/major division)

Inlet Left = 47°, Inlet Right = 165°, Exhaust Left = 225°, and Exhaust Right = 348°.

To determine the ideal weight location, the calculated weight placement for each end is averaged together. This results in adding weight at 106° in the Inlet and 287° in the Exhaust. Therefore, the ideal weight placement for the 2630 RPM second critical speed would be to add weight at these two locations.

Similar to the data from 2630 RPM, the data from the second critical at 2664 RPM in Fig. 5.23 also shows the expected 180° out of phase between the Exhaust and Inlet ends for the left versus left and the right versus right. This means that at this speed there is a dynamic imbalance exists. From the Lag Angle to Mode Shape Relationship plot of Fig. 5.13, we know that the critical is expected to have a 90-degree lag for the plane the weights would be installed. To reduce the imbalance in the rotor, the weight is required to be installed at the following:

Inlet Left = 60°, Inlet Right = 174°, Exhaust Left = 235°, and Exhaust Right = 359°.

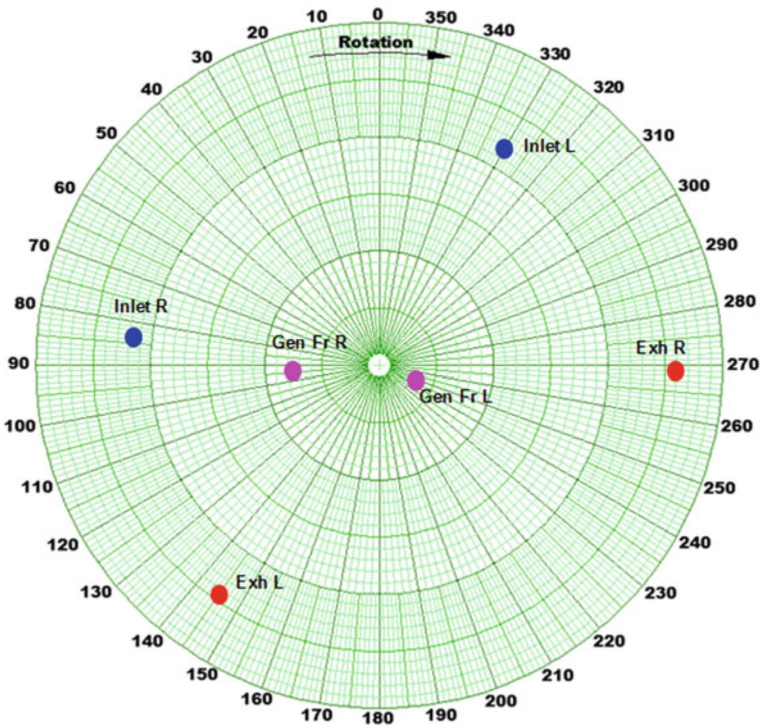

Fig. 5.23 As found second critical 2664 RPM (2 mils p-p/major division)

To determine the ideal weight location, the calculated weight placement for each end is averaged together. This results in adding weight at 117° in the Inlet and 297° in the Exhaust. Therefore, the ideal weight placement for the 2664 RPM second critical speed would be to add weight at these two locations.

As mentioned earlier, the turbine appears to be operating between the second and third critical. See Fig. 5.24. At 3600 RPM, the vibration still appears to have similar static and dynamic components. Knowing that as the rotor approaches the third mode, the lag angle in the two end planes would approach 90° and in the center plane it would approach 270°, the weight would be placed at a location between 257° and 356° in the Exhaust end and between 175° and 249° at the Inlet end. The following Table 5.7 shows a summary of the weight placements from the second critical and steady state (Tables 5.8 and 5.9).

After averaging both the Exhaust and Inlet ideal weight placements for both speeds, the placements are compared. It was found that the Exhaust plane had roughly the balance weight to correct both the second critical and the steady state condition. The Inlet weight placement shows there is 95° between the ideal weight placement locations (Table 5.10).

Averaging both the second critical and steady state weight placements resulted in 302° for the Exhaust end and 165° for the Inlet end. The weight placements

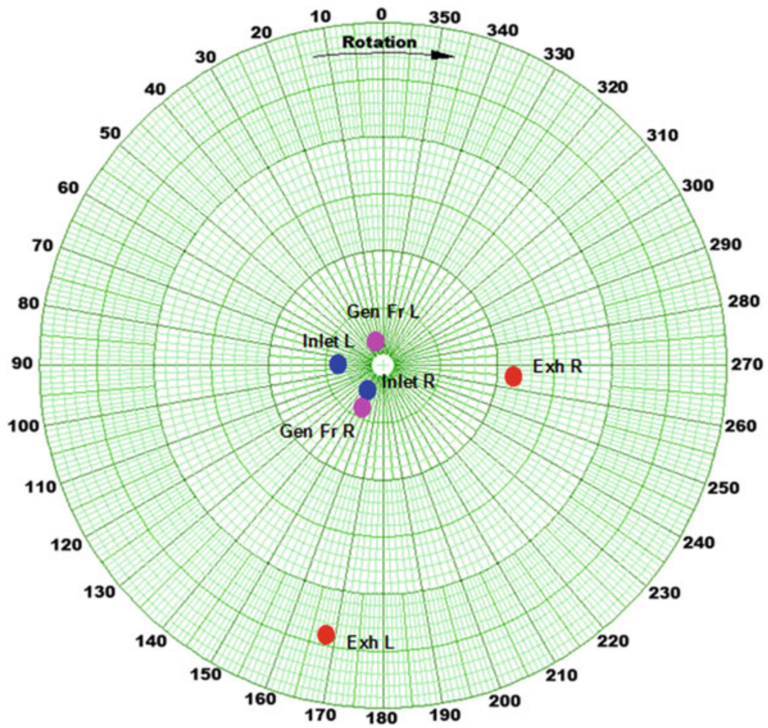

Fig. 5.24 As found online baseload 8 h 3600 RPM (2 mils p-p/major division)

Table 5.7 Rotor speed summary

Probe	Second critical	Second critical average	Steady state	Steady state average
Exhaust left	235	297	257	307
Exhaust right	359		356	
Inlet left	60	117	175	212
Inlet right	174		249	

Table 5.8 Balance data for the U-mode of the rotor

			Move 1 1035 RPM startup			Move 1 1245 RPM startup		
No.	TAG	Units	Total	1xAMP comp	1xPHS comp	Total	1xAMP comp	1xPHS comp
1	Exhaust left	mils p-p	0.827	0.535	263	2.951	1.512	89
2	Exhaust right	mils p-p	1.115	0.445	311	1.459	0.644	254
3	Inlet left	mils p-p	0.751	0.335	241	1.953	1.082	352
4	Inlet right	mils p-p	1.242	0.786	42	1.404	0.924	138
5	Gen front left	mils p-p	0.788	0.513	236	0.652	0.420	291
6	Gen front right	mils p-p	1.082	0.923	75	1.243	0.925	122
7	Gen rear left	mils p-p	1.119	0.587	310	1.456	1.236	62
8	Gen rear right	mils p-p	0.664	0.337	100	0.745	0.510	212

Table 5.9 Balance data for the S-mode of the rotor

			Move 1 2625 RPM startup			Move 1 2660 RPM startup		
No.	TAG	Units	Total	1xAMP comp	1xPHS comp	Total	1xAMP comp	1xPHS comp
1	Exhaust left	mils p-p	3.341	2.200	154	3.884	2.234	171
2	Exhaust right	mils p-p	4.116	2.637	290	3.919	2.541	299
3	Inlet left	mils p-p	1.500	1.142	341	1.782	1.285	357
4	Inlet right	mils p-p	1.826	1.601	106	1.904	1.578	117
5	Gen front left	mils p-p	0.947	0.711	243	0.928	0.693	246
6	Gen front right	mils p-p	1.703	1.432	95	1.692	1.427	98
7	Gen rear left	mils p-p	2.078	1.825	270	2.074	1.780	274
8	Gen rear right	mils p-p	0.896	0.751	51	0.854	0.723	55

Table 5.10 Rotor amplitudes/phase values of 1st balance move

			Move 1 Online 8 h		
No.	TAG	Units	Total	1xAMP comp	1xPHS comp
1	Exhaust left	mils p-p	3.183	2.287	214
2	Exhaust right	mils p-p	4.194	3.472	287
3	Inlet left	mils p-p	2.595	1.789	222
4	Inlet right	mils p-p	2.350	1.913	318
5	Gen front left	mils p-p	0.621	0.496	31
6	Gen front right	mils p-p	1.267	0.820	156
7	Gen rear left	mils p-p	2.540	2.019	297
8	Gen rear right	mils p-p	1.373	1.282	2

between the Inlet and Exhaust ends are 122° from each other meaning that there must be both dynamic and static components present. Adding weights in a single end plane will result in both static and dynamic response with most of the response being dynamic.

Since the Exhaust weight placement for both the second critical and the steady state ended up at roughly the same angle, it is easy to choose which end would be the ideal plane to use. The weight would be in installed at 302° into the Exhaust End plane.

After finding the angular location, the next step is to determine the amount of weight to be installed. A typical rule of thumb is to use the 10% Rule. This rule is defined as using a weight which produces a centripetal force which is equal to approximately 10% of the rotor weight at the highest rated speed of the rotor. To calculate the centripetal force the following formula is used. Where m_r = rotor mass, a_c = centripetal acceleration, v = tangential speed, r = radius of trial weight installation, and **w** = angular velocity.

$$F = (m_r)(a_c) = \frac{(m_r)(v^2)}{r} = (m_r)(r)\left(\omega^2\right)$$

Sometimes the rotor mass in given in mass and sometimes it is given in weight. To convert between weight and mass, the following formula can be used where W = weight and g = gravity. Note, for International System of units (SI) g = 9.8067 m/s^2 and for English units g = 386.088 in/s^2.

$$W = (m_r)(g)$$

Rearranging these equations and considering for only 10% of the rotor weight, the following formula is derived, where m_{tw} = trial weight.

$$m_{tw} = \frac{(0.10)(m_r)(g)}{(r)(\omega^2)}$$

It is extremely important to make sure that the correct units are used during the calculations. Failure to use the proper units will result in an invalid trial weight.

Using the information for this example, the recommended trial weight is calculated as follows. Note that rotor speed (θ) is in revolutions and will need to be converted to radians using the following formula, where p = 3.14159.

ω = (θ)(2)(π)
m_r = 71,875 lbs. or 1,150,000 oz.
θ = 3600 RPM or 60 revolutions/s
R = 18.60 inches
G = 386.088 in/s^2
P = 3.14159

Substituting the values into the trial weight equation above, the following is obtained.

$$m_{tw} = \frac{(0.10)(m_r)(g)}{(r)(\omega^2)} = \frac{(0.10)(1,150,000oz.)(386.088in/s^2)}{(18.60in.)\left(\left[\left(60\frac{rev}{s}\right)(2)(3.14159)\right]^2\right)} = 16.796\boldsymbol{oz}.$$

The above calculation together with the previous determination of the angular location for the weight placement in the Exhaust End plane results in the initial recommended balance move of ***16.796 oz. at 302***° in the Exhaust End plane of the Gas Turbine.

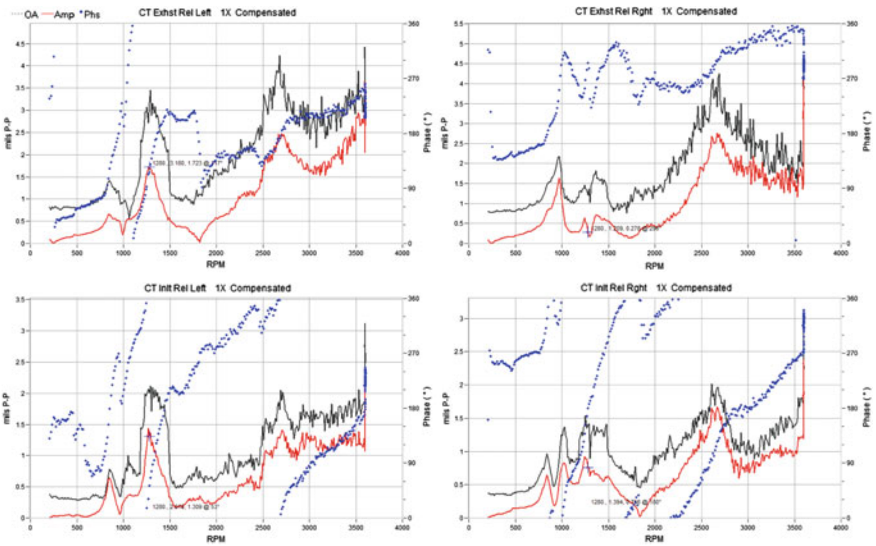

Fig. 5.25 Bode plots balance move 1 for turbine vibration

After reviewing the available weight sizes and balance holes' availability, it was determined that a weight move could be made using standard weight approximately the same as the calculated weight. This weight move referred to as Move 1 was ***19.14 oz. at 293°*** in the Exhaust End plane of the Turbine. The post Move 1 data compensated for slow roll runout and was placed in the following tables.

The Move 1 slow roll compensated data (See Fig. 5.25) when compared to the As Found slow roll compensated data for the same speed; there was minimal change at the First Critical speeds and significant changes at the Second Critical speeds and Steady State as expected. The best way to see the response from the balance move is to plot it on the same polar plots as were used for the As Found readings. By drawing a vector starting at the As Found readings and ending at the Move 1 readings, this will indicate the direction and the magnitude of the effect. These vectors are known as Effect Vectors. In addition to adding the effect vectors, it is a good practice to mark the angular location and magnitude of weight installed on each plot. This will allow for quick calculation of the effect lag angles.

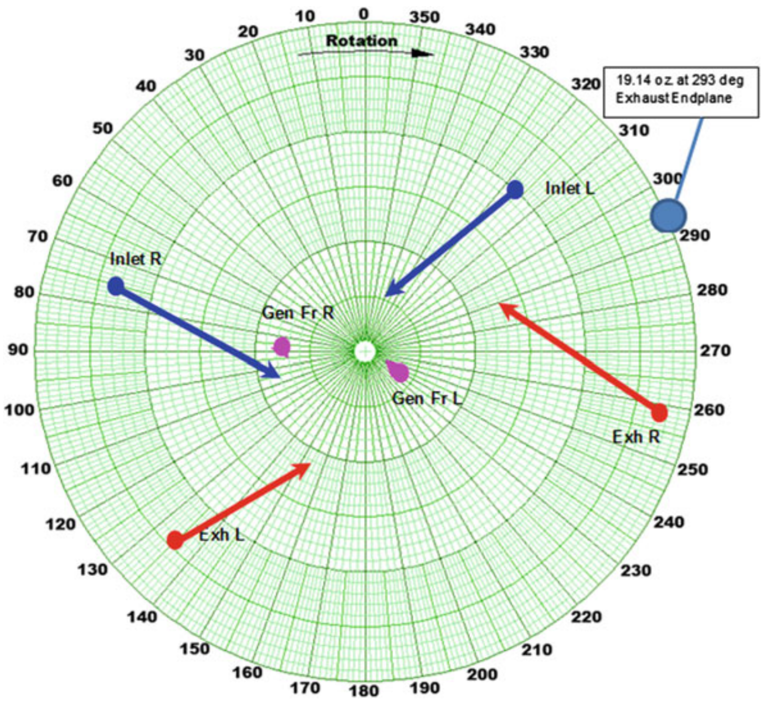

Fig. 5.26 Move 1 effect vectors second critical 2630 RPM (2 mils p-p/major division)

Since the First Critical speeds showed little change compared to the Second Critical speeds and Steady State, they will not be plotted. If they had shown similar changes, it would be best to plot them as well to determine their effects.

The polar plot in Fig. 5.26 shows that there is almost no effect on the generator. It also shows that the balance move had significant effect on the turbine. When the Inlet Left and Exhaust Left vectors were compared to each other, they are almost equal in length and in the opposite direction. This is also true for the right probes. This would indicate that the effect was almost pure dynamic as was expected. The vectors are slightly rotated towards the origin of the plot. These vectors are under rotated condition between approximately 5 and 25° and pointing to the origin. One of the fundamental rules of balancing is that rotating the weight will also rotate the effect by the same amount. This means that if the weight was rotated against shaft rotation by 10° from 293° to 303°, each vector would rotate counterclockwise by 10° as if the tail of the vector was the axis of rotation. The vectors are also about to reach the origin indicating that more weight could be used. Another fundamental rule of balancing is increasing the weight will increase the vector length proportionally. For example, if a 10-oz. weight resulted in an effect vector of 2 mils long, then a 15-oz. weight would result in an effect vector which would be 3 mils long.

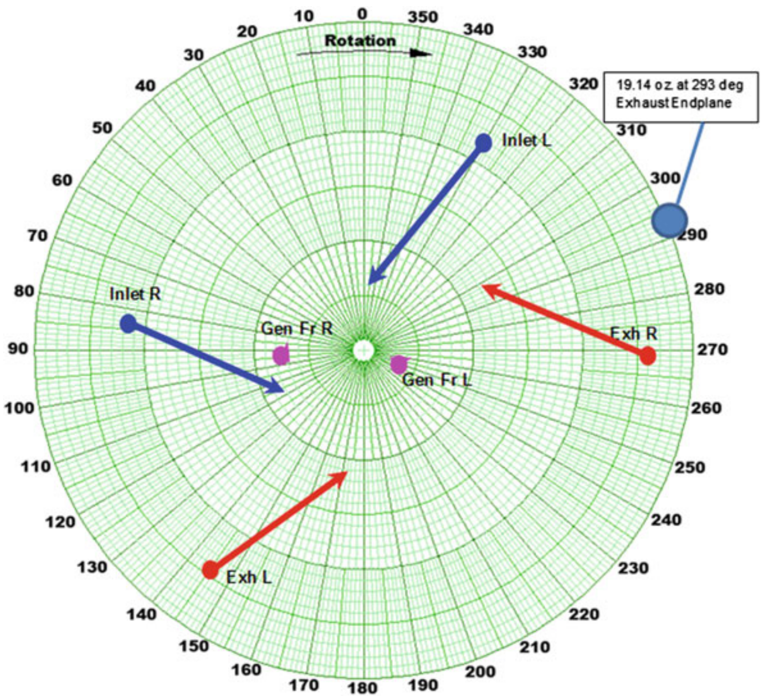

Fig. 5.27 Move 1 effect vectors second critical 2664 RPM (2 mils p-p/major division)

The polar plot in Fig. 5.27 shows similar characteristics as the previous polar plot at 2630 RPM. The generator end had little change, while the turbine end showed a dynamic effect on both the left and right probes as expected. The vectors are also not pointing directly towards the origin of the polar plot. They seem to indicate that the vectors are under rotated by approximately 10–25°. The effect vectors are short of reaching the origin of the plot, indicating that more weight could be added to increase their lengths.

The Steady State polar plot showed a different response than what was observed for the Second Rotor Critical speed plots. The polar plot of the generator again showed little change. See Fig. 5.28. The right probes of the turbine indicated slight difference in lengths, but are in the same direction. This indicates that the most effect was static with some dynamic. The dynamic component comes from the differences in the vector lengths. The left probe vectors of the turbine indicated almost twice the length of the Exhaust vector over the Inlet vector. The probes' effect-vector directions were also approximately 90° apart. This indicates that the effects were due to static and dynamic components. The plot also shows that both the Exhaust probes and the Inlet Left probe are under-rotated from the origin, while the Inlet Right almost passes straight through the origin. Both the Inlet vectors have passed the origin while both the Exhaust vectors fall short of the origin if rotated. Adding weight would benefit the Exhaust, but have negative effects on the Inlet probes.

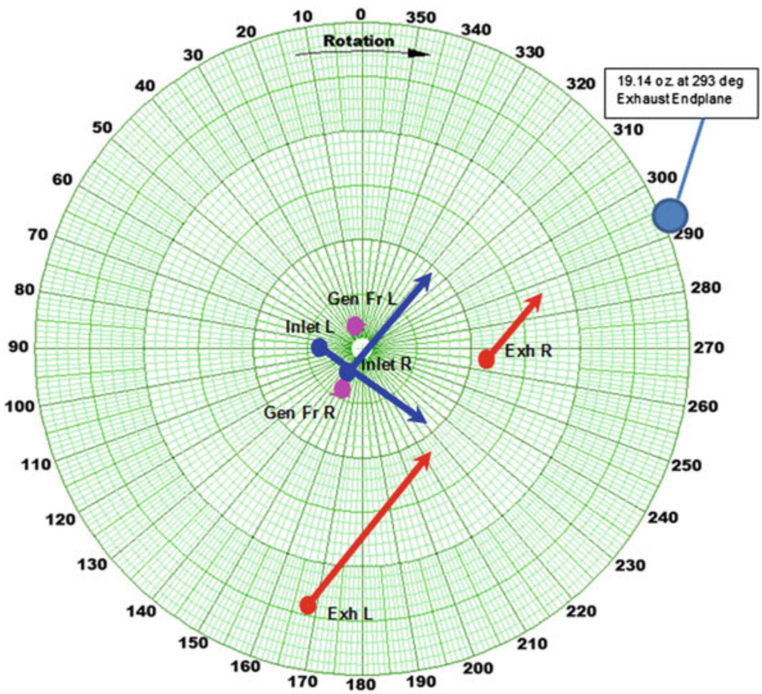

Fig. 5.28 Move 1 effect vectors online baseload 8 h 3600 RPM (2 mils p-p/major division)

5.9.1 Calculating Effect Coefficients and Lag Angles

The polar plots with the effect vectors provide valuable data. From the effect vectors, the Effect Coefficients and Lag Angles can be calculated for additional balancing or future balance of the same unit in the same plane. To calculate the Effect Coefficients and the Lag Angles, the effect vector direction and length must be known in relation to the origin of the polar plot. The weight and angular location must also be known.

In the polar plot, after plotting the effect vectors, plot the transpose the effect vectors to the origin. This makes it easy to find the direction of the vectors as well as measuring the length by using the polar plot scale. The following Fig. 5.29 for the 2664 RPM Second Critical shows the transposing.

After the effect vectors have been transposed to the origin, using the polar scale, the length of each vector is determined. The direction of the vectors is also read by following along the transposed vector from the origin to the outer ring of the polar plot and reading angle. The following Table 5.11 contains the data obtained from the polar plot for the four turbine probes. Errors can occur depending on how accurately the plot is generated; the values in the table were calculated using a vector calculator (current reading and subtracting the previous reading). Note: when

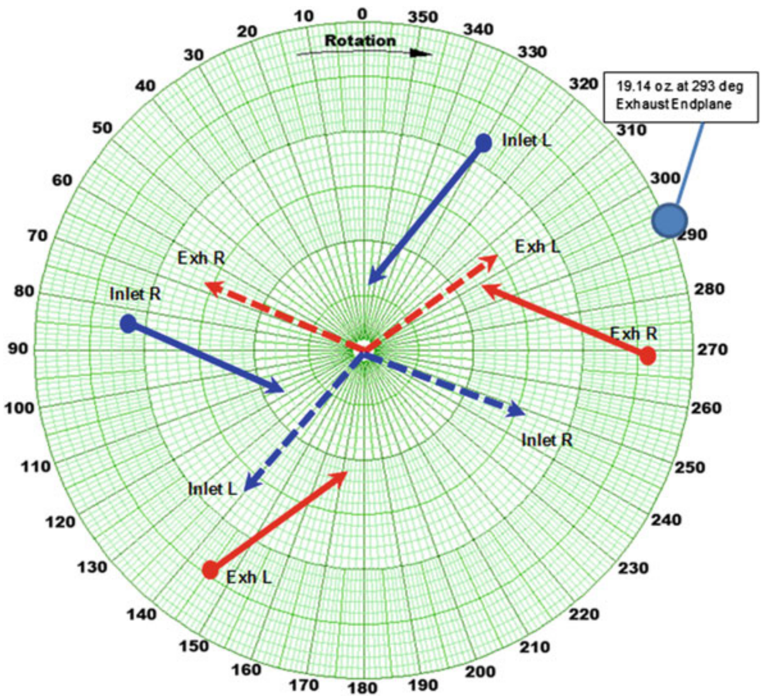

Fig. 5.29 Move 1 effect vectors transposed to the origin second critical 2664 RPM (2 mils p-p/ major division)

using the calculator method, make sure to check by drawing the plot as some calculators could reverse the initial position and final position resulting in the effect vector angle off by 180° (Table 5.12).

Table 5.11 Effect vectors for rotor 2nd critical speed

Effect vectors (2664 RPM startup, exhaust end plane 19.14 oz. at 293°)		
Probe	Effect vector length (mils p-p)	Effect vector angle
Exhaust left	3.089	306
Exhaust right	3.329	67
Inlet left	3.274	139
Inlet right	3.250	249

To calculate the Effect Coefficients, the Effect Vector Length is divided by the amount of weight installed. For this example, each of the Effector Vector Lengths would be divided by 19.14 oz. This will result in Effect Coefficients in mils p-p/oz.

The Effect Vector Angle is used to calculate the Effect Lag Angle. In order to calculate the Effect Lag Angle, the angular weight placement angle is subtracted from the Effect Vector Angle. If the result is negative, 360° is added to obtain a positive Effect Lag Angle. Note that the Effect Lag Angles are referenced from the plane where the weight is installed. In this example, this was the Exhaust Endplane. The following table gives the Effect Coefficients and Lag Angles for this example.

Table 5.12 Effect coefficients for rotor 2nd critical speed

Effect coefficients and lag angles (2664 RPM startup, exhaust end plane 19.14 oz. at 293°)		
Probe	Effect coefficients (mils p-p/oz.)	Lag angle (degrees)
Exhaust left	0.161	13
Exhaust right	0.174	134
Inlet left	0.171	206
Inlet right	0.170	316

This process of calculating effect coefficients and lag angles would be repeated for each of the speeds and for the Steady State data.

5.9.2 Applying Effect Coefficients and Lag Angles to Balance

The advantage of calculating effect coefficients and lag angles is that they make balancing effort more efficient. When unit specific effect coefficients and lag angles known and the effects are available, an evaluation can be performed to see if a specific balance plane will be the optimal balance plane to use for the operating condition. They also eliminate the need for a trial move, which reduces the number of runs needed on the unit since additional fuel and labor are required for these activities.

In the following example, the effects that were calculated for the Second Critical at 2664 RPM will be used to calculate an initial balance recommendation for the same unit which was unable to reach the running speed due to elevated vibration causing the unit to trip.

The following data in Table 5.13 was obtained from the last run of the unit as it tripped at 2650 RPM. This data has already been compensated for slow roll runout.

Table 5.13 Balance data obtained during unit trip

As found 2650 RPM startup tripped					
No.	TAG	Units	Total	1xAMP comp	1xPHS comp
1	Exhaust left	mils p-p	9.982	9.254	306
2	Exhaust right	mils p-p	7.841	7.777	64
3	Inlet left	mils p-p	10.001	9.891	137
4	Inlet right	mils p-p	8.243	8.169	237

Ideally, it is best if prior balancing data for all speeds are used to observe the vibration conditions. This helps to prevent additional moves; in some cases when the unit needs to be balanced prior to reaching rated speed due to tripping; the balance that corrects the transient vibration levels may have a negative influence on the steady state vibration. This was observed in the previous example, the effects at the Second Critical speeds showed additional weight being added to help the transient vibration levels, but it would hurt the Steady State vibration levels.

The first step is to plot the data on a polar paper to understand how the data looks when compared to the data from the Exhaust Left and right to the Inlet Left and Right. After plotting the data, the Exhaust and Inlet is almost 180° out of phase of each other indicating that the vibration is almost pure dynamic. Since this is the same unit, it should be known that in the past, this unit had its Second Critical speeds at 2630 RPM and 2664 RPM. In this case, the speed was 2650 RPM when the unit tripped before; so using effects from 2664 RPM should work to reduce the vibration levels. If it is not the same speed, it is likely that there will be variations in the effects as well.

Next, the angular position of the weight placement needs to be calculated. Similar to the method used for the trial weight angle, each angle from the four vibration probes will have 180° added to them. If there was no lag angle or the lag angle was equal to zero, then this is the position the weight would be installed. When lag angles are known, the ideal position of weight placement is determined by subtracting the lag angle from this new angle, Table 5.14, provides the data through these calculations.

Table 5.14 Weight placement with lag angles

Calculating weight placement with lag angles (as found 2650 rpm startup tripped)					
No.	TAG	1xPHS comp	Added 180°	Lag angle to be subtract	Ideal weight placement angle
1	Exhaust left	306	126	13	**113**
2	Exhaust right	64	244	134	**110**
3	Inlet left	137	317	206	**111**
4	Inlet right	237	57	316	**101**

From the calculation of the Weight Placement Angle in the previous Table 5.14, the values are averaged together to give the actual weight placement location that will benefit for each of the probes. In some cases, weighting might be desired if trying to bring down one of the readings more than the others. Weighting is used when an optimal solution for all the readings is required. To achieve this, select readings are favored and the balance move is designed to optimize those specific readings. The average of these readings was calculated to be **109°**. This is the ideal location for the weight placement in the Exhaust End plane. Figure 5.30.

The next step is to determine the amount of balance weight that needs to be installed. By taking the 2650 RPM vibration data from the Table 5.14 for each of the probes and dividing it by the corresponding Effect Coefficient will provide the amount of weight needed to decrease the vibration to zero. Generally, zero

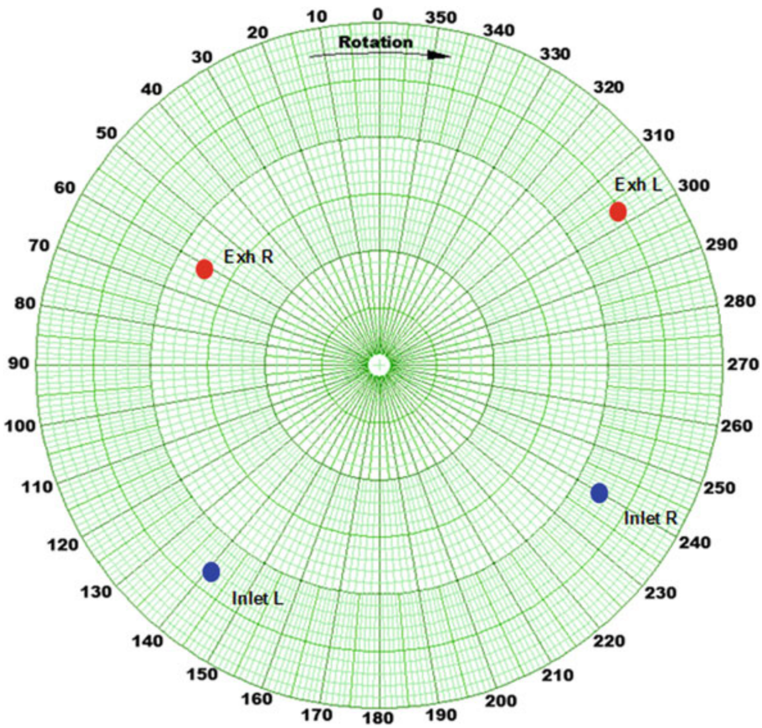

Fig. 5.30 As found tripped second critical 2650 RPM (4 mils p-p/major division)

balancing is difficult to achieve. Balancing is usually done to bring the vibration within acceptable levels based on manufacturer recommendations or vibration standards. As a side note, balancing to extremely low levels can have a negative effect on the stability of the system. This is experienced in high pressure steam turbines. This method of calculating the weight needed for zero vibration is being used to determine maximum and minimum weight range for a multi-probe rotor. The following Table 5.15 provides these calculations.

Table 5.15 Weight additions for zero-vibration

Calculating weight addition for zero vibration (As found 2650 RPM startup tripped)				
No.	TAG	1xAMP comp	Effect coefficients (mils p-p/oz.)	Amount weight to add (oz.)
1	Exhaust left	9.254	0.161	57.478
2	Exhaust right	7.777	0.174	44.695
3	Inlet left	9.891	0.171	57.842
4	Inlet right	8.169	0.170	48.053

The Table 5.15 indicates the weight range that should be installed is between 44.695 and 57.842 oz. Choosing a weight greater than 44.695 oz. will result in the effect vector for the Exhaust Right to pass through zero and start to increase from zero. Choosing a weight less than the values indicated in the Table 5.15 for the other probes will result in their effect vectors falling short of zero.

To begin the process, apply the smallest weight and then plot the expected effect vectors to see if this will be sufficient to meet the acceptable range on the other probes. To determine the length of the effect vectors, use the ***44.695 oz.*** Weight and multiply it by the corresponding Effect Coefficient. The Table 5.16 below shows these values. See Fig. 5.31 also.

Table 5.16 Calculation of effect vector length

Calculating effect vector length for 44.695 oz. (As found 2650 RPM startup tripped)				
No.	TAG	Amount weight added (oz.)	Effect coefficients (mils p-p/oz.)	Effect vector length (mils p-p)
1	Exhaust left	44.695	0.161	7.196
2	Exhaust right	44.695	0.174	7.777
3	Inlet left	44.695	0.171	7.643
4	Inlet right	44.695	0.170	7.598

The values in Table 5.16 give the length of the predicted response from the weight placement. In order to determine the direction of the effect vector, the difference between the weight placement being used and the ideal weight placement must be determined. Previously 109° was determined as the weight placement. Using each of the individual ideal weight placements and subtracting 109° from them will result in a positive or negative angle. This angle is how much the vector will be rotated from pointing directly towards the origin. A negative value means the weight needs to be moved clockwise to rotate the effect vector to point towards the origin and a positive value would need to move counterclockwise (Table 5.17).

Table 5.17 Calculation of effect vector direction

Calculating effect vector direction (As found 2650 RPM startup tripped)				
No.	TAG	Ideal weight placement angle	Actual weight placement	Angle from origin
1	Exhaust left	113	109	4
2	Exhaust right	110	109	1
3	Inlet left	111	109	2
4	Inlet right	101	109	−8

The following polar plot 5.31 shows the predicted response based on installing 44.695 oz. at 109° in the Exhaust End plane based on the previous effects at 2664 RPM for this unit. The pink dashed lines are used to show where the ideal weight placement would point the effect vector compared to where the actual weight placement is predicted to point the effect vectors.

The plot 5.31 shows that the vibration levels are expected to be below 4 mils p-p due to this balance move. It also shows that increasing the weight slightly could further improve the vibration levels on three of the four probes. If so desired, time could be spent to adjust the weight such that all the bearings have approximately the same vibration level. In this case that would not be practical. Adding weight in a certain probe direction would be practical.

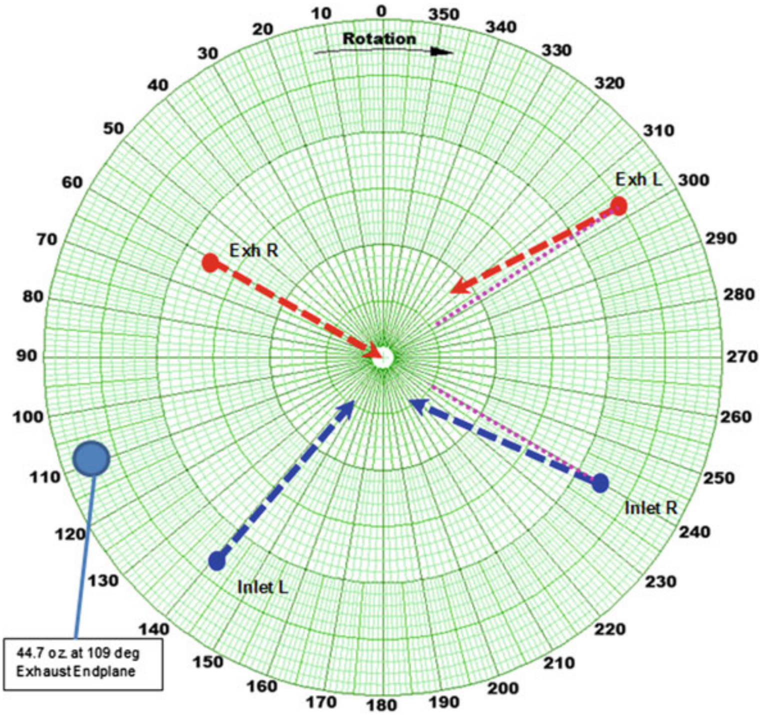

Fig. 5.31 Predicted response from balance move of 44.695 oz. at 109° in the exhaust end plane second critical 2650 RPM (4 mils p-p/major division)

5.10 Balancing of Rotors with Shared Bearings

A common bearing that supports two rotors is called a shared bearing. For balancing the shared bearing system, the rotors need to be analyzed as a system versus individual rotors. The imbalance vectors of the entire shaft system need to be

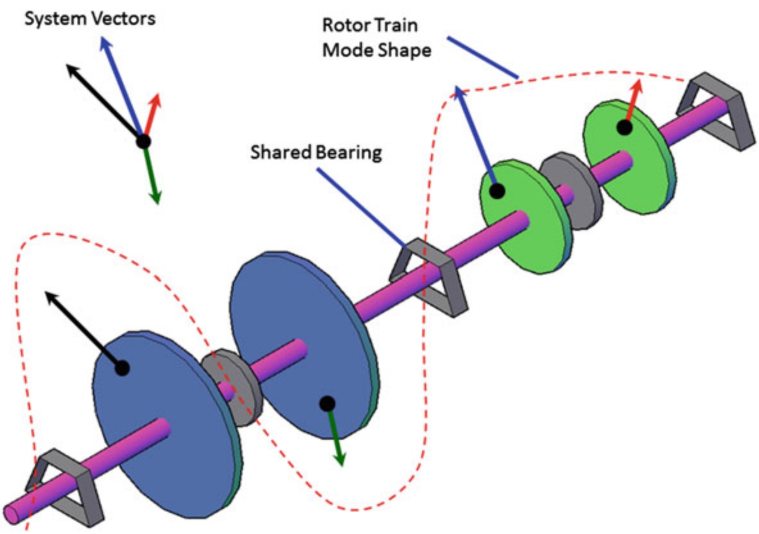

Fig. 5.32 Shared bearing rotor train with the mass imbalance vectors and system mode shape

calculated along with the mode shape of the system. The following Fig. 5.32 shows the system mode shapes and the imbalance vectors for a shared bearing rotor system.

In general, the same balancing techniques are used for shared bearing system as was used in a two bearing supported rotor systems. As observed in the rotor system mode shape, the rotor exhibits a static mode at the ends and a dynamic mode in the middle. Therefore, the end balance plane weights are installed at the same angle. However, for the mid plane, the weights are installed at 180° to those at the end planes of the rotor train.

5.11 Rotor Systems with Clutch

As shown in Fig. 5.33, the clutch is used to connect and disconnect the steam turbine from the rest of the train. The pawls used in the hydraulic clutch constantly engage and disengage in operation. As a result, they tend to wear away. This causes additional eccentricity than originally set in the pawls. As a result, mass imbalance in the clutch can increase and sometimes exceed the acceptable vibration levels. Therefore, for rotor systems with clutch need tighter shaft alignment tolerances to achieve lower vibration levels at the clutch bearings. If repeated vibration levels are experienced in clutch bearings, consider repairing or replacing the clutch.

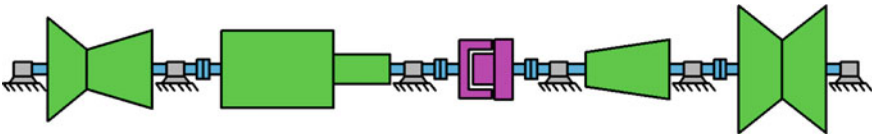

Fig. 5.33 Rotors engaged/disengaged with clutch

5.12 Commonly Used Balance Weights

Figure 5.34 shows some of the balance weights commonly used in rotor balancing. Two types of balance weights, in general, are used.

(a) Threaded Weights: They are fastened into matching drilled and tapped holes.
(b) Sliding Weights: Sliding weights are slid into machined grooves in the rotor

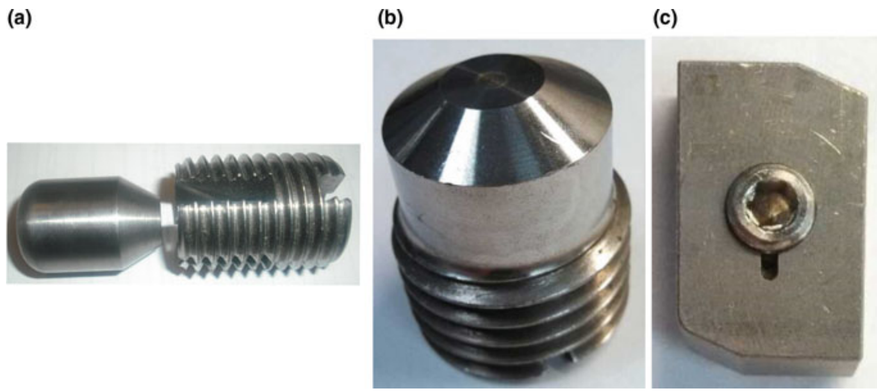

Fig. 5.34 Balance weights

Figures 5.34a and b show threaded weight configurations and Fig. 5.34c shows the sliding weight used in rotor grooves that are machined 360° on a rotor balance plane. The balance weights are made out of steel or platinum. Special alloys are used in boiled water reactor nuclear turbine applications.

Sliding balance weights installed at in the blower hub of a Generator rotor is shown in Fig. 5.35.

Fig. 5.35 Example of end balance plane weights on a generator rotor

5.13 Closure

The following discussions associated with rotor balancing were done in this chapter

- Rotor run outs cause eccentricity that gives rise to mass unbalances
- Definition of static and dynamic balance requirements
- Definition for rigid and flexible rotor balancing
- Slow roll vector and its importance in rotor balancing
- Practical examples of rotor balancing using real life experiences
- Commonly used balance weights and materials

References

1. ISO 7919-2 (2009) Mechanical vibration—evaluation of machine vibration by measurements on rotating shafts
2. ISO 10816-2 (2009) Mechanical vibration—evaluation of machine vibration by measurements on non-rotating parts

3. ISO 10814 Mechanical vibration - susceptibility and sensitivity of machines to unbalance
4. Bentley DE, Hatch CT, Grissom B (2002) Fundamentals of rotating machinery diagnostics. Bentley Pressurized Bearing, Minden
5. James ML (1994) Vibration of mechanical and structural systems: with Microcomputer applications. HarperCollins College, New York

Chapter 6
Rotor Train Alignment

6.1 Introduction

Although rotor dynamic characteristics are very important for smooth and continuous operation of machinery, static alignment of rotors is also equally important. This is because heavily misaligned shafts could cause excessive runouts that could lead to high vibration. Turbine train with misaligned shafts may not be operable until fixed. Shaft misalignment conditions could cost the industry dearly due to downtime and loss of revenue because of forced (un-scheduled) outages. Outage entails stopping machines, realigning shafts, sometimes opening of casing covers, etc. More than half of the forced outages in turbomachinery are caused by misalignment of shafts. This chapter discusses the key parameters that influence shaft alignment, measurement of those parameters, realignment methods and finally, verification of aligned shaft system to ensure smooth operation.

6.2 General

Dynamical aspects of rotors were discussed in the previous chapters. This chapter deals with rotor alignments, which are performed during assembly of rotor train in their stationary condition or when the rotor system is at rest at 0 RPM. As stated before, the misalignment of shafts costs the industry, thanks to downtime, cost of fixing the problem, lost power generation, and revenue due to non-availability of machines, etc. Shaft misalignment impacts can be realized in turbine parts such as (a) bearings, (b) rotor-to-stator seals, and (c) couplings due to clearance changes, galled bolts, and excessive shaft runouts.

Shaft alignment, also called "coupling alignment," is a process of adjusting shafts to stay colinear in vertical and horizontal planes. Rotor alignment can be achieved utilizing conventional tools, such as dial indicators, gages, calipers, straightedges. Modern and advanced methods use optics and/or laser systems.

R. Subbiah and J. E. Littleton, *Rotor and Structural Dynamics of Turbomachinery*,
Applied Condition Monitoring 11, https://doi.org/10.1007/978-3-319-73296-1_6

Shaft alignment process includes data acquisition and analytical calculations using the data that determines the final coupling radial displacements and axial gaps. Two different shaft alignment philosophies are common in the power industry. They are (1) align shafts with zero bending moments (BM) at the bearings and (2) align shafts with zero BMs at the couplings. There is no clear advantage of one over the other since they try achieving the same goal. However, it is a matter of convenience and/or vendor's preference or their design philosophy.

Two types of rotor support systems are:

(a) two bearing supports for one rotor and
(b) single shared bearing support for two rotors.

On a two bearing per rotor system, force disturbances that occur across the bearing span are confined within that component. As such, the shaft misalignment forces are distributed on the two couplings located on either side of the bearings. The resulting force amplitudes are relatively smaller, and it is easier to identify the coupling that caused misalignment. Consequently, rotor systems with two bearings per rotor can tolerate relatively larger coupling face and rim distortions.

In comparison, a single bearing support shares a significant amount of load of two rotors. As a result, one coupling is exposed to larger distortion than experienced on a two bearing rotor systems. Therefore, on shared bearing units, well-aligned shafts with tighter tolerances are required for smoother operation. If tighter tolerances are not applied in coupling assembly, it could give rise to unacceptable shaft vibration within short period of the unit's service life.

In addition, it is hard to identify which component initiated the excessive vibration on a shared bearing system. In some cases, it was also found that mass unbalance shifts in one rotor in the train could excite a different rotor that is not directly connected to the rotor that initiated mass unbalance. Shaft mode shapes at the operating speed, in some cases, may provide some clues.

Rotor trains with a clutch system are more sensitive even for minor shaft misalignments. Typically, increased eccentricity in the clutch engagement system opens excessive pawl clearances, resulting in high vibration. Hence, machines that operate with clutch systems need tighter shaft alignment tolerances for trouble-free operation for a long time.

This chapter discusses all elements of shaft alignment processes exclusively. A methodical approach covering all components that could affect the turbine alignment is discussed.

6.3 Turbine Assembly

A turbine consists of rotors that are assembled inside non-rotating stationary casings. These casings are secured circumferentially and axially and are supported and anchored on to the concrete foundation. Let us review the components that are part of the rotor-to-casing alignment.

They are

inner and outer casings,
gland casings,
thrust dummies,
bearing shells,
horizontal joints,
casing anchors,
centering beams, etc.

Key points for Better Turbine Assembly:

The primary function of the turbine assembly is to align the bottom casing to match the rotor sag curve. Once this is achieved, the seal clearances between the rotor-to-stationary parts should be set per design. Then, the cylinder is mounted and fixed on the foundation anchors. Axial stationary anchors are set to accommodate differential thermal expansion of rotors.

Turbine cylinder includes inner and outer casings that enclose the bladed-rotor. For steam turbines, inner casings mainly support stationary blade groups (that directs the steam flow through the rotating stages) and the thrust dummy seal rings. Outer casings enclose and support inner casings, inner gland seal rings and the exhaust hood structure designed to accommodate the end stage blades in LP turbines. Both inner and outer casings are split at the horizontal joint and are fastened by bolts. As such, each casing has a base and a cover for easy assembly and disassembly. A generic view is shown in Fig. 6.1. In some cases, the HP turbine is a one-piece barrel construction and is tilted vertically to assemble the rotor inside the barrel in the factory. The casings are supported firmly on the concrete foundation through anchor bolts.

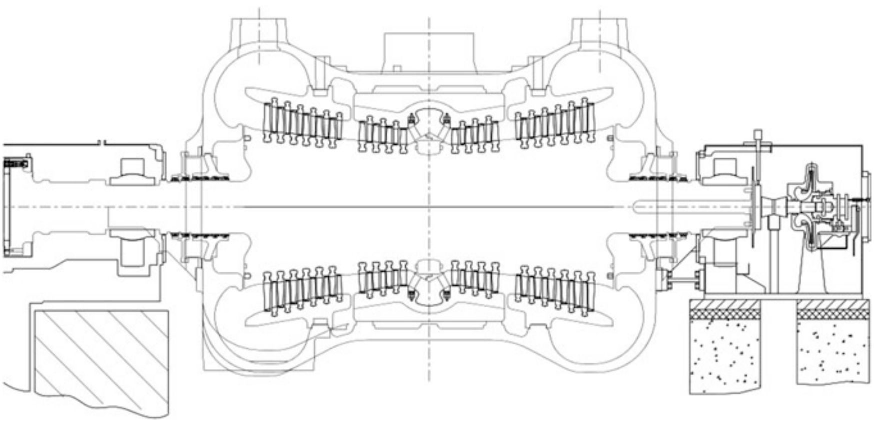

Fig. 6.1 Outer and inner casings and rotor assembly

The major part of the turbine alignment strategy is to have the rotor sag aligned to the shape of the cylinder base. In general, the stationary and rotating seals are set to as-designed cold clearances in such a manner that un-interrupted rotor position (no rubs between rotor and stationary seals) is achieved when the rotor runs in the maximum hot condition during operation. Turbine alignment accounts for rotor rise in bearing fluid film, thermal growth of rotor, blades, casings, and related parts including foundation settlement.

Anchor bolts keep the outer casings firmly bolted to concrete foundation. The foundation designer known as "architect engineer (AE)" uses the rotor dynamical design data to avoid the concrete foundation frequencies to interfere with rotor critical speeds. The concrete mat is designed for suitable earth quack standards in the area where the power plant is being built. The anchor bolts are suitably designed to withstand all types of anticipated loads as well. AE applies the following external loads in the design of foundation structure.

- Line-to-line short-circuit fault loads,
- shock loads emanating from nearby heavy-duty equipments and power plants,
- Local soil conditions and their ability to absorb additional loads. In some extreme cases, high quality sands are filled to make the foundation more rigid.

Thrust bearings are designed to control axial rotor motions, thus positioning the rotor within the design axial travel. The thrust cage that contains the thrust bearing is anchored to the foundation and secured by centering beams.

6.4 Rotor Train Alignment

Rotor alignments basically refer to aligning coupling rim and face to maintain concentricity and parallelism. Ideally, a perfectly aligned coupling has zero eccentricity at the coupling joints. This results in zero unbalance excitation at the couplings, and hence a good shaft system alignment can be maintained. In reality, some amount of eccentricity always exists that could trigger low levels of vibration and could add to overall shaft vibration. The coupling alignment data is discussed in detail in the next section using laboratory couplings.

6.4.1 Coupling Gaps and Displacements

A simple laboratory kit is used to demonstrate the coupling alignment measurements as illustrated in Fig. 6.2. Two ends of the coupling halves are shown in the

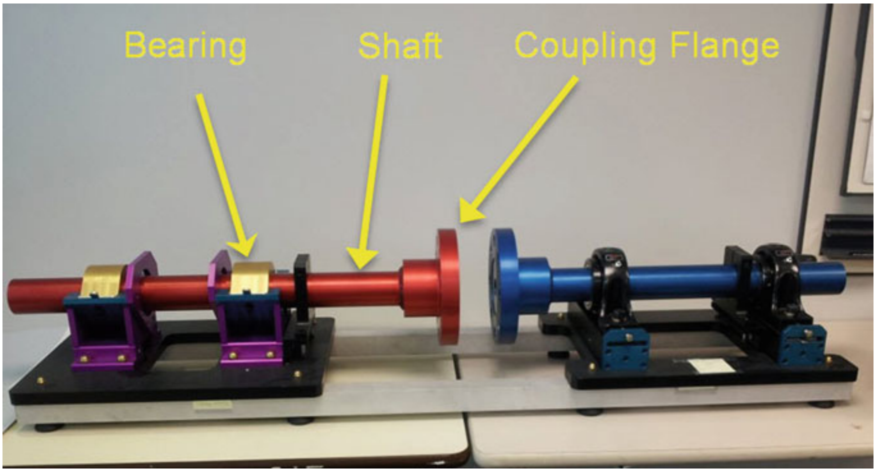

Fig. 6.2 Laboratory coupling kit (Courtesy of Siemens)

open (unbolted) condition. The shafts that support coupling flanges rest on the bearings. It is important to note that the two shaft ends must be concentric and coupling flange faces to be parallel to each other for an ideal shaft and coupling alignment condition.

As illustrated in Figs. 6.3a and b, the shaft centerlines are not concentric, but the shafts are parallel to each other. This condition of the shaft causes shaft offset called crank or eccentricity. This type of misalignment is known as "parallel shaft misalignment" [1, 2]. The eccentricity in the shaft would cause mass unbalance leading to vibration. The resulting mass unbalance produces centrifugal or unbalance forces, the magnitude of which depends on the shaft rotational speed. Large eccentricity in the coupling joint could build excessive unbalance force that could excite the coupling with unacceptable vibration. Such radial offset or eccentricity measured at the coupling flanges is called diametric eccentricity. Half of the diametric eccentricity is called "*displacement*" and is measured at the coupling rim assuming the flange faces are parallel.

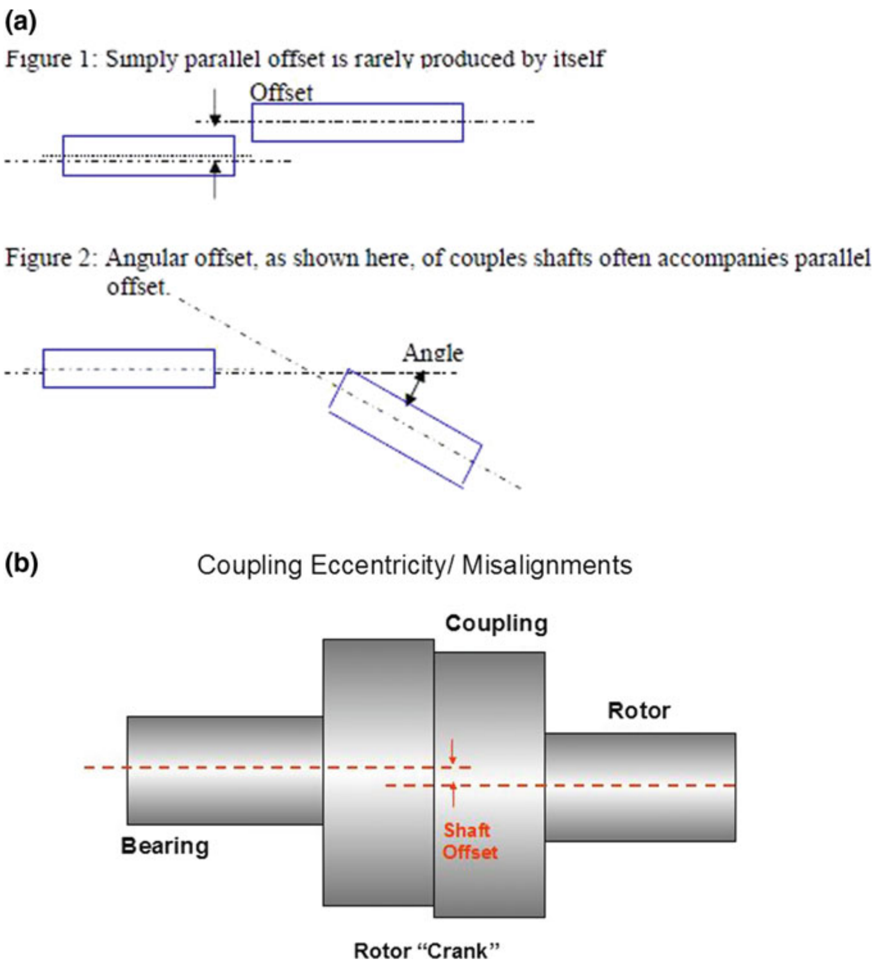

Fig. 6.3 **a** Shaft centerline offset, **b** coupling displacement showing shaft eccentricity/ misalignment, **c**Rotor crank

When shafts bend in such a way that the shaft centerlines intersect at an angle as shown in Fig. 6.4, the associated coupling flange faces become non-parallel. This type of misalignment is known as "angular misalignment." This gives rise to taper or non-parallel flange faces between the two couplings called "face runout" that produces "differential axial gap" between coupling faces. Offset between two coupling faces can have unequal axial distances around the periphery of the two coupling faces. By rotating one end of the coupling face while keeping the other end fixed, it is possible to align the coupling faces with minimal differential gaps across the coupling faces. This process is known as "clocking." Clocking helps equalizing gaps by matching the lows with the highs and vice versa. This brings the two faces almost parallel to each other. Gaps can be measured in the vertical plane as well as in the lateral plane.

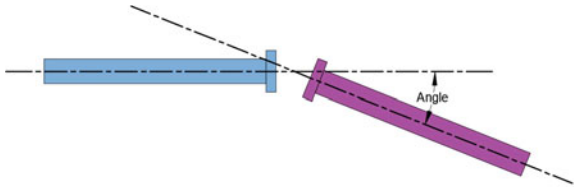

Fig. 6.4 Shaft angular offset

6.4.2 *How are Coupling Displacements and Gaps Measured in the Field?*

Some of the simple tools used to measure linear displacements are shown in Fig. 6.5. They are calipers, gages, liner ruler, etc.

Fig. 6.5 Simple tools used to measure linear displacements

Two views of Fig. 6.6 show the dial gage mounted on one end of the coupling half and measuring the rim readings of the other half of the coupling.

Fig. 6.6 Dial indicator measures rim readings (Courtesy of Siemens)

Indicator is mounted on one coupling rim (drive side) while measuring readings on the other coupling rim (driven side) as shown in Fig. 6.6. Record all dial readings in a data sheet starting with top dead center at 0 or 360°. It is common practice to obtain 16-point measurements (at an interval of 22.5°) for a decent set of rim offset data. Rotate the driven end of coupling until one full rotation is completed that brings the dial back to 0 or 360°. The coupling rim offset condition can be preciously obtained if more rim readings are taken. Switch the mounting to the other side and measure rim readings using the dial indicator as before. Again, perform 16-point readings. Determine an optimal rim position using the data obtained.

To measure the coupling axial face measurements, mount the alignment bracket on the drive side of the coupling face while the dial indicator is mounted on the driven end of the bracket as shown in Fig. 6.7. This measurement provides the face

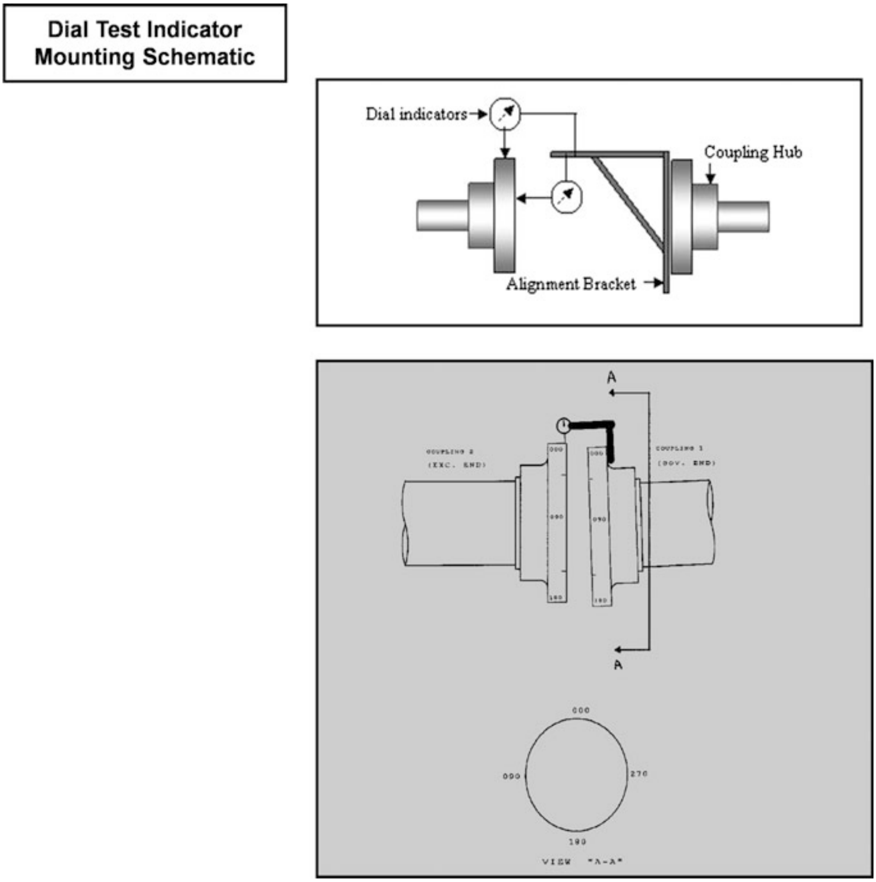

Fig. 6.7 Dial indicator measures face readings (Courtesy of Siemens)

readings on the driven end of the coupling face. 16-point readings are taken in the same way as it was done for the rim measurements. Switch the bracket to the other face (previous drive side) and measure face readings on the drive side. Again, perform 16-point readings.

Record the coupling rim displacements and axial face gaps as shown in an example record sheet shown in Fig. 6.8.

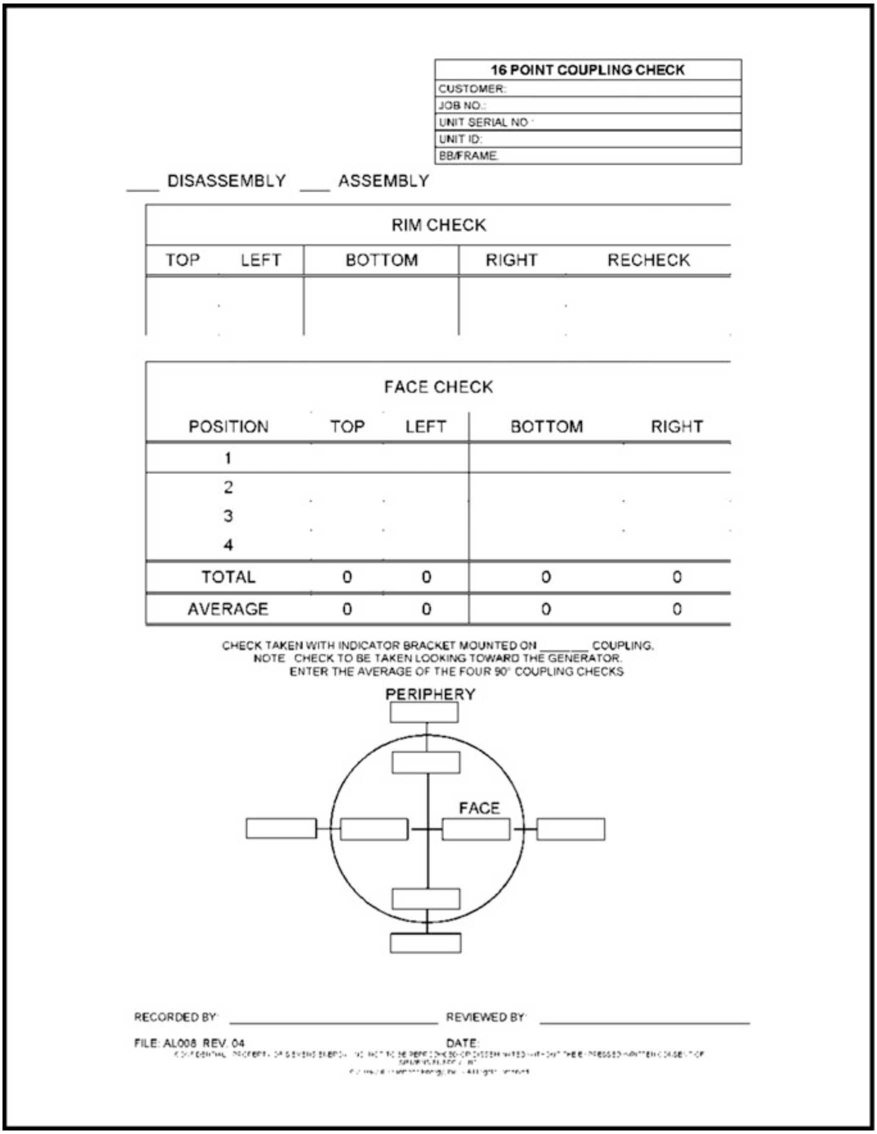

16 POINT COUPLING CHECK
CUSTOMER:
JOB NO.:
UNIT SERIAL NO.:
UNIT ID:
BB/FRAME:

___ DISASSEMBLY ___ ASSEMBLY

RIM CHECK

TOP	LEFT	BOTTOM	RIGHT	RECHECK

FACE CHECK

POSITION	TOP	LEFT	BOTTOM	RIGHT
1				
2				
3				
4				
TOTAL	0	0	0	0
AVERAGE	0	0	0	0

CHECK TAKEN WITH INDICATOR BRACKET MOUNTED ON _______ COUPLING.
NOTE: CHECK TO BE TAKEN LOOKING TOWARD THE GENERATOR.
ENTER THE AVERAGE OF THE FOUR 90° COUPLING CHECKS

PERIPHERY

FACE

RECORDED BY: ______________________ REVIEWED BY: ______________________

FILE: AL008 REV. 04 DATE:

Fig. 6.8 Example data sheet for the measured coupling displacements and gaps (Courtesy of Siemens)

6.4.3 Coupling Alignment Data from Measured Readings

The recorded rim readings can be converted to obtain coupling displacements as shown below:

$$\text{Vertical rim displacement} = (\text{Rim reading at } 0^\circ. - \text{Rim reading at } 180^\circ.) \div 2$$
$$\text{Lateral rim displacement} = (\text{Rim reading at } 90^\circ. - \text{Rim reading at } 270^\circ.) \div 2$$

Raising or lowering one end of the coupling with respect to the other end can help adjusting the coupling rim runouts or displacements. Runout reduction essentially reduces shaft eccentricity and results in reduced mass unbalances at the coupling joint. The radial runout or offset measured is known as "coupling crank." Excessive coupling crank leads to excessive vibration. Balance planes located in the body of the rotor may not help balancing the localized mass unbalances caused by the crank at the coupling. The effective way of balancing the coupling cranks is to drill balance holes on the rim of the coupling or behind the coupling faces that could be used to add balance correction weights.

Similarly, coupling axial gaps are assessed using face measurements on each face of the matching couplings. Measured gap readings at the same angular positions are subtracted to obtain final gaps.

For example, the vertical gap = gap at 0° − gap at 180°. If the gap reading at 0° is larger than that at 180°, the calculated vertical gap is called "negative gap." If the gap at 0° is smaller than the gap measured at 180°, the gap is called "positive gap."

$$\text{Similarly, lateral or horizontal gap} = \text{gap at } 90^\circ. - \text{gap at } 270^\circ.$$

Similarly, lateral or horizontal gap = gap at 90° − gap at 270°

Clocking of the coupling faces is done to reduce the axial differential gaps.

Figure 6.9a illustrates the differential gaps at the two ends of the LP coupling faces that match with the corresponding IP coupling on the left and with the generator coupling on the right. As shown, the IP and LP end coupling faces have smaller gap (lows) at the top and larger gap (highs) at the bottom. The gaps are just the opposite for the LP and the generator coupling faces.

Both LP coupling ends are clocked with their matching coupling halves of the IP and the Generator in such a way that the highs align with lows and vice versa. After alignment, the LP coupling face on either end is parallel with the matching IP and the generator coupling faces as shown in Fig. 6.9b. This example demonstrates how clocking can be effectively utilized to minimize the axial gaps between coupling faces.

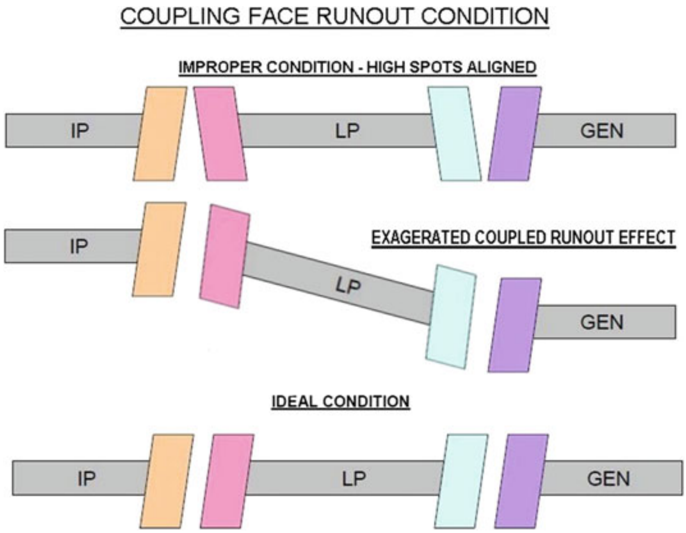

Fig. 6.9 **a** Both LP coupling faces have runout condition, **b** LP coupling faces were clocked to minimize gaps in the adjacent couplings

6.5 Two Different Philosophies of Rotor Alignments

As discussed earlier, the rotor coupling alignments can be made aligning the shafts with zero bending moments (BM) (a) at the bearings or (b) at the couplings. Setting Zero BM at the bearings is relatively easier to align shafts for two-bearings per rotor supports whereas zero BM at the couplings suits to align shafts for shared bearing systems because shafts are aligned using coupling spigots. Calculations are required to determine shaft alignment with zero BM either at the bearing or at the coupling.

6.5.1 Coupling Alignment Impacts: Shared Bearing System Versus Two Bearings System

As mentioned earlier, tighter tolerances on displacements and gaps are required for sustained low rotor vibration compared to two bearings per rotor system. Analysis is required to obtain range of displacements and gaps that meet acceptable bearing loading and high-cycle fatigue limits. This will help the site engineers to choose one of the acceptable alignments in the range.

6.5.2 Coupling Alignment for Two Bearings Per Rotor Supports

Let us discuss the coupling misalignment tolerances (of displacements and axial gaps) in two bearings per rotor system shown in Fig. 6.10 which has 6 rotor elements assembled in tandem; rotors are numbered from left to right. Alignment changes that exceed the set tolerances in coupling displacement and/or gap at one end of the coupling joint have little or no influence on the other end of the coupling joint in terms of vibration and bearing metal temperature. For example, in the rotor train shown in Fig. 6.10, a misalignment in the coupling joint between bearings 2 and 3 has little influence on the other end of the coupling joint that is between bearings 4 and 5. In other words, misalignment at one end of the rotor coupling can be corrected without affecting the alignment of the other couplings in the train.

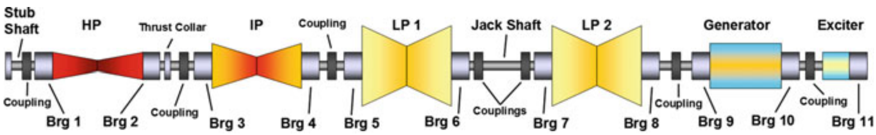

Fig. 6.10 Rotor train configuration of “two bearings per rotor system”

Another example is about the misaligned coupling between two adjacent bearings 2 and 3, and its impact on the bearing loads illustrated in Fig. 6.11. The bearings 2 and 3 are supported on the same bearing pedestal. Bearing 2 supports the generator end (GE) of the rotor 1, and the bearing 3 supports the turbine end (TE) of the rotor 2. Assume that the shaft misalignment occurs in the coupling joint between bearings 2 and 3. Say it unloads bearing 2. Then, bearing 3 loads up as a result. In this case, the unloaded bearing 2 will exhibit lower metal temperature than the nominal value compared to the loaded end of the bearing 3 that will experience higher than the nominal bearing temperature. This example demonstrates that the changes in bearing metal temperatures (from nominal condition) on two adjacent bearings could provide confirmation of shaft misalignment. The symptoms of misalignment are confined to one span only, and the advantage here is that it can be corrected without affecting the rest of the shaft system.

Rotors are mainly supported radially at the journal locations through fluid-film bearings as shown in Fig. 6.11. The generator end (GE) of the coupling flange (located after bearing 2) on the rotor 1 is assembled to the matching turbine end (TE) coupling flange (located before bearing 3) on the rotor 2 to make a coupling joint. The coupling joint thus assembled is secured and tightened by bolts. The processes involved in coupling alignment have been discussed in Sect. 6.4.1. (Fig. 6.12).

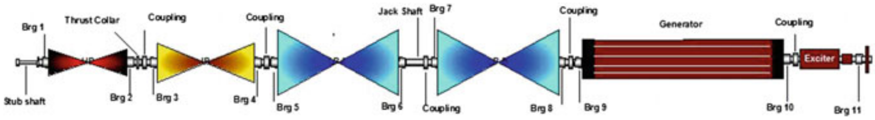

Fig. 6.11 Common coupling between two rotor components

6.5.3 *Alignment in Multi-span Rotor Systems*

For multi-span rotor systems, two bearings of a rotor can be set at zero positions known as "datum bearings" and the catenary curve can be set for the rest of the rotors with acceptable gaps and displacements at the respective couplings with acceptable bearing loadings. The three-rotor system shown in Fig. 6.13a has bearings 3 and 4 set at datum (or zero BM), and the rest of the shaft system is ready for alignment.

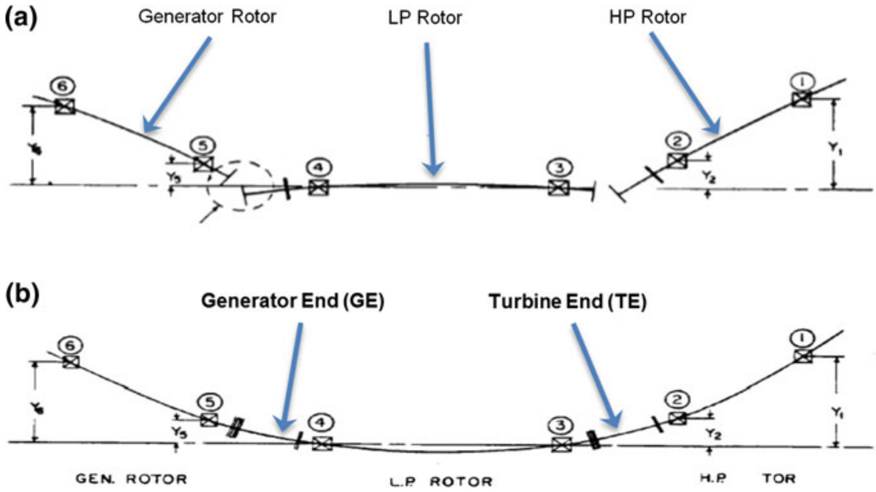

Fig. 6.12 **a**Uncoupled couplings at two ends of an LP rotor (Courtesy of Siemens), **b** final aligned shaft catenary curve (Courtesy of Siemens)

There are cases where the rotor couplings are connected to an extension shaft called "jack shaft" (JS). For example shown in Fig. 6.12a, JS are located between bearings 2 and 3 and between 4 and 5. Each JS has two coupling ends. In such cases, one coupling end of the JS is open when the other end is fixed or vice versa when performing coupling alignment.

The catenary curve for the rotor train is set after the coupling ends are aligned and bolted as shown in Fig. 6.12b.

6.5.4 *How Does Shaft Alignment Keep the Bending Stresses in Check?*

The other objective of shaft alignment is to reduce bending stresses at the small fillets and groove areas in the shaft, which are typically located in the overhang shaft areas adjacent to the bearings and/or glands. The stresses due to the combination of shaft bending loads, shaft torque loads (shear stresses due to rotor twist), and steam pressure forces could accumulate at the small fillet areas. With speed and load cycling, they could eventually exceed the design allowable stress limits. Continuous exposure to severe service loads could initiate rotor cracks. Therefore, it is important to keep them within the design allowable limits by properly aligning the shafts for continuous and trouble-free operation of the rotor train.

6.6 Coupling Alignment for Shared Bearing Rotor Supports

An example of a “shared bearing system” is shown in Fig. 6.13 with a common bearing that partially shares the loads of two rotors. In essence, two rotors are supported by 3 bearings in total. For trains with one HP-IP and 2 LP rotors, 4 common bearings support 3 rotor ends.

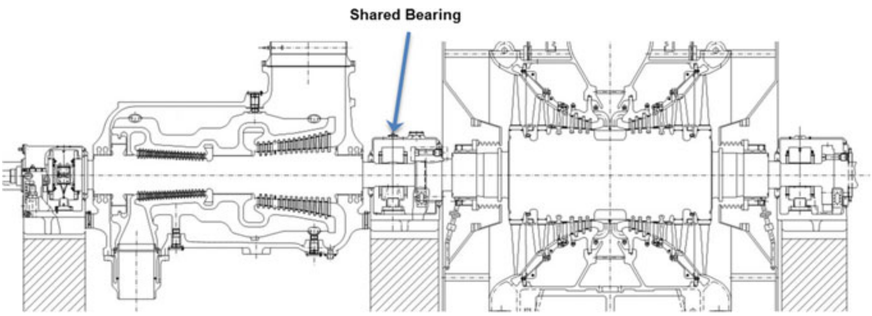

Fig. 6.13 Shared bearing rotor system (Courtesy of Siemens)

During factory balancing, the rotor end that does not have a bearing is supported by a stub shaft that serves as second bearing. For these rotor configurations, the couplings at the shared bearing end are aligned at the site by adjusting gaps only. To align the shafts for minimal runout conditions, the displacements are adjusted in the coupling spigots. To accommodate this, the two coupling halves are designed with clearances between the male and the matching female spigots. This enables supporting male spigot on the female counterpart. The concentricity or displacements in coupling halves on a shared bearing system cannot be adjusted using dial gages as it was done on open couplings in a two bearing per rotor system. The displacements are adjusted using feeler gages within spigots. The spigot alignment is discussed in Sect. 6.8.2.

Gaps can be measured at each quadrant setting at zero, 90, 180, 270° and recheck at zero. Use vertical or transverse gaps whichever is the highest.

In general, a maximum tolerance band of ±0.002 inches (0.05 mm) is recommended for aligning coupling displacements and gaps. However, the rotor design determines the nominal and the maximum coupling gaps and displacements.

6.7 General Guideline for Runout Measurements

It is always a good practice to measure the runouts at the coupling rims and at the adjacent shaft areas as shown in Fig. 6.14. A total of 4 radial runout measurements on the outer surface of the shaft and the couplings would help understanding the runout condition of the shaft system for better shaft alignment. These measurements also help machining excessive shaft runouts.

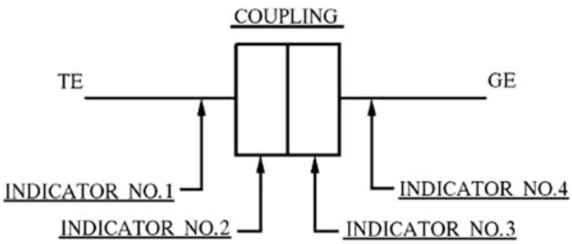

Fig. 6.14 Runout measurements of shafts and coupling faces

General tolerance guideline for displacements and gaps is provided for the two bearings per rotor system (45° lines) and shared bearing systems (hatched area) as illustrated in Fig. 6.15. As can be seen, tighter tolerances are recommended for shared bearing rotor systems because they become very sensitive even with minor shaft misalignments. A coupling misalignment can easily be diagnosed using vibration and bearing metal temperature data for a two bearing per rotor system. As

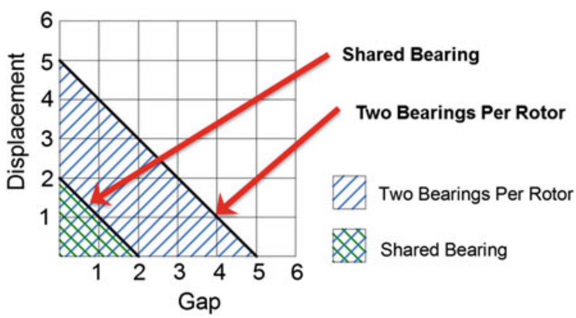

Fig. 6.15 Gap and displacement tolerance guidelines

discussed before, a misaligned coupling on a shared bearing system could trigger vibration in a rotor located at two or three spans away. Therefore, it becomes a challenge sometimes to diagnose the symptoms of vibration for the shared bearing rotor systems. Consequently, it is highly recommended to always maintain tighter tolerances for shared bearing rotor systems.

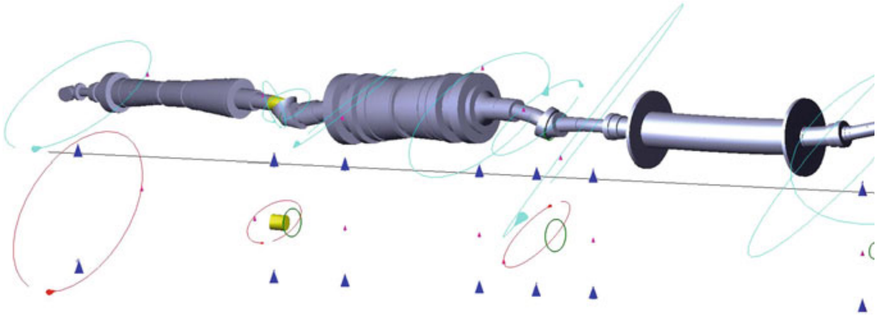

Fig. 6.16 An example shaft misalignment in a rotor train

Shaft cranking as illustrated in Fig. 6.16 introduces eccentricity in shafts and coupling rims as well. Consequently, misaligned shafts exhibit elevated vibration levels in operation depending on whether they unload or load bearings. Various shaft orbital plots highlight the sharp and narrow elliptical orbits shown at the bearing locations because of the shaft crank.

6.8 Other Guidelines for Better Shaft Alignments

To maintain as-designed alignments in rotor trains, it is important to have the rim and the face runouts within the design tolerances. However, in addition to the coupling gap/displacement alignments, there is another element that helps maintaining close tolerances in the coupling joint is the "coupling bolt." After the shafts and the coupling halves are aligned to recommended tolerances, the coupling holes are line-reamed or honed to receive the bolts that keep the two coupling halves aligned together as one solid joint. Bolts are prestretched, torqued, and tightened to the two outer end faces of the couplings by nuts for a tighter fit of the coupling halves.

6.8.1 Galling in Coupling Bolts

Galling occurs when pressure and friction at the matting coupling faces fret and joints cause bolt threads to seize. This is also known as "cold welding." Once fasteners have seized by galling, it is virtually impossible to remove them without cutting the bolt or splitting the nut.

The bolt shank diameter and the number of bolts are determined based on the torque transmitted by the coupling joint. In service, the coupling bolts may gall at the contact point between the inner faces of the nuts and the outer face of the coupling. Galling could cause uneven bolt diameters along the body of the bolt (such as variable diameters at points 1 and 2 in Fig. 6.17). This could lead to loosen couplings and eventual misalignment. So, coupling bolts are made of high-strength material to match with the coupling flange material.

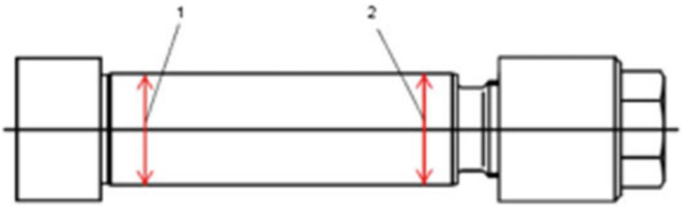

Fig. 6.17 Coupling bolt conditions

Sometimes, the bolt holes or bolt surfaces may be machined uneven. Bolt holes in locations 1 through 4 shown in Fig. 6.18 may be uneven. Such uneven surfaces in both holes and bolts could lead to loose bolting and misalignment. Sometimes, uneven holes could produce “ovality” or non-circular holes. If ovality was measured, recommendation is to clean up bolt holes to circular shape. Uneven bolt sizes lead to shearing of bolts and eventual misalignment.

Fig. 6.18 Coupling hole conditions

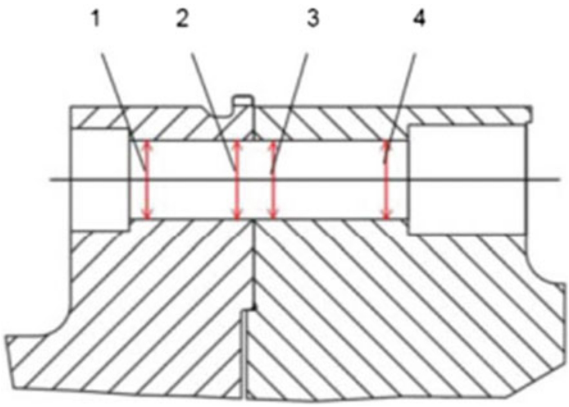

6.8.2 Requirements of Spigot Clearances/Interferences

Coupling Spigots are used to maintain tighter coupling joint. A spigot coupling is shown in Fig. 6.19. In the case of two bearings per rotor system, typically, the coupling spigots are assembled with shrink-fit or negative clearances. Shafts are aligned by moving the coupling halves to correct for displacements and gaps.

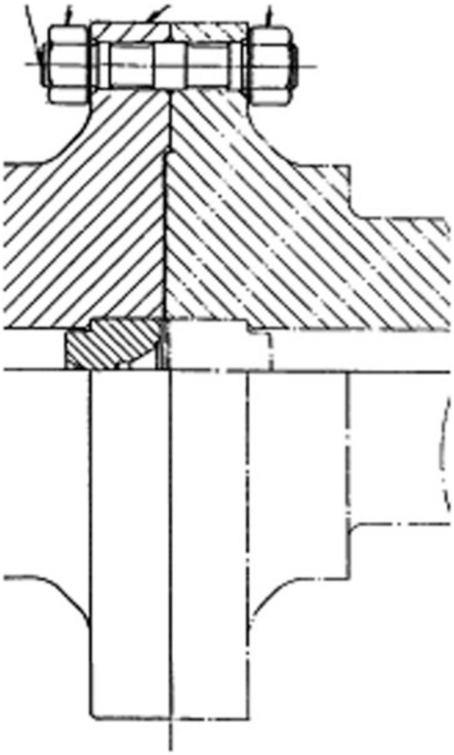

Fig. 6.19 Coupling spigot fittings

However, for rotor systems with shared bearings, spigots have positive clearances and any smaller radial runout due to kinks or permanent bow is adjusted in the spigot clearances, whereas the gaps or axial runouts are clocked (one face is rotated relative to the other) before the couplings are bolted together. Uneven spigot clearances give rise to eccentric fit of coupling faces and lead to eventual misalignment.

6.9 Other Shaft Alignment Methods

Apart from the conventional mechanical tools used to obtain the shaft alignment data described here, modern tools such as "laser alignment" techniques are also applied in some cases to measure the same data. Laser alignment equipment utilizes laser beam transmitters and receivers to measure alignment within high tolerances.

Laser beams are used to measure shaft elevations and coupling displacements with respect to a reference point when the rotor system was aligned when built. This reference data is continuously used to capture or monitor the changes of shaft movements in operation by permanently installed laser equipment.

In certain cases, bearing structures have distorted laterally (or horizontal) causing bearing misalignment condition. The distortion was significant that the clearances between the bearing shell and the journal became uneven. As a result, the bearing was reported as unloaded causing sub-synchronous whirl in the lateral (or horizontal) direction.

6.10 Closure

The following materials were covered in this chapter:

- Precise casing-to-rotor alignments help avoiding seal rub conditions in operation.
- The impact of shaft or coupling radial and axial runouts on rotor alignment.
- Distinct differences between the two different rotor support systems known as (a) two bearing supports per rotor and (b) shared bearing rotor systems and their sensitivity to rotor train alignment.
- Stringent alignment tolerances are required for shared bearing systems to maintain a good shaft alignment.
- Importance of bolt machining to tight tolerances and their role in maintaining alignment.

References

1. Piotroswski J (1995) Shaft alignment handbook. Marcel Dekker, Inc.
2. Wowk V Machinery vibration: alignment. McGraw Hill

Chapter 7
Condition Monitoring of Rotors

7.1 Introduction

After learning rotor and structural dynamic theory and the tools to evaluate the most relevant parameters, it becomes important to apply them systematically to solve turbo-machinery issues. Parallels can be drawn between the health diagnostic processes applied in humans versus machines. To understand the source of a problem in a human body, physicians analyze the basic or vital information that could provide symptoms. Information such as (a) Body temperature, (b) Heart/pulse rate are used for initial analysis. Additional data may be needed for in-depth diagnosis of problems. Similarly, vital symptoms (key data) can be used to diagnose machinery problems. Diagnostic details of turbo-machinery issues are discussed in the following sections.

7.2 General

This chapter addresses the diagnostic procedures applied to problems experienced in turbo-machinery and the diagnostic tools used to record and monitor data. Results from the diagnosis can be used to determine whether the machine is operable continuously or monitor for a while until things settle or stop the machine when levels exceed the limits specified by ISO vibration standards.

To understand the health condition of a turbo-machinery, two primary parameters such as (a) Bearing metal temperatures and (b) Vibration levels are required. Based upon the initial diagnosis, additional data may be required to perform an in-depth analysis of problems. This chapter goes through the step-by step process that would lead to the root-cause of machinery problems. Diagnosis includes the tools used in acquiring relevant data, and the detail description of analyses carried out towards identifying and solving the issues.

R. Subbiah and J. E. Littleton, *Rotor and Structural Dynamics of Turbomachinery*,
Applied Condition Monitoring 11, https://doi.org/10.1007/978-3-319-73296-1_7

7.3 Diagnostic Data and Tools

The diagnostic tools vary depending upon the type of data to be monitored for analysis. The most basic data sets such as vibration and bearing metal temperatures are needed for condition monitoring of rotating machinery.

The data needed for machinery diagnosis are:

- Vibration
- Oil film Pressure and Temperature of Bearings
- Speed and Load
- Steam/Gas Pressure at relevant points in a turbine.

The basic vibration measurements used in machine diagnosis are shown in Fig. 7.1

They are:

(1) acceleration (a)
(2) velocity (v)
(3) displacement (d).

The plots represent shaft amplitudes versus time. The amplitudes have distinct phase relationships between them as shown. The velocity lag 90° from the acceleration and the displacement lags 90° from the velocity. The phase difference between the acceleration and the displacement is 180°.

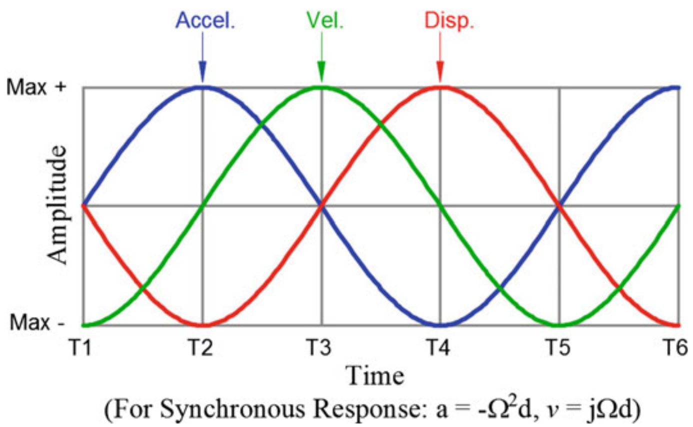

Fig. 7.1 Various types of vibration data

Primarily, vibrations in turbo-machinery are measured for rotors and the bearing support structures. The instruments used to measure shaft vibration are non-contact proximity probes, otherwise known as "rotor motion or shaft-displacement measuring sensors". The structural vibration is measured by accelerometers placed directly on the body of the structure. Shaft vibration data is usually referred as "Shaft Relative Vibration (SRV)" which is measured with respect to the stationary structure, where the vibration probes are mounted directly on a bearing structure or on a structure in proximity to bearings overseeing the rotor as shown in Fig. 7.2a.

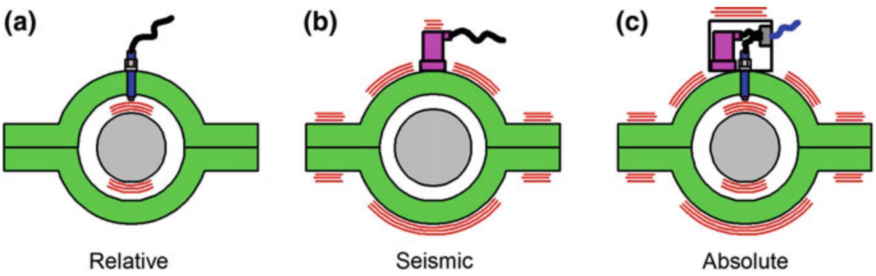

Fig. 7.2 Various rotor vibration data measurements

7.3.1 *Shaft Relative Vibration (SRV) Measurement*

SRV data helps primarily to understand the magnitude of shaft motions inside the bearing oil film. The measured data provides shaft's relative position inside the bearing clearance. The response patterns of the rotor provide indications of what forces could have caused the problem; such as a mass unbalance or mass loss or rotor-stator rubs or oil whirl or steam whirl and/or other transient events etc.

The inductive type, non-contact proximity sensors have been in practice for measuring shaft relative vibration data since early 1970s. The probe tips are positioned facing the outer surface of the rotating shaft. The gap between the sensor tip and the shaft surface must be within the linear measuring range of the sensor's electric field. Essentially, a varying DC gap voltage due to the shaft motion is measured in the shaft relative measurement. Thus, the variations in DC gap voltage correspond to the rotor motions inside the clearance space. The DC gap voltage variations are calibrated to the corresponding shaft motions and are measured in mils or microns.

SRV measures help identifying rotor critical speeds, unbalance responses, rotor-to-casing rubs, rotor cracks and any rotor related abnormalities. Spectrum plots of rotor harmonics are measured as shaft relative motions as well. ISO 20816-2 [1] (International Standards Organization) provides guidelines for shaft relative vibration levels for large turbo-machinery. API (American Petroleum Institute) standard can also be used for small industrial turbines, process equipments applied in chemical, food processing, sugar and paper mills etc. Figure 7.2a shows the proximity probe positions that are used to measure shaft relative vibration. Brackets on the stationary structure support the proximity probes as shown in Fig. 7.3.

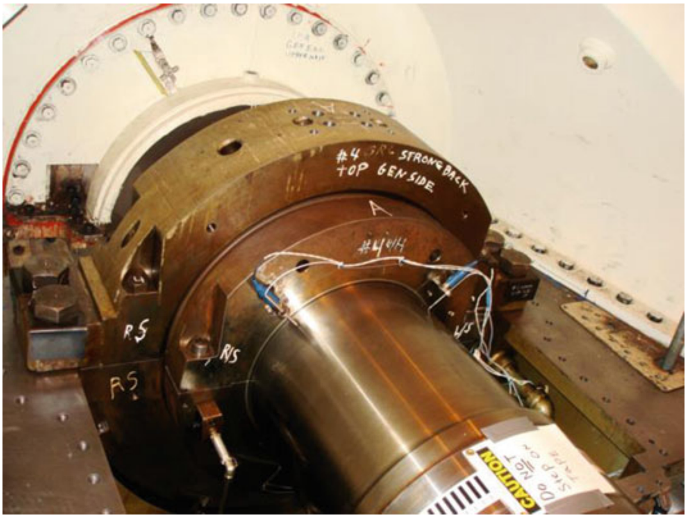

Fig. 7.3 Proximity probes installed on the shaft to measure vibration signature

7.3.2 Seismic Vibration (SV) Measurement of Structures

SV is the measure of amplitudes of structural components such as bearing shell and the associated pedestal structures connected to it. For seismic vibration measurement, accelerometer or velocity sensor is typically attached to the body of the structure as shown in Fig. 7.2b. They are measured in RMS or in/s or mm/s units. The acceleration or velocity signals measured are being converted to displacement in inches or microns to monitor shafts at steady-state operating speed. For steam turbines, gas turbines and generators, SV provides the bearing support pedestal vibration. Although, the support structures respond to forces imparted by the unbalance forces in the rotor, SV cannot be used to identify rotor critical speeds and other rotor driven frequencies. ISO 20816-2 provides exclusive guidelines for bearing structure vibration levels as well. Shaft and seismic probes are shown in Fig. 7.4. The probes are positioned almost at similar angular positions (30°, 45° or other angles) on either side of the 12 O'clock position.

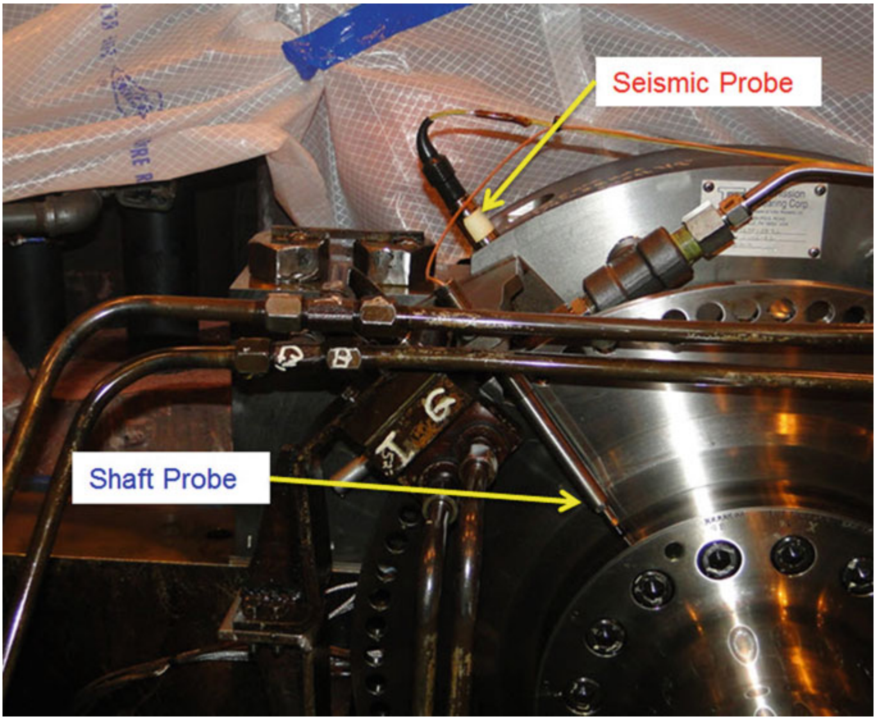

Fig. 7.4 Shaft and seismic probes

7.3.3 Shaft Absolute Vibration (SAV) Measurement

SAV is the measure of the net effect of the shaft and the bearing structure motions including their phase angle positions. Probes used to measure SAV is illustrated in Fig. 7.2c. When the angular positions of the shaft and the bearing structure probes are identical, the absolute vibration can be obtained by directly adding the levels of SRV and SV. A rule of thumb is a direct addition of SRV and SV amplitudes which would be equivalent to direct SAV measurement, if the phase angle differences between SRV and SV stay within 30°. This is almost equal to direct SAV amplitude measurement. Table 7.2 lists SRV, SV and SAV vibration amplitudes at several bearing locations of a T-G system. They clearly show the relationship between the three measurements.

An example of real rotor responses is shown in Table 7.1. Rotor vibration levels at four bearing locations (bearings 3 through 6) are reported. For example, the 3X and 5X shaft and seismic phase angles are very close (within 30°). Hence, directly adding SRV and SV magnitudes (not including their phase angle effects) match with the directly measured SAV levels. Rest of the data in the table suggests that exact phase angle information should be accounted for SRV and SV amplitude positions to arrive at the correct SAV levels (Table 7.2).

The seismic vibration sensor, which is an accelerometer, measures the bearing structure vibration. The rotor displacement sensor, which is a proximity probe, measures the relative vibration.

SRV and SV measurements are sufficient to identifying most problems related to shaft and/or support structures accurately. ISO 20816-2 provides guidelines for shaft and bearing structure vibration levels (or sometimes called bearing cap).

Table 7.1 Shaft vibration measurements at various bearing locations

Brg	Ips[a] pk	Degree	RPM	Seismic mils pk-pk (SV)		Rel mils pk-pk (SRV)		Absolute mils p-p (SAV)	
#	Amp	Phase	Freq	Amp	Phase	Amp	Phase	Amp	Phase
3Y	0.15	334	1800	1.6	64	1.40	15	2.7	41
3X	0.17	348	1800	1.8	78	1.20	98	3.0	86
4Y	0.14	143	1800	1.5	233	0.97	301	2.1	259
4X	0.10	168	1800	1.1	258	0.39	137	1.0	237
5Y	0.17	18	1800	1.8	108	1.64	65	3.2	88
5X	0.19	32	1800	2.0	122	1.83	149	3.8	135
6Y	0.17	189	1800	1.8	279	0.44	106	1.3	277
6X	0.10	202	1800	1.1	292	0.81	259	1.8	278

[a]Ips represents inches per second

Some old power plants still use SAV levels to monitor vibration using shaft riders shown in Fig. 7.5. A shaft rider uses spring-loaded Teflon probe tip that always in contact with the rotor surface and is used to measure the SAV. When the Teflon tip wears away, the measured vibration shows a lower value than the reference normal, at which point, it is an indication that the Teflon tip needed replacement. It is cautioned that the SAV measurement may not indicate definitively whether the measured amplitude is dominated by the rotor or by the structure. So, it is always encouraged to measure SRV and SV separately for accurate diagnosis of vibration.

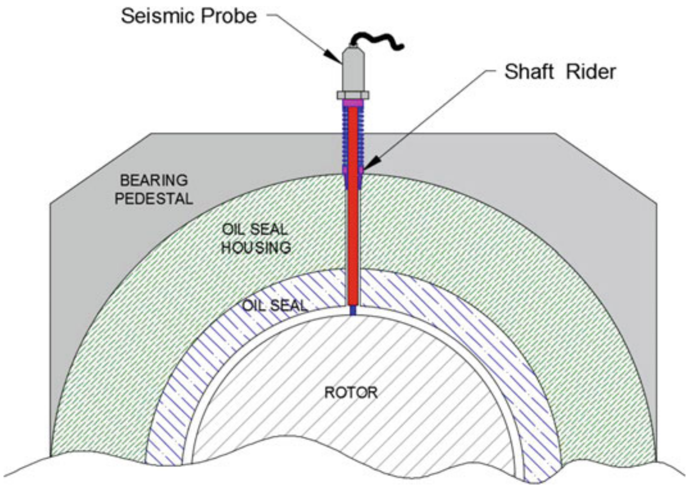

Fig. 7.5 Shaft riders to measure shaft absolute vibration

7.3.4 Bearing Metal Temperature Measurements

Bearing metal temperatures are measured between the journal and the bearing at or closer to the minimum oil film location. The tip of the thermocouple is placed as close to the bearing Babbitt metal surface as possible at the minimum oil film thickness zone (sometimes, thermocouple tips are positioned half way into the Babbitt thickness).

Bearing thermocouples are small and compact measuring devices and are used to detect oil film temperature increases in the journal and the thrust bearings. Some of the physical and material requirements for thermocouples are as follows:

- Low mass and flexible sensors which are fast responding.
- Sizes from 0.125 inch (3 mm) in diameter single or double insulated lead or lead-bronze or copper-constantan or iron-constantan wire etc. Selection of thermo-couple materials and configurations must match with those already exist at the T-G unit.
- Thermocouple materials are wear resistant and typically housed in stainless steel braided jacket.
- Designed for temperatures from −50 to 177 °C (−58–350°F) and
- Wires have spring loaded mounting and retaining thrust washer
- Vibration and moisture proof design.

Measured bearing metal temperatures indicate whether the bearings are unloaded, adequately loaded and/or heavily loaded. They may provide symptoms (together with shaft relative vibration data) of unloaded bearings, shaft misalignment, oil whirl, and/or steam whirl etc.

7.4 Load Variations

Steam/gas load variations in turbines could unload the bearings resulting in shaft vibration increase. This happens in machines designed for partial-arc operating conditions where steam-induced load unbalance excitations could trigger "steam whirl" related self-excitation.

7.5 Pressure Variations

Steam pressure variations in a steam turbine could cause temperature variations between the cylinder base and the cover. Excessive temperature differentials in the cylinder base to cover could lead to casing distortions, rotor-to-stationary seal rubs and water ingress into the casings, all of which eventually could increase rotor vibration.

7.6 Diagnostic Data

Most useful machine diagnostic information can be obtained using plots such as (a) Bode, (b) Polar, (c) Spectrum, (d) Shaft Centerline and (e) Spectrum Waterfall [2–7].

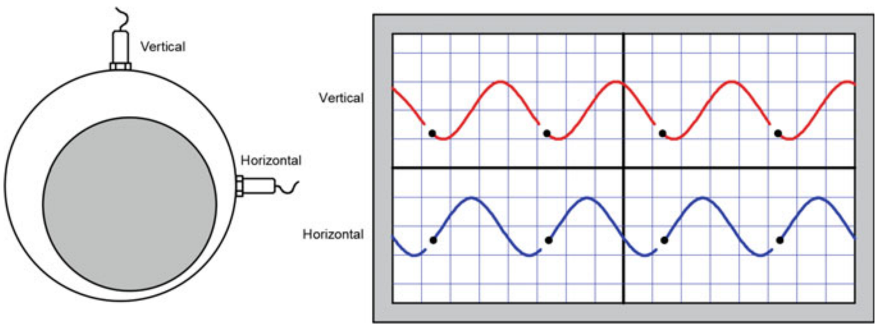

Fig. 7.6 Probe positions in orthogonal directions (X-vertical, Y-horizontal)

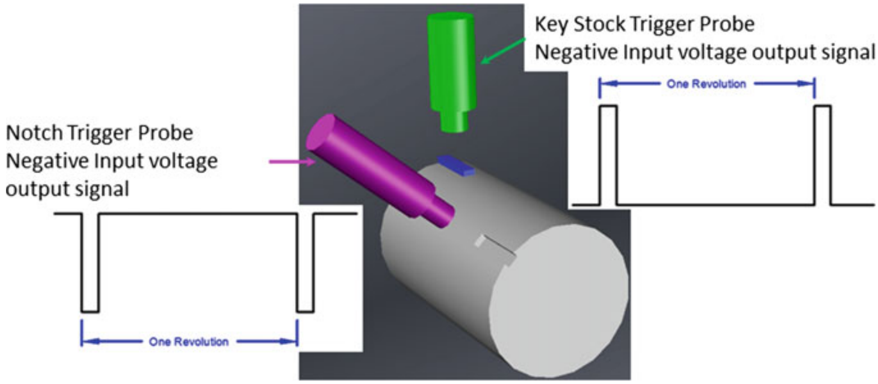

Fig. 7.7 Shaft reference key notch or key stock

Orthogonal probe positions in X (Vertical) and Y (Horizontal) directions are shown in Fig. 7.6. They measure rotor motions. Signal discontinuity caused by a notch or a material stock can be observed on both X and Y recordings as shown in Fig. 7.7. Both measures provide shaft positions with respect to phase angle references related to the notch positions. Typically, the probes are positioned at 45-degrees from the top dead center (or 12 O' clock position), one for each side.

7.6.1 Bode Plot

A Bode plot displays vibration magnitudes as a function of rotor speeds and the associated phase angles at any chosen shaft locations. An example is shown in Fig. 7.8. The phase angles are measured with respect to the reference notch position in the rotor shaft. They help in locating and positioning the balance weights in the shaft train as needed. Bode plots are used to view rotor displacements and phase angles during rotor run-up (startup) and run-down (coast down) conditions. A Bode plot helps identifying the resonance speeds (or critical speeds) of a rotor.

It can be noticed in a bode plot that whenever the rotor passes through one of the resonance speeds, the rotor amplitude reaches a peak value. For the case presented in Fig. 7.8, the rotor critical speed occurs at approximately 1,364 RPM. Correspondingly, the phase angle shifts to 90° when the rotor speed passes through the resonance.

The first vertical rotor critical speed response can be observed at about 89 μ or 3.5 mills p-p/$\underline{90}^{o}$ when zero phase angle reference is assumed. Phase angle increases opposite to the direction of shaft rotation. The second vertical rotor critical speed can be observed at 3800 RPM and has a response at about 114 μ or 4.5 mills p-p/$\underline{90}^{o}$.

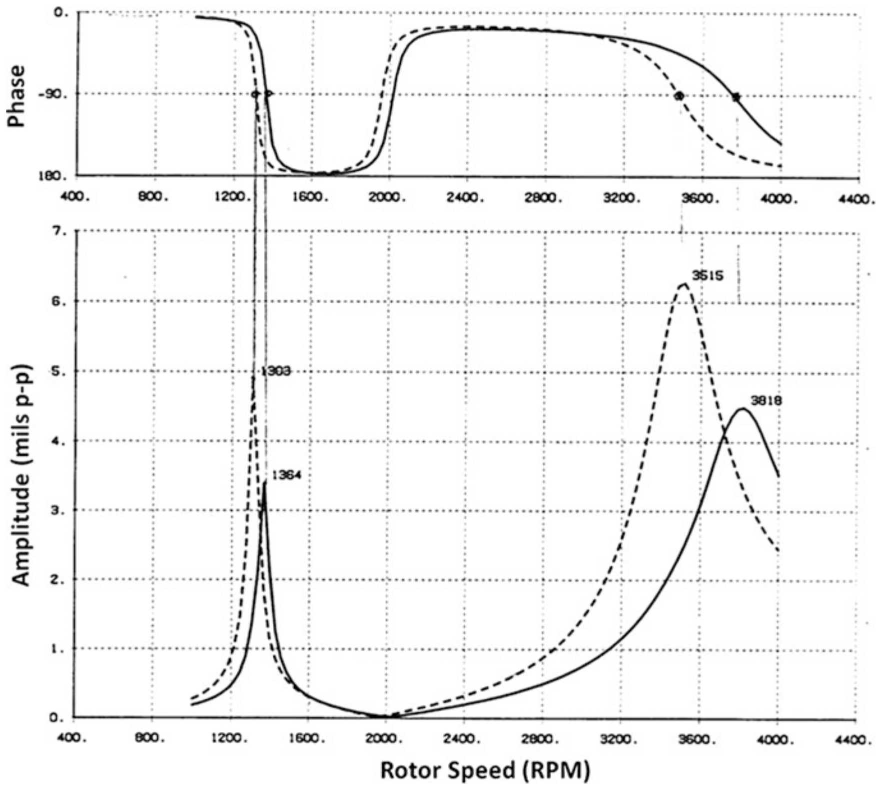

Fig. 7.8 Bode plot

7.6.2 Polar Plot

The data plotted in a polar plot are identical to Bode plot discussed before. A polar plot is illustrated in Fig. 7.9 that displays rotor amplitudes and the associated phase angle data in polar coordinates. This plot provides the phase changes in the range of zero to 360°. The zero degree in a polar plot points to the angular position of a transducer. It is easy to visualize and compare the rotor data from the orthogonally mounted proximity probe pairs with a polar plot. A polar plot consists of constant amplitude circles begin at 0 mils (or microns) which is the origin of the polar plot with increasing amplitudes in increments of 1 mil (25 μ) as illustrated in Fig. 7.9.

The rotor critical speed line on the polar plot is the one that connects the origin and the maximum rotor amplitude, which in this case occurs at 3600 RPM.

It is easy to evaluate Q-factor from a polar plot as follows:

With reference to the Fig. 7.9, the central frequency of the rotor is obtained at 3600 RPM. The two side band frequencies can be obtained, by drawing two 45-degree lines from the origin on either side of the central frequency, at 3420 and

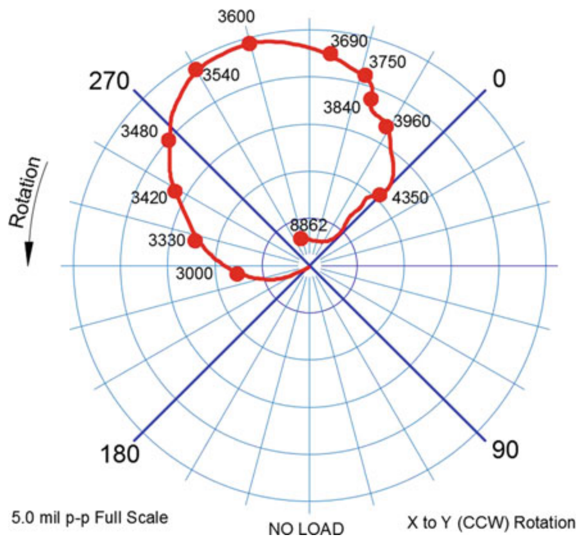

Fig. 7.9 Example of a polar plot

3960 RPMs. As we know, the Q-factor is the ratio of the rotor speed at the peak amplitude and the difference of the two side band speeds. The calculated Q- factor, in this case, is 6.7.

Phase angles increase in the direction counter to the shaft rotation in a polar plot.

1x polar plot shows the location of rotor high spot (peak amplitude) relative to the transducer. This is true for 1x circular orbits and almost true for 1x elliptical orbits as well.

Identical rotor responses and phase angles are displayed in a bode and a polar plots side by side as shown in Fig. 7.10. In the polar plot shown in Fig. 7.10a, the amplitude and the speed of the rotor can be noticed as increasing from zero at the center and reaching the maximum for the 1st rotor critical speed at about 1850 RPM. The same peak response amplitude can be seen at about 1850 RPM in the bode plots in Fig. 7.10b. Similarly, the 2nd rotor critical speed at 5250 RPM can be found identical in both plots.

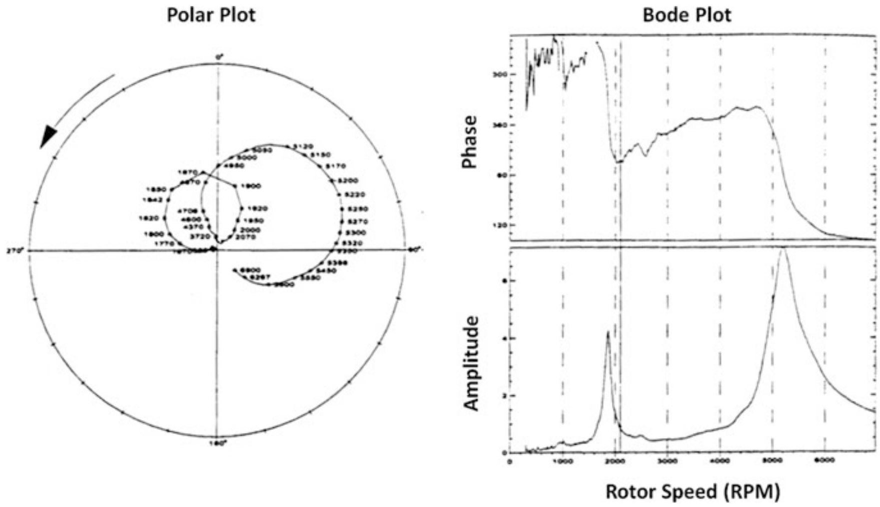

Fig. 7.10 Polar and the corresponding bode plots

7.6.3 Shaft Centerline Plot

Shaft relative amplitudes displayed in Bode and Polar plots provide the rotor vibration data; but do not display the locus of the journal positions inside the oil film bearing. When a rotor, supported in hydrodynamic bearings, varies in speed and/or load, the oil film stiffness and damping characteristics also vary. Consequently, the radial position of the journal inside the bearing varies. Thus, the shaft centerline plot provides locus of the rotor positions inside the oil film bearing at any instant. The trend of the shaft centerline plot enables to understand several malfunctions of the machinery such as

(a) Unloading of bearing due to operating conditions
(b) Shaft misalignment
(c) Fluid-induced instability (Oil whirl, Oil whip)
(d) Steam/gas-induced instability (steam whirl)
(e) Seal rubs etc.

Samples of shaft centerline plot in Figs. 7.11a, b show the unloaded rotor conditions in the vertical and the lateral planes respectively.

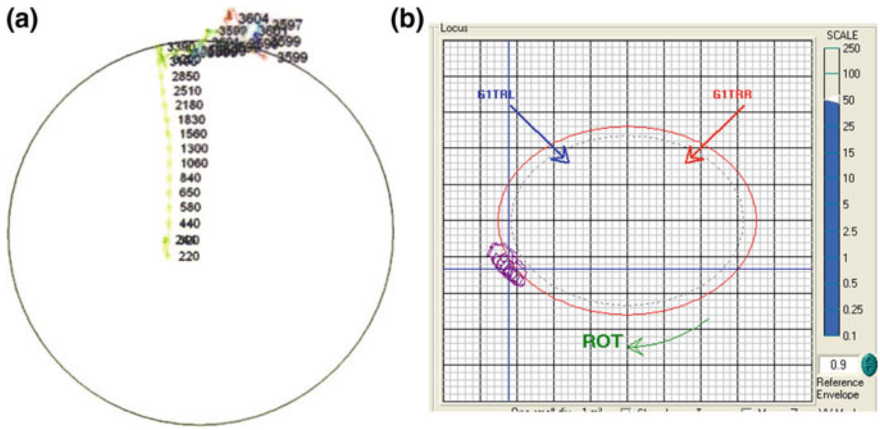

Fig. 7.11 **a** Shaft centerline plot-vertically unloaded bearing. **b** Shaft centerline plot-lateral unloading

They primarily produce variations of rotor's radial position within the bearings and/or seals. Secondarily, correlation of shaft centerline data along with the rotor vibration and the operation data provides the total behavior of the rotor inside a bearing.

Hence, it is important to note that the shaft centerline plots are just as important an indicator of the health condition of the machinery as the rotor vibration data.

7.6.4 Spectrum Plot

Commonly used terminologies of a spectrum plot include:

Fundamental Frequency: 1st bending mode of the rotor

Resonant Frequency—Frequency at which the highest rotor amplitude occurs.

Synchronous Frequency—Frequency of the rotor at which both spin and whirl speeds are identical.

Non-synchronous Frequency—Rotor spin and whirl frequencies are different

Sub-synchronous Frequency—Rotor resonance frequency below the synchronous or operating frequency of the rotor.

A spectrum plot comprises of:

- Fourier Transform—This process is based on the principle of superposition of individual signals into one periodic signal as shown in green in Fig. 7.12. The periodic signal can be broken down into individual frequency components (sinusoidal signals) with their associated frequencies and amplitudes. It essentially breaks down the signals into the fundamental frequency and its harmonics.
- The vibration is sampled over a pre-determined period.

For rotor dynamic space, spectrum plots provide the following symptoms:

- The complex signal is made up of rotor 1x rpm component (mass unbalance), a 2x rpm component (dissimilar shaft stiffness) and a 5x (typically blade pass frequency) of the rotor train.
- There can be other influences—misalignment, bearing problems, soft foot, loosened coupling bolts, frequency modulation, amplitude modulation etc.
- Time domain plots show periodic waveform of multiple frequencies
- Periodic frequency spectrums (in time domain) seen in green can be broken down into individual frequency components as 1x, 2x… etc. by spectrum analyzer as shown in Fig. 7.12.

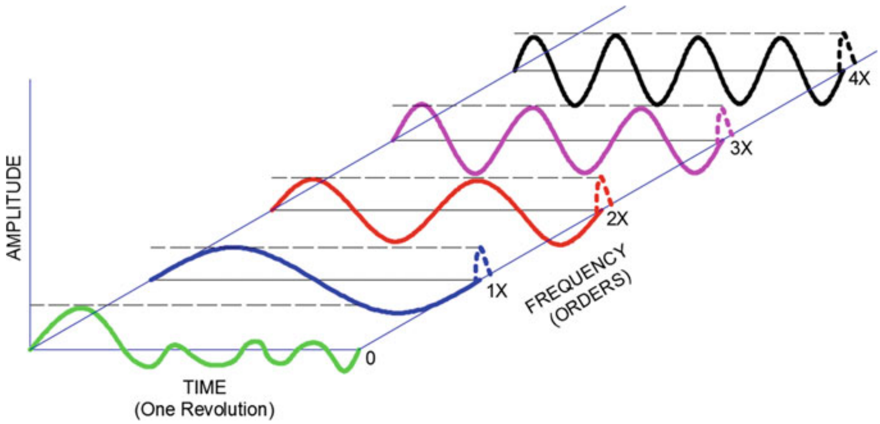

Fig. 7.12 Periodic spectrum consists of multiple frequencies

7.7 Frequency/Time Domain Plots

Steady-state time domain spectrum (top one in Fig. 7.13) shows steady amplitude in the vertical axis and time in the horizontal axis. This information consists of all frequencies involved in the periodic spectrum. The periodic frequency data in the time domain can be discretized into individual frequencies as displayed in frequency spectrum (amplitude in vertical axis and frequencies in horizontal axis) shown at the bottom of the Fig. 7.13. It is very important to check that the two spectrums agree.

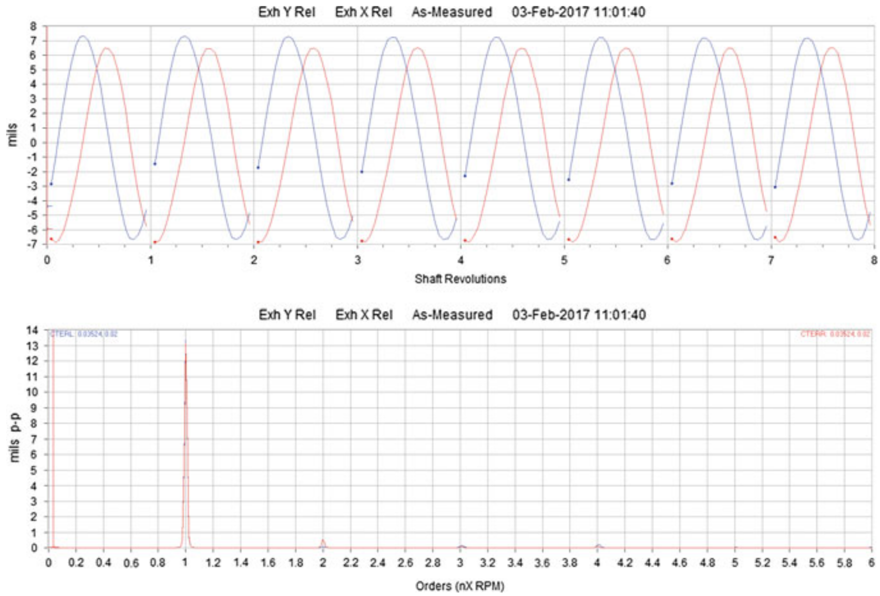

Fig. 7.13 Time (top) and frequency (bottom) domain frequency spectrums

7.7.1 Spectrum Water Fall Plot

A waterfall plot is a three-dimensional plot in which multiple spectrum data are obtained at various periods of operation. A waterfall is a presentation of both frequency and the instantaneous occurrence of an event on a single graph. This is also known as time domain data and captures the rotor vibration as a function of time, usually in the form of a measured impulse (instantaneous) responses. The frequency domain version is the decomposition of the time domain impulse responses into periodic cosine waveforms via Fourier analysis.

The waterfall plots in time domain is shown in Fig. 7.14a that provides the details of the time line showing the sub-synchronous amplitudes increased progressively and initiated oil whip. This condition is associated with high rotor response under the same operating condition. The same time domain information is plotted in frequency domain as shown in Fig. 7.14b which provides the vibration spectrum components of a machine when oil whip occurred. The sub-synchronous vibration component at 12.9 Hz (in both time and frequency domain plots) is seen increasing in amplitudes causing oil whip.

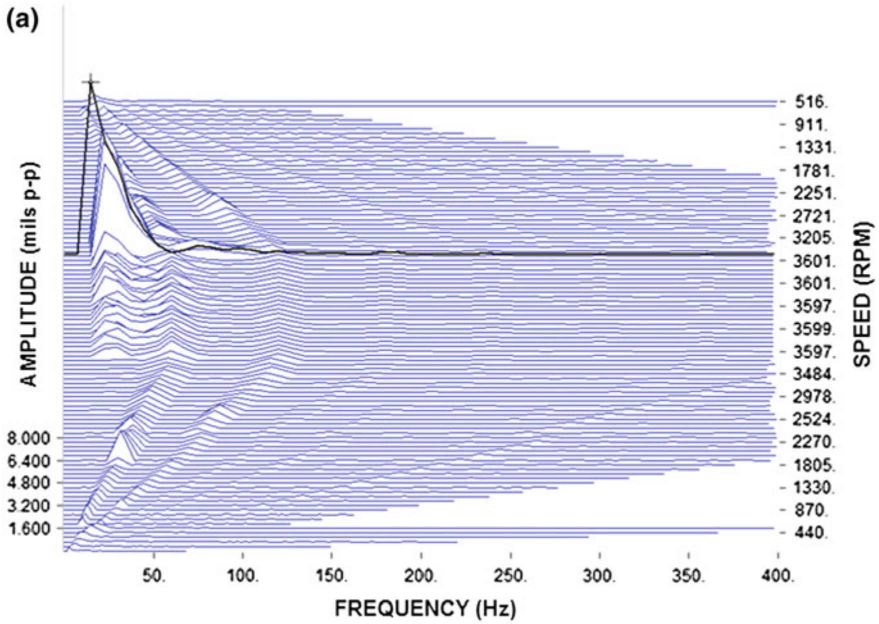

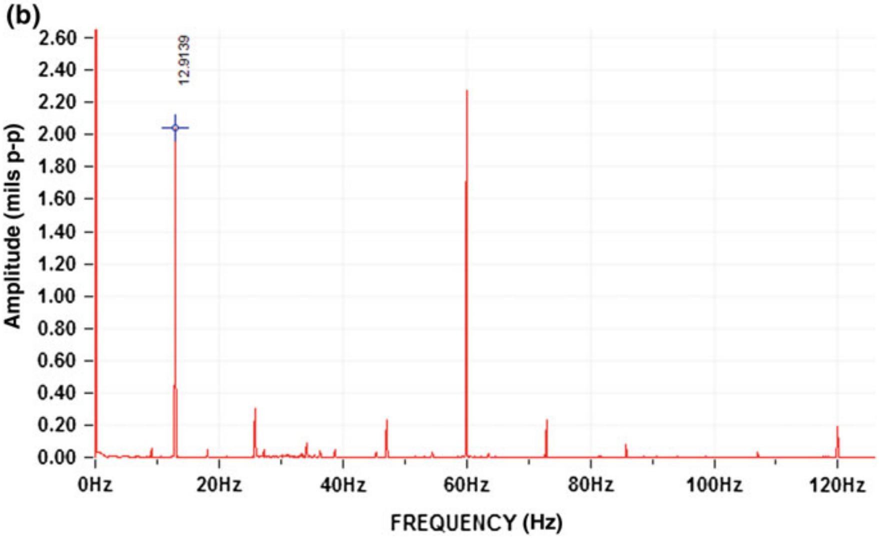

Fig. 7.14 **a** Waterfall diagram showing the instantaneous and the total duration at which oil whip occurred (time domain plot). **b** Spectrum plots showing the frequency (12.9 Hz) at which oil whip occurred (frequency domain plot)

7.8 General Information

Proximity probes are installed in vertical and lateral (horizontal) directions. (It is reminded to readers that Y and Z were used for vertical and horizontal axes in earlier chapters.) Sign conventions may change depending on how the axes are defined and their corresponding probe locations. So, what is important is to look for vertical and horizontal motions of the rotor for tracking related critical speeds and responses. In this example, X and Y rotor amplitudes with their associated phase angles are used to obtain the maximum rotor vibration amplitude. When transduces are used on a casing in the X and Y planes, corresponding casing motions can be obtained.

Now, let us discuss the identification of rotor critical speeds and the related mode-shapes using the probe planes located along the rotor shaft axis. Use the polar plots shown in Fig. 7.15 at each shaft location to compare various rotor mode-shapes.

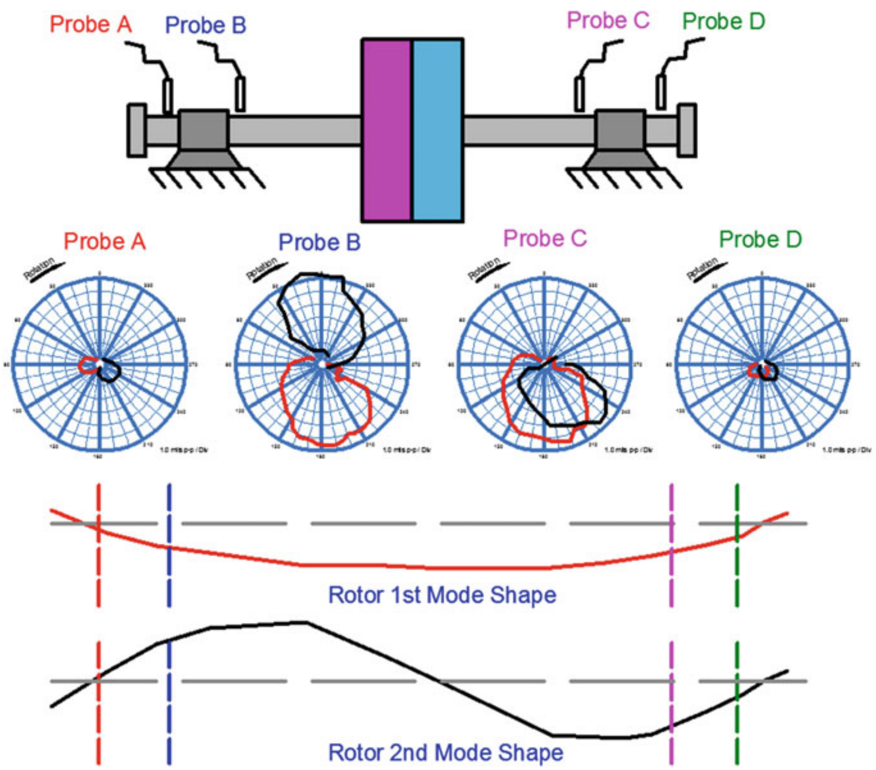

Fig. 7.15 Polar plots at the various probe planes along the rotor shaft

Follow the first and the second rotor mode shape plots in red and black respectively in Fig. 7.15 (from left to right on the rotor axis). At probe position A, which is located just before the bearing 1, the first and the second rotor modes in red and black respectively are about 180° apart. Since rotor amplitudes are relatively smaller at this probe location, the polar orbits that represent 1st and 2nd critical speeds are also smaller.

At the probe location B, where the rotor amplitudes are relatively larger (or well pronounced responses) than those at location A, the polar plots shown for the 1st and 2nd rotor modes are 180-degrees apart to each other. Moving further to the right on the probe planes C and D, the phase angles for the 1st and 2nd rotor modes are very similar. Consequently, mode shapes appear to be very similar as well. However, only the rotor critical speed information corresponding to either of their modes are different and can be clearly identified at the peak response points. This exercise demonstrates the importance of choosing the probe locations in order to identify rotor modes.

By connecting key-phasor points on all the bearings, the rotor system mode-shape can be obtained as shown in Fig. 7.16.

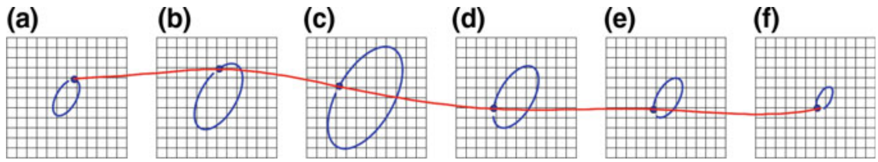

Fig. 7.16 Rotor mode shape connecting key phasor points

It is important to understand that if the bearing clearances are maintained equally in all directions, the rotor is expected to have a circular whirl. However, the unsymmetrical nature of fluid-film dynamic coefficients in combination with the support pedestal stiffness would change the circular shape into ellipse due to stiffness asymmetry provided by the fluid-film in the orthogonal directions. Sometimes, severely preloaded bearings exhibit shaft orbits as “Figure 8” as shown in Fig. 7.17.

Rotor misalignments were discussed in Chap. 6 in detail and are not repeated here. We know that rotor crank causes shaft eccentricity that leads to shaft misalignment. Excessive misalignment triggers increased rotor vibration.

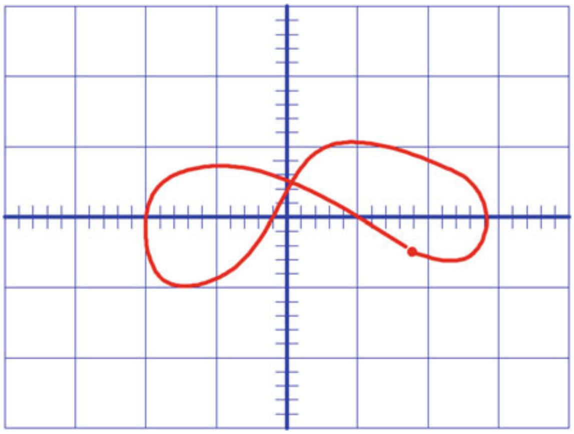

Fig. 7.17 Highly pre-loaded bearing

7.9 Torsional Shaft Vibration Measurement

Thus far, we have discussed diagnostic methods applied to lateral vibrations in rotors. We learnt proximity probes are used to measure shaft motion and accelerometers mounted on structures measure seismic vibration. Shaft twist or angular displacements associated with torsional vibration cannot be measured using a proximity probe or an accelerometer unless a calibrated system suitable to measure angular twist is installed. This section discusses diagnostic methods used in measuring rotor torsional vibration.

7.9.1 Angular Velocity Measuring Methods in Shafts [6–8]

The digital measurement technique for torsional vibration is based on time sampling at equidistant angular intervals around the rotating shaft. This is accomplished by one of two methods: (i) magnetic pickups that measure angular motion of a toothed wheel which is part of the rotor and typically located at a Turning Gear (TG), (ii) tracking alternative reflective and non-reflective (black/white) equi-distant bar patterns recognized by an optical sensor. The sensor electronics generate an angular velocity signal. The frequency of the pulse is directly proportional to the angular velocity of the shaft. Thus, shaft torsional motion is recorded and used to identify torsional frequencies and amplitudes.

Angular velocity measurements provide a fixed number of samples per revolution and are independent of rotational speeds. When time sampling is used, the number of measurement values per revolution varies with rotational speed. Assuming that the angular velocity is constant between adjacent pulses, the instantaneous angular velocity values may be calculated by dividing the actual angular spacing of the physical steps (between gear teeth) by the elapsed time from one positive edge to the next as shown in Fig. 7.18a. Not all rotor trains have TGs. In that case, shaft angular displacements can be tracked by reflective or bar code tapes or by optical probes. Figure 7.18b shows rotor lateral test configuration where proximity probes are used to measure rotor motions.

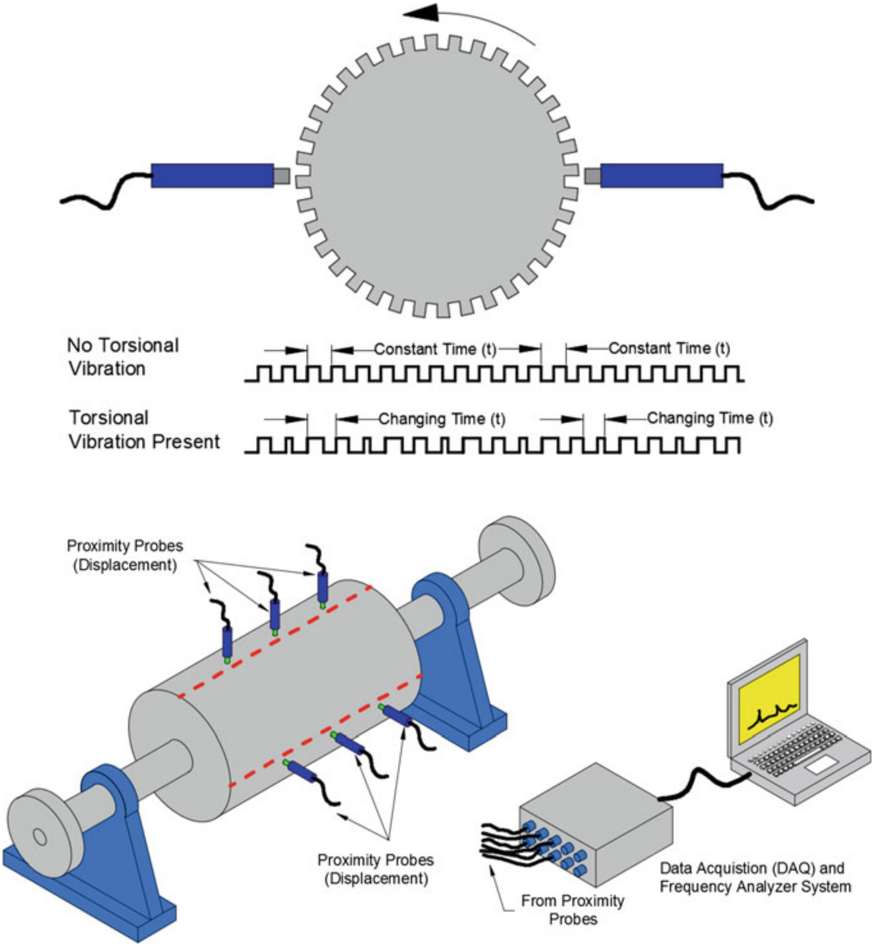

Fig. 7.18 Shaft torsional (**a**) and Lateral (**b**) Vibration measurements

Factory torsional testing can be done on a single rotor which is identified as the critical component in the train. One end of the rotor is connected to a torsional exciter, which applies torsional excitation at varying frequencies. Whenever a rotor torsional natural frequency matches with an excitation frequency, a peak response appears in the frequency spectrum and it is recorded along with the phase angle. The test is run to capture all frequencies of interest. Factory test configuration is illustrated in Fig. 7.19.

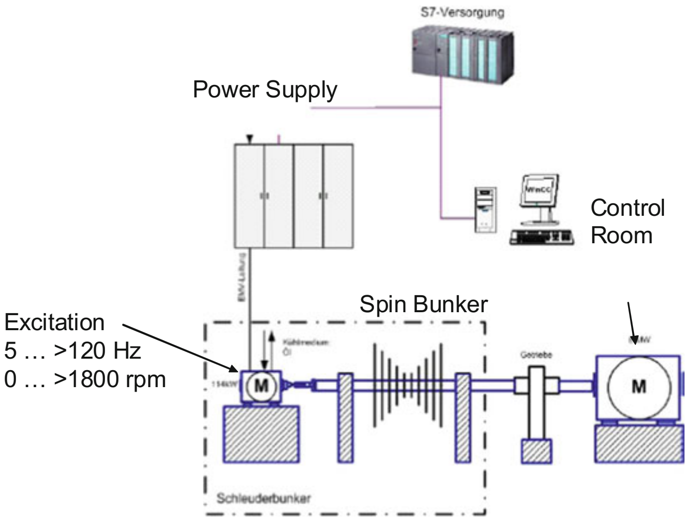

Fig. 7.19 Factory torsion testing of a single span LP rotor

In general, the following data are collected during a factory testing:

- Measure torsional natural frequencies (3–150 Hz range)
- Measure applied torque
- Measure relative response amplitudes and phase angles at various locations of the shaft to obtain mode shapes
- Measure off-resonant response of modes near 50, 100 Hz (50 Hz machines) or near 60, 120 Hz (for 60 Hz machines).
- Calibrate the single rotor model to test results and use it in the train to compute train frequencies.

Although single component frequencies are verified by factory testing, uncertainties of train frequencies still remain. On-site testing could help validating all the calculated frequencies of the train.

Two types of on-site torsional testing can be performed. They are (a) Active Test and (b) Passive Test

(a) An active test utilizes low, controllable generator excitation torques as a source of torsional excitation. Although the excitation force is small, it can be applied precisely at the dominant torsional resonant frequencies of concern, and thus it is sufficient to excite and detect the torsional natural frequencies that may not be typically identified in a passive test.
(b) A passive test is performed by sensing torsional responses during normal operations of the unit, typically during a startup involving an off-line speed ramp to rated speed or during synchronization to the grid, or subsequent on-line operation. Passive testing relies on the strength of the random mechanical and electrical torque perturbations that occur during normal operation. This test captures most of the excitable and/or dominant rotor train frequencies when transducers are positioned at dominant mode shape locations of the shaft.

The determination of probe locations is made using the calculated frequencies and their associated mode shapes of interest. The mode shape in Fig. 7.20 indicates a critical rotor frequency at 116 Hz, which is close to 120 Hz (for a 60 Hz machine). As can be seen, the most effective locations to place probes in order to capture this frequency are (a) at the turning gear and (b) at the shaft area between the LP and the Generator rotors.

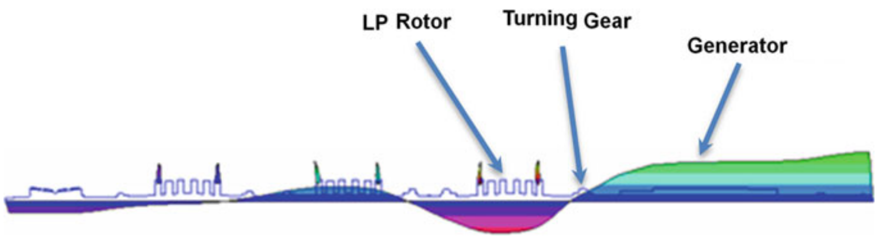

Fig. 7.20 Mode shape and typical probe locations (use the uploaded figure)

The commonly applied transducers to measure torsional responses are:

(a) non-contact magnetic or inductive probes that sense the rotation of tooth or gear wheels such as typically exists from a turning gear,
(b) strain gage(s) applied to the shaft, requiring special telemetry to detect the signal, and
(c) optical methods with fiber optics probes sensing the rotation of black/white stripes applied to the shaft.

Among these, the strain gage is the most sensitive element used to detect even low amplitude torsional responses and modes.

An example of a torsional on-site test configuration of a rotor train is shown in Fig. 7.21.

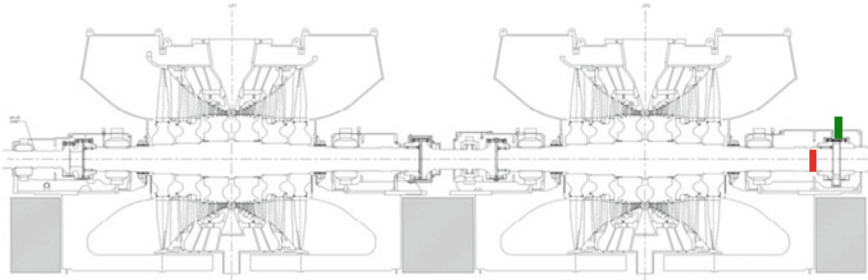

Fig. 7.21 An example of on-site torsional test rotor train configuration

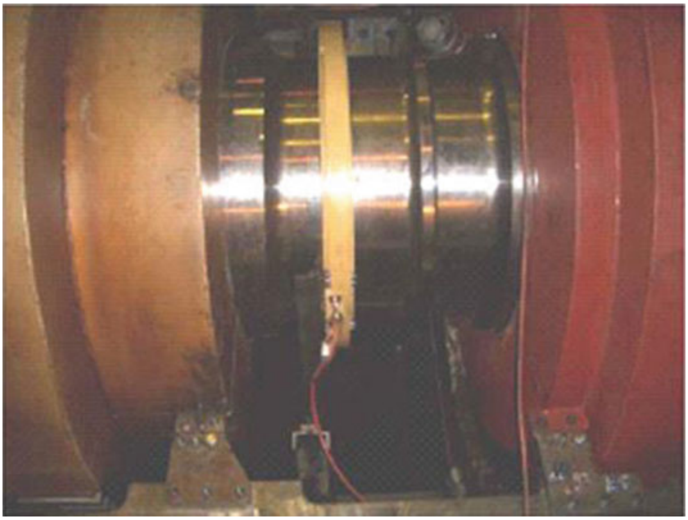

Fig. 7.22 Strain gage attached to an LP shaft

Figure 7.22 shows the strain gage mounted on an LP shaft. Figures 7.23 and 7.24 show the measured frequency spectrums using magnetic probes at the TG and the strain gages on the shaft respectively on an LP shaft. In Figs. 7.23 and 7.24, the horizontal axes represent frequencies in Hz and torsional strain amplitudes in the vertical axes. The main reason to show these plots are to caution the readers to be aware of the fact that additional frequencies can be measured with strain gages, which are very sensitive to varying torsional displacements, although those frequencies may be less responsive in operation and may not harm the unit.

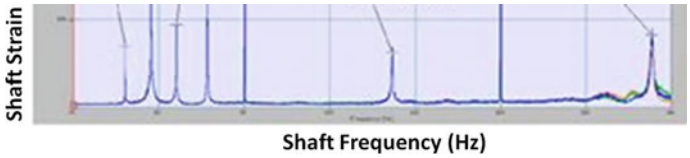

Fig. 7.23 Signals measured at the TG Location

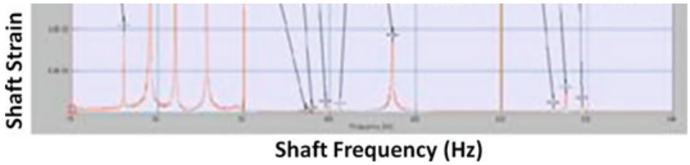

Fig. 7.24 Signals measured by a strain gage

7.10 Operational Influences on Rotor Vibration

Most of the discussions in this book described vibrational phenomenon that occur due to design, manufacturing, and/or assembly of the rotating machinery. This section exclusively describes the operational influences that could lead to vibration in turbo machinery. They will be broken into several categories as listed below. However, some are interrelated.

- Closing of rotor-stator clearances
- Cylinder Distortion/Misalignment
- Ingress of a cooling media such as cool steam and/or water induction
- Lube Oil System Influences.

7.10.1 Closing of Rotor-Stator Clearances

One of the most commonly experienced rotor vibration conditions in a steam or a combustion turbine is when the rotor comes into contact with the seals segments in a stationary casing or a cylinder. In a turbine, seals are typically attached to stationary components (in some designs, rotor also has staked-in seals) and have pre-determined design clearances between them and the rotor surfaces. Whenever a section of the rotor contacts a seal segment, the clearances between them are essentially closed and rub starts to occur. The extent of the rub depends on the degree of contact between the rotor and the stator. During a rub, the contact point at the rotor gets locally heated increasing the rotor sag or runout as a result. Consequently, the bent rotor excites its 1st lateral natural frequency and increases its response or vibration. The extent of the rub can be defined as soft when clearances are just closed. A hard rub is one where rub forces keep building and the rotor vibration elevates to a point where the turbine supervisory system trips the unit. Hard rubs are associated with high vibration and phase angle rotation that could either go with or against rotation depending on whether other elements in the turbine system participated in the rub-process. At times, rubs could reach a non-linear state, where the rotor could stall. Rubs can be classified as pure radial or pure axial or a combination of radial and axial. The following scenarios could initiate rubs in a turbine; however, all of these scenarios boil down to the same symptom, known as "vibration".

(a) Misalignment of casing to rotor,
(b) Casing distortion due to temperature differences between base and cover
(c) Weakened bearing support structures and
(d) Settling of the concrete foundation of the entire turbine structure.

Figure 7.25 shows an example of a steam turbine rotor that experienced a radial rub near the steam gland area where the design clearance was less than the maximum rub indicated. Reported in the illustration are the radial clearances along the rotor length.

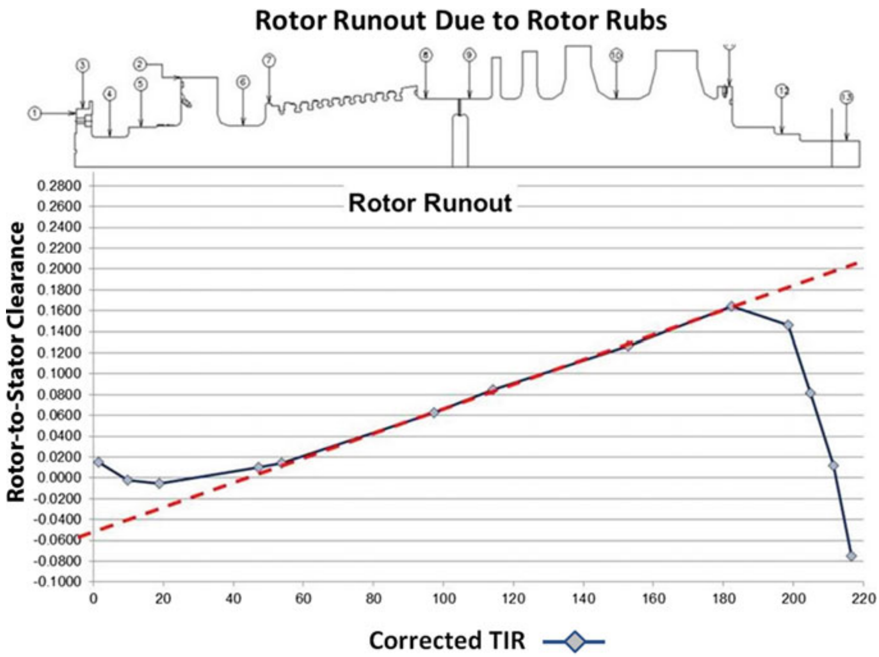

Fig. 7.25 An example of rotor runout leading to rub

7.10.2 Cylinder Distortion/Misalignment

A turbine is designed with adequate radial/axial clearances between the rotating and the stationary parts in the cold state. In the radial direction (which comprises of vertical and horizontal directions), the design clearance settings mainly account for thermal growth and increased mechanical forces (centrifugal forces) of the rotor, blades and other turbine components. Additionally, the design clearances between rotor and stationary parts account for (a) the rotor rise due to oil film dynamics, (b) vacuum loading and (c) settling of bearing supports in operation.

In the axial direction, the design clearances account for axial expansion due to steam pressure and temperature variations under the transient and the steady state operating conditions. The radial and axial gaps between the rotor and the stationary parts reduce from the as-designed cold condition when they reach full operating load (both thermal + mechanical) condition. In the event of a casing incorrectly aligned to a rotor inadvertently, the likelihood of a radial rub increases as a function of the relative misalignment to the original design alignment.

Both radial and axial rubs manifest themselves in the form of vibratory responses of the rotor and the structure. Most likely, the vibratory responses tend to show up during unit start up or coast down as the shaft speed is increased or decreased respectively.

In the case of axial expansion, rotors typically expand faster than the stationary parts during the unit start up. Opposite trend occurs during shutdown. Turbines can experience axial rubs when the casing-to-rotor clearances fall short of the design condition. As stated previously, the thermal expansion of rotors and casings typically occur at different rates which could lead to closing of clearances in the axial direction. The rate of expansion is different for startup and shut down operating conditions.

In both axial and radial rub situations, the rotor is directly impacted; as a result, rotor vibration increase is imminent. Pure radial rub causes lateral; however, pure axial rub causes excessive rotor axial expansion and/or increased rotor travel. Excessive rotor travel individually or combined with radial rub could cause "rotor stall or standstill". Depending on the orientation of the cylinder distortion, rubs could either be predominantly radial or predominantly axial.

For units with sliding pedestals and/or casings, unsteady (or intermittent) axial movement on the sliding surface can lead to both cylinder base axial and radial rubs that could show up in elevated vibration levels. For these types of behaviors, it is highly recommended to monitor the casing vibration and the differential expansion as well.

There are several potential scenarios where the casing can distort. The causes could include improper drainage, poor insulation, and non-uniform heating or cooling of the casings. Any one of the potential issues can lead to casing distortion.

7.10.3 Ingress of a Cooling Media Such as Cool Steam and/or Water Induction

Usually, water ingress (or sometimes known as water induction) occurs in a steam turbine whenever the cover-to-base cylinder temperature differentials become significant. An example case of water ingress that occurred in an IP turbine is illustrated in Fig. 7.26. The temperature differential was almost 500 F (260 C) which is significant amount than normally allowed. Such huge delta temperature difference in a turbine is responsible for transformation of gaseous working fluid into liquid. In this case, the hot steam transforms into water and damages the rotating blades.

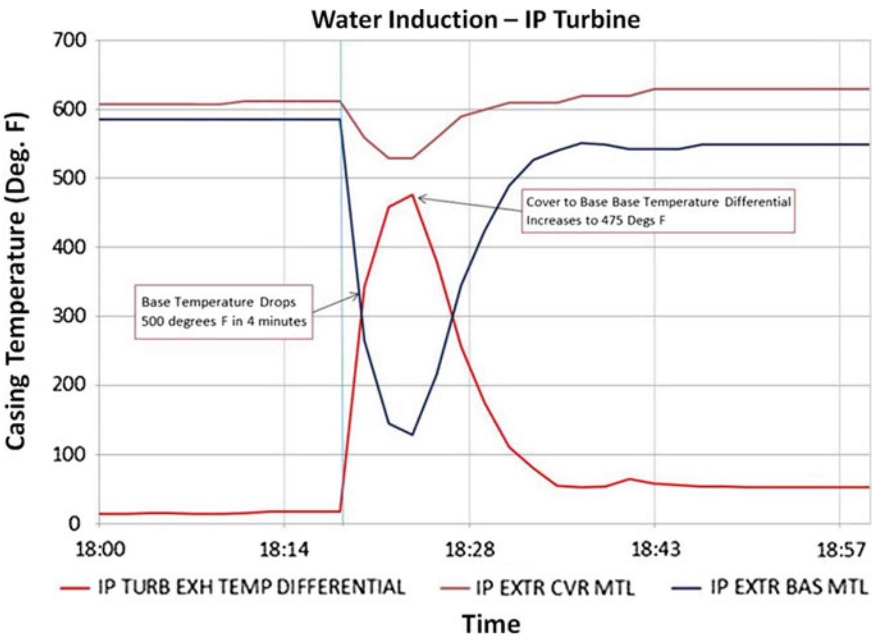

Fig. 7.26 Cover to base steam temperatures of an IP turbine

In another LP turbine incident, last row LP blades were damaged which was attributed to water impingement or induction. Instrumentation installed on the LP Steam turbine confirmed that the outer cylinder was filling with water up to the horizontal joint. When the direction and velocity of steam flow during bypass operation were included in a computational flow analysis, it was concluded that the water entrained into the LP steam turbine was causing damage to last row LP blades. Computational Fluid Dynamic calculations were applied to understand the flow mechanism and to come up with a permanent solution avoiding water induction in those designs.

7.10.4 Lube Oil Influences on Increased Rotor Vibration

Lube oil inlet temperatures to bearings can impact rotor dynamic behavior. Since oil viscosity is directly related to film stiffness and damping, it could affect the dynamic characteristics of a rotor, specially, stability conditions of the rotor. It was found that increasing or decreasing the oil film temperature had a noticeable shift in the rotor dynamic behavior from a steady operating condition to un-steady state oil whip condition on a cylindrical bearing. It is recommended to maintain lube oil temperatures within acceptable levels. Typical lube oils applied in turbine industry are VG 32 or VG 46. Recommended nominal oil inlet temperature is about 120 F (49 C) Roughly ±10% variation from the nominal value are allowed.

Table 7.2 Provides general symptoms, probable causes and potential mitigation measures

Sl. no	Observed symptoms	Probable cause	Potential mitigation	Remarks
1	1x Vibration increase followed by phase angle shift against rotation	Mass unbalances due to loss of blade-foil segments or solid particle erosion of blades and rotor surfaces (essentially causing mass unbalance)	Balance the rotor; if balancing does not help, replace the damaged parts. Bore-scope exams may help identifying damage areas	Full blade loss generates very high vibration followed by damages to bearings and turbine parts. Rotor is not balanceable in this condition. Replace the blade or repair damaged parts
2	Gradual increase of total vibration with dominant 1x	Blade tip erosion	Check steam temperatures for wet steam conditions and correct them as necessary	Balancing won't help
3	Dominant 1x vibration increase after a torsional event such as lightning strike, grid fault or short-circuit event	Instantaneous slip at the coupling resulting in severe damage to coupling bolts or galling of bolts or loose spigots or loss of shrink-fit at the shrunk-on disks and shrunk-on couplings	Correct coupling clearances, preload bolts, maintain bolt stretch and restore spigots to design. Maintain shrink fits to design	

(continued)

Table 7.2 (continued)

Sl. no	Observed symptoms	Probable cause	Potential mitigation	Remarks
4	Overall vibration increase: predominantly sub-synchronous with decreasing bearing metal temperature	Unloaded bearing in general: When two bearings are located adjacent to each other and on the same pedestal, one bearing unloads when the other bearing load up. Unloaded bearing exhibits increasing vibration and decreasing bearing metal temp. Opposite trend is noticed for a loaded bearing	Balance moves wouldn't be effective. Milder form of oil whirl (with sub-synch. component between 1 to 3 mils (0.025–0.075 mm)). Sub-sync. vibration above 3 mils with a sharp peak indicates potentially increasing trend of bearing unloading. Vibration above 6 mils points to oil whip and may need bearing replacement	Load up bearing when sub-sync. vibration below 3 mils Load up + tighten bearing clearances for sub-sync. vibration above 3 mils Sub-sync. increasing unabated indicating oil whip, replace bearing
5	Sub-synchronous vibration amplitude is dominant and larger than 1x amplitude	Oil Whirl: Oil film cross-coupled dynamic stiffnesses become dominant and cause increasing sub-synchronous vibration (typically occur in cylindrical bearings)	Tightening bearing clearances or load up bearings. May help in case of milder form of oil whirl situation	If bearing experiences oil whip, none of the mitigations resolve the issues. The bearing is going through the extreme case of oil whirl
6	In partial-arc steam turbines where steam is admitted at selected sector of the nozzle chamber, the resultant load pushes the rotor to one side and imparts uneven load on bearings	Steam whirl occurs in partial-arc designs exhibiting high sub-synchronous or sometimes 1x. Partial-arc steam admission causes load unbalance and creates uneven rotor-to-stator clearances by moving the bladed-rotor more towards one side than the other. Resultant tangential steam loads act in a similar fashion as the dominant	(a) Milder form of steam whirl (vibration increase below 5 mils) can be controlled by pre-loading the bearings or tightening bearing clearances or re-sequencing the valve openings. (b) To control the medium steam whirl condition (vibration above 5 mils), test different valve sequence schemes and choose the best operating sequence for acceptable	

(continued)

Table 7.2 (continued)

Sl. no	Observed symptoms	Probable cause	Potential mitigation	Remarks
		cross-coupled forces act on a fluid-film bearing, resulting in unequal loads on the bearing supports	vibration. (c) in case of classical steam whirl, apply anti-swirl vanes and/or flow dams to control steam whirl, mainly at the control stage, nozzle chamber and the first few stages of rotating blade rows	
7	Un-abated 1X vibration to begin with and changing to dominant 2X vibration in advanced stages followed by reduction of 1st rotor bending natural frequency	Shaft Cracks: Increase of 1X vibration may mislead to mass unbalance; but balancing may help temporarily in the initial stages. However, vibration continues to increase unabated even after rotor balancing	Remove the cracked rotor and excavate the cracked area, inspect and weld repair before re-installing the rotor or replace the entire rotor or part of a rotor depending on the crack location	Approximately 30–40% loss of shaft diameter may lead to sudden breakage of rotor. Therefore, when vibration keep increasing beyond trip, stop the machine and inspect for cracks
8	Rotor relative vibration increases at the 1st natural frequency and exceeds ISO 20816-2 C/D limits. And/or seismic vibration of support structure exceeds C/D levels	Rotor-stator rubs could be the probable cause due to tighter clearances in assembly. *or* improper rotor-to-stator alignment *or* excessive shaft run out or permanent thermal bow in the rotor *or* support structure subsidence *or* loss of oil lift on heavier rotor designs *or* unit left at standstill while still hot and did not have adequate turning gear time	Correct rotor-stator alignment, balance rotor for mild to medium shaft runouts. Remove permanent and excessive thermal bow or shaft run out; need machining of the rotor in the lathe. To address subsidence, strengthen the pedestal supports by welding braces as needed. Oil lift pressure should be checked and maintained for TG oil lift related issues.	

(continued)

Table 7.2 (continued)

Sl. no	Observed symptoms	Probable cause	Potential mitigation	Remarks
			To address and correct rotor standstill condition, run the unit for several hours on turning gear speed. TG duration is unit specific	
9	Excessive seismic vibration of supports	Possible Support structure subsidence *or* weakened structural members *or* weakened sub-structures that are connected to the main structure *or* sinking of concrete foundation *or* loosened bolts at bearing strong-backs, pedestals, or other turbine support areas	Perform structural testing by electrical shaker to understand the structural conditions. If tests indicate the pedestal stiffnesses have dropped from original design, stiffen the supports. Tighten loose bolts in joints. If concrete structure is weak, let architect engineer review and take appropriate steps to fix the condition of the concrete foundation. Check and correct bolt torques at all joints in the support system	
10	Vibration due to sub and super synchronous and their harmonic component excitations	Loosened coupling bolts *or* unequal frame foot loading *or* asymmetric rotor stiffness leads to excessive 2x vibration (due to insufficient compensation of slots in the generator rotor body) This condition is mainly related to Generators	If harmonic frequencies are equal to the number of coupling bolts in a joint, then tighten bolts or replace them if galled or broken. Fix the frame foot loading Fill the machined slots in the generator rotor for proper compensation	

(continued)

Table 7.2 (continued)

Sl. no	Observed symptoms	Probable cause	Potential mitigation	Remarks
11	Chatter (screeching, singing or growling noise) resulting from repeated sticking and slipping of journal in oil film bearing at low operating speeds	Stick-Slip: (a) heavily loaded bearings without oil-lift >400 psi (2.8 MPa) experience this phenomenon or (b) Lightly loaded bearings (350 psi or 2.4 MPa) due to low damping or (c) Insufficient break-away torque also could lead to stick-slip	(a) Journal running at the boundary film (with virtually no damping) could lead to film breakage results in sticking and slipping of journal. This could lead to chatter of longer last row LP blades. Resolution is to install oil lifts	
12	Impulse loading from the steel mill or an arc furnace or other heavy equipment operating nearby to a power plant. Both lateral and torsional modes are excited	Impact loading from a steel mill or an arc furnace in the vicinity of a power plant could impart sharp impulse loads on the power plant equipment that could reduce fatigue life of the shafts, blades or other parts	Analyze the shafts for expended fatigue life due to impact loads from the steel mill or arc furnace at the impact frequencies. Evaluate shaft stresses and the remaining life of rotors and blades. Detune torsional frequencies and/or strengthen the shafts against high cycle fatigue damages	
13	Excessive axial travel or rotor stall	Excessive differential expansion due to internal load changes or loss of thrust balance due to heaters out of service. Running the unit for extended periods at full speed-no Load or below minimum recommended loads could cause rotor	Fix the heaters that are out of service or reevaluate the thrust loading and reset the thrust bearing with adequate clearances. Increase cold clearances to accommodate axial expansions. Return the unit to turning gear operation to allow steady shaft	

(continued)

Table 7.2 (continued)

Sl. no	Observed symptoms	Probable cause	Potential mitigation	Remarks
		long (heating of the rotor longer than the stationary component)	temperatures that will reduce shaft bows or runouts	
14	Large cylinder distortions	Unequal cylinder base-to cover differential temperatures	Measure cylinder corners to check for square-ness. Correct the cylinder structure if distorted. Also check the insulation effectiveness or check for total loss or partial damages to insulation. Fix them as needed	
15	Increased thrust bearing temperature	(a) Oil flow may be low (b) Play in the thrust bearing leveling plates (c) thrust unbalance (d) thrust anchor points damaged or weakened (e) centering beam bolts loose	(a) Increase oil flow by turning the control knob by one and a half turns (b) Check levelling plates for wear and replace them as needed (c) Adjust the thrust bearing alignment for the revised thrust balance condition (d) Repair or replace parts as needed (e) tighten all loose bolts	
16	Discoloration of bearing babbitted area	Electrical discharge	Check and replace grounding brush	
17	Bearing fatigue damage at the upper half of the bearing	Probable cavitation due to oil pressure variations between the upper and lower halves of the bearing. Probable solid particle entry and blockage in oil passage ways	Correct flow discontinuities in the bearing to reduce oil pressure variations. Use fine oil filters (10 μ) in the oil lines to block the entry of oversize particles. Frequent oil flush is recommended	

(continued)

Table 7.2 (continued)

Sl. no	Observed symptoms	Probable cause	Potential mitigation	Remarks
18	Babbitt fatigue damage at the lower half	High temperature hot spots in the babbitted areas that could cause fatigue damage. Poor bonding during the babbitting process could as well lead to material fatigue	Remove old babbitt thoroughly and re-babbitt the bearings	
19	Bearing temperature increase due to calked spherical seat	When spherical bearing surfaces do not conform to spherical seats of the fixed yoke or saddle, bearings can slip or slide and could calk to one position which may lead to unintended journal to bearing contact or unloading of journal to one side	Blue check the spherical contact surfaces to verify the fit at the spherical contacts Prepare the spherical surfaces to have at least 80% of fit for better seating of the bearing	
20	Unloaded bearings in a certain category of LP turbines installed with water cooled condensers (typically full speed machines)	Due to changes in condenser vacuum pressure, the bearing structures are pulled down in operation, thus causing bearing unloading	For those category of LP bearings that are unloaded in operation, resolution is to load them up when the unit is in stationary condition (at 0 RPM) to the amount that it would unload during operation	

7.11 Closure

Commonly applied diagnostic methods in turbo-machinery were discussed in detail along with the diagnostic tools applied in lateral and torsional frequency response spectrum analyses. Test verification methods in both lateral and torsion were described. They form a sound basis for understanding the diagnosis and solutions applied in rotating machinery. Most related references are listed that would help obtaining additional information on machine diagnostics.

References

1. ISO 20816, Mechanical vibration- measurement and evaluation of machine vibration- part 2: land based gas turbines, steam turbines and generators in excess of 40 MW, with fluid-film bearings and rated speeds of 1500 r/min, 1800 r/min, 3000 r/min and 3600 r/min
2. Bently DE, Hatch CT (2001) Fundamentals of rotating machinery diagnostics, Chaps 6 and 7, ISBN 0-9714081-0-6
3. Eiselmann Sr RC, Eiselmann Jr RC (1998) Machinery malfunction diagnostics and correction, pp 410–415, 418, 578, 752, Chaps 9, 11, 14, ISBN 0-13-240946-1
4. Thomas GR (2006) No vibration–no problem: or is there? In: The 24th Canadian machinery vibration association machinery vibration seminar and annual general meeting, 25–27 Oct 2006, Montreal, Quebec, Canada
5. Smith JD (1999) Gear noise and vibration, ISBN: 0-8247-6005-0. Marcel Dekker, New York
6. Adamson S (2000) Measurement and analysis of rotational vibration and other test data from rotating machinery. SAE Paper No 2000-01-1333
7. Nestorides EJ (1958) A handbook on torsional vibration. Cambridge University Press, Cambridge
8. Heisler H (1995) Advanced engine technology, ISBN: 1 56091 734 2. Arnold Publishers, London

Chapter 8
Case Studies

8.1 Introduction

Various case histories of turbo-machinery problems are discussed in this chapter.

8.2 General

Utilizing the knowledge gained on the diagnostic methods, it is high time to discuss some commonly observed issues in turbo-machinery. This chapter discusses eleven test cases of practical importance in turbo-machinery followed by diagnosis and recommended measures.

Incidences such as oil whip, steam whirl, unloaded bearings due to rotor misalignments, torsional vibration, distorted casings, rotor cracks etc. are discussed. In general, variations in bearing metal temperature and shaft vibration are inter-related in such a manner that symptoms indicated by one could lead to clues in resolving the other. Axial vibration issues were rarely reported. However, thrust bearing temperature issues are not uncommon. Eleven case studies, that are typical in turbo-machines, are discussed in this chapter. The test cases cover both torsional and lateral vibration occurrences. They include fossil and nuclear turbo-machinery issues as well.

R. Subbiah and J. E. Littleton, *Rotor and Structural Dynamics of Turbomachinery*,
Applied Condition Monitoring 11, https://doi.org/10.1007/978-3-319-73296-1_8

8.3 Description of a Problem for Test Case-1

Excessive unbalance loads generated by steam pipe hangers on a HP-IP turbine caused bearing shell distortion and closed nominal clearances between the journal and the shell. This caused high bearing metal temperature. See Fig. 8.1 for unit configuration.

8.3.1 Data Review

Excessive steam loads distorted the bearing 1 casing and closed the clearances between the journal and the shell. The bearing metal temperature increased as a result. This condition is also known as “Canting or tilting” of the bearing structure in the lateral direction that led to shell distortion.

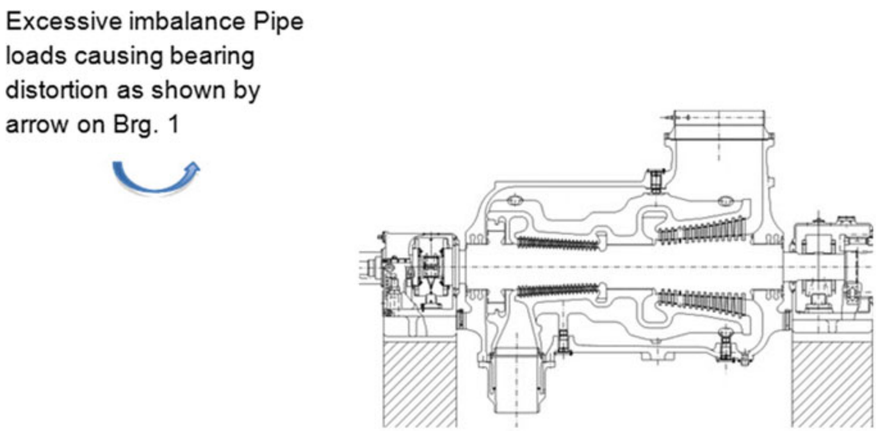

Fig. 8.1 Unbalance pipe loads create a moment on bearing

- 13.4” (336 mm) diameter elliptical or lemon bearing 1 experienced high temperature and kept rising.
- Vertical pedestal motions due to unbalance pipe hanger loads led the bearing shell distortion in the lateral direction.
- Measured bearing metal temperatures and the corresponding journal orientation were utilized to simulate equivalent loading on the bearing configuration.

In general, bearing failures are attributed to rotor misalignment, oil whip, steam whirl and/or excessive mass unbalance loads due to loss of blade segments in part or in full. In all of these cases, the rotor responds to applied forces and passes them on to the bearings.

However, in this particular case, the steam pipe hanger unbalance loads triggered excessive distortion of the bearing structure. This bearing was instrumented with four thermo-couples; two at the top and the other two at the bottom. Left and right thermo-couples at the top were mounted at 45° on either side of the 12 o'clock position. Bottom thermocouples were located at about 20° on either side of the 6 o'clock position.

The measured bearing metal temperatures are shown in Fig. 8.2 and reported in Table 8.1. Highest temperature was recorded at 221 F (105 C) which was at the top right. To understand the shell distortion, the estimated steam forces and the measured temperature variations were simulated using a Finite Element Model (FEM) and discussed in the following section.

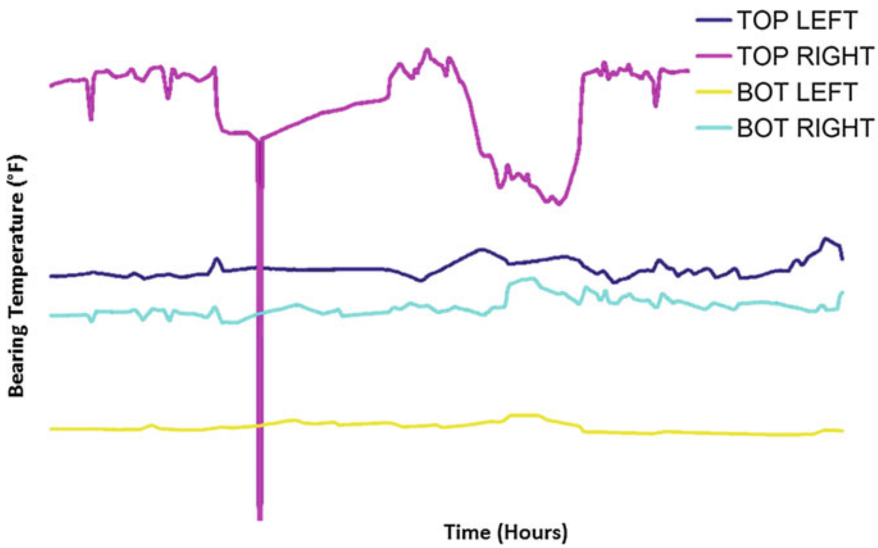

Fig. 8.2 Measured bearing metal temperatures

Table 8.1 Measured temperatures

Average temperatures
Top left: 176 F (80 °C)
Top right: 221 F (105 °C)
Bot. left: 131 F (55 °C)
Bot. right: 158 F (70 °C)

8.3.2 Simulation

An FEM of the interior surface of the bearing (which is an ellipse) was simulated using the measured bearing metal temperatures. Since the right half of the bearing was of interest, the details of the right side only are shown in Fig. 8.3. The ratio of measured temperatures between the top right and the top left is plotted. The maximum temperature ratios evaluated closely matched with the measured values between the range of 1.2 and 1.3. The temperature profile thus simulated was converted to equivalent mechanical loads in a thermo-elastic analysis. The mechanical loads applied were found to match with the estimated pipe hanger unbalance loads.

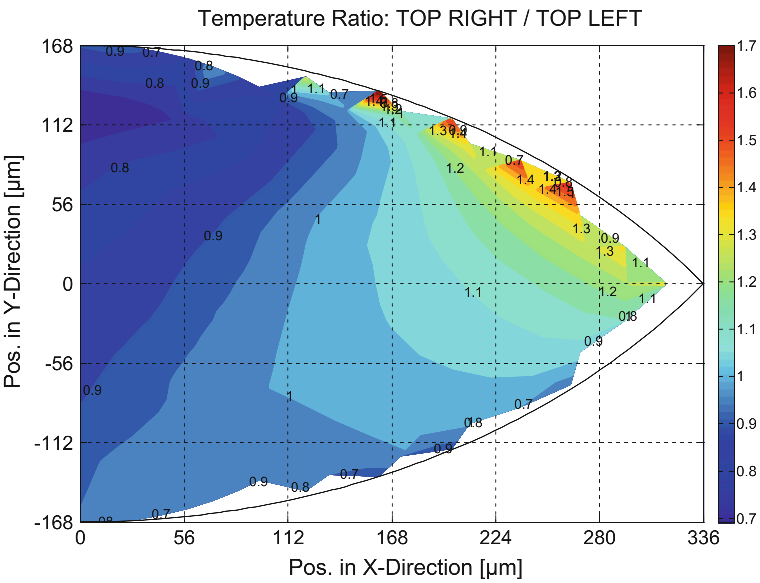

Fig. 8.3 Thermal analysis of bearing structure

It was found that the thermal loads, combined with the unbalance pipe hanger loads caused thermo-elastic distortions of the bearing shell. Estimated pipe hanger loads were: Lateral load at 27,000 N and Vertical loads at 45,000 N.

Influence of thermo-elastic distortion plus the measured canting of the bearing shell was simulated in a 3-D Finite Element model of the bearing shell. The findings matched with the observed bearing damage as shown on the right of the Fig. 8.4.

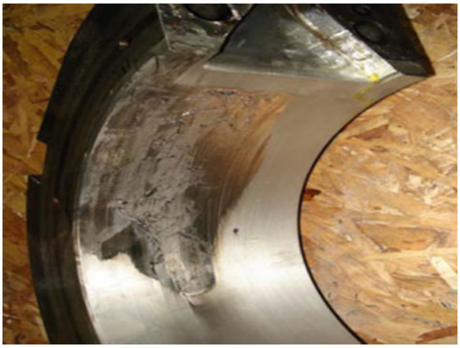

Fig. 8.4 FE simulation of observed high temperature on the top right

Based on good correlation of the analytical results to actual findings, the following recommendations were made:

> Primary Solution: Reduce the pipe hanger steam unbalance loads. This will help reducing the bearing shell distortions in the lateral and in the vertical directions.
>
> Additional recommendation was made to replace the elliptical bearing with a self-aligning pad bearing, preferably a 5-pad with pre-loading.

8.3.3 Solution

When the pipe hanger loads were minimized and the bearing replaced by a five-pad tilt-pad, bearing metal temperatures dropped below 190-degree F (88 C), approximately 30-degree reduction from before. The unit was acceptable for continuous operation.

8.4 Description of a Problem for Test Case-2

An unloaded generator bearing #5 shown in Fig. 8.5 was the cause of excessive sub-synchronous vibration. All rotors in this configuration are individually supported by two bearings. Only HP-IP bearings 1 and 2 are tilt-pad type. The rest of

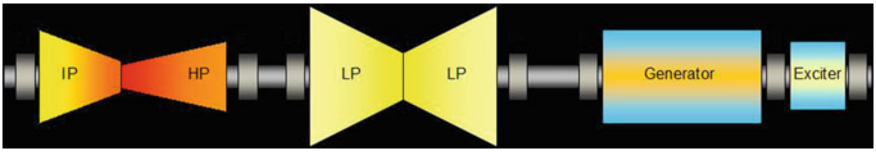

Fig. 8.5 Steam turbine-generator configuration

the bearings are partial-arc types. The geometrical details of bearing 5 are described in Table 8.2 below.

Table 8.2 Geometrical description of bearing 5

Bearing type	Diameter
Partial arc-cylindrical	17 in. (432 mm)

8.4.1 Data Review

High vibration was reported on bearing 5, which is the turbine end of the Generator bearing. Bearing 5 was found heavily unloaded in the *lateral direction* (Horizontal plane of the bearing) as shown by the shaft centerline plot in Fig. 8.6. The journal moved significantly away from the bearing center indicating unloaded condition in the lateral direction.

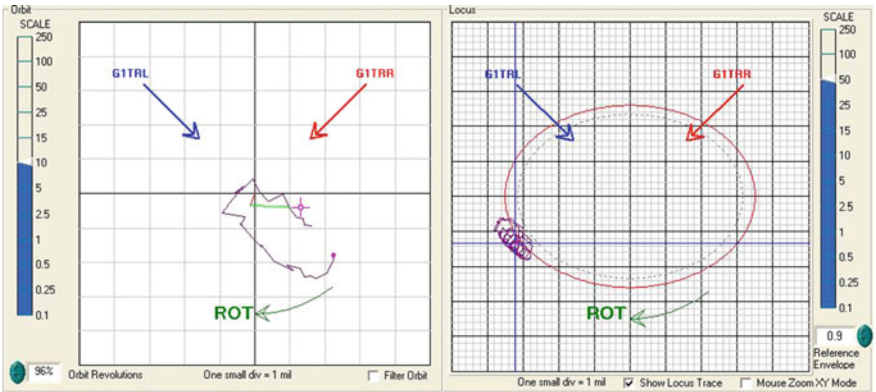

Fig. 8.6 Shaft centerline plot of bearing 5

Vibration spectrum in Fig. 8.7 confirms the unloaded bearing condition with a high amplitude of about 15 mils (380 μ) at the sub-synchronous frequency around 15 Hz. The sub-synchronous vibration by itself exceeded the vibration trip limit of 10 mils set for the machine. In general, unloaded journal lowers the oil film damping significantly and results in high vibration.

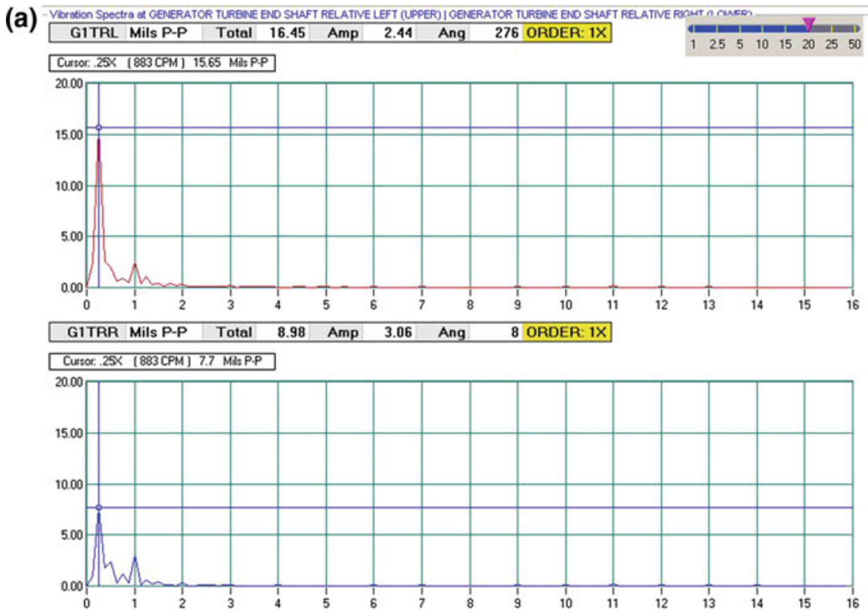

Fig. 8.7 Vibration spectrum plot

The measured bearing metal temperature on bearing #5 was at around 140°F (60 C) that is considered very low. This is another indicator of unloaded bearing (Fig. 8.8).

Fig. 8.8 Bearing structure shift in the horizontal direction

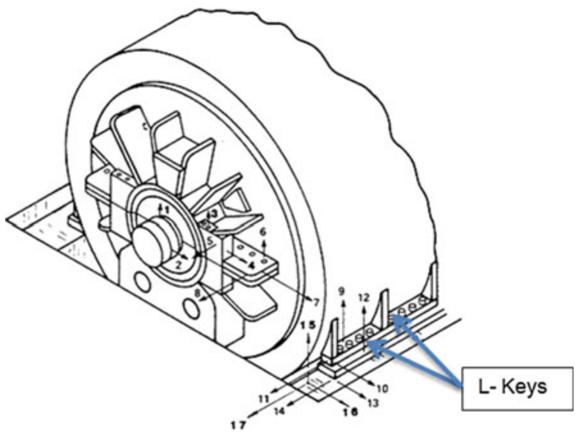

Since the bearing unloading occurred in the lateral direction, the traditional solution of loading the bearing in the vertical plane won't resolve the issue. In this case, the journal needs to be moved towards the center of the bearing. It was thought that by physically moving the bearing structure in the lateral direction, could bring the journal closer to the bearing center. This is accomplished by loosening the bolts on the bearing support L-keys and then moving the entire bearing structure from Right to Left.

The corrective measures discussed above are an example of adjusting the bearing clearances to accommodate the journal towards the center of the bearing. This action brought the bearing to an adequate loading condition. The sub-synchronous vibration came down to below 0.0002" (5 μ) after the bearing was moved. See the sub-synchronous vibration component dropped in the spectrum plots shown in Fig. 8.9 after the bearing structure move.

8.4.2 Solution

Unloaded bearing in the lateral direction was corrected by moving the bearing structure to position the journal to the center. This action brought an unloaded bearing to an adequately loaded condition.

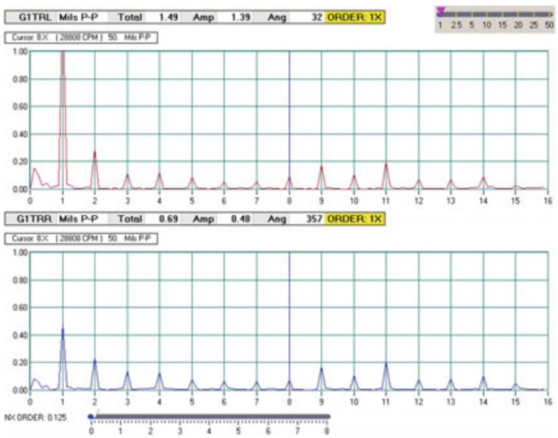

Fig. 8.9 Vibration spectrum plot after the bearing structure was adjusted laterally

8.5 Description of a Problem for Test Case-3

This is the case of a HP turbine that suffered steam whirl. The affected HP turbine was a symmetric and opposed flow machine. Because of the symmetry, only one half of the cross-section is shown in Fig. 8.10. The delta P across the control stage (CS) seal segments was about 12 bars. Primarily, the large delta P across the CS inlet seal area was found responsible for producing excessive circumferential steam velocity that led to steam whirl.

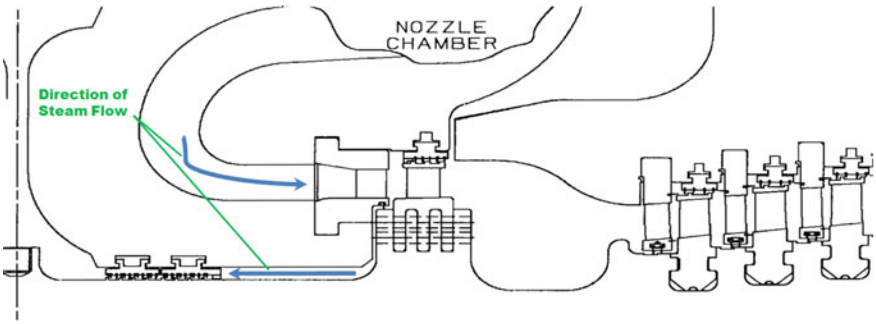

Fig. 8.10 Opposed flow HP rotor

8.5.1 Data Review

The HP rotor was supported on 4-pad tilt-pad bearings (Fig. 8.11) at the two ends.

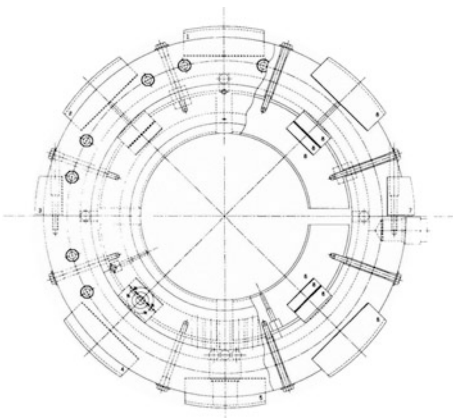

Fig. 8.11 4-pad tilting pad bearing

This HP turbine was built to operate at part steam load conditions when boiler was unable to supply the 100% steam due to fluctuating boiler loads. Typically, some selected valve segments are closed to accommodate the partial steam supply, known as, "partial-arc loading". The partial loading caused unbalance steam conditions on one side of the turbine vs the other side. This resulted in larger steam loads on one bearing and lighter load on the other bearing. This is the beginning of steam induced vibration. Continuous operation with this condition increases sub-synchronous vibration component related to steam whirl. (For details, readers are directed to steam whirl discussions in Chap. 4) Consequently, the rotor exhibited very high sub-synchronous vibration.

The vibration in bearing 2 reached the highest at around 0.023" (580 μ) in the vertical direction; most of it was sub-synchronous whereas the bearing 1 vibrations are comparatively lower. The bearing vibration trends for bearings 1, 2 and 3 (Y-axis) at various times (X-axis) are shown in Fig. 8.12.

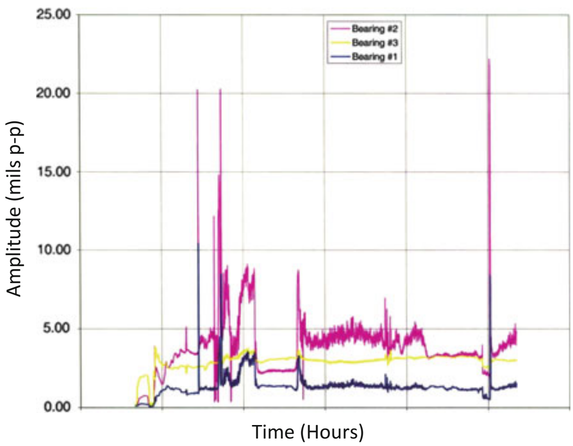

Fig. 8.12 Shaft relative vibration trends for bearings 1, 2 and 3

The bearing metal temperature data in bearings 1 through 3 was obtained as shown in Fig. 8.13. Lowest temperature (about 155 F = 68 C) was recorded on the bearing 2, which additionally supports the bearing un-loaded condition.

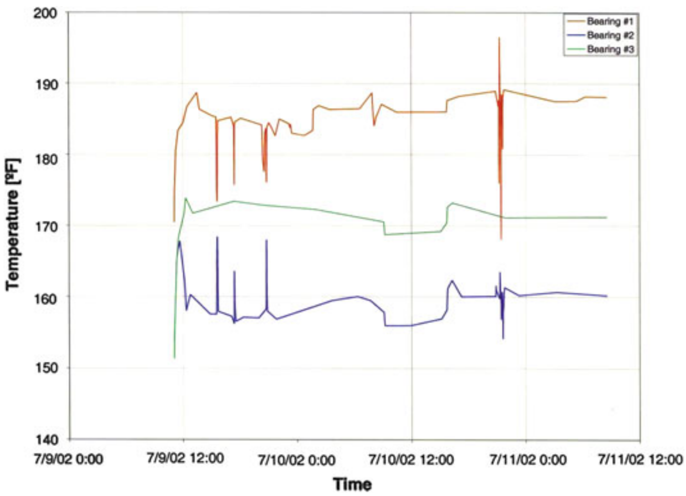

Fig. 8.13 Bearing metal temperatures at bearings 1, 2 and 3

Shaft centerline plots were collected for bearing 2 as shown in Fig. 8.14. It clearly points to the unloaded bearing condition and matched with the lower bearing metal temperature and the excessive vibration measured on this unit.

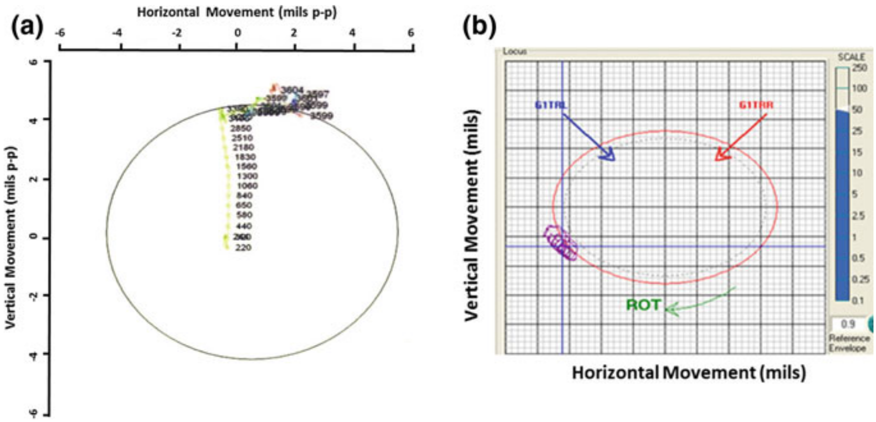

Fig. 8.14 Shaft centerline plot of bearing 2

Actions such as (a) raising bearing 2 to increase loading (b) valve re-sequencing to balance the steam loads and (c) tightening bearing clearances to improve damping did not help resolving this issue.

8.5.2 *Analyses*

Since the sub-synchronous vibration was unprecedentedly high, traditional solutions did not resolve this issue. Hence, this case was considered as an example of "Classical Steam Whirl" where conventional solutions did not work. Rotor dynamic analysis, when seal dynamical coefficients were not applied, did not predict rotor instability. Seal dynamical coefficients were then applied at the control stage (at Sect. 8.2) and at the nozzle chamber (NZC) (at Sect. 8.3) seal areas as shown in the rotor dynamic model in Fig. 8.15. The calculated log-dec. value of −0.0475 indicated a negative damping confirming steam-induced instability as shown in the rotor whirl plots. Additional analyses were performed simulating with anti-swirl vanes across the rotating seals at CS and NZC. Resulting analyses showed positive damping and resolved the steam-whirl condition of the machine.

Based on the analyses, anti-swirl vanes (as shown in Figs. 8.16a, b and c) were installed (a) at the inlet to the rotating shroud seals on the CS and at (b) at the inlet to NZC seal areas. The function of the anti-swirl vanes is to reduce the circumferential steam velocity that is responsible for excessive steam unbalance forces. The vibration was reduced to acceptable levels and the unit started operating without steam whirl issues after the installation of anti-swirl features.

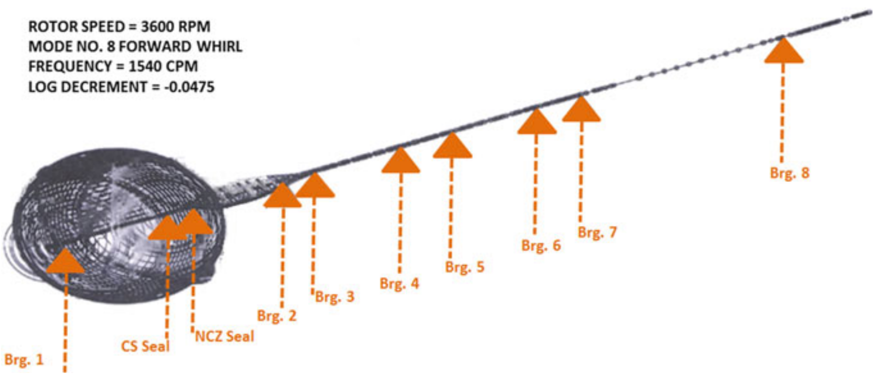

Fig. 8.15 Rotor dynamic model simulating HP rotor steam whirl

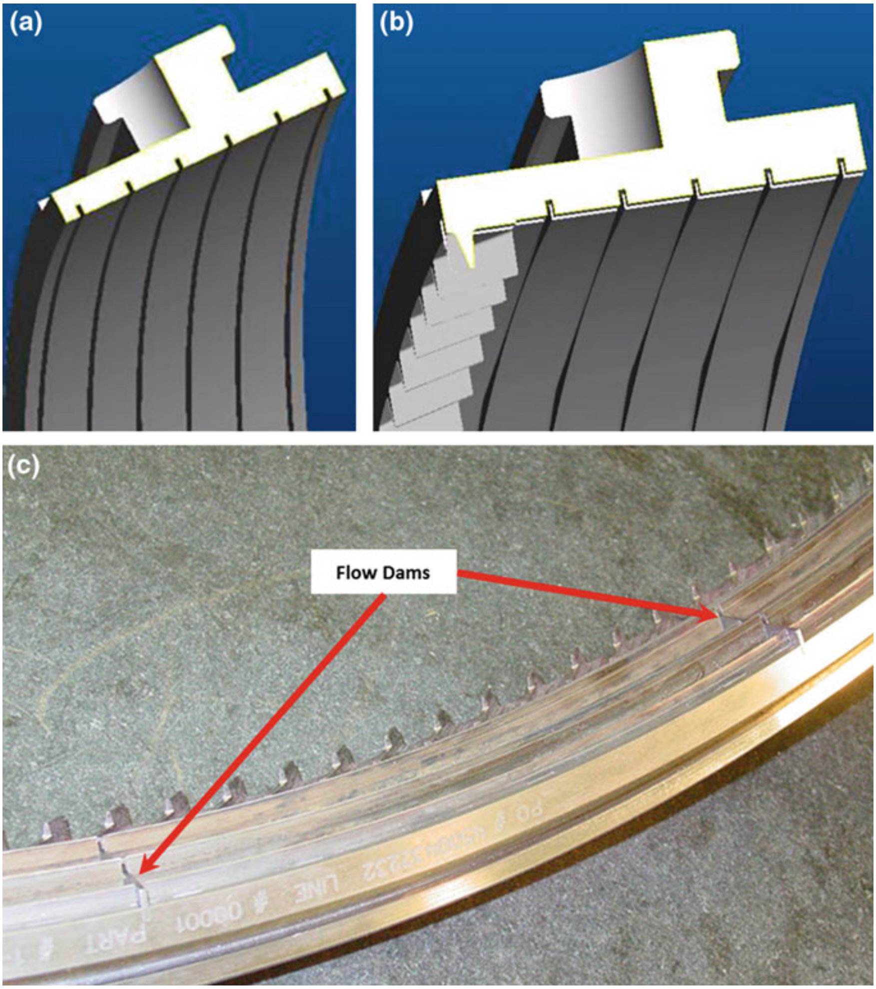

Fig. 8.16 **a** Original configuration. **b** Anti-swirl vanes installed. **c** Actual hardware with anti-swirl vanes on control stage shroud seals

8.5.3 Solution

When anti-swirl vanes were installed at the control stage, a high percentage of steam unbalance forces were reduced due to its location at a higher diameter. Additionally, flow dams were installed in front of the nozzle chamber seal rings as shown in Fig. 8.17. These anti-swirl features helped reducing the steam unbalance forces to acceptable levels. High sub-synchronous vibration originally found at about 0.023" (580 μ) came down to less than 0.001" (25 μ), a 23-fold reduction of steam unbalance forces.

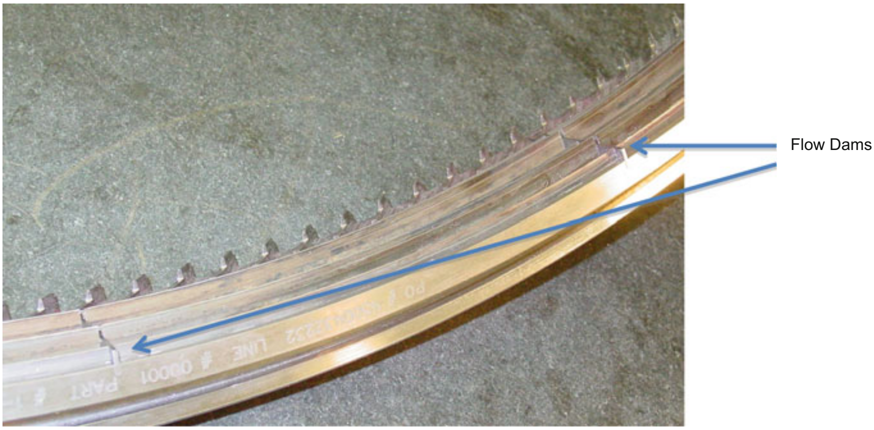

Fig. 8.17 Flow dams

8.6 Description of a Problem for Test Case-4

High Vibration was reported due to uneven cylinder Base-to-Cover Temperature at normal operating speed and load in an HP-IP rotor shown in Fig. 8.18.

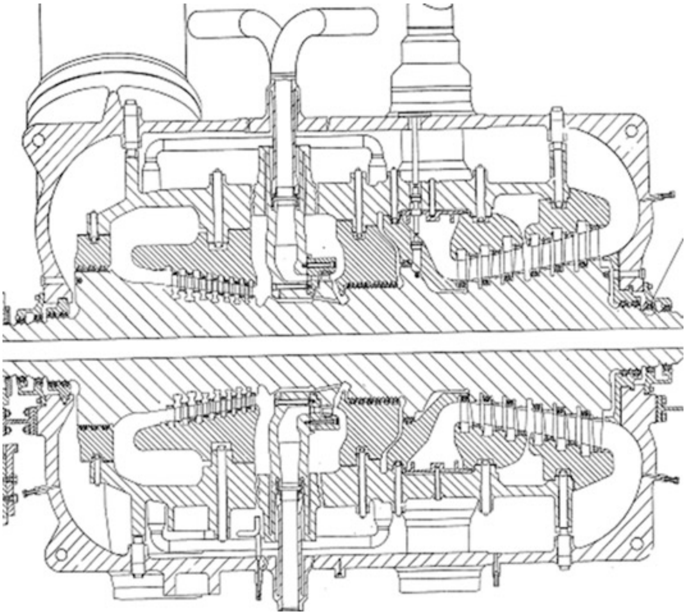

Fig. 8.18 HP-IP turbine (courtesy of Siemens)

8.6.1 Analyses: The Following Data Were Reviewed

- Rotor NDE (Non-Destructive testing such as magnetic particle, MT or ultrasonic, UT or dye-penetrant PT)
- Run out
- Valve Parts Inspection
- Rotor alignment
- Bearing Clearances/Temperatures
- Axial Expansion
- Cylinder Thermal Growth
- Bearing Support Structure Seismic data
- Operation Data
- Steam Chemistry

Rotor NDE—No indications were found that otherwise could have initiated rotor vibration

Rotor Run Out—Rotor charting indicated the runouts were within acceptable limits

Rotor Alignment—Coupling gaps and displacements between HP and LP were within design tolerance limits

Valves Operation—Deviations in valve operating sequence could cause steam-induced vibration due to steam unbalance loads.

Field outage report did not indicate any abnormal wear in valve seating that would otherwise cause pressure differentials leading to steam-induced vibration.

Valves operation was normal and did not contribute to rotor vibration.

Bearing Clearances/Temperatures—Increased bearing clearances tend to reduce damping and cause vibration. Review of bearing clearance data indicated no abnormal wear in bearings. Bearing operating temperatures were normal at 180 F (82 C)

Bearing Support Seismic data—Bearing pedestal seismic vibration could trigger shaft vibration. However, seismic vibration was within allowable limits

Axial Expansion—Differential axial expansion was measured and did not indicate abnormal behavior

Cylinder Thermal Growth—Uneven HP turbine base-to-cover thermal expansions could have caused cylinder distortion leading to seal rubs and triggered rotor vibration. But, temperatures of cylinder base/cover were within normal.

Internal Steam Leakage—Based on the data review on IP cylinder base and cover temperature differentials, MW load and the shaft vibration as shown in Fig. 8.19, internal steam leakage was considered as a likely scenario during start up at low MW load where non-uniform cylinder heating was observed. This could have caused instantaneous, but temporary IP cylinder distortion that led to seal rubs resulting in instantaneous high vibration of the rotor.

8.6.2 Solution

Internal steam leakage at the IP inlet was confirmed as the root-cause of increased shaft vibration. Actions were taken to reduce internal steam leakage that corrected the high vibration issue.

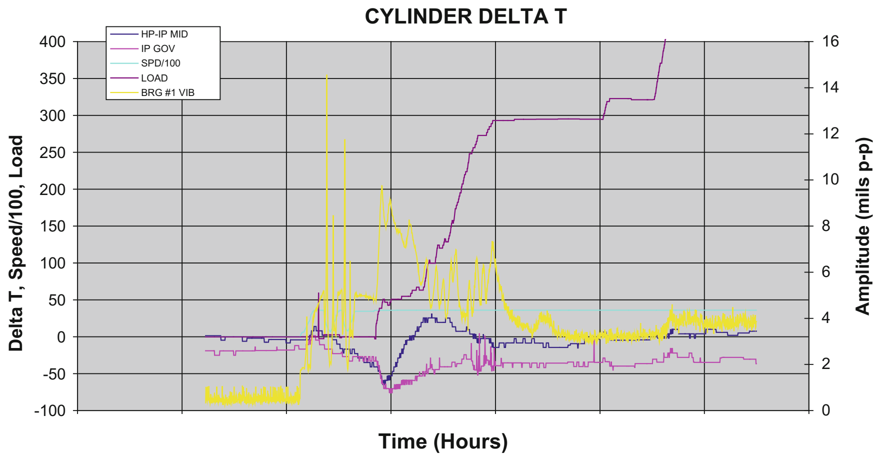

Fig. 8.19 Vibration, load and IP cylinder temperature data during start-up

8.7 Description of a Problem for Test Case-5

Torsional Frequency Shift due to Inertia Changes in the rotors as described below:

The example rotor train consisted of an HP, three LPs, generator and exciter rotors. This rotor train experienced high torsional vibration due a sudden loss of rotor inertia. This unit was operating without any torsional incident for about 15 years. During service, a sudden loss of inertia in the turbine system shifted the torsional frequencies closer to operating resonance.

8.7.1 Analyses

Detailed FE analyses of the LP rotor last row disc were performed in an effort to identify the source of the problem. Analyses were conducted by varying the thickness of the disc neck area. Calculations indicated potential for shifting the torsional frequency away from the operating zone by a comfortable margin. Consequently, the rotor disc re-profiling as shown in Fig. 8.20a was carried out to study their effects on frequency shifts.

Finite element modeling of the LP rotor last row disc area was carried out with finer mesh elements. The neck area of the disc was progressively reduced and an optimal profile was arrived that was found shifting the frequency from that of the original configuration. The disc profile was finally optimized to the shape shown in Fig. 8.20b that shifted the torsional frequency of the train away from resonance with comfortable margin from the operating speed. The new disc profile also kept the disc shear stresses within acceptable levels as required.

Additionally, inertia ring was added to the connector shaft (or jack shaft, JS) as shown in Fig. 8.21 which also participated in the mode of interest. Introduction of inertia ring on the JS helped further reducing the frequency and the shear stress of the rotor train for the torsional mode of interest.

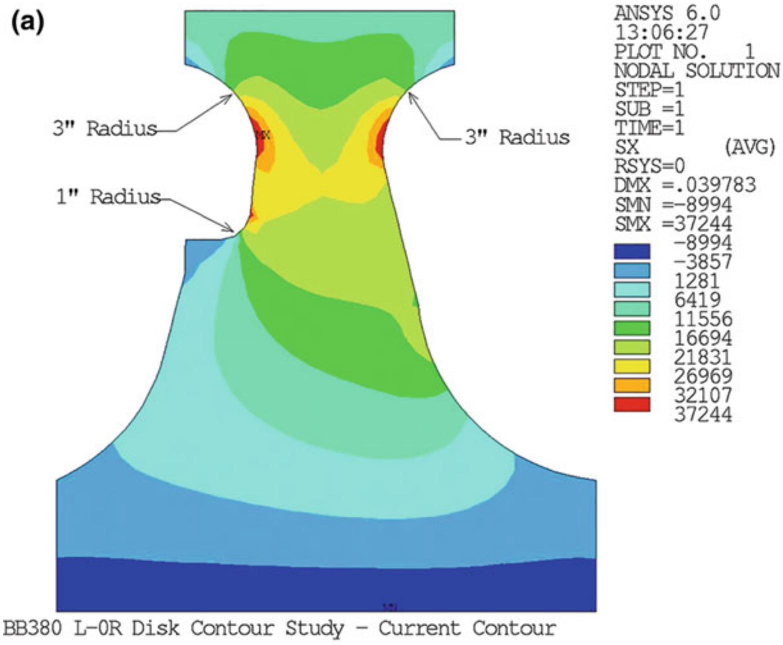

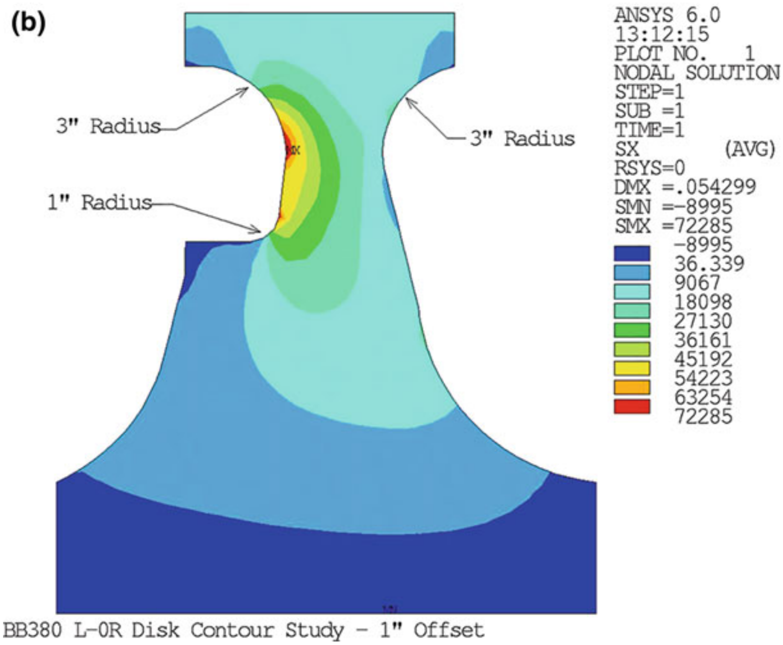

Fig. 8.20 **a** Before disc machining. **b** After disc machining

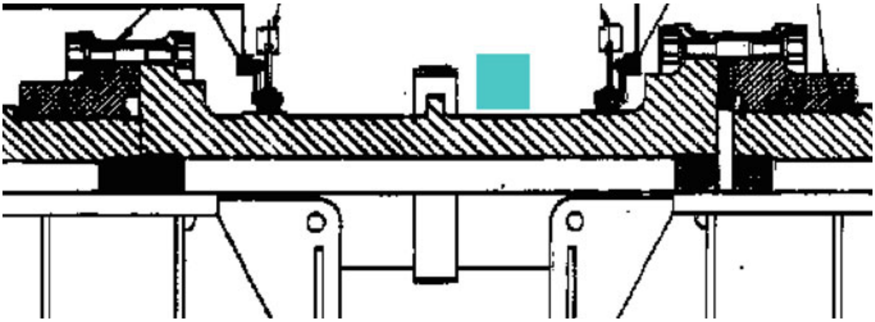

Fig. 8.21 Added Inertia at a shaft location helped to reduce vibratory stresses

8.7.2 Solution

Reduced neck areas of the LP discs shifted torsional frequency away from the operating frequency. In addition, the inertia ring that was shrunk on to the connector shaft, further reduced frequency and shear stresses for the frequency of interest.

8.8 Description of a Problem for Test Case-6

An HP rotor experienced high vibration when it was operating in partial-arc steam admission mode. The rotor was supported on 4-pad tilt-pad bearings on both ends and the vibration observed was 1x dominant and not ½ x (typically observed in steam turbines) on bearing 2.

8.8.1 Data Analysis

Measured data confirmed that the sub-synchronous (or ½ x) vibration was about 20 times smaller than 1X vibration as shown in Fig. 8.22. In this case, the rotor had overall vibration of 0.010” (250 μ) dominated by 1X at part load conditions (or sequential valve operation).

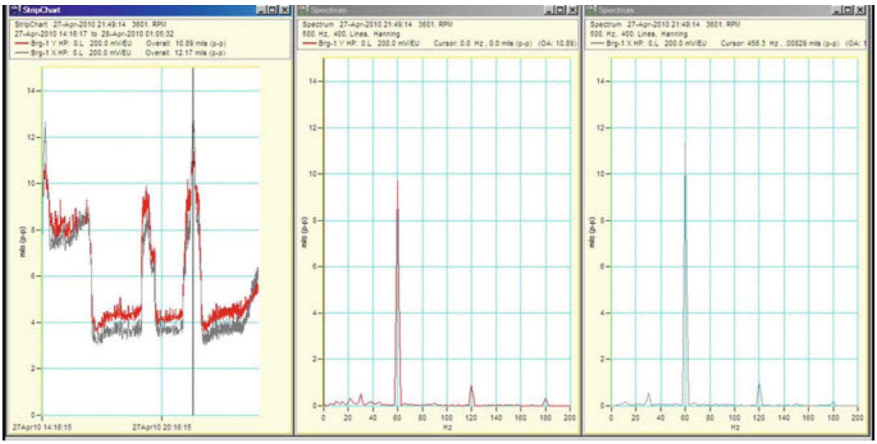

Fig. 8.22 Vibration spectrum plots

At part-load operation, the bearing 1 vibration levels were about 0.004 inches (50 μ) p-p as shown in Fig. 8.23 whereas the vibration levels on bearing 2 were recorded as high as 0.012 inches (about 300 μ) p-p as shown in Fig. 8.24.

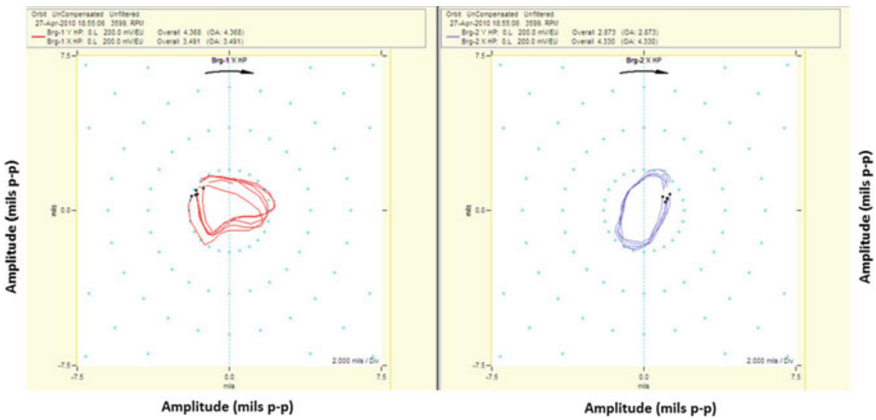

Fig. 8.23 Bearing 1 vibration orbits on LH and RH bearings

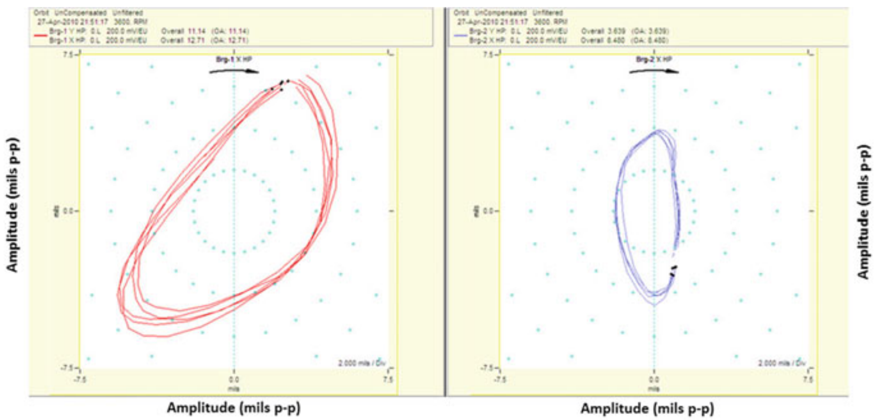

Fig. 8.24 Bearing 2 vibration orbits on LH and RH bearings

The following actions were taken with the intent of reducing 1X vibration:

a. Multiple rotor balance attempts failed to reduce vibration
b. Valve re-sequencing to suppress steam induced forces failed
c. Tightening of bearing clearances did not improve vibration levels
d. Bearing load increase on bearing 2 to improve damping did not help either.

Associated orbital plots were obtained and reviewed. Additionally, the loci of the journal positions *before, during and after* the high vibration event were reviewed. Studies concluded that the current 4-pad bearings were not capable of controlling the steam unbalance forces. Consequently, studies were conducted simulating 5 and 6 pad bearings to control the excessive steam loads. It was found that the 6-pads with variable lengths and pre-loading helped controlling the steam whirl predominantly at 1x.

The customized 6-pad bearing configurations were applied to control the orbital behavior. Vibration was brought below 0.003" (75 μ) and were acceptable for continuous operation. 6-pad bearings, when suitably pre-loaded, were found to contain unbalance steam forces.

8.8.2 Solution

6-pad bearings with variable pad lengths and suitable pad-preloading helped reducing vibration. In this case, 6-pad bearings were applied on both bearings 1 and 2.

8.9 Description of a Problem for Test Case-7

Elevated vibration and increased metal temperatures were noticed and reported on a 6-pad bearing (see Fig. 8.25). Details are discussed below.

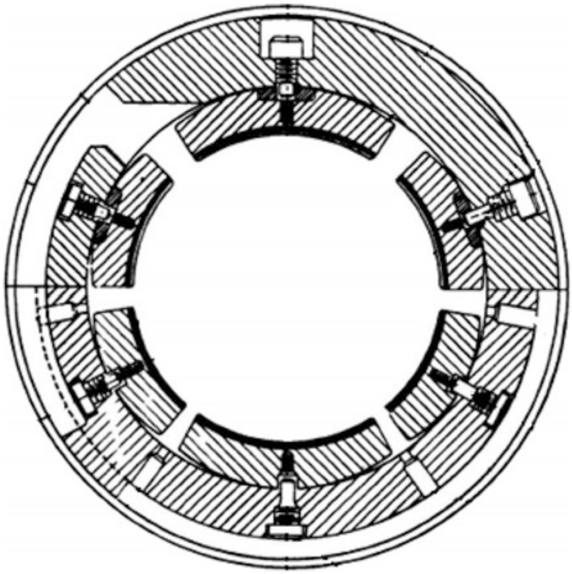

Fig. 8.25 6-pad bearing

8.9.1 Data Analysis

A vintage steam turbine rotor, originally supported on 4-pad tilt-pad bearings, had frequent vibration issues due to inadequate pad support loads. One of the bearings had excessive sub-synchronous vibration due to steam induced unbalance forces. This bearing was replaced with a 6-pad type. The 6-pad bearing, at installation, had three pads on the top and the other three at the bottom as shown in Fig. 8.25. Even after installing 6-pad bearing, the unit experienced high vibration that sometimes exceeded alarm limits. Close review of the pad installation revealed that the pad orientations and preloading were not adequate to address the un-controlled journal motions at the operating condition.

Orbital plots showed the journal was rocking towards the bottom pad (the pad at 6 O'clock position was load-on-pad) at intermediate steam loads. Experience shows that the load-on-pad condition eventually reduces the damping and become unstable; sometimes known as, "*lightly loaded bearing condition*".

In the first attempt to reduce vibration, the bearing was raised to increase the bearing load. This action increased oil film damping and reduced shaft vibration. However, the bearing metal temperature started increasing to 230 F (110 C) at full load.

While the bearing loading helped addressing the vibration problem, it created another problem namely, "*heavily loaded bearing condition*".

In the second attempt, the bearing was lowered towards the lateral direction slightly and the bearing pad assembly was rotated about 20° clockwise from the original configuration. The rotation of the pad-assembly brought the journal between the two pads (load between pads) and closer to the minimum oil film position. The journal positioned between pads increased the oil film stiffness and kept the rotor loaded adequately. The combination of bearing moves helped lowering the bearing metal temperature to 200 F (93 C) and the vibration as well at full load operation.

Pad orientations and pre-loading were optimized with respect to journal position using measured orbital plots in conjunction with the installed vibration probe angular positions.

8.9.2 Solution

Utilizing the shaft orbital plots in relation to vibration probe orientations, the locus of the journal inside the 6-pad bearing was optimized. This approach helps reducing vibration and the bearing metal temperature at the same time.

8.10 Description of a Problem for Test Case-8

An HP-IP rotor installed with brush seals experienced steam whirl. Rotor dynamic studies confirmed possibility of steam whirl occurrences with brush seals (Fig. 8.26a) at a specific brush seal clearance. Brush seals on a HP turbine blade path is shown in Fig. 8.26.

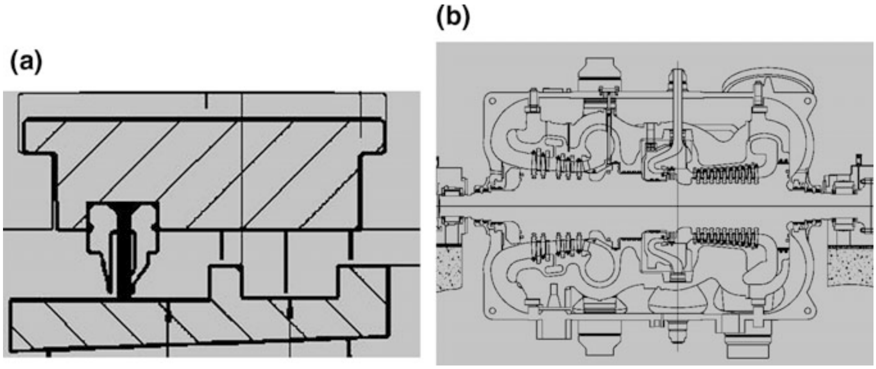

Fig. 8.26 Brush seals installed on rotating row shrouds of a HP turbine blade path

8.10.1 Analysis

The main function of brush seals is to improve thermal performance in a HP turbine by reducing steam leakage across the seals. Brush seals are meant to provide ideally zero clearances between the rotor surface and the associated stationary seal segments.

During the initial operation, this unit experienced a steam whirl incident. A rotor dynamic study was conducted to understand the behavior of brush seals.

Rotor dynamic model was built including bearing oil film, pedestal stiffness and brush seal dynamic coefficients for the configuration shown in Fig. 8.26. Seal dynamic coefficients were calculated for all the rotating blade shrouds. Rotor stability studies were performed. The resulting log-dec values of the mode of interest were plotted against brush seal clearances as shown in Fig. 8.27.

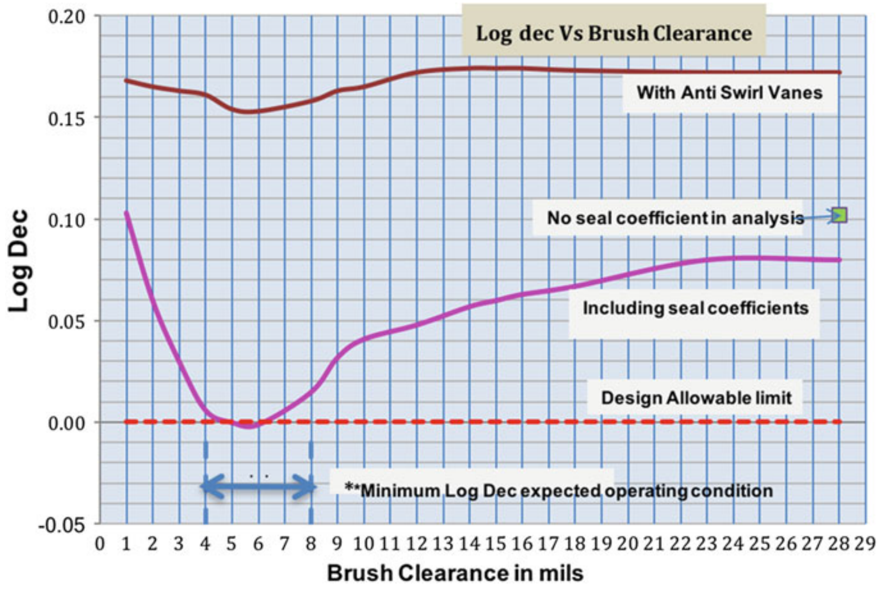

Fig. 8.27 Rotor dynamic studies with and without anti-swirl vanes

The analysis indicated that when the seal clearances reached between 0.004” ($\sim$100 μ) and 0.008” ($\sim$200 μ), rotor became unstable. The rotor instability due to steam whirl was not predicted when the seal dynamic coefficients were not included in the model as shown by the green log-dec. values. Additionally, when the seal dynamic coefficients for the anti-swirl vanes were introduced in the rotor dynamic model at the inlet to CS, NZC and blade path, significant improvement in damping was realized as noted in Fig. 8.27.

8.10.2 Solution

Rotor dynamic studies were performed including brush seal dynamic coefficients. Mild form of steam whirl was predicted for a small range of brush seal clearances. Predictions matched with the actual rotor instability behavior as illustrated in Fig. 8.27.

8.11 Description of a Problem for Test Case-9

This is a case about uneven Frame Foot Loading for a Generator. Vibration spectrum plots provided symptoms of uneven frame foot loading. See spectrum plot in Fig. 8.28 where 1x, 2x and harmonic responses provided clues about frame vibration. Additionally, the polar plot was observed as abnormal and irregular and the X and Y response components on the right side were seen unusual for a shaft vibration. They all provide symptoms that foot vibration could be a suspect.

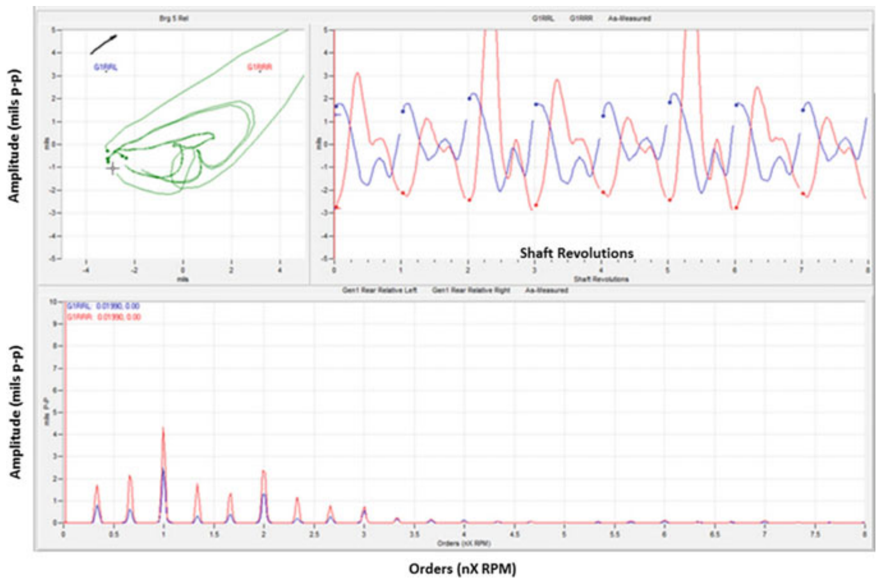

Fig. 8.28 Spectrum plots obtained at the generator feet

8.11.1 *Data Analysis*

Rarely, generator shaft relative vibration spectra show a pattern of unusual trends as noticed in Fig. 8.28. The spectrum plots show several vibration components atypical to generator rotor behavior. These symptoms do not match with behaviors that are exclusively related to the rotor and/or the fluid-film bearings. Close monitoring of the generator feet data indicated that the multiple spectral amplitudes at harmonic frequency intervals were measured at the feet. Such symptoms correlated with insufficient frame foot loading.

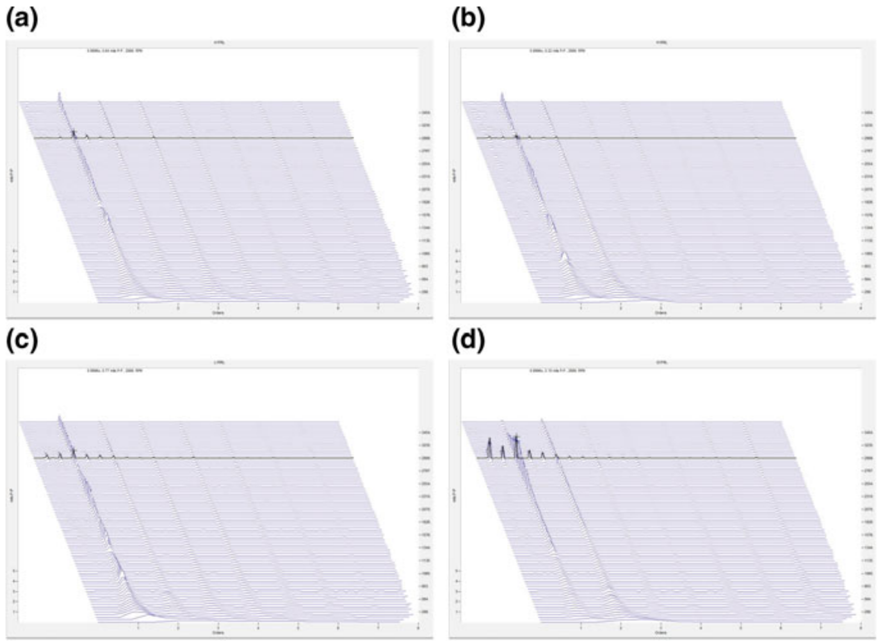

Fig. 8.29 Waterfall diagram showing frame foot issues

Additionally, waterfall diagrams shown in Fig. 8.29 further corroborated with the observed vibration data.

8.11.2 Solution

Spectrum, shaft relative, seismic and waterfall vibration plots can be used to identify and confirm the generator uneven frame-foot loading.

8.12 Description of a Problem for Test Case-10

Several shrunk-on discs of an LP rotor and the two shrunk-on LP coupling flanges were disassembled and re-assembled at the factory as part of the repair. When the repaired LP rotor was assembled with the Generator on-site, the LP coupling outer rim diameter (shown in Fig. 8.30) was found to have excessive runout (kink) with a maximum of 11 mils TIR (Total Indicated Reading).

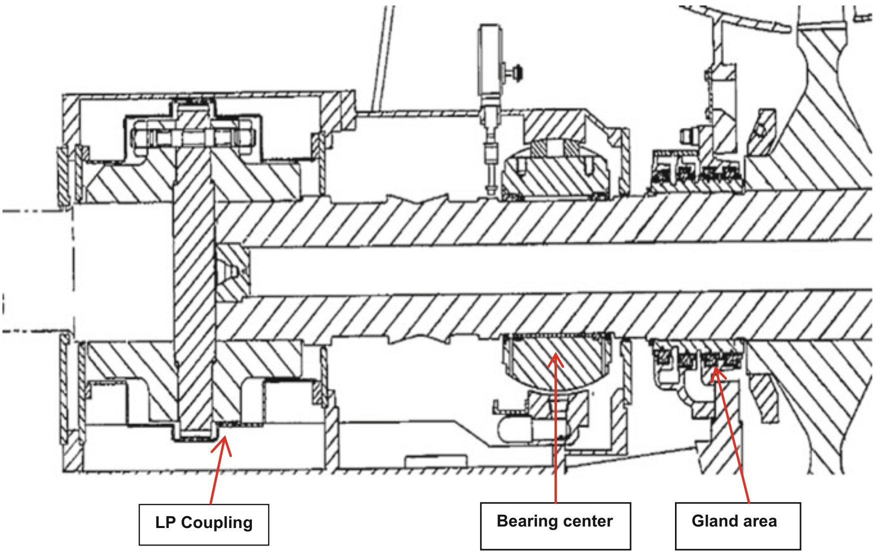

Fig. 8.30 LP-generator coupling overhang

8.12.1 Historical Data Review

Recorded Data in the Factory Before Shipment to Site:

- In the as-shipped condition, the rotor center through the gland area had an average recorded TIR at 0.00275” which is considered as low runout.
- TIRs were recorded <0.001” at the LP overhang sections that consist of journal, vibrometer land, coupling spigot and the truth track at the coupling rim.
- Coupling spigot TIR was machined to suit the stub shaft that was attached to the LP rotor for factory balancing. The stub shaft was necessary to support the long shaft over hang via a third bearing.
- Rotor was high speed balanced without any observed vibration issues on the shaft overhang.

8.12.2 Field Measurements with Excessive Runout at the Coupling End

- When the rotors were assembled on-site, excessive TIR (about 0.011”) was measured at one portion on the LP coupling OD as shown in Table 8.3.

Table 8.3 Recorded TIR at the LP shaft overhang

Position	Location to journal CL	TIR
Journal CL	0.00	0.000
Differential expansion inboard	16.188	0.003
Differential expansion outboard	24.813	0.005
Inboard side Gnn coupling	37.469	0.006
Middle Gnn cplg flange at OD	49.188	0.011
LP coupling truth track	50.750	0.002

- The Spigot diameter and the coupling truth track (a narrow machining area at the rim of the coupling used as reference point for all TIRs measurements on the shaft) are running true to the LP journal center
- The overhang shaft TIRs starting from the coupling rim are continuously decreasing through the overhang section that ends with 0.0” at the journal center.
- The local kink at the LP coupling flange caused mismatch of bolt holes between the LP rotor and the adjacent Generator rotor. This delayed coupling assembly on-site.

8.12.3 Concerns

- Primary concern was the coupling assembly on-site due to the holes being eccentric in assembled condition.
- Secondary concern was the excessive TIR at the LP coupling rim. If the rotor system is allowed to operate with the high TIR, vibration at the coupling would increase.
- Major effort was needed to remove the coupling runout at one location. So, alternate solutions were reviewed.

8.12.4 Resolution

- Since the entire shaft line on both sides of the couplings were concentric with low TIR, the shaft line does not have eccentricity large enough to trigger vibration due to unbalance condition.
- The coupling holes on the two halves of the coupling joint were line-reamed to maintain concentricity of the joint and with the LP shaft line. In addition, LP spigot was machined concentric with the shaft line.
- The above actions ensure the shaft line is concentric.
- Although the local TIR at one point on the rim of the coupling was high, the majority of the shaft line had lower TIR. So, this coupling assembly is not expected to cause vibration at the bearing.
- Earlier, the rotor was balanced with this condition at the factory without issues.
- However, the site was cautioned to prepare for additional balance moves at the coupling area in case of high vibration.

8.12.5 Conclusion

As expected, the large TIR in the local area on the coupling rim did not adversely impact the vibration at the bearing location. Unit operated with acceptable vibration.

8.13 Description of a Problem for Test Case-11

A large linear surface crack was observed in the fillet area between the gland and the disc seat diameter of an LP rotor as shown in Fig. 8.31. The goal was to determine the most likely cause of shaft cracking, and to develop potential remedial actions to reduce the likelihood of reoccurrence (Fig. 8.32).

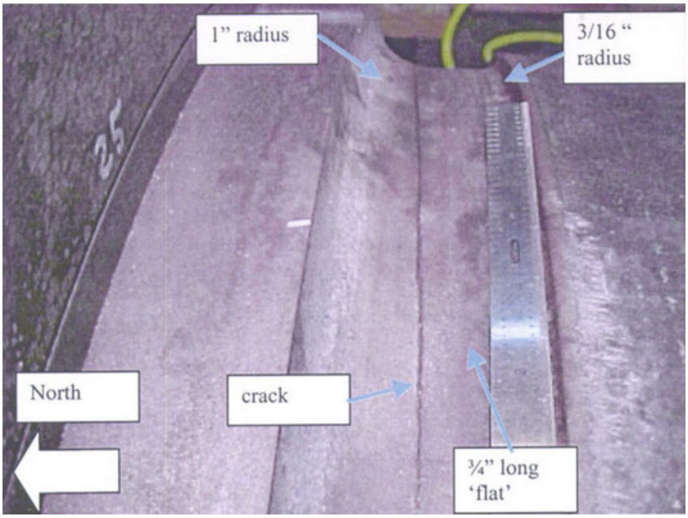

Fig. 8.31 Shaft crack

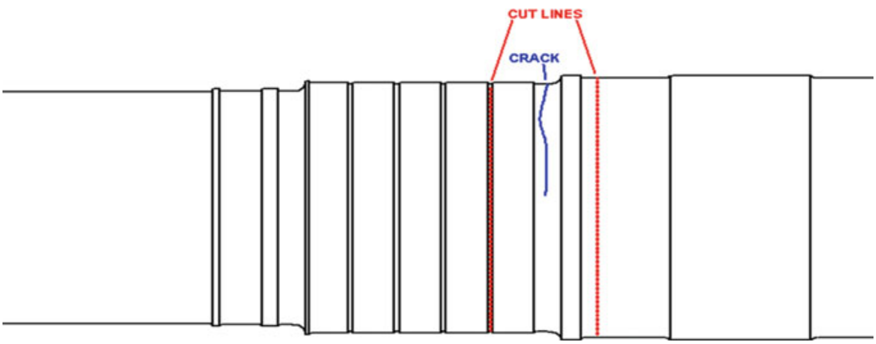

Fig. 8.32 Cracked zone in the shaft is shown in red lines

8.13.1 Analysis

The scope of the root cause analyses was:

- Develop a rotor model and apply the operational data to study the cause of the rotor crack.
- Estimate stresses resulting from normal operation, bearing elevation misalignment, lateral vibration, torsional vibration and other circumstances of interest defined by the operational review.
- Simulate crack initiation/propagation mechanisms and use a fracture mechanics approach to match which scenario best fits the conditions observed on the shaft fracture surface.
- Based on review, conclude findings.

Gland temperature-MW load data was used as representative of a typical operation. Whenever supply steam temperature fell below 250 F (121 C), the supply steam was no longer superheated. Alternate hot and cold gland steam temperature occurred over approximately 2 h, and generated thermal stresses in the shaft. The probable effects of these thermal cycles on shaft cracking were discussed in the stress and fracture mechanics evaluations.

8.13.2 Thermal Stress Analysis

The possible contribution of the gland system behavior to shaft cracking was as follows:

- The wet steam supplied at 215 F (102 C) to the LP turbine glands throttled outward to the LP exhaust pressure. As the steam exited the gland, it flashed to vapor due to the lower temperature. When this occurred, contaminants in the steam tend to concentrate on the shaft surface. This resulted in pitting on the shaft at the gland area. Metallurgical investigations confirmed evidence of chloride deposits in the pits. Pits provided initiation site for cracks.
- The daily thermal transients associated with the gland steam temperature changes as the unit load changes could result in thermal stresses in the shaft surface. These cycles could potentially drive cracks. An evaluation of thermal stresses resulting from the thermal transients is provided in the next section.

Maximum stresses (as shown MX) were calculated at the fillet area near the gland. See Fig. 8.33. The shaft locations where the stresses were predicted higher correlated well with the actual location on the shaft where the cracks initiated as shown in Fig. 8.31.

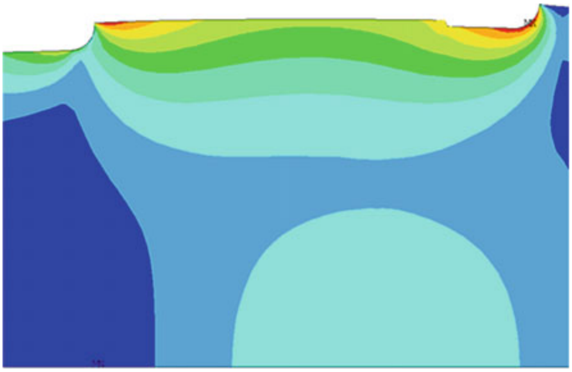

Fig. 8.33 Thermal stress at the gland area

8.13.3 Metallurgical Findings

The metallurgical evaluation of the shaft crack correlated to corrosion pitting both on the shaft surface and at the areas of the fracture face. The depth of the pit was 0.022" (0.56 mm) and looked crack-like at the bottom. The alternating stress level required to start crack propagation by high cycle fatigue for the 0.022" (0.56 mm) corrosion pitted area was calculated around 10 ksi (69 MPa). If the pitting crack were at 0.100" deep (2.5 mm), the alternating stresses needed to propagate the crack was about half.

The estimated nominal shaft bending stress at the gland area was approximately 5 ksi (35 MPa) that matched with the crack depth of 0.1" when the actual bearing alignment data was applied. When the 0.1" initial crack was applied in the fracture mechanics evaluation, it was estimated that a normal shaft bending is all that is needed to cause the flaw to grow in HCF.

8.13.4 Conclusions

The most probable causes of shaft cracking on the rotor are:

- Poor performance of the LP gland steam system.
- Insufficient superheat and variations in steam supply conditions resulted in pitting of the shaft and significant thermal transient stresses that helped the crack to initiate
- Crack propagation was mostly by high cycle fatigue with alternating bending stress provided by normal shaft rotation.

8.14 Closure

Eleven case studies related to key turbo-machinery issues were discussed throughout this chapter. They help providing symptoms and diagnosis leading to solutions to those problems.

Appendix A: Behavioral Similarities Between a Structure and a Human Body

Disclaimer: Discussions advanced here are the sole opinion of the author. Any exercise or workout-routine must be discussed with the primary care physician before embarking on a program.

The author has done limited research on behavioral similarities of a structure (a simple example is a cantilever beam) and the human body. The fundamental mode of a cantilever beam is known to provide the most energetic and flexible condition among all the modes it excites. Analogous to a cantilever beam, a human body bent in that shape can attain most energy and flexibility. See Fig. 8.34. A few body stretches/workouts are discussed.

Three main working systems of the human body and are responsible for healthy living are:

(a) Digestive System
(b) Respiratory System
(c) Immune System.

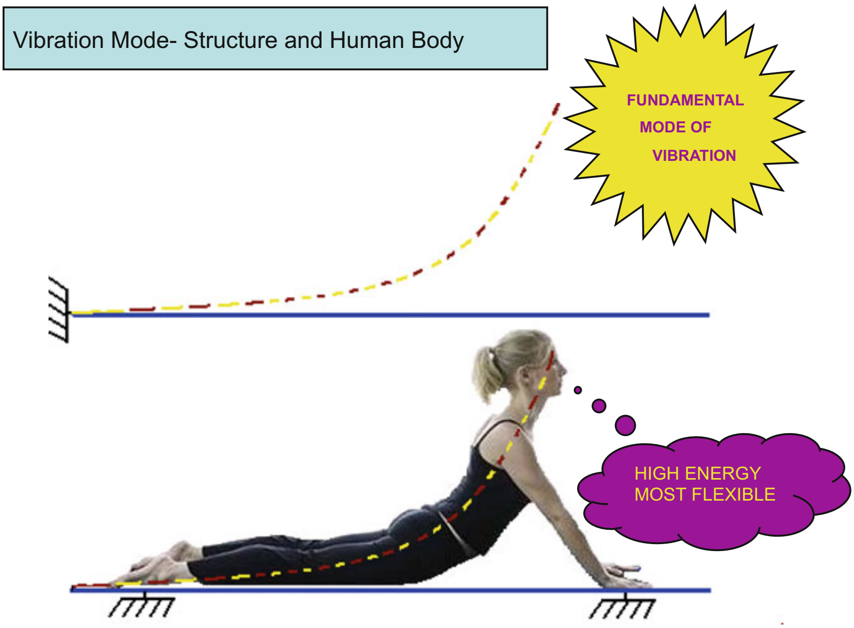

Fig. 8.34 Fundamental mode shape of a cantilever beam and the human body bent in a similar shape

The human body bent in the fundamental mode shape of a cantilever beam, illustrated in Fig. 8.34, in general, strengthens the three systems of the human body mentioned above; the benefits are discussed below:

Due to high-energy and flexibility, this posture shown in A1 helps stretching the following body parts/organs

- Organs in the abdominal area that participate in the digestive system are: (a) small and large intestines, (b) pancreas, (c) liver, (d) kidneys, (e) spleen and (f) gallbladder. These organs stretch during the exercise routine shown in Fig. 8.34.
- Toes, legs, and back bone structure
- Muscles in the arm
- Bent upper body helps chest expansion
- This posture supports about a third of the body weight, an optimal measure considered in weight lifting
- These exercise routines strengthen the immune system.
- Holding the breath for an extended period of time and releasing it regulates the respiratory system and blood pressure.

- Digestive system is strengthened and regulated since most organs that are responsible for digestion (such as liver, pancreas, intestines and kidneys etc.) participate in this posture.
- Respiratory system is regulated when breath is held in this posture (about 30 s or more) and released after the completion of each routine [1–3].
- Immune system improves when the various muscle groups, bones and other organs in the entire body get work-out [4, 5].
- Muscles at the tonsil area stretch with the head bent backwards in this posture; this could improve tonsil conditions.
- Stomach muscles stretch while holding and releasing the breath.
- These exercises activate enough muscle fibers to directly impact mitochondria or reverse the genetic process of aging.
- By working multiple muscle groups simultaneously, as illustrated in Figs. 8.34 and 8.35, complete activation of mitochondria at a level that can impact gaining processes of multiple muscle groups [6–8].

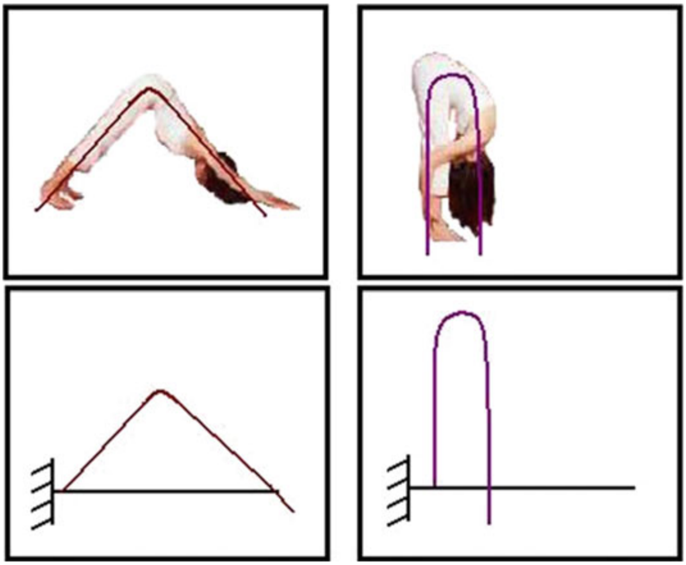

Fig. 8.35 Similarity between the second mode shape of a cantilever beam and the human body posture

Again, second bending mode shape of a cantilever beam and the equivalent human body postures are compared side-by-side in Fig. 8.35. Benefits discussed above apply here as well.

References

1. Brown RP, Gerbarg PL (2005) Sudarshan Kriya, "Yogic breathing in the treatment of stress, anxiety, and depression", part I-neurophysiologic model. J Altern Complement Med 11(1), 189–201
2. Brown RP, Gerbarg PL (2005) Sudarshan Kriya, "Yogic breathing in the treatment of stress, anxiety, and depression", part II: clinical applications and guidelines. J Altern Complement Med 11(4):711–717
3. Harinath K, Malhotra KS, Pal K et al (2004) Effects of Hatha yoga and Omkar meditation on cardiorespiratory performance, psychologic profile, and melatonin secretion. J Altern Complement Med 10(2):261–268
4. Arora S, Bhatacharjee J (2008) Modulation of immune responses in stress by yoga. Int J Yoga 1(2):45–55
5. Kolasinski SL, Garfinkel M, Tsai AG et al (2005) Iyengar yoga for treating symptoms of osteoarthritis of the knees: a pilot study. J Altern Complement Med 11(4):689–693
6. Carlson LE, Speca M, Patel KD, Goodey E (2004) Mindfulness-based stress reduction in relation to quality of life, mood, symptoms of stress and levels of cortisol, dehydroepiandrosterone sulfate (DHEAS) and melatonin in breast and prostate cancer outpatients. Psychoneuroendrocrinology 29(4):448–474
7. Waelde LC, Thompson L, Gallagher-Thompson D (2004) A pilot study of a yoga and meditation intervention for dementia caregiver stress. J Clin Psychol 60(6):677–687
8. West J, Otte C, Geher K, Johnson J, Mohr DC (2004) Effects of Hatha yoga and African dance on perceived stress, affect, and salivary cortisol. Ann Behav Med 28(2):114–118